Non-genetic mechanisms leading to local and distant metastasis

M.J. Teeuwssen

Non-genetic Mechanisms Leading to Local and Distant Metastasis

Niet-genetische mechanismen betrokken bij lokale en metastasering op afstand

Thesis

to obtain the degree of Doctor from the
Erasmus University Rotterdam
by command of the
rector magnificus

Prof. dr. A.L. Bredenoord

and in accordance with the decision of the Doctorate Board.
The public defence shall be held on

Wednesday 18 May 2022at 10.30hrs
By

Maria Johanna Teeuwssen
born in Delft, Netherlands.

Table of contents

**CHAPTER I**

1

General introduction

Cancer consists of a heterogeneous group of diseases including colon cancer, ovarian cancer and tumors of the head and neck region, and is the final outcome of uncontrolled cell growth. Cancer is the most important cause of death worldwide with 18.1 million cases in 2018, and it is expected that 29.5 million cases will be diagnosed in 2040 [1]. Cancer develops through a gradual accumulation of genetic alterations in specific tumor suppressor and oncogenes that result in a stepwise transformation of normal epithelial cells into precursor lesions and eventually towards malignancy [2] (**Figure 1**). Frequently, cancer results in metastatic dissemination, an event where tumor cells invade into the adjacent tissues and spread to other distant organs. Of note, up to 90% of cancer-related mortality for solid tumors is due to sequelae of metastasis [3]. In addition, with the improvement of therapeutic and management strategies, the number of patients living with metastatic disease has been rising [4]. This reality highlights the heavy public health burden of metastatic disease and accentuates the critical need to understand and more effectively intervene clinically in the late stages of cancer progression.
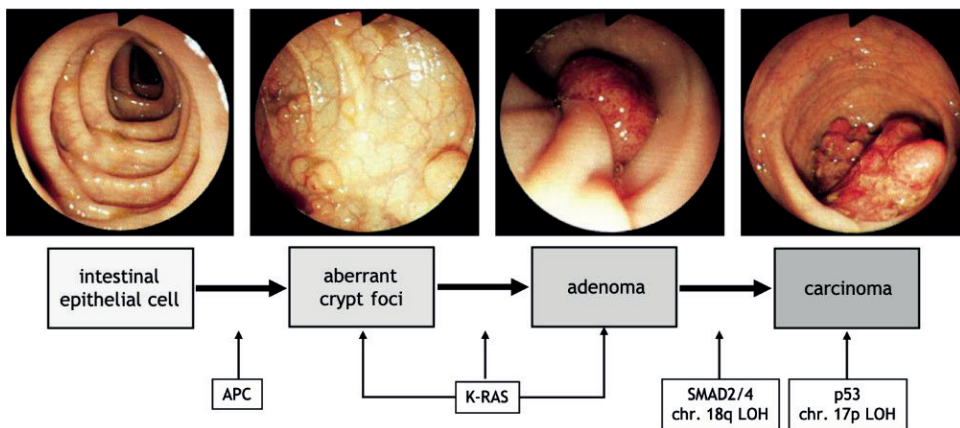
Figure 1. The adenoma-carcinoma sequence. The adenoma-carcinoma sequence refers to a stepwise pattern of mutational activation of oncogenes (e.g. *K-RAS*) and inactivation of tumor suppressor genes (e.g. *P53*) that results in cancer. This phenomenon starts with the transformation of normal epithelium to an adenoma, proceeding to an *in situ* carcinoma, and ultimately to an invasive and metastatic tumor. In colon cancer development, the genomic changes include the activation of proto-oncogene *K-RAS* and the inactivation of at least three tumor suppression genes, including, loss of *APC* (chromosome region 5q21, loss of *P53* (chromosome region 17p13, and loss of heterozygosity for the long arm of chromosome 18 (18q LOH) [2].

The formation of metastases is an extremely complex process in which tumor cells escape from the primary tumor, disseminate to a secondary site, survive and adapt to the ectopic location and finally colonize and proliferate to form lesions while evading immune surveillance [5] (**Figure 2**). The dissemination of metastatic tumor cells from the primary tumor to secondary locations may be conducted via the blood circulation, via the lymphatic system, or through direct extension [6,7]. Hematogenous spread of metastatic cells is responsible for the majority of distant metastasis [8]. Alternatively, tumor cells can disseminate through the lymphatic system, which is considered to be a common event in cancer [9]. However, ultimately the lymphatic system drains into the systemic venous

system, and so, these metastatic cells will eventually spread via the hematogenic system. Yet, both metastatic cells disseminated by either blood or lymphatic flow to distant organs actively leave the vasculature through extravasation. These extravasated cancer cells may then grow out to form secondary tumors (**Figure 2**). Lastly, the spreading of malignant cells can also occur into body cavities via penetrating the surface of the peritoneal, pleural, pericardial, or subarachnoid spaces. This transcoelomic spread is fairly uncommon, and appears to be restricted to ovarian carcinomas and mesotheliomas [6].
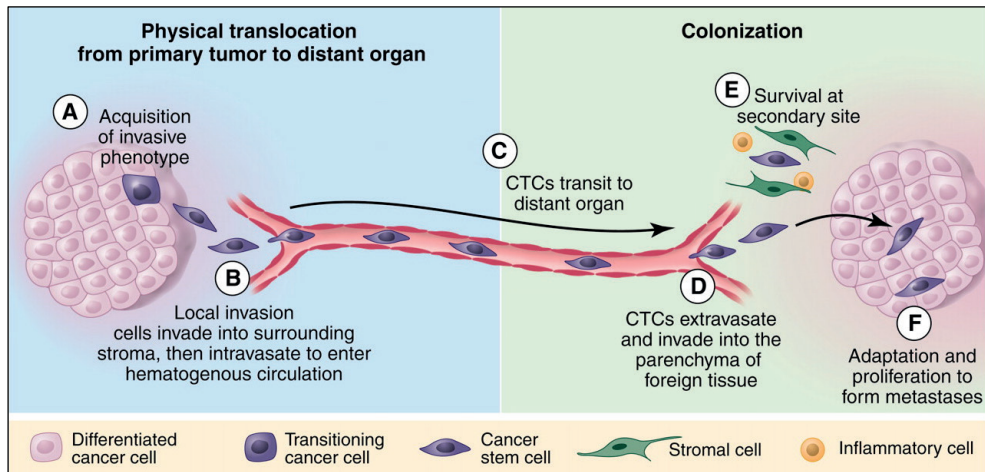
Figure 2. The metastatic cascade. In order to metastasize tumor cells, have to address two major aspects: i. the physical detachment of cancer cells from the primary tumor and ii. the colonization of the metastatic cells within the distant organ. (**A**) To begin the metastatic cascade, tumor cells within the primary tumor have acquire an invasive phenotype. (**B**) Cancer cells can then invade into the local stroma and towards blood vessels, where they intravasate into the blood circulation. (**C**) Circulating tumor cells (CTCs) travel through the circulation to distant sites and display features that lead to anchorage-independent survival. (**D**) At the foreign organ, CTCs extravasate and invade into the microenvironment of this tissue. (**E**) Here, tumor cells must be able to survive as single cells (or as a small cluster of cells) and need to be able to escape the innate immune response. (**F**) To give rise to a macrometastatic tumor, the cancer cells need to adapt to the local microenvironment and initiate proliferation. Figure adapted from [5].

In order to successfully complete these challenging series of events, the most important feature of metastasizing tumor cells is the capacity to adapt to the ever-changing environmental contexts by undergoing reversible changes in its cellular identity. This 'Dr. Jekyll and Mr. Hide' feature of migrating cancer cells is often referred to as phenotypic plasticity [10] and is controlled by epigenetic mechanisms which regulate, among other processes, epithelial-to-mesenchymal transition (EMT) and the reverse mesenchymal-to-epithelial transition (MET) [11]. Thus, EMT is thought to play key roles in each step of the metastatic cascade including invasion [11], intra- and extravasion [12], and the colonization of distant organ sites [13,14].

In this thesis, we discuss the role and underlying mechanisms leading to of phenotypic plasticity in metastasis formation in tongue, colon and ovarian cancer. In **Chapter II** we summarize the current knowledge of phenotypic plasticity in tumor heterogeneity and metastasis formation and the contribution of EMT in this process. The alleged role of hybrid epithelial/mesenchymal (E/M) in collective and/or single-cell migration during local dissemination at the primary site and systemic spreading will be highlighted. In **Chapter III** we employ an epigenetic mechanism underlying MET in tongue cancer by investigating the molecular function of DOC1 (deleted in oral cancer 1). **Chapter IV** and **VI** reports the identification and molecular characterization of a subpopulation of respectively colon and ovarian cancer cells earmarked by phenotypic plasticity and by highly invasive and metastasizing properties. Following, in **Chapter V** we review the latest knowledge of the role of Wnt signaling in ovarian cancer stemness, EMT, and therapy resistance. In addition, the proposed role of exosomes in the paracrine activation of Wnt signaling and pre-metastatic niche formation will be highlighted. Next, in **Chapter VII** we present experimental evidence for the dual role of Wnt signaling in regulating metastasis formation in high grade serous ovarian cancer. And lastly, in **Chapter VIII** different therapeutic strategies hypothesized to target cancer cell plasticity will be discussed including its associated challenges.

References

1. Ferlay J, E.M., Lam F, Colombet M, Mery L, Piñeros M, Znaor A, Soerjomataram I, Bray F. Global Cancer Observatory: Cancer Tomorrow. Availabe online: https://gco.iarc.fr/tomorrow (accessed on 15 November).
2. Fearon, E.R.; Vogelstein, B. A genetic model for colorectal tumorigenesis. *Cell* **1990**, *61*, 759-767.
3. Mehlen, P.; Puisieux, A. Metastasis: a question of life or death. *Nat Rev Cancer* **2006**, *6*, 449-458.
4. Sundquist, M.; Brudin, L.; Tejler, G. Improved survival in metastatic breast cancer 1985-2016. *Breast* **2017**, *31*, 46-50, doi:10.1016/j.breast.2016.10.005.
5. Chaffer, C.L.; Weinberg, R.A. A perspective on cancer cell metastasis. *Science* **2011**, *331*, 1559-1564, doi:10.1126/science.1203543.
6. Tan, D.S.; Agarwal, R.; Kaye, S.B. Mechanisms of transcoelomic metastasis in ovarian cancer. *Lancet Oncol* **2006**, *7*, 925-934, doi:10.1016/S1470-2045(06)70939-1.
7. Wong, S.Y.; Hynes, R.O. Lymphatic or hematogenous dissemination: how does a metastatic tumor cell decide? *Cell Cycle* **2006**, *5*, 812-817, doi:10.4161/cc.5.8.2646.
8. Weinberg, R.A. Is metastasis predetermined? *Mol Oncol* **2007**, *1*, 263-264; author reply 265-266, doi:10.1016/j.molonc.2007.07.001.
9. Naxerova, K.; Reiter, J.G.; Brachtel, E.; Lennerz, J.K.; van de Wetering, M.; Rowan, A.; Cai, T.; Clevers, H.; Swanton, C.; Nowak, M.A., et al. Origins of lymphatic and distant metastases in human colorectal cancer. *Science* **2017**, *357*, 55-60, doi:10.1126/science.aai8515.
10. Varga, J.; Greten, F.R. Cell plasticity in epithelial homeostasis and tumorigenesis. *Nat Cell Biol* **2017**, *19*, 1133-1141.
11. Nieto, M.A.; Huang, R.Y.; Jackson, R.A.; Thiery, J.P. Emt: 2016. *Cell* **2016**, *166*, 21-45.
12. Frose, J.; Chen, M.B.; Hebron, K.E.; Reinhardt, F.; Hajal, C.; Zijlstra, A.; Kamm, R.D.; Weinberg, R.A. Epithelial-Mesenchymal Transition Induces Podocalyxin to Promote Extravasation via Ezrin Signaling. *Cell Rep* **2018**, *24*, 962-972.
13. Ocana, O.H.; Corcoles, R.; Fabra, A.; Moreno-Bueno, G.; Acloque, H.; Vega, S.; Barrallo-Gimeno, A.; Cano, A.; Nieto, M.A. Metastatic colonization requires the repression of the epithelial-mesenchymal transition inducer Prrx1. *Cancer Cell* **2012**, *22*, 709-724.
14. Stankic, M.; Pavlovic, S.; Chin, Y.; Brogi, E.; Padua, D.; Norton, L.; Massague, J.; Benezra, R. TGF-beta-Id1 signaling opposes Twist1 and promotes metastatic colonization via a mesenchymal-to-epithelial transition. *Cell Rep* **2013**, *5*, 1228-1242.

CHAPTER II

2

Cell heterogeneity and phenotypic plasticity in metastasis formation: the case of colon cancer

Teeuwssen M.J. and Fodde R.

Abstract

The adenoma-to-carcinoma progression in colon cancer is driven by a sequential accumulation of genetic alterations at specific tumor suppressors and oncogenes. In contrast, the multistage route from the primary site to metastasis formation is underlined by phenotypic plasticity, i.e., the capacity of disseminated tumor cells to undergo transiently and reversible transformations in order to adapt to the ever-changing environmental contexts. Notwithstanding the considerable body of evidence in support of the role played by epithelial-to-mesenchymal transition (EMT)/mesenchymal-to-epithelial transition (MET) in metastasis, its rate-limiting function, the detailed underlying cellular and molecular mechanisms, and the extension of the necessary morphologic and epigenetic changes are still a matter of debate. Rather than leading to a complete epithelial or mesenchymal state, the EMT/MET-program generates migrating cancer cells displaying intermediate phenotypes featuring both epithelial and mesenchymal characteristics. In this review, we will address the role of colon cancer heterogeneity and phenotypic plasticity in metastasis formation and the contribution of EMT to these processes. The alleged role of hybrid epithelial/mesenchymal (E/M) in collective and/or single-cell migration during local dissemination at the primary site and more systemic spreading will also be highlighted.

Keywords: colon cancer; Wnt signaling; tumor heterogeneity; phenotypic plasticity; EMT; hybrid E/M; collective and single-cell migration; beta-catenin paradox

Abstract

1. Introduction—Tumor Heterogeneity in Colon Cancer

Colon cancer is the third most commonly diagnosed malignancy and the second leading cause of cancer-related death worldwide. It is predicted that its mortality burden will increase by 75% by 2040 [1]. Apart from its clinical impact, colon cancer also represents a unique study model to elucidate the cellular and molecular mechanisms underlying tumor onset, progression towards malignancy, and metastasis formation at distant organ sites [2].

It is generally accepted that primary colon carcinomas are heterotypic, i.e., they feature a heterogeneous composition of epithelial cancer cells intermingled with lymphocytes, stromal fibroblasts, endothelial, and other cell types from the micro- and macro-environment [3]. This heterogeneity is matched by the diversity of parenchymal cancer cells encompassing a broad spectrum of morphologies, gene expression profiles, and functional characteristics [4–6]. Likewise, heterogeneity within the stromal compartment, i.e., the tumor microenvironment, has also been demonstrated [5,7].

Intrinsic, i.e., (epi)genetic, as well as extrinsic factors, such as spatial location within the tumor (e.g., at the invasive front vs. tumor center), inflammation, and treatment history underlie the observed intra-tumor heterogeneity. Consequently, different cellular subpopulations within the primary tumor mass and its metastatic lesions are observed [8,9]. Next to 'spatial' heterogeneity, 'temporal' heterogeneity has also been demonstrated relative to changes in the (epi)genetic landscape of colon cancer within individual tumors over time [10]. Of note, tumor heterogeneity is thought to underlie the disappointing results of many currently employed anti-cancer therapies as it not only supports tumor progression and metastatic dissemination but it also lies at the basis of the development of therapy resistance and of overall poor clinical prognosis [11].

Metastasis formation is a process encompassing multiple steps: (1) Local tumor invasion across the basement membrane into the surrounding stroma, (2) intravasation into the vasculature, (3) survival in the circulatory system, (4) extravasation into the parenchyma of the distant organ, (5) colonization into a distal organ, and (6) re-initiation of proliferation to form macroscopic metastases [12]. In order to successfully complete this challenging series of events, the most important feature of the metastasizing cancer cell is the capacity to adapt to the ever-changing environmental contexts by undergoing reversible changes in its cellular identity. This *'Dr. Jekyll and Mr. Hide'* feature of migrating cancer cells is often referred to as phenotypic plasticity [13] and is controlled by epigenetic mechanisms which regulate, among other processes, epithelial-to-mesenchymal transition (EMT) and the reverse mesenchymal-to-epithelial transition (MET) [14].

A variety of chromatin remodeling complexes such as Polycomb and NuRD, play a central role in the transcriptional regulation of EMT-related transcription factors (EMT-TFs) and micro RNAs (miRs) by determining the accessibility of regulatory DNA elements and positioning of nucleosomes [15,16]. In addition, post-translational histone modifications which modulate chromatin folding and influence recruitment of regulatory proteins and control gene expression [17]. Accordingly, contextual EMT-promoting signals epigenetially modify the repression of epithelial genes and consequently drive the transition of cells into more mesenchymal-like states. These are epigenetically sustained unless the presence of EMT-promoting signals is discontinued leading to the reversion to more epithelial phenotypes [15].

Notwithstanding the considerable body of evidence in support of the role played by EMT/MET in metastasis, its rate-limiting function, and the detailed underlying cellular and molecular mechanisms, and the extension of the necessary morphologic and epigenetic changes are still a matter of debate [14,18,19]. Rather than leading to a complete epithelial or mesenchymal state, the EMT/MET programs generate migrating cancer cells displaying intermediate phenotypes featuring both epithelial and mesenchymal characteristics. These hybrid E/M cancer cells have been the focus of much attention in the most recent scientific literature as they are likely to be metastable and as such very efficient in causing metastasis [20].

Here, we will address the role of tumor cell heterogeneity and phenotypic plasticity in colon cancer metastasis formation and the contribution of EMT to these processes. The alleged role of hybrid E/M in collective and/or single-cell migration during local dissemination at the primary site and more systemic spreading will be highlighted.

2. The Adenoma-Carcinoma Sequence in Colon Cancer: The β-Catenin Paradox

Colon cancer arises and progresses through a well-defined series of histologic stages along which normal colonic epithelial cells transform in stepwise fashion into precursor lesions which eventually evolve to increasingly more invasive and malignant stages. This sequence, often referred to as 'the adenoma-carcinoma sequence', features a gradual accumulation of genetic alterations in specific tumor suppressors and oncogenes generally regarded as the main underlying and driving forces in the progression of colonic adenomas towards malignancy [21].

The initiating and rate-limiting event in the vast majority of sporadic colon cancer cases is represented by the constitutive activation of canonical Wnt signaling through loss of function mutations at the *APC* (adenomatous polyposis coli) tumor suppressor gene. Alternatively, gain of function or 'activating' mutations in Wnt agonists such as the β-catenin (*CTNNB1*) oncogene have functionally equivalent consequences, i.e., the ligand-independent and constitutive signaling activation of the pathway [2]. The reason for the pivotal role of the Wnt/β-catenin signal transduction pathway in colon cancer onset mainly resides in its functional role in the intestinal crypt of Lieberkühn where it regulates the homeostatic equilibrium between stemness, proliferation, and differentiation [22]. In the bottom third of the crypt, where stem cells reside, Wnt signaling is particularly active due to signals from the surrounding stromal environment. Moving along the crypt-villus axis however, Wnt is progressively less active in a decreasing gradient inversely proportional to the grade of differentiation of the epithelial lining [23]. Here, in the absence of canonical Wnt ligands such as Wnt3a, intracellular β-catenin levels are controlled by the formation of a multiprotein "destruction complex" encompassing protein phosphatase 2A (PP2a), glycogen synthase kinase 3 (GSK3β) and casein kinase 1α (CK1α), and the scaffold proteins adenomatous polyposis coli (APC), and Axin1/2. This complex binds and phosphorylates β-catenin at specific serine and threonine residues, thereby targeting it for ubiquitination and proteolytic degradation by the proteasome [23] (Figure 1a). In the presence of Wnt ligands instead, i.e., in the stem cell compartment, co-activation of the Frizzled and LRP5/6 (low-density lipoprotein receptor-related proteins) receptors prevents the formation of the destruction complex thus resulting in the stabilization and consequent

Chapter 2

translocation of β-catenin from the cytoplasm to the nucleus. Here, β-catenin interacts with members of the TCF/LEF family of transcription factors and modulates the expression of a broad spectrum of Wnt downstream target genes with cellular functions ranging from stemness to proliferation [23] (Figure 1a). Consequently, loss- and gain-of-function genetic alterations in *APC* and β-catenin respectively, result in the constitutive signaling of β-catenin to the nucleus [2].

This genetic model predicts that the vast majority of colon cancers, initiated by the constitutive activation of Wnt signaling, should feature nuclear β-catenin localization throughout the entire tumor mass. However, extensive immunohistochemical analysis of sporadic colon cancers has contradicted this prediction. In fact, only a minority of colon cancer cells, non-randomly distributed along the invasive front of the primary mass and of quasi-mesenchymal morphology, show nuclear β-catenin accumulation. In contrast, the majority of more differentiated (epithelial-like) tumor cells localized inside the tumor mass are characterized by an apparently normal (membrane-bound) subcellular distribution of β-catenin together with increased cytoplasmic staining [25] (Figure 1b). This "β-catenin paradox" is generally explained by the fact that the *APC* and β-catenin mutations are necessary for the constitutive activation of the pathway though insufficient for nuclear β-catenin accumulation and full-blown Wnt signaling [24] (Figure 1b). The latter is only achieved in colon cancer cells located at the invasive front where they are exposed to stromal cues capable of further promoting the nuclear translocation of β-catenin from the cytoplasm [26].

Of note, the same heterogeneous β-catenin distribution, with nuclear staining in less differentiated cells located in closer proximity to the microenvironment and membranous staining in more differentiated cells in the center of the lesion, has also been observed in colon cancer metastases [27]. The reacquisition of epithelial features at the metastatic sites is required for cancer cell proliferation, as mesenchymal-like cells are generally hindered in their proliferative activity and are therefore not able to underlie the expansion of the metastasis.

Hence, different levels of Wnt signaling activity between the tumor center and the invasive front are likely to account for the 'spatial' intra-tumor heterogeneity and to underlie distinct Wnt downstream cellular effectors such as proliferation and EMT leading to tumor growth and invasion, respectively [28]. These observations have led to the hypothesis according to which, apart from its role in colon cancer initiation, Wnt signaling and the consequent downstream EMT activation, also underlies the onset of migrating cancer stem cells (mCSC) at the invasive front of the primary lesion which locally invade the tumor microenvironment and eventually form distant metastases [29].

This paracrine—and presumably epigenetic—control of local invasion and metastasis also offers an explanation to the so-called "progression puzzle" [30], i.e., the lack of main genetic and expression differences between matched primary tumors and metastases as reported in colon cancer and other tumor types [31–33]. This suggests that although the adenoma-carcinoma progression at the primary site is clearly driven by the sequential accumulation of genetic mutations at key genes, the multistage route from dissemination into the tumor microenvironment to metastasis formation is underlined by phenotypic plasticity, i.e., the capacity of circulating tumor cells (CTCs) to undergo transient phenotypic changes to adapt to the ever-changing cellular contexts en route to distant organ sites.

As previously and eloquently proposed by Thomas Brabletz and collaborators, EMT and its reverse program MET play pivotal roles in regulating phenotypic plasticity of CTCs [29].

In the next section, we will discuss the current understanding of the role of EMT in local invasion and metastasis.
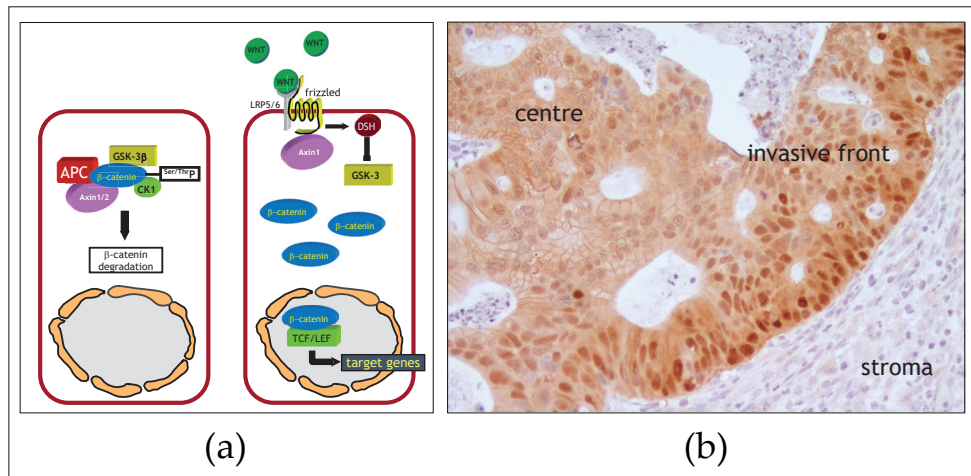
Figure 1. The Wnt/β-catenin signal transduction pathway and the β-catenin paradox in colon cancer. (**a**) Illustration of the canonical Wnt signaling in homeostasis. Left panel: In the absence of Wnt ligands, intracellular β-catenin levels are controlled by a destruction complex encompassing protein phosphatase 2A (PP2a), glycogen synthase kinase 3 (GSK3β) and casein kinase 1α (CK1α), adenomatous polyposis coli (APC), and Axin1/2. This complex binds and phosphorylates β-catenin at serine and threonine residues, thereby targeting it for ubiquitination and proteolytic degradation by the proteasome. Right panel: In presence of Wnt, co-activation of the Frizzled and LRP5/6 (low-density lipoprotein receptor-related proteins) receptors prevents the formation of the destruction complex leading to the stabilization and consequent translocation of β-catenin from the cytoplasm to the nucleus. Here, β-catenin interacts with members of the TCF/LEF family of transcription factors and modulates the expression of a broad spectrum of Wnt downstream target genes. Adapted from [24]. (**b**) The β-catenin paradox in colon cancer. β-catenin IHC analysis of the invasive front of a colon carcinoma show marked nuclear β-catenin accumulation in the proximity of the stromal microenvironment. In contrast, the majority of tumor cells localized inside the tumor mass are characterized by membrane-bound and cytoplasmic β-catenin staining. Scale bar: 50 μm.

3. Epithelial to Mesenchymal Transition in Local Invasion and Metastasis

As pointed out in the previous section, tumor cells within primary and metastatic tumor masses, as well as CTCs, display substantial phenotypic heterogeneity representing various intermediate stages of the EMT program [34,35]. EMT is a developmental program exploited by carcinoma cells to switch from their epithelial state, featuring cell–cell contacts and apical–basal polarity, to more motile and invasive quasi-mesenchymal phenotypes with spindle-like morphology and front-back-end polarity. During cancer invasion, EMT provides cells with the ability to produce, interact with, and digest the surrounding extracellular matrix (ECM), detach from the primary tumor, and invade into

the surrounding tissue [14]. In addition to promoting cellular migration and invasion, the transient phenotypic changes associated with formation of the mesenchymal state during EMT have been associated with the acquisition of stem-like properties, resistance to therapy, and immune suppression [36–39]. The epigenetic, and as such reversible nature of EMT is crucial as the reverse mesenchymal-to-epithelial (MET) process allows migrating cancer (stem-like) cells to regain proliferative and epithelial characteristics to colonize distant organ sites [14]. The initiation and execution of EMT are orchestrated by a set of transcription factors (i.e., *ZEB1/2*, *SNAIL1/SLUG*, and *TWIST1/2*) and miRNAs (e.g., the miR200 family) [40]. Hallmarks of EMT include the silenced expression of integral members of epithelial cell adhesion structures such as adherens- and tight-junctions, and desmosomes, and/or proteins involved in cytoskeleton (re)organization and in cell-matrix adhesion. Next, EMT-TFs can also activate the expression of mesenchymal cell markers resulting in changes in cell morphology, enhanced migratory properties, and ECM remodeling. EMT is induced by cytokines and growth factors secreted from the tumor microenvironment in response to metabolic changes, hypoxia, innate and adaptive immune responses, and treatment by cytotoxic drugs [40]. In addition, the mechanical composition and properties of the ECM also play an important role in EMT regulation. Both shear stress of cancer cells and increasing matrix stiffness in the microenvironment activate EMT, tumor invasion and metastasis [41–43]. In turn, as noted before, EMT also stimulates the composition and mechanics of the ECM, thereby forming a tightly controlled feedback loop that is often dysregulated in cancer.

As mentioned above, colon carcinomas display nuclear β-catenin accumulation at the invasive front simultaneously with the acquisition of mesenchymal-like morphologic features [24]. In this respect, it has been shown that EMT can be activated downstream of canonical Wnt/β-catenin signaling as GSK3β kinase activity inhibition stabilizes SLUG, thereby initiating EMT [44]. Alternatively, active Wnt signaling also inhibits SNAIL1 phosphorylation, leading to increased protein levels of this transcriptional repressor of E-cadherin, EMT initiation, and local invasion [45]. In colon cancer, overexpression of the Wnt ligand Wnt3a is associated with EMT and cancer progression. Accordingly, Wnt3a overexpression in both in vitro and in vivo models was shown to induce *SNAIL* expression thus promoting EMT, an effect that is abrogated by the Wnt antagonist Dickkopf1 (Dkk1) [28].

More recently, the intestinal microbiome has also been shown to contribute to EMT. A variety of enterotoxins secreted by microbes, including *Bacteriodes fragilis*, *Fusobacterium nucleatum,* and *Enterococcus faecalis* have been demonstrated to alter normal cell–cell adhesion by interfering with E-cadherin function [46–48]. *F. nucleatum* adheres through FadA (*Fusobacterium adhesion A*), an adhesion protein, to E-cadherin in colon cancer cells. The FadA/E-cadherin interaction leads to activation of β-catenin signaling and of oncogenic and inflammatory responses [48]. Interestingly, *Fusobacterium* and its associated microbiome (including *Bacteroides*, *Selenomonas*, and *Prevotella*) are sustained in distal metastases and mouse xenografts of primary colorectal tumors. Treating tumor-bearing mice with the antibiotic metronidazole reduced the amount *Fusobacterium* and abrogated cancer cell proliferation and growth [49].

3.1. Role of EMT in Metastasis under Debate

EMT is often defined by the respective down- and up-regulation of epithelial (e.g., E-cadherin, catenins, and cytokeratins) and mesenchymal markers (e.g., vimentin, fibronectin, and N-cadherin) by the above-mentioned *ZEB1/2*, *SNAIL1/SLUG*, and *TWIST1/2* transcription factors (EMT-TFs). However, no single transcription factor (TF) or downstream target can universally define EMT throughout different cancer types and cellular contexts. Distinct EMT-TFs are likely to act in a tumor- and dosage-specific manner and as such differentially repress or enhance the transcription of specific downstream target genes. From this perspective, the recent debate on whether EMT is an essential requirement for metastasis to occur [14,50] reflects the complexity of the network of transcription factors and their downstream targets in the activation of the EMT program. Two provocative studies, in particular, have raised questions on the relative importance of the role played by EMT along the multistep sequence of events leading to metastasis. Fischer et al. (2015) employed in vivo mesenchymal GFP reporters to study EMT onset in the MMTV-PyMT mammary cancer model. Notwithstanding the observed mesenchymal expression within the primary lesions, albeit in low proportion, and its enrichment in CTCs, GFP-positive tumor cells did not contribute to distant metastases [18]. Moreover, *Zeb1/2* inhibition by miR-200 overexpression did not reduce lung metastasis incidence. In a second study by Zheng et al. (2015) it was shown, by taking advantage of a pancreatic ductal carcinoma mouse model, that genetic ablation of *Snail1* or *Twist1* did not affect dissemination and lung metastasis development [19]. The latter is in contrast with a later study by Krebs et al. (2017), showing that *Zeb1* downregulation in the same pancreatic cancer models negatively affects the formation of precursor lesions, tumor grading, invasion, and metastasis [51]. Additionally, other studies using different cancer mouse models point to a key role of *Snail1*- and *Twist1*-driven EMT in metastatic colonization [52–54].

Although compelling, the Fischer et al. (2015) and Zheng et al. (2015) studies are mainly based on the analysis of individual transcription factors and downstream targets in specific tumor models [39,40] and cannot as such be used to discard EMT's role in metastasis against an overwhelming body of experimental evidence from the scientific literature. Several TFs are known to cooperate in eliciting EMT and in controlling the extension of the execution of the trans-differentiation program. Also, EMT-TFs are known to act in a cooperative and context-dependent fashion, and loss of individual factors in specific organ sites may well not suffice to initiate EMT and facilitate metastasis formation. The same is true for the employed mesenchymal markers the expression of which cannot be employed as universal readouts of EMT activation [14,50].

3.2. Hybrid E/M Phenotypes and Partial EMT: Many Shades of Gray

As mentioned above, the transient and reversible nature of EMT represents an essential feature for a metastatic lesion to develop [52,54,55]. Recent experimental evidence indicates that EMT, rather than acting as a binary switch where cells transit between fully epithelial and mesenchymal states, generates a broad spectrum of intermediate E/M stages where cells co-express both types of markers [14] (Figure 2). These partial EMT states are metastable and as such confer to the cancer cell enhanced phenotypic plasticity, an essential hallmark of the migrating/metastatic cancer (stem) cell [14].
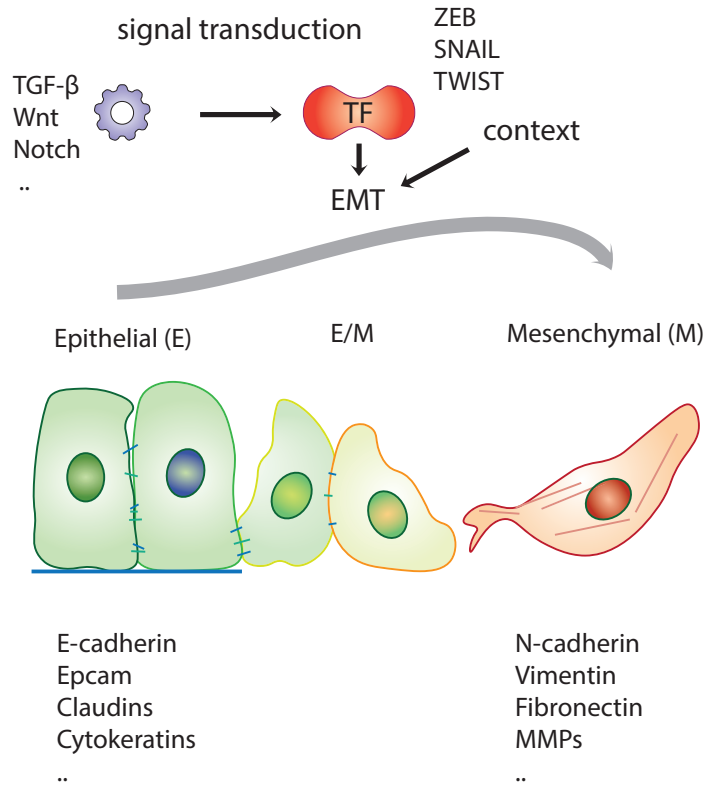
Figure 2. Epithelial to mesenchymal transition (EMT). Schematic overview of epithelial (E) cells transitioning to mesenchymal (M) phenotypes through an intermediate E/M state, and vice versa. EMT can be induced by various stimuli and is dependent on the environmental context.

Two recent studies, in particular, have highlighted the relevance of partial EMT in metastasis. In a mouse model of pancreatic ductal adenocarcinoma (PDAC), Aiello et al. (2018) sorted primary tumor cells according to their membranous expression of E-cadherin (*Cdh1*). Additional RNAseq and protein analysis of *Cdh1*-negative cancer cells revealed the presence of two distinct groups of tumors: while the first resulted from the transcriptional downregulation of E-cadherin (and of other epithelial markers), the second and major group showed E-cadherin expression both at the mRNA and protein levels. However, rather than being presented at the membrane, E-cadherin was internalized in recycling endosomes [34]. These two distinct E-cadherin negative and EMT-competent subpopulations of tumor cells were also earmarked by different invasive and metastatic behavior. Whereas cancer cells featuring a complete EMT (i.e., E-cadherin downregulated at the transcriptional level) invaded the tumor microenvironment mostly as single cells, cells with internalized E-cadherin in a partial EMT state (E/M) migrate collectively as multicellular clusters which are also found in the blood of the pancreatic cancer mouse model [34]. Of note, it has also been shown that the different degrees of epithelial-mesenchymal plasticity affect the tumor cells' metastatic organotropism, i.e., their capacity to metastasize a spectrum of different organ sites [56].

In a second study, Pastushenko et al. (2018) employed a mouse model of squamous cell carcinoma (SCC) and, by taking advantage of the different expression levels of the CD106, CD61, and CD51 cell-surface markers, identified six distinct EpCAM-negative tumor cell subpopulations, each characterized by a different degree of EMT. The different SCC subpopulations, encompassing both fully mesenchymal (complete EMT) and hybrid E/M subtypes (partial EMT), were characterized by distinct chromatin landscapes and gene expression profiles. Similar EMT-heterogeneity was also found in mouse models for metaplastic and luminal breast cancer [35]. Although the tumor-propagating capacity of hybrid E/M EpCAM-negative SCC cells was found to be comparable with that of their fully mesenchymal equivalents, those with a partial EMT phenotype showed increased CTC multiplicities and metastasis formation at distant organs [35]. Overall, partial EMT seems to confer increased phenotypic plasticity to the cancer cells especially when it comes to regaining epithelial characteristic (by MET), an essential requirement for metastasis formation at specific organ sites [14]. Of note, HNSCC (head and neck squamous cell carcinoma) cells with partial EMT are preferentially localized at the invasive front of the primary tumors in close proximity to CAFs (cancer-associated fibroblasts) [57], reminiscent of the "β-catenin paradox" in colon cancer [24].

The elucidation of the molecular mechanisms underlying partial EMT is still in its early days. Nonetheless, the different intermediate E/M phenotypes are likely to be driven by specific epigenetic and transcriptional modifications. Kröger et al. (2019) isolated subpopulation tumor cells stably residing in a hybrid E/M state from both in vitro and in vivo models using a human immortalized and transformed mammary epithelial cell line. These E/M tumor cells were characterized by upregulation of the SNAIL EMT-TF and of canonical Wnt-signaling. Ectopic *ZEB1* expression resulted in a fully mesenchymal transformation of the E/M cells accompanied by a reduction of their tumorigenic potential and a switch from canonical to non-canonical Wnt signaling [58].

Apart from SNAIL, other transcription factors including NUMB, GRLH2, and OVOL have been proposed to act as '*phenotypic stability factors*' which promote, control, and stabilize the hybrid E/M state, possibly by interfering with the core EMT decision-making circuit [59,60].

As mentioned above, the cancer cell's ability to revert back from EMT-induced phenotypes is critical for metastasis formation in distant organs and full mesenchymal transformation may result in the irreversible loss of MET capacity [58,61,62]. For example, activation of TGF-β signaling triggers EMT in carcinoma cells in a dosage-dependent fashion. Upon short-term treatment, the induced EMT is reversible. However, prolonged exposure of cancer cells to TGF-β result in more stable and irreversible transitions even upon ligand withdrawal [62].

Next to the specific expression signatures of EMT-related transcription factors and their downstream signaling pathways driving hybrid E/M and fully mesenchymal states in cancer cells, the existence of other alternative EMT-programs with distinct outcomes has been proposed [34,56].

Overall, it is still unclear whether hybrid E/M cells represent a metastable population or are just captured in a time frame transitioning from the epithelial to mesenchymal phenotype. Also, it remains uncertain which context-dependent environmental factors and downstream signaling paths are responsible for driving heterogeneous phenotypic fates during tumor progression. Nonetheless, as mentioned earlier, ample experimental

evidence clearly indicates that the hybrid E/M cells state is involved in the collective invasion, migration, and dissemination of tumor cells en route to form distant metastases. In the next sections, we will portray the role of EMT in collective cell invasion into the local tumor stroma and dissemination as CTC-clusters, when compared with single migrating cancer cells that complete the full EMT-program.

4. Single versus Collective Cell Migration

The initial detachment of the cancer cell from the primary mass and its invasion in the surrounding stromal microenvironment represent critical and rate-limiting steps in the metastatic cascade responsible for 90% of deaths in patients with malignancies [12,63]. In order to invade, cancer cells employ distinct invasion modalities: single (amoeboid or mesenchymal invasion) and collective cell migration. Of note, cancer cells can switch between these invasion modes, an important feature when it comes to the development of anti-invasive and anti-metastatic therapies [64].

4.1. Single Cell Migration

Cancer cells lacking interactions with neighboring tumor cells can detach from the primary mass and migrate individually into the microenvironment. There are two different mechanisms of single-cell invasion, namely amoeboid and mesenchymal migration [64]. The involvement of one of these two modes is dependent on the rigidity of the cell-matrix adhesions, the tumor cell's capacity to remodel the extracellular matrix, and the contractility of the cytoskeleton [65]. In amoeboid invasion, an EMT-independent mechanism, cancer cells have a characteristic rounded cell shape. Here, migration relies on the contractility of cortical actomyosin, promoted by the Rho/ROCK signaling pathway [66]. The proteolysis-independent actomyosin contractility results in membrane blebbing, i.e., the formation of membrane protrusions that enable cancer cells to squeeze through gaps within the ECM [66,67]. In contrast, during mesenchymal single-cell invasion, cells adopt an elongated spindle-like phenotype with front-back polarity as a result of EMT [68,69]. Additionally, cells that engage the mesenchymal mode are dependent on the activity of enzymes such as matrix metalloproteinases (MMPs) and serine protease seprase that degrade the ECM and, as tumor cells invade, progressively create channels which can be used for the cells lagging behind the leading ones [70]. Interestingly, inhibition of ECM remodeling leads to amoeboid migration with cancer cells squeezing through pre-existing pores by actomyosin contractility [67]. Of note, MMPs are generally regarded as integral members of the EMT program. In hepatocellular carcinoma (HCC), upregulation of the EMT-TF Snail not only repressed E-cadherin transcription but also increased expression of MMP-1, MMP-2, MMP-7, and MT1-MMP leading to accelerated invasion [71,72]. Alternatively, several ECM components and even MMPs can, in some cases, act as EMT initiators [73,74]. Induction of MMP-3, also known as stromelysin-1 (SL-1), in the mammary epithelium resulted in cleavage of E-cadherin leading to removal of E-cadherin and catenins from adherens junctions, downregulation of cytokeratins, upregulation of vimentin and of endogenous MMPs [73].

Although single-cell invasion is linked to tumor cells undergoing the full EMT-program leading to suppression of E-cadherin and induction of vimentin [68,69], there is evidence that partial EMT, i.e., the retention of epithelial features, can also feature

single-cell migration [75,76]. Additionally, cancer cells can switch between amoeboid and mesenchymal states spontaneously or through changes in ECM composition [67].

4.2. Collective Cell Migration and the Role of EMT

In collective cell migration, cancer cells retain intact cell–cell adhesions while invading the tumor microenvironment, the vasculature, and distant organ sites [77]. A variety of migration modalities feature collective cell migration, ranging from narrow linear connected cell strands to broad sheets or compact cluster/budding of cells [77]. Unlike single-cell migration resulting from fully mesenchymal cells, the role of EMT in collective migration is subtler. Recently, using a *Drosophila melanogaster* model of colon cancer, it was shown that the Snail homolog *Sna* can activate partial EMT in tumor cells leading to their collective invasion through the basement membrane and muscle fibers [78]. Additional evidence pointing at the correlation between hybrid E/M and collective cell migration lies in the onset of 'leader' cells at the invasive margin that are selected to guide other 'following' cancer cells [79]. These leader cells show a bi-phenotypic state with mesenchymal features as altered polarity and development of protrusions at their front. Yet, they also maintain attachments to their follower cells at their rear end. The follower cells, on the other hand, retain apical–basal polarity and migrate taking advantage of the pulling force generated by leader cells [80]. Knockdown of the epithelial marker cytokeratin 14 in leader cells is sufficient to block collective migration suggesting that the hybrid E/M state is mandatory for establishment of the leader cells [79]. The onset, activity, and maintenance of leader cells are coordinated by environmental stimuli, i.e., the local increase of compression [81], soluble factors, and chemokines [82], but is also controlled within the collective tumor group by autocrine or juxtacrine fashion. Of note, also in this case several MMPs are expressed at the leading edge to facilitate ECM degradation and to create a migration path for the cell clusters [83].

Notably, non-cancer cells can also contribute to collective cell migration. The movement of cancer cells can be conducted by migratory stromal cells such as fibroblasts [84,85]) or macrophages [86,87]. Labernadie et al. (2017) demonstrated that cancer-associated fibroblasts (CAFs) exert a physical force on cancer cells that leads to their collective migration. This intercellular force transduction is achieved by the formation of heterophilic adhesion complexes between N-cadherin on the CAF membrane and E-cadherin on the cancer cell membrane [85]. Moreover, CAFs are also a source of ECM-degrading proteases such as MMPs thereby creating micro tracks used by cancer cells to migrate through [84]. In addition to degrading the ECM, CAFs also secrete growth factors and chemokines that generate chemotactic gradients to direct cell migration [88]. Last, cancer cells can ingest exosomes secreted by CAFs thereby activating intracellular pathways known to trigger EMT [89]. In colon cancer, CAFs release exosomes containing miR-92a-3p and promote invasion and chemotherapy resistance. miR-92a-3p directly binds to FBXW7 and MOAP1 thereby activating Wnt-induced EMT and mitochondrial apoptosis [89].

Overall, single and collective cell migration share some of the underlying mechanisms (e.g., cell–cell and cell-matrix communication, and the establishment of a migratory polarity). Moreover, during invasion tumor cells can switch between different modes of migration depending on intrinsic (cell adhesion) and extrinsic cues (ECM composition and density). In general terms, a complete EMT is associated with single-cell migration, whereas collective cell migration seems to result from partial EMT. Nonetheless, the

mechanisms underlying the role of EMT in determining the invasion modalities, the intercellular communication among invading cells, and the tumor microenvironmental cues leading to collective migration are yet poorly defined. This is further complicated by the fact that invasion modalities are likely to be cell type-, tissue-, and time-dependent. The plasticity of cancer cells to switch between different invasion modes is a key feature and a putative target for the development of novel therapeutic strategies [90].

5. Circulating Tumor Cells

Circulating tumor cells (CTCs) are defined as those cancer cells disseminated from the primary tumor mass and intravasated into blood vessels which are thought to underlie metastasis at distant organ sites [91]. CTCs have been identified at different multiplicities in many carcinomas including colon, breast, prostate, lung, bladder, and gastric cancer, while they are extremely rare in healthy individuals or in patients with non-malignant disease [91]. However, even in cancer patients, CTCs are extremely rare and, accordingly, their prospective isolation and characterization have proven to be a challenge [91]. Heterogeneity also exists among CTCs, possibly reflecting the above discussed intra-tumor heterogeneity. Likewise, the existence of both single CTCs, as well as CTC clusters comprising multiple (from few to hundreds) cells, has been well established in the scientific literature [92,93]. Of note, CTC clusters are not exclusively composed of epithelial cancer cells but are often intermingled with immune cells, cancer-associated fibroblasts, tumor stroma, and platelets [94–98]. In addition to this heterogeneity, CTCs and CTC clusters have been captured that express both epithelial and mesenchymal features [93,99–101].

5.1. Single CTCs versus CTC Clusters

Single CTCs disseminate into distant organs upon EMT [14]. However, the discovery of CTC clusters has raised questions on the relative role of EMT in local invasion and systemic dissemination from the primary tumor mass. CTC clusters are defined as a group of 2–3 or more tumor cells that travel as a group through the bloodstream [91]. In 1954, Watanabe showed that, by injecting bronchogenic carcinoma cells in the jugular vein of recipient mice, tumor clumps, in contrast to single cells, were able to form metastasis [102]. Accordingly, aggregated colon cancer cells also showed increased metastatic efficiency in the liver when compared with single cells after intra-portal injection in rat [103]. These initial observations, however, did not explain how and where CTC clusters are formed. More recently, it has been demonstrated that CTC clusters do not derive from the intravascular aggregation of single CTCs or from proliferating single CTCs, but rather from clumps of primary tumor cells that collectively detach from the primary mass and enter the vasculature as CTC clusters [104–106]. Moreover, it was also shown that the metastatic capacity of CTC clusters was up to fifty-fold higher when compared with single CTCs [104]. Genome-wide single-cell DNA methylation analysis demonstrated distinct methylomes between CTC clusters and single CTCs in human breast cancer patients. CTC clusters were shown to be hypo-methylated at stemness- and proliferation-associated transcription regulators including OCT4, NANOG, SOX2, and SIN3A, and hyper-methylated at Polycomb target genes [107]. Lastly, the presence of circulating tumor micro emboli in peripheral blood of patients with cancer arising from colon, breast, and lung was predictive of poor survival [104,108,109].

5.2. CTC Cluster Heterogeneity

The heterogeneous composition of CTC clusters encompassing parenchymal cancer cells together with immune cells, cancer-associated fibroblasts, tumor stroma, and platelets, seems to reflect the heterogeneity of the primary tumors they originate from [94–98]. The presence of non-malignant cells within CTC clusters contributes to their improved survival and metastatic capacity. Normal epithelial cells undergo cell anoikis upon the detachment from the extracellular matrix (ECM), which establishes an important defense mechanism to prevent abnormal growth in inappropriate places. However, EMT can circumvent anoikis in individual cells during dissemination and metastasis [110]. The transition of single CTCs to a mesenchymal phenotype results in the expression of adherence-independent survival signals that compensate for the loss of attachment to the ECM [111]. Alternatively, CTC clusters may prevent tumor cell anoikis by retaining epithelial cell–cell interactions and thus contributing to the activation of survival stimuli [104,105]. Next, the non-malignant cell microenvironment can protect CTC cells from immune cells [112,113], shield cells from mechanical stress, and promotes adhesion to the endothelium [114,115]. It also has been shown that platelets can induce EMT in CTCs via TGF-β and NF-κB signaling while enhancing their metastatic potential [97]. Thus, secretion of growth factors and cytokines by the non-cancer cells may represent an additional survival advantage for the CTC clusters in the vasculature. Last, yet another advantage of the CTC clusters when compared to single CTCs is the capacity of remodeling the microenvironment at the metastatic site, thereby facilitating colonization [95].

5.3. EMT in CTC Clusters

Next to the heterogeneity of CTC clusters in terms of cell lineage composition, the degree of EMT activation among the parenchymal cancer cells within CTCs can also vary considerably. CTC clusters display epithelial cell–cell interactions as shown by the retention of expression of several epithelial-specific genes such as K5, K8, K14, E-cadherin, P-cadherin, and plakoglobin in metastatic breast CTC clusters [116]. Accordingly, knockdown of plakoglobin, a member of the catenin protein family and homologous to β-catenin, led to disaggregation of the CTC clusters, thereby compromising metastasis formation [104]. Also, disruption of K14 expression negatively affected the expression of key downstream effectors in metastatic niche remodeling and metastasis survival, leading to compromised efficiency in metastasis formation [105]. However, CTC clusters with predominant hybrid E/M or fully mesenchymal features have been observed in human colon, prostate, lung, and breast cancer patients [93,99–101]. At least one-third of cancer cells from within CTC clusters derived from colon cancer patients were negative for cytokeratin expression [100]. In breast cancer, CTC clusters show shifts in their EMT status according to treatment modalities with predominant mesenchymal expression patterns during cancer progression and/or in refractory disease [93] (Figure 3). This dynamic EMT profile allows for cellular plasticity and adaptation to the diverse cellular contexts encountered by CTCs during dissemination and metastasis formation, and to different treatments regimes. The latter is also of relevance for the use of prognostic epithelial markers of CTCs likely to fail to detect cancer cells that have undergone EMT. Additional mesenchymal CTCs markers are needed for more accurate prognostic studies [117].

As mentioned above, alternative EMT-programs accounts for different CTC phenotypes. Aiello et al. (2018) suggested that single CTCs arise from cancer cells that have completed

a full EMT-program, whereas tumor cells characterized by partial EMT tend to present as clusters resulting from collective migration [34]. However, it has been demonstrated that, next to those mainly composed by CTCs, cell clusters have been isolated from colon cancer patients which consist of endothelial cells without any genetic aberrations found in their matched primary tumor of origin. These cell clusters were positive for both epithelial and mesenchymal markers and are thought to result from the direct release of clusters from the tumor vasculature due to impaired neo-angiogenesis [118].

6. Partial EMT, Collective Cell Migration, and Metastasis: Therapeutic strategies

Metastasis formation involves the successful completion of a sequential series of challenging steps. Phenotypic plasticity refers to the key feature of the metastasizing cancer cell to adapt to the environment where it resides through reversible changes of its cellular identity [13]. This '*Dr. Jekyll and Mr. Hide*' feature of migrating cancer cells is controlled by epigenetic mechanisms which regulate E-to-M and M-to-E transitions (EMT and MET) [14]. However, EMT cannot be regarded as a binary process as it generates hybrid E/M cancer cells encompassing a range of intermediate stages. Partial EMT has been correlated with collective cell migration and with the presence of CTC clusters with enhanced metastatic potential in the peripheral blood of cancer patients [119]. Moreover, the unaffected CTC clusters multiplicity upon chemotherapy is indicative of treatment failure in colorectal cancer [120]. From this perspective, the elucidation of the underlying intrinsic and extrinsic mechanisms is bound to lead to the development of novel therapeutic and even preventive strategies based on the targeting of cell–cell and/or cell-matrix interactions and the disruption of CTC clusters. Gkountela et al. (2019) tested a library of approximately 2500 FDA-approved compounds and identified Na^+/K^+ ATPase inhibitors able to disaggregate derived CTC clusters derived from breast cancer patients into single cells. Mechanistically, Na^+/K^+ ATPase inhibition in tumor cells leads to an increase of intercellular Ca^{2+} concentration and to the consequent inhibition of formation of cell–cell junctions. In an in vivo xenograft model using NSG mice injected with patient-derived breast cancer cells in their fat pad, treatment with the Na^+/K^+ ATPase inhibitor ouabain resulted in a marked reduction of CTC cluster formation together with the increase of single CTC multiplicity. Although the size of the primary tumor was unaffected upon ouabain treatment, the overall number of metastatic lesions, corresponding to the number of CTC clusters, was reduced [107].

An alternative approach towards the development of therapeutic strategies based on CTC clusters may be represented by inhibition of platelet function. Platelets make integral part of CTC clusters where they are thought to protect the cancer cells from shear stress and immune attacks [121]. Acetylsalicylic acid (i.e., aspirin) inhibits platelet function by acetylation of cyclooxygenase (COX) thereby preventing arachidonic acid (and prostaglandin) production and consequently resulting in irreversible inhibition of platelet-dependent thromboxane formation. Based on this, aspirin has been employed as an anticoagulant for the prevention of thrombosis [122]. In experimental cancer models and clinical trials, inhibiting the interaction between cancer cells and platelets have been shown to hamper tumor cell survival, growth and metastasis formation [123,124].
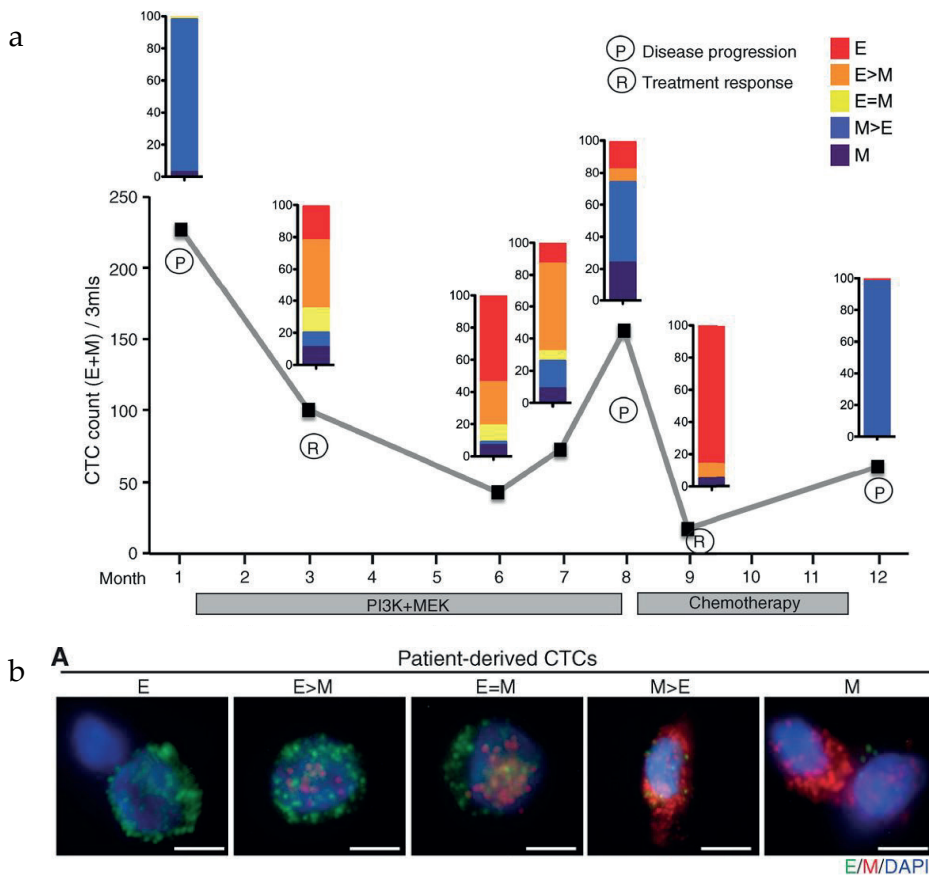
Figure 3. EMT features in single circulating tumor cells (CTCs) and CTC clusters from a metastatic breast cancer patient. (**a**) Longitudinal monitoring of EMT features in CTCs. The *Y*-axis indicates the number of CTCs per 3 mL of blood. The patient was monitored over time (*X*-axis) during treatment with inhibitors targeting the PI3K and MEK pathways (months 1–8), followed by chemotherapy with Adriamycin (8–12). The color-coded quantification bars indicate the EMT status of the CTCs based on RNA-ISH (in situ hybridization) analysis at each indicated time point. P = disease progression; R = tumor response. (**b**) RNA-ISH analysis of EMT markers in CTCs derived from patients with metastatic breast cancer. Green dots represent epithelial (E) and red marks mesenchymal (M) markers. Scale bar: 5 μm. Adapted from [93].

Notwithstanding the above promising and innovative therapeutic strategies based on CTC clusters, their allegedly high degree of plasticity—as a mechanism to escape targeted treatment—is also likely to result in therapy resistance. Nonetheless, future research towards the identification of novel therapeutic targets to lower the risk of CTC cluster formation is expected to improve the efficacy of cancer treatment in the long run.

Chapter 2

7. Final Remarks and Conclusions

EMT contributes to a considerable degree of cellular heterogeneity in both primary tumors and metastatic lesions as it affects a broad spectrum of cellular functions beyond the transitions between epithelial and mesenchymal states associated with enhanced invasive and metastatic abilities. Changes in stem cell behavior, escape from apoptosis and senescence, ECM and tumor-microenvironment remodeling, and resistance to cytotoxic treatments are only a few among the broad spectrum of downstream EMT effectors which contribute to intra-tumor cell heterogeneity with profound implications for cancer therapeutics, especially in the decade of personalized treatments [11].

In fact, EMT is thought to play key roles in each and every step of the metastatic cascade including intra- and extravasation [125], and the colonization of distant organ sites [126,127]. For the sake of brevity, these latter aspects are not discussed in this review. The observed broad spectrum of EMT effectors may well reflect the pleiotropic functional roles of the EMT-TFs such as ZEB1 [128] that go well beyond the E to M (and vice versa) trans-differentiation, and include angiogenesis, remodeling of the tumor microenvironment, immune escape, mechanotransduction, and possibly many more.

The identification and elucidation of the complex network of intrinsic and extrinsic mechanisms driving EMT at "just-right" (E/M) levels to trigger collective migration, generate CTC clusters and successfully metastasize distant organ sites represent the major future research challenge in the translation of our fundamental understanding of metastasis into therapy. From this perspective, single-cell epigenetic and transcriptomic analysis will provide powerful approaches to address this challenge. These high-resolution techniques will be key to elucidate the heterogeneous composition of malignancies including the identification of distinct and rare cell types arising transiently in time and at specific locations within tumors. Moreover, single-cell profiles will help to investigate the variability among individuals, disease states, microenvironments, and treatment history.

Overall, the realization of the importance of epigenetics and the elucidation of the mechanisms underlying transient changes in the cellular identity of individual circulating and metastasizing tumor cells will lay the basis for the development of novel treatment modalities. These will complement the current 'personalized cancer medicine' mainly directed at somatic gene mutations arisen at the primary site and unlikely to be rate-limiting in the clinical management of a more advanced malignant disease.

Conflicts of Interest: The authors declare no conflict of interest.

References

1. Ferlay, J., E.M., Lam F, Colombet M, Mery L, Piñeros M, Znaor A, Soerjomataram, I., Bray, F. Global Cancer Observatory: Cancer Tomorrow. Availabe online: https://gco.iarc.fr/tomorrow (accessed on 02 May).

2. Fodde, R.; Smits, R.; Clevers, H. APC, signal transduction and genetic instability in colorectal cancer. *Nat. Rev. Cancer* **2001**, *1*, 55–67, doi:10.1038/35094067.

3. Hanahan, D.; Weinberg, R.A. Hallmarks of cancer: The next generation. *Cell* **2011**, *144*, 646–674, doi:10.1016/j.cell.2011.02.013.

4. Dalerba, P.; Kalisky, T.; Sahoo, D.; Rajendran, P.S.; Rothenberg, M.E.; Leyrat, A.A.; Sim, S.; Okamoto, J.; Johnston, D.M.; Qian, D., et al. Single-cell dissection of transcriptional heterogeneity in human colon tumors. *Nat. Biotechnol.* **2011**, *29*, 1120–1127, doi:10.1038/nbt.2038.

5. Li, H.; Courtois, E.T.; Sengupta, D.; Tan, Y.; Chen, K.H.; Goh, J.J.L.; Kong, S.L.; Chua, C.; Hon, L.K.; Tan, W.S., et al. Reference component analysis of single-cell transcriptomes elucidates cellular heterogeneity in human colorectal tumors. *Nat. Genet.* **2017**, *49*, 708–718, doi:10.1038/ng.3818.

6. Roerink, S.F.; Sasaki, N.; Lee-Six, H.; Young, M.D.; Alexandrov, L.B.; Behjati, S.; Mitchell, T.J.; Grossmann, S.; Lightfoot, H.; Egan, D.A., et al. Intra-tumour diversification in colorectal cancer at the single-cell level. *Nature* **2018**, *556*, 457–462, doi:10.1038/s41586-018-0024-3.

7. Fiori, M.E.; Di Franco, S.; Villanova, L.; Bianca, P.; Stassi, G.; De Maria, R. Cancer-associated fibroblasts as abettors of tumor progression at the crossroads of EMT and therapy resistance. *Mol. Cancer* **2019**, *18*, 70, doi:10.1186/s12943-019-0994-2.

8. Lamprecht, S.; Schmidt, E.M.; Blaj, C.; Hermeking, H.; Jung, A.; Kirchner, T.; Horst, D. Multicolor lineage tracing reveals clonal architecture and dynamics in colon cancer. *Nat. Commun.* **2017**, *8*, 1406, doi:10.1038/s41467-017-00976-9.

9. van der Heijden, M.; Miedema, D.M.; Waclaw, B.; Veenstra, V.L.; Lecca, M.C.; Nijman, L.E.; van Dijk, E.; van Neerven, S.M.; Lodestijn, S.C.; Lenos, K.J., et al. Spatiotemporal regulation of clonogenicity in colorectal cancer xenografts. *Proc. Natl. Acad. Sci.* **2019**, *116*, 6140–6145, doi:10.1073/pnas.1813417116.

10. Saito, T.; Niida, A.; Uchi, R.; Hirata, H.; Komatsu, H.; Sakimura, S.; Hayashi, S.; Nambara, S.; Kuroda, Y.; Ito, S., et al. A temporal shift of the evolutionary principle shaping intratumor heterogeneity in colorectal cancer. *Nat. Commun.* **2018**, *9*, 2884, doi:10.1038/s41467-018-05226-0.

11. Fisher, R.; Pusztai, L.; Swanton, C. Cancer heterogeneity: Implications for targeted therapeutics. *Br. J. Cancer* **2013**, *108*, 479–485, doi:10.1038/bjc.2012.581.

12. Fidler, I.J. The pathogenesis of cancer metastasis: The 'seed and soil' hypothesis revisited. *Nat. Rev. Cancer* **2003**, *3*, 453–458, doi:10.1038/nrc1098.

13. Varga, J.; Greten, F.R. Cell plasticity in epithelial homeostasis and tumorigenesis. *Nat. Cell Biol.* **2017**, *19*, 1133–1141, doi:10.1038/ncb3611.

14. Nieto, M.A.; Huang, R.Y.; Jackson, R.A.; Thiery, J.P. Emt: 2016. *Cell* **2016**, *166*, 21–45, doi:10.1016/j.cell.2016.06.028.

15. Tam, W.L.; Weinberg, R.A. The epigenetics of epithelial-mesenchymal plasticity in cancer. *Nat. Med.* **2013**, *19*, 1438–1449, doi:10.1038/nm.3336.

16. Mohd-Sarip, A.; Teeuwssen, M.; Bot, A.G.; De Herdt, M.J.; Willems, S.M.; Baatenburg de Jong, R.J.; Looijenga, L.H.J.; Zatreanu, D.; Bezstarosti, K.; van Riet, J., et al. DOC1-Dependent Recruitment of NURD Reveals Antagonism with SWI/SNF during Epithelial-Mesenchymal Transition in Oral Cancer Cells. *Cell Rep.* **2017**, *20*, 61–75, doi:10.1016/j.celrep.2017.06.020.

17. Zentner, G.E.; Henikoff, S. Regulation of nucleosome dynamics by histone modifications. *Nat. Struct Mol. Biol.* **2013**, *20*, 259–266, doi:10.1038/nsmb.2470.

18. Fischer, K.R.; Durrans, A.; Lee, S.; Sheng, J.; Li, F.; Wong, S.T.; Choi, H.; El Rayes, T.; Ryu, S.; Troeger, J., et al. Epithelial-to-mesenchymal transition is not required for lung metastasis but contributes to chemoresistance. *Nature* **2015**, *527*, 472–476, doi:10.1038/nature15748.

19. Zheng, X.; Carstens, J.L.; Kim, J.; Scheible, M.; Kaye, J.; Sugimoto, H.; Wu, C.C.; LeBleu, V.S.; Kalluri, R. Epithelial-to-mesenchymal transition is dispensable for metastasis but induces chemoresistance in pancreatic cancer. *Nature* **2015**, *527*, 525–530, doi:10.1038/nature16064.

20. Pastushenko, I.; Blanpain, C. EMT Transition States during Tumor Progression and Metastasis. *Trends Cell Biol.* **2019**, *29*, 212–226, doi:10.1016/j.tcb.2018.12.001.

21. Fearon, E.R.; Vogelstein, B. A genetic model for colorectal tumorigenesis. *Cell* **1990**, *61*, 759–767, doi:10.1016/0092-8674(90)90186-i.

22. Reya, T.; Clevers, H. Wnt signalling in stem cells and cancer. *Nature* **2005**, *434*, 843–850, doi:10.1038/nature03319.

23. Gregorieff, A.; Clevers, H. Wnt signaling in the intestinal epithelium: From endoderm to cancer. *Genes Dev.* **2005**, *19*, 877–890, doi:10.1101/gad.1295405.

24. Fodde, R.; Brabletz, T. Wnt/beta-catenin signaling in cancer stemness and malignant behavior. *Curr. Opin. Cell Biol.* **2007**, *19*, 150–158.

25. Brabletz, T.; Jung, A.; Hermann, K.; Gunther, K.; Hohenberger, W.; Kirchner, T. Nuclear overexpression of the oncoprotein beta-catenin in colorectal cancer is localized predominantly at the invasion front. *Pathol. Res. Pract.* **1998**, *194*, 701–704.

26. Le, N.H.; Franken, P.; Fodde, R. Tumour-stroma interactions in colorectal cancer: Converging on beta-catenin activation and cancer stemness. *Br. J. Cancer* **2008**, *98*, 1886–1893, doi:10.1038/sj.bjc.6604401.

27. Brabletz, T.; Jung, A.; Reu, S.; Porzner, M.; Hlubek, F.; Kunz-Schughart, L.A.; Knuechel, R.; Kirchner, T. Variable beta-catenin expression in colorectal cancers indicates tumor progression driven by the tumor environment. *Proc. Natl. Acad. Sci.* **2001**, *98*, 10356–10361, doi:10.1073/pnas.171610498.

28. Qi, L.; Sun, B.; Liu, Z.; Cheng, R.; Li, Y.; Zhao, X. Wnt3a expression is associated with epithelial-mesenchymal transition and promotes colon cancer progression. *J. Exp. Clin. Cancer Res.* **2014**, *33*, 107, doi:10.1186/s13046-014-0107-4.

29. Brabletz, T.; Jung, A.; Spaderna, S.; Hlubek, F.; Kirchner, T. Opinion: Migrating cancer stem cells-an integrated concept of malignant tumour progression. *Nat. Rev. Cancer* **2005**, *5*, 744–749, doi:10.1038/nrc1694.

30. Bernards, R.; Weinberg, R.A. A progression puzzle. *Nature* **2002**, *418*, 823, doi:10.1038/418823a.

31. Reiter, J.G.; Makohon-Moore, A.P.; Gerold, J.M.; Heyde, A.; Attiyeh, M.A.; Kohutek, Z.A.; Tokheim, C.J.; Brown, A.; DeBlasio, R.M.; Niyazov, J., et al. Minimal functional driver gene heterogeneity among untreated metastases. *Science* **2018**, *361*, 1033–1037, doi:10.1126/science.aat7171.

32. Goswami, R.S.; Patel, K.P.; Singh, R.R.; Meric-Bernstam, F.; Kopetz, E.S.; Subbiah, V.; Alvarez, R.H.; Davies, M.A.; Jabbar, K.J.; Roy-Chowdhuri, S., et al. Hotspot mutation panel testing reveals clonal evolution in a study of 265 paired primary and metastatic tumors. *Clin. Cancer Res.* **2015**, *21*, 2644–2651, doi:10.1158/1078-0432.CCR-14-2391.

33. Brannon, A.R.; Vakiani, E.; Sylvester, B.E.; Scott, S.N.; McDermott, G.; Shah, R.H.; Kania, K.; Viale, A.; Oschwald, D.M.; Vacic, V., et al. Comparative sequencing analysis reveals high genomic concordance between matched primary and metastatic colorectal cancer lesions. *Genome Biol.* **2014**, *15*, 454, doi:10.1186/s13059-014-0454-7.

34. Aiello, N.M.; Maddipati, R.; Norgard, R.J.; Balli, D.; Li, J.; Yuan, S.; Yamazoe, T.; Black, T.; Sahmoud, A.; Furth, E.E., et al. EMT Subtype Influences Epithelial Plasticity and Mode of Cell Migration. *Dev. Cell* **2018**, *45*, 681–695 e684, doi:10.1016/j.devcel.2018.05.027.

35. Pastushenko, I.; Brisebarre, A.; Sifrim, A.; Fioramonti, M.; Revenco, T.; Boumahdi, S.; Van Keymeulen, A.; Brown, D.; Moers, V.; Lemaire, S., et al. Identification of the tumour transition states occurring during EMT. *Nature* **2018**, *556*, 463–468, doi:10.1038/s41586-018-0040-3.

36. Dongre, A.; Rashidian, M.; Reinhardt, F.; Bagnato, A.; Keckesova, Z.; Ploegh, H.L.; Weinberg, R.A. Epithelial-to-Mesenchymal Transition Contributes to Immunosuppression in Breast Carcinomas. *Cancer Res.* **2017**, *77*, 3982–3989, doi:10.1158/0008-5472.CAN-16-3292.

37. Morel, A.P.; Lievre, M.; Thomas, C.; Hinkal, G.; Ansieau, S.; Puisieux, A. Generation of breast cancer stem cells through epithelial-mesenchymal transition. *PLoS ONE* **2008**, *3*, e2888, doi:10.1371/journal.pone.0002888.

38. Mani, S.A.; Guo, W.; Liao, M.J.; Eaton, E.N.; Ayyanan, A.; Zhou, A.Y.; Brooks, M.; Reinhard, F.; Zhang, C.C.; Shipitsin, M., et al. The epithelial-mesenchymal transition generates cells with properties of stem cells. *Cell* **2008**, *133*, 704–715, doi:10.1016/j.cell.2008.03.027.

39. Smith, B.N.; Bhowmick, N.A. Role of EMT in Metastasis and Therapy Resistance. *J. Clin. Med.* **2016**, *5*, doi:10.3390/jcm5020017.

40. Puisieux, A.; Brabletz, T.; Caramel, J. Oncogenic roles of EMT-inducing transcription factors. *Nat. Cell Biol.* **2014**, *16*, 488–494, doi:10.1038/ncb2976.

41. Lee, H.J.; Diaz, M.F.; Price, K.M.; Ozuna, J.A.; Zhang, S.; Sevick-Muraca, E.M.; Hagan, J.P.; Wenzel, P.L. Fluid shear stress activates YAP1 to promote cancer cell motility. *Nat. Commun.* **2017**, *8*, 14122, doi:10.1038/ncomms14122.

42. Wei, S.C.; Fattet, L.; Tsai, J.H.; Guo, Y.; Pai, V.H.; Majeski, H.E.; Chen, A.C.; Sah, R.L.; Taylor, S.S.; Engler, A.J., et al. Matrix stiffness drives epithelial-mesenchymal transition and tumour metastasis through a TWIST1-G3BP2 mechanotransduction pathway. *Nat. Cell Biol.* **2015**, *17*, 678–688, doi:10.1038/ncb3157.

43. Rice, A.J.; Cortes, E.; Lachowski, D.; Cheung, B.C.H.; Karim, S.A.; Morton, J.P.; Del Rio Hernandez, A. Matrix stiffness induces epithelial-mesenchymal transition and promotes chemoresistance in pancreatic cancer cells. *Oncogenesis* **2017**, *6*, e352, doi:10.1038/oncsis.2017.54.

44. Wu, Z.Q.; Li, X.Y.; Hu, C.Y.; Ford, M.; Kleer, C.G.; Weiss, S.J. Canonical Wnt signaling regulates Slug activity and links epithelial-mesenchymal transition with epigenetic Breast Cancer 1, Early Onset (BRCA1) repression. *Proc. Natl. Acad. Sci.* **2012**, *109*, 16654–16659.

45. Yook, J.I.; Li, X.Y.; Ota, I.; Fearon, E.R.; Weiss, S.J. Wnt-dependent regulation of the E-cadherin repressor snail. *J. Biol. Chem.* **2005**, *280*, 11740–11748.

46. Yang, Y.; Wang, X.; Huycke, T.; Moore, D.R.; Lightfoot, S.A.; Huycke, M.M. Colon Macrophages Polarized by Commensal Bacteria Cause Colitis and Cancer through the Bystander Effect. *Transl. Oncol.* **2013**, *6*, 596–606, doi:10.1593/tlo.13412.

47. Wu, S.; Lim, K.C.; Huang, J.; Saidi, R.F.; Sears, C.L. Bacteroides fragilis enterotoxin cleaves the zonula adherens protein, E-cadherin. *Proc. Natl. Acad. Sci.* **1998**, *95*, 14979–14984, doi:10.1073/pnas.95.25.14979.

48. Rubinstein, M.R.; Wang, X.; Liu, W.; Hao, Y.; Cai, G.; Han, Y.W. Fusobacterium nucleatum promotes colorectal carcinogenesis by modulating E-cadherin/beta-catenin signaling via its FadA adhesin. *Cell Host Microbe* **2013**, *14*, 195–206, doi:10.1016/j.chom.2013.07.012.

49. Bullman, S.; Pedamallu, C.S.; Sicinska, E.; Clancy, T.E.; Zhang, X.; Cai, D.; Neuberg, D.; Huang, K.; Guevara, F.; Nelson, T., et al. Analysis of Fusobacterium persistence and antibiotic response in colorectal cancer. *Science* **2017**, *358*, 1443–1448, doi:10.1126/science.aal5240.

50.   Maheswaran, S.; Haber, D.A. Cell fate: Transition loses its invasive edge. *Nature* **2015**, *527*, 452–453, doi:10.1038/nature16313.

51.   Krebs, A.M.; Mitschke, J.; Lasierra Losada, M.; Schmalhofer, O.; Boerries, M.; Busch, H.; Boettcher, M.; Mougiakakos, D.; Reichardt, W.; Bronsert, P., et al. The EMT-activator Zeb1 is a key factor for cell plasticity and promotes metastasis in pancreatic cancer. *Nat. Cell Biol.* **2017**, *19*, 518–529, doi:10.1038/ncb3513.

52.   Tran, H.D.; Luitel, K.; Kim, M.; Zhang, K.; Longmore, G.D.; Tran, D.D. Transient SNAIL1 expression is necessary for metastatic competence in breast cancer. *Cancer Res.* **2014**, *74*, 6330–6340, doi:10.1158/0008-5472.CAN-14-0923.

53.   Xu, Y.; Lee, D.K.; Feng, Z.; Xu, Y.; Bu, W.; Li, Y.; Liao, L.; Xu, J. Breast tumor cell-specific knockout of Twist1 inhibits cancer cell plasticity, dissemination, and lung metastasis in mice. *Proc. Natl. Acad. Sci. U S A* **2017**, *114*, 11494–11499, doi:10.1073/pnas.1618091114.

54.   Tsai, J.H.; Donaher, J.L.; Murphy, D.A.; Chau, S.; Yang, J. Spatiotemporal regulation of epithelial-mesenchymal transition is essential for squamous cell carcinoma metastasis. *Cancer Cell* **2012**, *22*, 725–736, doi:10.1016/j.ccr.2012.09.022.

55.   Schmidt, J.M.; Panzilius, E.; Bartsch, H.S.; Irmler, M.; Beckers, J.; Kari, V.; Linnemann, J.R.; Dragoi, D.; Hirschi, B.; Kloos, U.J., et al. Stem-cell-like properties and epithelial plasticity arise as stable traits after transient Twist1 activation. *Cell Rep.* **2015**, *10*, 131–139, doi:10.1016/j.celrep.2014.12.032.

56.   Reichert, M.; Bakir, B.; Moreira, L.; Pitarresi, J.R.; Feldmann, K.; Simon, L.; Suzuki, K.; Maddipati, R.; Rhim, A.D.; Schlitter, A.M., et al. Regulation of Epithelial Plasticity Determines Metastatic Organotropism in Pancreatic Cancer. *Dev. Cell* **2018**, *45*, 696–711 e698, doi:10.1016/j.devcel.2018.05.025.

57.   Puram, S.V.; Tirosh, I.; Parikh, A.S.; Patel, A.P.; Yizhak, K.; Gillespie, S.; Rodman, C.; Luo, C.L.; Mroz, E.A.; Emerick, K.S., et al. Single-Cell Transcriptomic Analysis of Primary and Metastatic Tumor Ecosystems in Head and Neck Cancer. *Cell* **2017**, *171*, 1611–1624 e1624, doi:10.1016/j.cell.2017.10.044.

58.   Kroger, C.; Afeyan, A.; Mraz, J.; Eaton, E.N.; Reinhardt, F.; Khodor, Y.L.; Thiru, P.; Bierie, B.; Ye, X.; Burge, C.B., et al. Acquisition of a hybrid E/M state is essential for tumorigenicity of basal breast cancer cells. *Proc. Natl. Acad. Sci.* **2019**, *116*, 7353–7362, doi:10.1073/pnas.1812876116.

59.   Bocci, F.; Jolly, M.K.; Tripathi, S.C.; Aguilar, M.; Hanash, S.M.; Levine, H.; Onuchic, J.N. Numb prevents a complete epithelial-mesenchymal transition by modulating Notch signalling. *J. R. Soc. Interface* **2017**, *14*, doi:10.1098/rsif.2017.0512.

60.   Jolly, M.K.; Tripathi, S.C.; Jia, D.; Mooney, S.M.; Celiktas, M.; Hanash, S.M.; Mani, S.A.; Pienta, K.J.; Ben-Jacob, E.; Levine, H. Stability of the hybrid epithelial/mesenchymal phenotype. *Oncotarget* **2016**, *7*, 27067–27084, doi:10.18632/oncotarget.8166.

61.   Biddle, A.; Gammon, L.; Liang, X.; Costea, D.E.; Mackenzie, I.C. Phenotypic Plasticity Determines Cancer Stem Cell Therapeutic Resistance in Oral Squamous Cell Carcinoma. *EBioMedicine* **2016**, *4*, 138–145, doi:10.1016/j.ebiom.2016.01.007.

62.   Katsuno, Y.; Meyer, D.S.; Zhang, Z.; Shokat, K.M.; Akhurst, R.J.; Miyazono, K.; Derynck, R. Chronic TGF-beta exposure drives stabilized EMT, tumor stemness, and cancer drug resistance with vulnerability to bitopic mTOR inhibition. *Sci. Signal.* **2019**, *12*, doi:10.1126/scisignal.aau8544.

63.   Mehlen, P.; Puisieux, A. Metastasis: A question of life or death. *Nat. Rev. Cancer* **2006**, *6*, 449–458.

64.   Friedl, P.; Wolf, K. Tumour-cell invasion and migration: Diversity and escape mechanisms. *Nat. Rev. Cancer* **2003**, *3*, 362–374, doi:10.1038/nrc1075.

Chapter 2

65. Ridley, A.J.; Schwartz, M.A.; Burridge, K.; Firtel, R.A.; Ginsberg, M.H.; Borisy, G.; Parsons, J.T.; Horwitz, A.R. Cell migration: Integrating signals from front to back. *Science* **2003**, *302*, 1704–1709, doi:10.1126/science.1092053.

66. Sahai, E.; Marshall, C.J. Differing modes of tumour cell invasion have distinct requirements for Rho/ROCK signalling and extracellular proteolysis. *Nat. Cell Biol.* **2003**, *5*, 711–719, doi:10.1038/ncb1019.

67. Wolf, K.; Mazo, I.; Leung, H.; Engelke, K.; von Andrian, U.H.; Deryugina, E.I.; Strongin, A.Y.; Brocker, E.B.; Friedl, P. Compensation mechanism in tumor cell migration: Mesenchymal-amoeboid transition after blocking of pericellular proteolysis. *J. Cell Biol.* **2003**, *160*, 267–277, doi:10.1083/jcb.200209006.

68. Beerling, E.; Seinstra, D.; de Wit, E.; Kester, L.; van der Velden, D.; Maynard, C.; Schafer, R.; van Diest, P.; Voest, E.; van Oudenaarden, A., et al. Plasticity between Epithelial and Mesenchymal States Unlinks EMT from Metastasis-Enhancing Stem Cell Capacity. *Cell Rep.* **2016**, *14*, 2281–2288, doi:10.1016/j.celrep.2016.02.034.

69. Zhao, Z.; Zhu, X.; Cui, K.; Mancuso, J.; Federley, R.; Fischer, K.; Teng, G.; Mittal, V.; Gao, D.; Zhao, H., et al. In Vivo Visualization and Characterization of Epithelial-Mesenchymal Transition in Breast Tumors. *Cancer Res.* **2016**, *76*, 2094–2104, doi:10.1158/0008-5472.CAN-15-2662.

70. Friedl, P.; Wolf, K. Proteolytic interstitial cell migration: A five-step process. *Cancer Metastasis Rev.* **2009**, *28*, 129–135, doi:10.1007/s10555-008-9174-3.

71. Miyoshi, A.; Kitajima, Y.; Kido, S.; Shimonishi, T.; Matsuyama, S.; Kitahara, K.; Miyazaki, K. Snail accelerates cancer invasion by upregulating MMP expression and is associated with poor prognosis of hepatocellular carcinoma. *Br. J. Cancer* **2005**, *92*, 252–258.

72. Miyoshi, A.; Kitajima, Y.; Sumi, K.; Sato, K.; Hagiwara, A.; Koga, Y.; Miyazaki, K. Snail and SIP1 increase cancer invasion by upregulating MMP family in hepatocellular carcinoma cells. *Br. J. Cancer* **2004**, *90*, 1265–1273.

73. Lochter, A.; Galosy, S.; Muschler, J.; Freedman, N.; Werb, Z.; Bissell, M.J. Matrix metalloproteinase stromelysin-1 triggers a cascade of molecular alterations that leads to stable epithelial-to-mesenchymal conversion and a premalignant phenotype in mammary epithelial cells. *J. Cell Biol* **1997**, *139*, 1861–1872.

74. Shintani, Y.; Wheelock, M.J.; Johnson, K.R. Phosphoinositide-3 kinase-Rac1-c-Jun NH2-terminal kinase signaling mediates collagen I-induced cell scattering and up-regulation of N-cadherin expression in mouse mammary epithelial cells. *Mol. Biol. Cell* **2006**, *17*, 2963–2975, doi:10.1091/mbc.e05-12-1123.

75. Ilina, O.; Campanello, L.; Gritsenko, P.G.; Vullings, M.; Wang, C.; Bult, P.; Losert, W.; Friedl, P. Intravital microscopy of collective invasion plasticity in breast cancer. *Dis. Model. Mech.* **2018**, *11*, doi:10.1242/dmm.034330.

76. Shamir, E.R.; Pappalardo, E.; Jorgens, D.M.; Coutinho, K.; Tsai, W.T.; Aziz, K.; Auer, M.; Tran, P.T.; Bader, J.S.; Ewald, A.J. Twist1-induced dissemination preserves epithelial identity and requires E-cadherin. *J. Cell Biol.* **2014**, *204*, 839–856, doi:10.1083/jcb.201306088.

77. Friedl, P.; Locker, J.; Sahai, E.; Segall, J.E. Classifying collective cancer cell invasion. *Nat. Cell Biol.* **2012**, *14*, 777–783, doi:10.1038/ncb2548.

78. Campbell, K.; Rossi, F.; Adams, J.; Pitsidianaki, I.; Barriga, F.M.; Garcia-Gerique, L.; Batlle, E.; Casanova, J.; Casali, A. Collective cell migration and metastases induced by an epithelial-to-mesenchymal transition in Drosophila intestinal tumors. *Nat. Commun.* **2019**, *10*, 2311, doi:10.1038/s41467-019-10269-y.

79. Cheung, K.J.; Gabrielson, E.; Werb, Z.; Ewald, A.J. Collective invasion in breast cancer requires a conserved basal epithelial program. *Cell* **2013**, *155*, 1639–1651, doi:10.1016/j.cell.2013.11.029.

80. Friedl, P.; Mayor, R. Tuning Collective Cell Migration by Cell-Cell Junction Regulation. *Cold Spring Harb. Perspect. Biol.* **2017**, *9*.

81. Tse, J.M.; Cheng, G.; Tyrrell, J.A.; Wilcox-Adelman, S.A.; Boucher, Y.; Jain, R.K.; Munn, L.L. Mechanical compression drives cancer cells toward invasive phenotype. *Proc. Natl. Acad. Sci.* **2012**, *109*, 911–916.

82. Scarpa, E.; Mayor, R. Collective cell migration in development. *J. Cell Biol.* **2016**, *212*, 143–155, doi:10.1083/jcb.201508047.

83. Wolf, K.; Wu, Y.I.; Liu, Y.; Geiger, J.; Tam, E.; Overall, C.; Stack, M.S.; Friedl, P. Multi-step pericellular proteolysis controls the transition from individual to collective cancer cell invasion. *Nat. Cell Biol.* **2007**, *9*, 893–904.

84. Gaggioli, C.; Hooper, S.; Hidalgo-Carcedo, C.; Grosse, R.; Marshall, J.F.; Harrington, K.; Sahai, E. Fibroblast-led collective invasion of carcinoma cells with differing roles for RhoGTPases in leading and following cells. *Nat. Cell Biol.* **2007**, *9*, 1392–1400.

85. Labernadie, A.; Kato, T.; Brugues, A.; Serra-Picamal, X.; Derzsi, S.; Arwert, E.; Weston, A.; Gonzalez-Tarrago, V.; Elosegui-Artola, A.; Albertazzi, L., et al. A mechanically active heterotypic E-cadherin/N-cadherin adhesion enables fibroblasts to drive cancer cell invasion. *Nat. Cell Biol.* **2017**, *19*, 224–237.

86. Condeelis, J.; Pollard, J.W. Macrophages: Obligate partners for tumor cell migration, invasion, and metastasis. *Cell* **2006**, *124*, 263–266.

87. DeNardo, D.G.; Barreto, J.B.; Andreu, P.; Vasquez, L.; Tawfik, D.; Kolhatkar, N.; Coussens, L.M. CD4(+) T cells regulate pulmonary metastasis of mammary carcinomas by enhancing protumor properties of macrophages. *Cancer Cell* **2009**, *16*, 91–102.

88. Roussos, E.T.; Condeelis, J.S.; Patsialou, A. Chemotaxis in cancer. *Nat. Rev. Cancer* **2011**, *11*, 573–587, doi:10.1038/nrc3078.

89. Hu, J.L.; Wang, W.; Lan, X.L.; Zeng, Z.C.; Liang, Y.S.; Yan, Y.R.; Song, F.Y.; Wang, F.F.; Zhu, X.H.; Liao, W.J., et al. CAFs secreted exosomes promote metastasis and chemotherapy resistance by enhancing cell stemness and epithelial-mesenchymal transition in colorectal cancer. *Mol. Cancer* **2019**, *18*, 91, doi:10.1186/s12943-019-1019-x.

90. Gandalovicova, A.; Rosel, D.; Fernandes, M.; Vesely, P.; Heneberg, P.; Cermak, V.; Petruzelka, L.; Kumar, S.; Sanz-Moreno, V.; Brabek, J. Migrastatics-Anti-metastatic and Anti-invasion Drugs: Promises and Challenges. *Trends Cancer* **2017**, *3*, 391–406.

91. Aceto, N.; Toner, M.; Maheswaran, S.; Haber, D.A. En Route to Metastasis: Circulating Tumor Cell Clusters and Epithelial-to-Mesenchymal Transition. *Trends Cancer* **2015**, *1*, 44–52.

92. Finkel, G.C.; Tishkoff, G.H. Malignant cells in a peripheral blood smear: Report of a case. *N. Engl. J. Med.* **1960**, *262*, 187–188.

93. Yu, M.; Bardia, A.; Wittner, B.S.; Stott, S.L.; Smas, M.E.; Ting, D.T.; Isakoff, S.J.; Ciciliano, J.C.; Wells, M.N.; Shah, A.M., et al. Circulating breast tumor cells exhibit dynamic changes in epithelial and mesenchymal composition. *Science* **2013**, *339*, 580–584.

94. Ao, Z.; Shah, S.H.; Machlin, L.M.; Parajuli, R.; Miller, P.C.; Rawal, S.; Williams, A.J.; Cote, R.J.; Lippman, M.E.; Datar, R.H., et al. Identification of Cancer-Associated Fibroblasts in Circulating Blood from Patients with Metastatic Breast Cancer. *Cancer Res.* **2015**, *75*, 4681–4687, doi:10.1158/0008-5472.CAN-15-1633.

Chapter 2

95. Duda, D.G.; Duyverman, A.M.; Kohno, M.; Snuderl, M.; Steller, E.J.; Fukumura, D.; Jain, R.K. Malignant cells facilitate lung metastasis by bringing their own soil. *Proc. Natl. Acad. Sci.* **2010**, *107*, 21677–21682.

96. Gasic, G.J.; Gasic, T.B.; Galanti, N.; Johnson, T.; Murphy, S. Platelet-tumor-cell interactions in mice. The role of platelets in the spread of malignant disease. *Int. J. Cancer* **1973**, *11*, 704–718, doi:10.1002/ijc.2910110322.

97. Labelle, M.; Begum, S.; Hynes, R.O. Direct signaling between platelets and cancer cells induces an epithelial-mesenchymal-like transition and promotes metastasis. *Cancer Cell* **2011**, *20*, 576–590.

98. Szczerba, B.M.; Castro-Giner, F.; Vetter, M.; Krol, I.; Gkountela, S.; Landin, J.; Scheidmann, M.C.; Donato, C.; Scherrer, R.; Singer, J., et al. Neutrophils escort circulating tumour cells to enable cell cycle progression. *Nature* **2019**, *566*, 553–557, doi:10.1038/s41586-019-0915-y.

99. Lecharpentier, A.; Vielh, P.; Perez-Moreno, P.; Planchard, D.; Soria, J.C.; Farace, F. Detection of circulating tumour cells with a hybrid (epithelial/mesenchymal) phenotype in patients with metastatic non-small cell lung cancer. *Br. J. Cancer* **2011**, *105*, 1338–1341.

100. Molnar, B.; Ladanyi, A.; Tanko, L.; Sreter, L.; Tulassay, Z. Circulating tumor cell clusters in the peripheral blood of colorectal cancer patients. *Clin. Cancer Res.* **2001**, *7*, 4080–4085.

101. Yadavalli, S.; Jayaram, S.; Manda, S.S.; Madugundu, A.K.; Nayakanti, D.S.; Tan, T.Z.; Bhat, R.; Rangarajan, A.; Chatterjee, A.; Gowda, H., et al. Data-Driven Discovery of Extravasation Pathway in Circulating Tumor Cells. *Sci. Rep.* **2017**, *7*, 43710, doi:10.1038/srep43710.

102. Watanabe, S. The metastasizability of tumor cells. *Cancer* **1954**, *7*, 215–223.

103. Topal, B.; Roskams, T.; Fevery, J.; Penninckx, F. Aggregated colon cancer cells have a higher metastatic efficiency in the liver compared with nonaggregated cells: An experimental study. *J. Surg. Res.* **2003**, *112*, 31–37.

104. Aceto, N.; Bardia, A.; Miyamoto, D.T.; Donaldson, M.C.; Wittner, B.S.; Spencer, J.A.; Yu, M.; Pely, A.; Engstrom, A.; Zhu, H., et al. Circulating tumor cell clusters are oligoclonal precursors of breast cancer metastasis. *Cell* **2014**, *158*, 1110–1122.

105. Cheung, K.J.; Padmanaban, V.; Silvestri, V.; Schipper, K.; Cohen, J.D.; Fairchild, A.N.; Gorin, M.A.; Verdone, J.E.; Pienta, K.J.; Bader, J.S., et al. Polyclonal breast cancer metastases arise from collective dissemination of keratin 14-expressing tumor cell clusters. *Proc. Natl. Acad. Sci.* **2016**, *113*, E854–E863.

106. Maddipati, R.; Stanger, B.Z. Pancreatic Cancer Metastases Harbor Evidence of Polyclonality. *Cancer Discov.* **2015**, *5*, 1086–1097.

107. Gkountela, S.; Castro-Giner, F.; Szczerba, B.M.; Vetter, M.; Landin, J.; Scherrer, R.; Krol, I.; Scheidmann, M.C.; Beisel, C.; Stirnimann, C.U., et al. Circulating Tumor Cell Clustering Shapes DNA Methylation to Enable Metastasis Seeding. *Cell* **2019**, *176*, 98–112 e114, doi:10.1016/j. cell.2018.11.046.

108. Hou, J.M.; Krebs, M.G.; Lancashire, L.; Sloane, R.; Backen, A.; Swain, R.K.; Priest, L.J.; Greystoke, A.; Zhou, C.; Morris, K., et al. Clinical significance and molecular characteristics of circulating tumor cells and circulating tumor microemboli in patients with small-cell lung cancer. *J. Clin. Oncol.* **2012**, *30*, 525–532.

109. Zhang, D.; Zhao, L.; Zhou, P.; Ma, H.; Huang, F.; Jin, M.; Dai, X.; Zheng, X.; Huang, S.; Zhang, T. Circulating tumor microemboli (CTM) and vimentin+ circulating tumor cells (CTCs) detected by a size-based platform predict worse prognosis in advanced colorectal cancer patients during chemotherapy. *Cancer Cell Int.* **2017**, *17*, 6, doi:10.1186/s12935-016-0373-7.

110. Frisch, S.M.; Schaller, M.; Cieply, B. Mechanisms that link the oncogenic epithelial-mesenchymal transition to suppression of anoikis. *J. Cell Sci.* **2013**, *126*, 21–29, doi:10.1242/jcs.120907.

111. Mahauad-Fernandez, W.D.; Naushad, W.; Panzner, T.D.; Bashir, A.; Lal, G.; Okeoma, C.M. BST-2 promotes survival in circulation and pulmonary metastatic seeding of breast cancer cells. *Sci. Rep.* **2018**, *8*, 17608, doi:10.1038/s41598-018-35710-y.

112. Nieswandt, B.; Hafner, M.; Echtenacher, B.; Mannel, D.N. Lysis of tumor cells by natural killer cells in mice is impeded by platelets. *Cancer Res.* **1999**, *59*, 1295–1300.

113. Palumbo, J.S.; Talmage, K.E.; Massari, J.V.; La Jeunesse, C.M.; Flick, M.J.; Kombrinck, K.W.; Jirouskova, M.; Degen, J.L. Platelets and fibrin(ogen) increase metastatic potential by impeding natural killer cell-mediated elimination of tumor cells. *Blood* **2005**, *105*, 178–185.

114. Borsig, L.; Wong, R.; Hynes, R.O.; Varki, N.M.; Varki, A. Synergistic effects of L- and P-selectin in facilitating tumor metastasis can involve non-mucin ligands and implicate leukocytes as enhancers of metastasis. *Proc. Natl. Acad. Sci.* **2002**, *99*, 2193–2198, doi:10.1073/pnas.261704098.

115. Leblanc, R.; Peyruchaud, O. Metastasis: New functional implications of platelets and megakaryocytes. *Blood* **2016**, *128*, 24–31, doi:10.1182/blood-2016-01-636399.

116. Cheung, K.J.; Ewald, A.J. A collective route to metastasis: Seeding by tumor cell clusters. *Science* **2016**, *352*, 167–169.

117. Gorges, T.M.; Tinhofer, I.; Drosch, M.; Rose, L.; Zollner, T.M.; Krahn, T.; von Ahsen, O. Circulating tumour cells escape from EpCAM-based detection due to epithelial-to-mesenchymal transition. *BMC Cancer* **2012**, *12*, 178, doi:10.1186/1471-2407-12-178.

118. Cima, I.; Kong, S.L.; Sengupta, D.; Tan, I.B.; Phyo, W.M.; Lee, D.; Hu, M.; Iliescu, C.; Alexander, I.; Goh, W.L., et al. Tumor-derived circulating endothelial cell clusters in colorectal cancer. *Sci. Transl. Med.* **2016**, *8*, 345ra389, doi:10.1126/scitranslmed.aad7369.

119. Mu, Z.; Wang, C.; Ye, Z.; Austin, L.; Civan, J.; Hyslop, T.; Palazzo, J.P.; Jaslow, R.; Li, B.; Myers, R.E., et al. Prospective assessment of the prognostic value of circulating tumor cells and their clusters in patients with advanced-stage breast cancer. *Breast Cancer Res. Treat.* **2015**, *154*, 563–571, doi:10.1007/s10549-015-3636-4.

120. Molnar, B.; Floro, L.; Sipos, F.; Toth, B.; Sreter, L.; Tulassay, Z. Elevation in peripheral blood circulating tumor cell number correlates with macroscopic progression in UICC stage IV colorectal cancer patients. *Dis. Markers* **2008**, *24*, 141–150, doi:10.1155/2008/941509.

121. Sharma, D.; Brummel-Ziedins, K.E.; Bouchard, B.A.; Holmes, C.E. Platelets in tumor progression: A host factor that offers multiple potential targets in the treatment of cancer. *J. Cell Physiol.* **2014**, *229*, 1005–1015, doi:10.1002/jcp.24539.

122. Schror, K. Aspirin and platelets: The antiplatelet action of aspirin and its role in thrombosis treatment and prophylaxis. *Semin. Thromb. Hemost.* **1997**, *23*, 349–356, doi:10.1055/s-2007-996108.

123. Kanikarla-Marie, P.; Lam, M.; Sorokin, A.V.; Overman, M.J.; Kopetz, S.; Menter, D.G. Platelet Metabolism and Other Targeted Drugs; Potential Impact on Immunotherapy. *Front. Oncol.* **2018**, *8*, 107, doi:10.3389/fonc.2018.00107.

124. Guillem-Llobat, P.; Dovizio, M.; Bruno, A.; Ricciotti, E.; Cufino, V.; Sacco, A.; Grande, R.; Alberti, S.; Arena, V.; Cirillo, M., et al. Aspirin prevents colorectal cancer metastasis in mice by splitting the crosstalk between platelets and tumor cells. *Oncotarget* **2016**, *7*, 32462–32477, doi:10.18632/oncotarget.8655.

Chapter 2

125. Frose, J.; Chen, M.B.; Hebron, K.E.; Reinhardt, F.; Hajal, C.; Zijlstra, A.; Kamm, R.D.; Weinberg, R.A. Epithelial-Mesenchymal Transition Induces Podocalyxin to Promote Extravasation via Ezrin Signaling. *Cell Rep.* **2018**, *24*, 962–972, doi:10.1016/j.celrep.2018.06.092.

126. Stankic, M.; Pavlovic, S.; Chin, Y.; Brogi, E.; Padua, D.; Norton, L.; Massague, J.; Benezra, R. TGF-beta-Id1 signaling opposes Twist1 and promotes metastatic colonization via a mesenchymal-to-epithelial transition. *Cell Rep.* **2013**, *5*, 1228–1242, doi:10.1016/j.celrep.2013.11.014.

127. Ocana, O.H.; Corcoles, R.; Fabra, A.; Moreno-Bueno, G.; Acloque, H.; Vega, S.; Barrallo-Gimeno, A.; Cano, A.; Nieto, M.A. Metastatic colonization requires the repression of the epithelial-mesenchymal transition inducer Prrx1. *Cancer Cell* **2012**, *22*, 709–724, doi:10.1016/j.ccr.2012.10.012.

128. Sanchez-Tillo, E.; Siles, L.; de Barrios, O.; Cuatrecasas, M.; Vaquero, E.C.; Castells, A.; Postigo, A. Expanding roles of ZEB factors in tumorigenesis and tumor progression. *Am. J. Cancer Res.* **2011**, *1*, 897–912.

CHAPTER III

3

DOC1-dependent recruitment of NURD reveals antagonism with SWI/SNF during epithelial-mesenchymal transition in oral cancer cells

A. M. Mohd-Sarip, M.J. Teeuwssen, A.G. Bot, M. J. De Herdt, S.M. Willems, R. J. Baatenburg de Jong, L.H.J. Looijenga, D. Zatreanu, K. Bezstarosti, J. van Riet, E. Oole, W.F.J. van IJcken, H.J.G. van de Werken, J.A. Demmers, R. Fodde, C.P. Verrijzer

Abstract

The Nucleosome Remodeling and Deacetylase (NURD) complex is a key regulator of cell differentiation that has also been implicated in tumorigenesis. Loss of the NURD subunit Deleted in Oral Cancer 1 (DOC1) is associated with human oral squamous cell carcinomas (OSCCs). Here, we show that restoration of DOC1 expression in OSCC cells leads to a reversal of epithelial-mesenchymal transition (EMT). This is caused by the DOC1-dependent targeting of NURD to repress key transcriptional regulators of EMT. NURD recruitment drives extensive epigenetic reprogramming, including eviction of the SWI/SNF remodeler, formation of inaccessible chromatin, H3K27 deacetylation, and binding of PRC2 and KDM1A, followed by H3K27 methylation and H3K4 demethylation. Strikingly, depletion of SWI/SNF mimics the effects of DOC1 re-expression. Our results suggest that SWI/SNF and NURD function antagonistically to control chromatin state and transcription. We propose that disturbance of this dynamic equilibrium may lead to defects in gene expression that promote oncogenesis.

Abstract

Chapter 3

Introduction

ATP-dependent chromatin remodeling complexes (remodelers) control expression of the eukaryotic genome through mobilization of nucleosomes. The nucleosome is the basic repeat unit of eukaryotic chromatin, comprising 147 base pairs (bp) of DNA, wrapped tightly around a protein core formed by an octamer of histones [1]. Nucleosome positioning and stability determines the accessibility of regulatory DNA elements, thereby providing a pervasive mode of gene expression control. Consequently, remodelers play a central role in transcriptional regulation by mediating the assembly, sliding, restructuring, or ejection of nucleosomes [2,3]. There are four major families of remodelers, each named after its ATPase subunit: SWI/SNF, INO80, ISWI and CHD. In addition to the central ATPase, remodeler complexes have unique sets of tightly associated proteins that determine targeting and regulate activity.

A second mechanism to control chromatin state involves a plethora of post-translational histone modification, which can direct recruitment of regulatory proteins (including remodelers) and modulate the folding of the chromatin fiber [4,5]. Prominent modifications include acetylation, methylation, and phosphorylation of specific residues on the histone N-terminal tails, which protrude from the nucleosome. There is a clear correlation between specific histone modifications and transcriptional state. For example, acetylation of histone H3K27 (H3K27ac) marks active genes, whereas tri-methylation of the same residue (H3K27me3) is associated with gene silencing by the Polycomb system. Although they mediate completely different biochemical reactions, remodelers and histone modifying enzymes function in a closely integrated manner to determine chromatin state [6]. In agreement with their central role in gene expression control, cancer genome sequencing studies have revealed frequent mutations in remodelers and histone modifying enzymes across a broad spectrum of cancer types [7-9].

NURD refers to a family of protein assemblages that harbors one of the chromodomain ATP-dependent helicases CHD3, CHD4 or CHD5 (CHD3/4/5), and the histone deacetylases HDAC1/2 [10,11]. In addition to these two enzymatic activities, NURD comprises the scaffolding proteins GATAD2A/B, histone chaperones RBP4/7, histone tail- and DNA-binding proteins MTA1/2/3, and either one of the CpG-binding proteins MBD2 or MBD3. Notably, MBD2, but not MBD3, binds methylated CpG residues [12]. MBD2-NURD, rather than MBD3-NURD, has been implicated in the formation of repressive chromatin [12,13]. Finally, DOC1 (Deleted in Oral Cancer 1) is an initially overlooked yet integral subunit of NURD, conserved from *Drosophila* to humans [14,15]. DOC1 has also been identified as an interaction partner and negative regulator of CDK2, hence its alternate name: Cyclin-Dependent Kinase 2 Associated Protein 1 (CDK2AP1) [16,17]. *Doc1* knock-out mice are embryonic lethal at around day 3.5-5.5 p.c. [17,18]. Embryonic stem cells lacking *Doc1* self-renew, but form exclusively mesodermal lineages in teratoma differentiation assays [18]. NURD has been functionally connected to histone H3K27 methylation by Polycomb-Repressive Complex 2 (PRC2) [19,20], and H3K4me2 demethylation by KDM1A/LSD1 [7,21]. NURD plays essential roles in various developmental processes, pluripotent stem cell differentiation, and has been implicated in oncogenesis [7,22-25].

The gene encoding the 115 amino acids (aa) DOC1 protein was first discovered as a potential tumor suppressor in oral cancer [26]. Indeed, DOC1 is absent or down-regulated in ~ 70% of human oral cancers [27,28]. Moreover, loss of DOC1 expression has also been

observed in nasopharyngeal-, gastric- and esophageal carcinomas [29-31]. Pertinently, in these studies low DOC1 expression correlated strongly with tumor invasion, metastasis and adverse prognosis for patients. However, the molecular pathway through which loss of DOC1 promotes oncogenesis has remained unclear.

Epithelial-mesenchymal transition (EMT) is a reversible process that plays a central role in tumor malignancy [32,33]. EMT is an integral part of normal development, allowing embryonic epithelial cells to become mobile and capable to colonize specific areas of the embryo. In cancer, however, EMT enables carcinoma cells to detach from the primary tumor, invade surrounding tissue, and disseminate to distant sites to form metastases. EMT is orchestrated by a transcriptional program directed by a small set of evolutionary conserved master transcription factors, including TWIST, SNAIL, ZEB, and SLUG [32]. EMT transcription factors exert additional oncogenic activities, e.g. escape from senescence or apoptosis, adoption of stem cell-like properties and drug resistance, even in cancer cells retaining epithelial features.

Here, we investigated the molecular function of DOC1 in oral cancer. We found that tumor suppression by DOC1 involves reversal of EMT, which is caused by NURD-dependent repression of EMT transcription factors. DOC1 mediates the recruitment of NURD, initiating comprehensive epigenetic reprogramming and transcriptional silencing. Our results reveal that NURD and SWI/SNF function antagonistically to control gene expression, through modulation of nucleosome remodeling and Polycomb recruitment.

Results

Loss of the NURD subunit DOC1 in oral cancer cells

Similar to the better studied SWI/SNF remodelers, the sequencing of cancer genomes has uncovered frequent mutations in genes encoding NURD subunits (Figure S1A; http://www.cbioportal.org). These observations suggest that inactivation of NURD might contribute to oncogenesis. Although rarely mutated in most cancer types, DOC1 levels are reduced in the majority of human oral cancers, and the loss of DOC1 correlates with tumor invasion and metastasis [27,28]. Prompted by these findings, we examined DOC1 expression in normal and cancerous tongue tissue (Figure 1A-E). Immunohistochemistry (IHC) of normal tongue tissue suggests a relationship between DOC1 expression and epithelial cell differentiation (Figure 1A). DOC1 is mostly undetectable in the basal layer (BL) where the epithelial stem cells reside. However, DOC1 is induced during cell differentiation, and is robustly expressed in nuclei within the stratified squamous epithelial layer (SSEL). However, when the keratinocytes undergo terminal differentiation and cornification within the stratum corneum (SC), DOC1 levels are reduced again. Analysis of a cohort of 36 OSCCs of the tongue revealed a small percentage (~8%) that were completely negative for DOC1 (Figure 1B), whereas the majority showed a mixture of negative and positive cells (Figure 1C), and ~20% were positive (Figure 1D-E). Moreover, we found that DOC1 was lacking in all 4 different human oral squamous cell carcinoma (OSCC) cell lines that we examined (SCC4, SCC9, SCC15 and SCC25), while it was readily detected in HaCaT keratinocytes (Figure 1F-G and Figure S1B-C). Thus, in agreement with previous studies, we observed reduced DOC1 expression in the majority of OSCCs.

Chapter 3
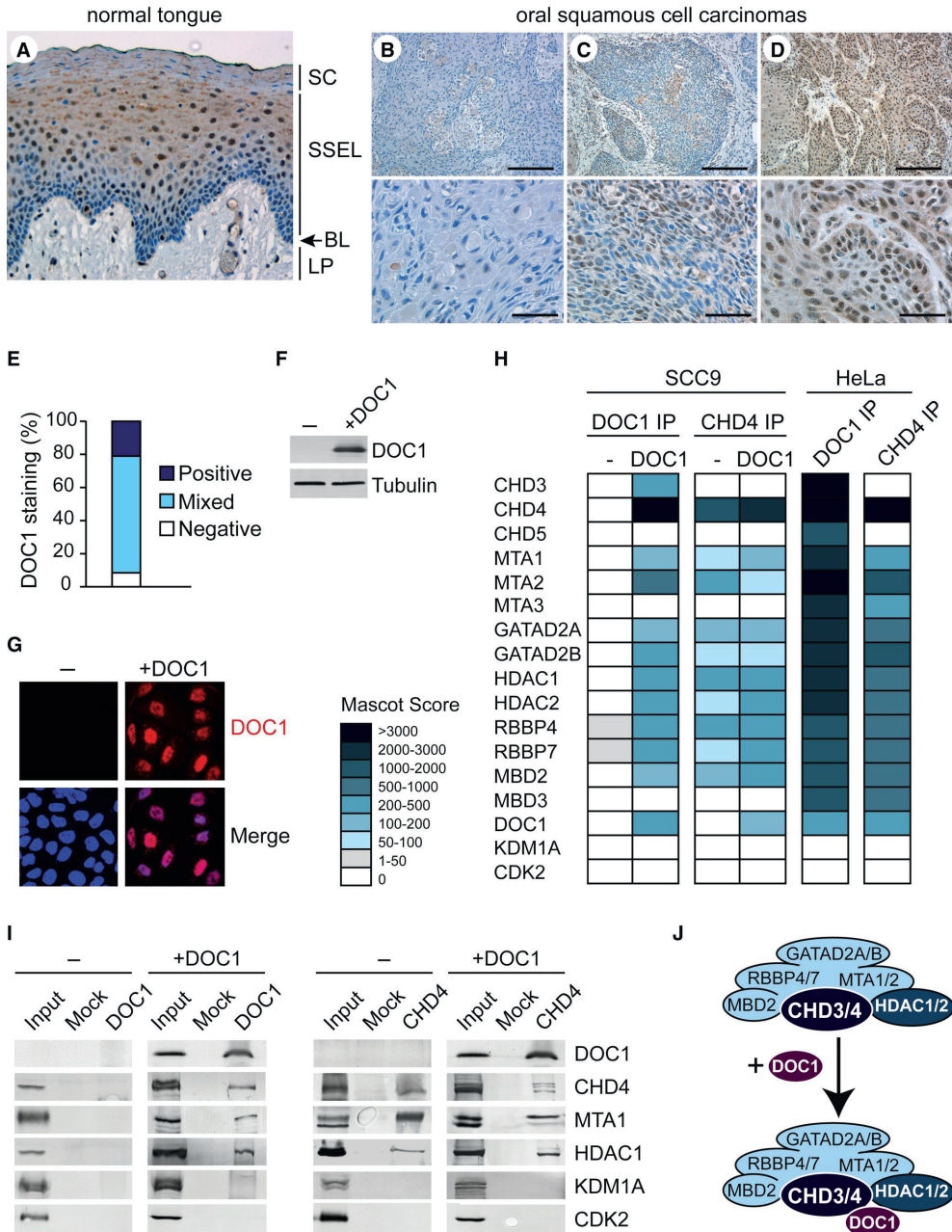
Figure 1. Re-expressed DOC1 in OSCC cells integrated into NURD. (**a**) Photomicrograph depicting DOC1 (brown), detected by immunohistochemistry, in a hematoxylin counterstained section of normal tongue epithelium. The underlying connective tissue of the lamina propria (LP), the basal layer (BL) stratified squamous epithelial layer (SSEL) and keratinized stratum corneum (SC) are indicated. Our anti-DOC1 antibodies strongly stain the nuclei of the SSEL. (**b-d**) DOC1 expression in tongue carcinoma. Examples of tumors that were: (**b**) negative for DOC1, (**c**) comprise a mixture of DOC1-negative and positive cells

(**d**) strongly positive for DOC1. Scale bars: 200 μm (top panels) or 50 μm (bottom). (**e**) Quantification of the DOC1 expression in 36 tongue carcinomas. (**f**) Immunoblotting analysis of DOC1 expression in SCC9 cells transduced with lentiviruses expressing either an irrelevant control (LacZ, -) or DOC1. Tubulin serves as a loading control. (**g**) Indirect IF of SCC9 cells treated as described above. Cells were fixed and stained with antibodies against DOC1 (red). Nuclei were visualized by DAPI staining of DNA (blue). See Figure S1B-C for additional OSCC cell lines. (**h**) Interaction heatmap, based on mascot scores, depicting associated factors identified by mass spectrometry after IP of DOC1 or CHD4 from SCC9 cells transduced with lentiviruses expressing either an irrelevant control (LacZ, -) or DOC1. In addition, endogenous DOC1 and CHD4 were IPed from HeLa cells. See Table S1 for details and IPs from SCC4 cells. (**i**) Co-IPs of DOC1 or CHD4 from SCC9 cells. Associated proteins were detected by immunoblotting with antibodies against the indicated proteins. Input represents 10% of the binding reactions. See Figure S1D for co-IPs from HeLa cells. (**j**) Cartoon summarizing the proteomics results. See also Table S1 and Figure S1.

To study its role in OSCC cells, we re-expressed *DOC1* by lentiviral transduction (Figure 1F-G and Figure S1B). Next, we immuno-purified (IPed) DOC1 from whole cell extracts (WCE) prepared from SCC9 cells transduced with either LacZ- or DOC1-expressing virus. Mass spectrometric analysis revealed the association of DOC1 with CHD3, CHD4, MTA1 MTA2, GATA2A, GATA2B, HDAC1, HDAC2, RBBP4, RBBP7, and MBD2 (Figure 1H and Table S1). Purification of CHD4 revealed a similar complex, but lacking CHD3. CHD5, MTA3 and MBD3 were absent in the IPs from SCC9 cells. The presence- or absence of DOC1 did not substantially affect the composition of the NURD complex, although there were subtle changes in the mass spectrometric scores for specific subunits. Thus, DOC1 does not appear to play a major architectural role in the NURD complex. IPs of DOC1 and CHD4 from SCC4 cells yielded similar results (Table S1). Mass spectrometric analysis of endogenous DOC1 IPed from HeLa cells revealed the full complement of NURD-class proteins, including CHD3/4/5, MBD2/3 and MTA1/2/3 (Figure 1H and Table S1). CHD4 IPed from HeLa cells was associated with a similar set of proteins, but CHD3 and CHD5 were absent. Immunoblotting of DOC1- and CHD4-bound proteins confirmed the mass spectrometric results (Figure 1I and Figure S1D). Under the conditions used (buffers including 600 mM KCl and 0.1% NP-40), CDK2 was not present in our DOC1 IPs. Likewise, we did not detect the association of KDM1A with NURD, which has been debated in the literature (Laugesen and Helin, 2014). We conclude that DOC1 is an integral subunit of the MBD2/3/CHD3/4/5-NURD family of complexes. OSCC cells lack DOC1, but when re-expressed DOC1 integrates into NURD (Figure 1J). Next, we examined the effects of DOC1 re-expression in OSCC cells.
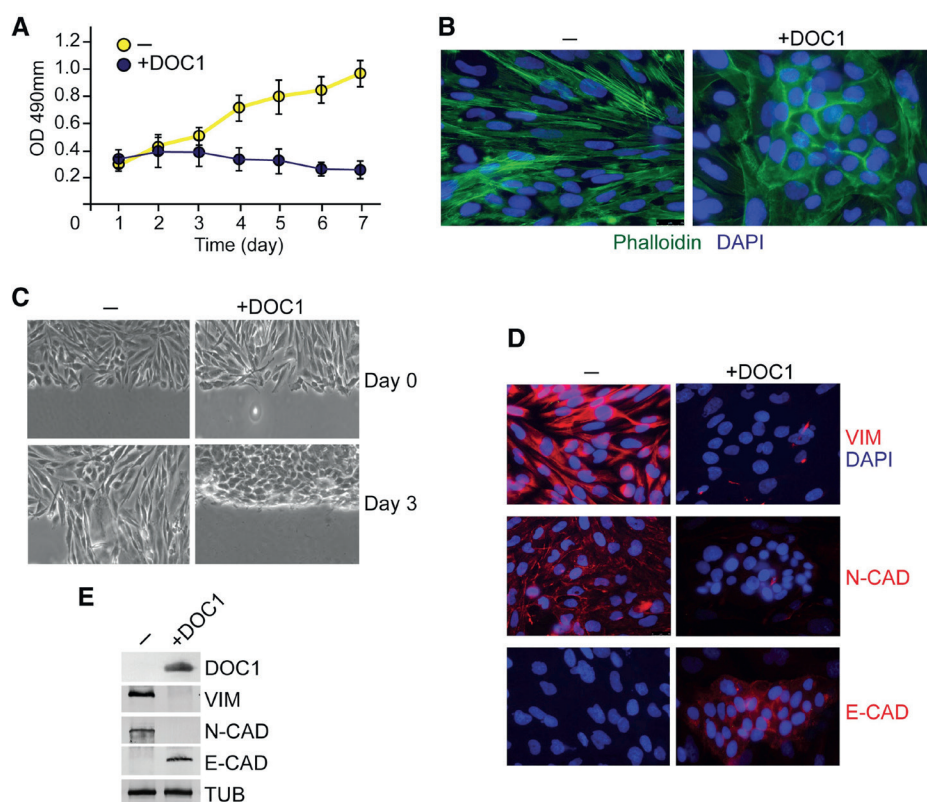
DOC1 attenuates OSCC cell proliferation and induces MET
DOC1 expression in SCC9 cells causes a marked attenuation of cell proliferation (Figure 2A; throughout this paper, yellow graphs refer to mock-treated cells, whereas blue graphs refer to OSCC cells expressing DOC1). We did not observe an arrest at a defined stage of the cell cycle, increased apoptosis or cellular senescence (Figure S2A). Most likely, this is due to the inactivation of the p53- and p16INK4a tumor suppressor pathways in these OSCC cells (http://www.lgcstandards-atcc.org). DOC1 also inhibited proliferation of the other OSCC cell lines (SCC4, SCC15, and SSC25; Figure S2B-D). Surprisingly, DOC1 re-expression induced marked changes in SCC9 cell morphology and actin organization, as visualized by phalloidin staining (Figure 2B). Compared to cells transduced with a control vector, which have a more fibroblast-like appearance, DOC1-expressing cells acquire a more cobblestone-like morphology with epithelial features. Moreover, upon DOC1 expression, prominent stress fibers are replaced by a more cortical actin organization. A scratch test revealed that DOC1 expressing SCC9 cells are less migratory and form layers of

tightly attached cells (Figure 2C). These results suggest that expression of DOC1 induces a mesenchymal-to-epithelial transition (MET). To test this possibility, we examined the expression of a number of canonical EMT markers. Immunofluorescence (IF) microscopy revealed a strong reduction of the mesenchymal markers vimentin (VIM) and N-cadherin (N-CAD) after DOC1 expression, whereas the epithelial marker E-cadherin (E-CAD) was up-regulated (Figure 2D and Figure S2E). The observed changes in expression of these EMT markers were confirmed by immunoblotting (Figure 2E).

In conclusion, we examined the effects of DOC1 re-expression in OSCC cells that lack this integral subunit of NURD. DOC1 efficiently incorporates into NURD, and triggers the differentiation of cells from a quasi-mesenchymal (SCC9 and SCC15) or quasi-epithelial

Figure 2. DOC1 expression causes MET in OSCC cells. (**a**) Re-expression of DOC1 attenuates cell proliferation. Proliferation curves of SCC9 cells transduced with lentiviruses expressing either LacZ (yellow graph) or DOC1 (blue graph), as determined by the Aqueous One Proliferation Assay (Promega). Means and standard error of mean (SEM) were derived from three independent biological replicates. See Figure S2A for cell cycle analysis and Figure S2B-D for additional OSCC cell lines. (**b**) DOC1 affects cell shape and actin organization in OSCC cells. Indirect IF of SCC9 cells that either lack (-) or express DOC1. F-actin was visualized by Phalloidin staining (green), and nuclei were visualized by DAPI staining of DNA (blue). See Figure S2E for other OSCC cell lines. (**c**) DOC1 inhibits migration of SCC9 cells. The effect of DOC1 on migratory behavior of SCC9 cells was tested by a wound healing assay. Light microscopic images were taken directly following scratching a monolayer of cells (day 0) and 3 days later. (**d**) DOC1

induces MET in OSCC cells. Indirect IF of SCC9 cells stained (red) with antibodies against Vimentin (VIM), N-cadherin (N-CAD) and E-cadherin (E-CAD). Nuclei were visualized by DAPI staining of DNA (blue). See Figure S2E for other OSCC cell lines. (**e**) Immunoblotting analysis of the effect of DOC1 on expression of EMT markers. Tubulin serves as a loading control. See also Figure S2.

(SCC4 and SCC25) appearance towards an epithelial phenotype. Therefore, DOC1-induced cell differentiation is strictly speaking a partial MET. For the sake of brevity, however, we will here refer to this process as MET. This transition involves changes in actin organization, cell shape, expression of key EMT markers, reduced cell migration, and attenuated cell proliferation. These observations suggest that loss of DOC1 contributes to the development of OSCC by inhibiting epithelial differentiation and by conferring tumor cells with a mesenchymal-like and possibly more invasive phenotype.

DOC1 functions as part of NURD

To test if the effects of DOC1 re-expression in OSCC cells depend on the chromatin remodeling activity of the NURD complex, we depleted its ATPase CHD4 (Figure 3A). Following shRNA-mediated knockdown of CHD4 in SCC9 cells, DOC1 expression failed to trigger MET. There was no induction of E-CAD, whereas VIM and N-CAD expression was not reduced. Loss of CHD4, in the absence of DOC1 expression, did not affect expression of EMT markers. Irrespective of the presence or absence of DOC1, knockdown of CHD4 led to reduced cell proliferation (Figure 3B). Likewise, depletion of MBD2 or MTA2 caused a loss of cell viability and blocked the ability of DOC1 to promote MET (Figure S3A and B). Thus, once NURD lacks DOC1, loss of additional NURD subunits compromises cell viability, but has little effect on the expression of EMT markers. Thus, the capacity of DOC1 to drive MET depends on NURD, and that cells lacking DOC1 still depend on the remaining NURD for viability.

Next, we used shRNAs to deplete either DOC1, CHD4, MBD2 or MTA2 in HaCaT cells, a spontaneously immortalized, human keratinocyte line (Figure 3C-D and Figure S3C-E). Under our culture conditions HaCaT cells have an epithelial phenotype. Upon knock down of DOC1 or other NURD subunits, there was reduced expression of the epithelial marker E-CAD, whereas the mesenchymal markers N-CAD and VIM were induced (Figure 3C and Figure S3C). In agreement with our earlier results (Figure 1J), loss of DOC1 did not affect the stability of other NURD subunits (Figure S3D). However, loss of MBD2 or MTA2 affected CHD4 levels, suggesting that these subunits are important for the structural integrity of NURD. Importantly, depletion of either DOC1, CHD4, MBD2 or MTA2 caused substantially reduced cell numbers (Figure 3D and Figure S3E). Thus, the intact NURD complex is required for optimal viability of HaCaT cells. Collectively, these observations support the notion that DOC1 functions as an integral part of NURD.

DOC1-dependent recruitment of NURD drives MET

The EMT program is orchestrated by a set of master regulators that form an integrated transcriptional network with extensive cross-regulation. Expression of DOC1 in OSCC cells leads to downregulation of all major EMT transcription factors, concomitant with cell differentiation towards an epithelial phenotype (Figure 4A). To determine which of these might be directly regulated by NURD, we used quantitative chromatin immunoprecipitations (ChIP-qPCR). We monitored CHD4 binding to selected promoter regions in either the absence- or presence of DOC1. CHD4 ChIPs revealed strong DOC1-

dependent binding to the promoters of *Twist1*, *Twist2* and *Zeb2* and weaker binding to the *Snail*, *Slug* and *Zeb1* promoters (Figure 4B). CHD4 binding to 2 previously identified targets of NURD, *Crabp1* and *Rassf10* (Gunter et al., 2013), was independent of DOC1. The binding pattern of DOC1 was similar to that of CHD4 (Figure 4C). Collectively, these results suggest that DOC1 is a gene-selective subunit of NURD, required for the binding and repression of key EMT transcription factor genes.
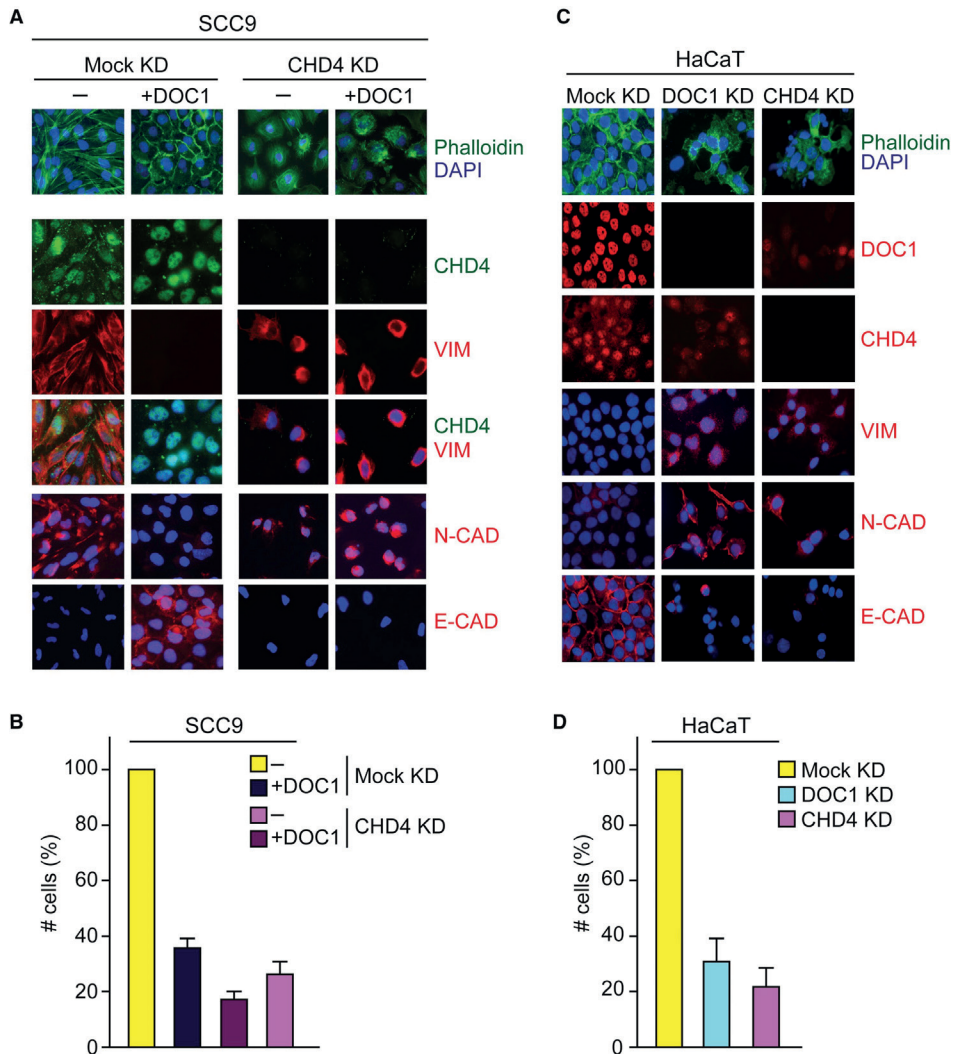

Figure 3. DOC1-induced MET depends on CHD4. (**a**) Indirect IF of SCC9 cells that either lack or express DOC1, in combination with shRNA-mediated knockdown of CHD4. Cells were stained using the indicated antibodies. (**b**) Effects of DOC1 expression in combination with CHD4 KD on cell proliferation were determined 3 days after KD, as described in the legend to Figure 2A. (**c**) Indirect IF of HaCaT cells after KD of DOC1 or CHD4. Cells were stained using the indicated antibodies. (**d**) HaCaT cell numbers were determined 3 days following KD of DOC1 or CHD4. Means and SEM were derived from three independent biological replicates. See also Figure S3.

NURD-mediated repression of crucial master regulators of EMT provides an attractive molecular mechanism to explain DOC1-induced MET in OSCC cells. To test this hypothesis, we transduced lentiviruses that expressed shRNAs directed against either *Twist1* or *Twist2* or a control virus (mock). Depletion of either TWIST1 or TWIST2, in the absence of DOC1 expression, suffices to induce MET, as indicated by actin reorganization, down-regulation of VIM and N-CAD, and induction of E-CAD (Figure 4D-E). TWIST1 and TWIST2 appear both to be required for EMT. As observed for DOC1 re-expression in OSCC cells, loss of TWIST1/2 inhibited cell proliferation (Figure 4F). These results establish that down regulation of TWIST1 or TWIST2 can mimic the main effects of DOC1 re-expression in OSCC cells. These results suggest that DOC1 initiates MET in oral cancer cells by directing NURD to repress master regulators of EMT.

NURD recruitment causes extensive chromatin reorganization

To explore the impact of NURD recruitment on the local chromatin structure, we first determined its precise localization within ~900 bp of the *Twist1* promoter region (-500 to +400 bp, relative to the transcription start site, TSS). ChIP-qPCR revealed DOC1-dependent CHD4 binding, directly upstream of the *Twist1* transcription start site (Figure 5A). Histone H3 ChIPs revealed a prominent nucleosome-depleted region (NDR), in the absence of DOC1 when *Twist1* is expressed (Figure 5B). Following DOC1 expression and NURD binding, there is a dramatic nucleosome repositioning leading to occupancy of the NDR. High resolution MNase sensitivity mapping showed that, in the absence of DOC1, the *Twist1* promoter DNA was highly accessible to nuclease digestion (Figure 5C). In addition, MNase mapping established that the ~250 bp NDR is flanked by well positioned nucleosomes. DOC1 expression induces extensive chromatin reorganization, leading to complete occlusion of the NDR and a shift in the position of the flanking nucleosomes. Thus, DOC1-mediated recruitment of NURD to the *Twist1* promoter induces a switch from an open to closed nucleosomal organization.

In addition to nucleosome remodeling, NURD mediates histone deacetylation. As expected, HDAC1 was readily recruited to the *Twist1* and *Twist2* promoters following DOC1 expression (Figure 5D). Concomitantly, there was a drop in the level of H3K27 acetylation, corrected for histone H3 occupancy (Figure 5E). Similar to the *Twist1* promoter, histone H3 ChIP revealed DOC1-induced nucleosome occupancy at the *Twist2* promoter (Figure 5F). H3K27 deacetylation by NURD has been linked to the recruitment of PRC2 [20]. Indeed, in the presence of DOC1, we observed binding of the PRC2 enzymatic subunit EZH2, accompanied by increased levels of H3K27me3 (Figure 5G-H). Moreover, DOC1 expression was followed by binding of KDM1A, with concomitant loss of H3K4me2 and H3K4me3 (Figure 5I-K). The transfer from an active- to a repressed chromatin state was accompanied by loss of RNA polymerase II (RNAPII; Figure 5L). Similar to what we observed for the *Twist1/2* promoters, DOC1-dependent binding of NURD to the promoter region of *Zeb2* induced formation of a repressive chromatin structure (Figure S4A-K). Thus, NURD recruitment initiates the comprehensive epigenetic reprogramming of the *Twist1/2* and *Zeb2* genes.

Chapter 3
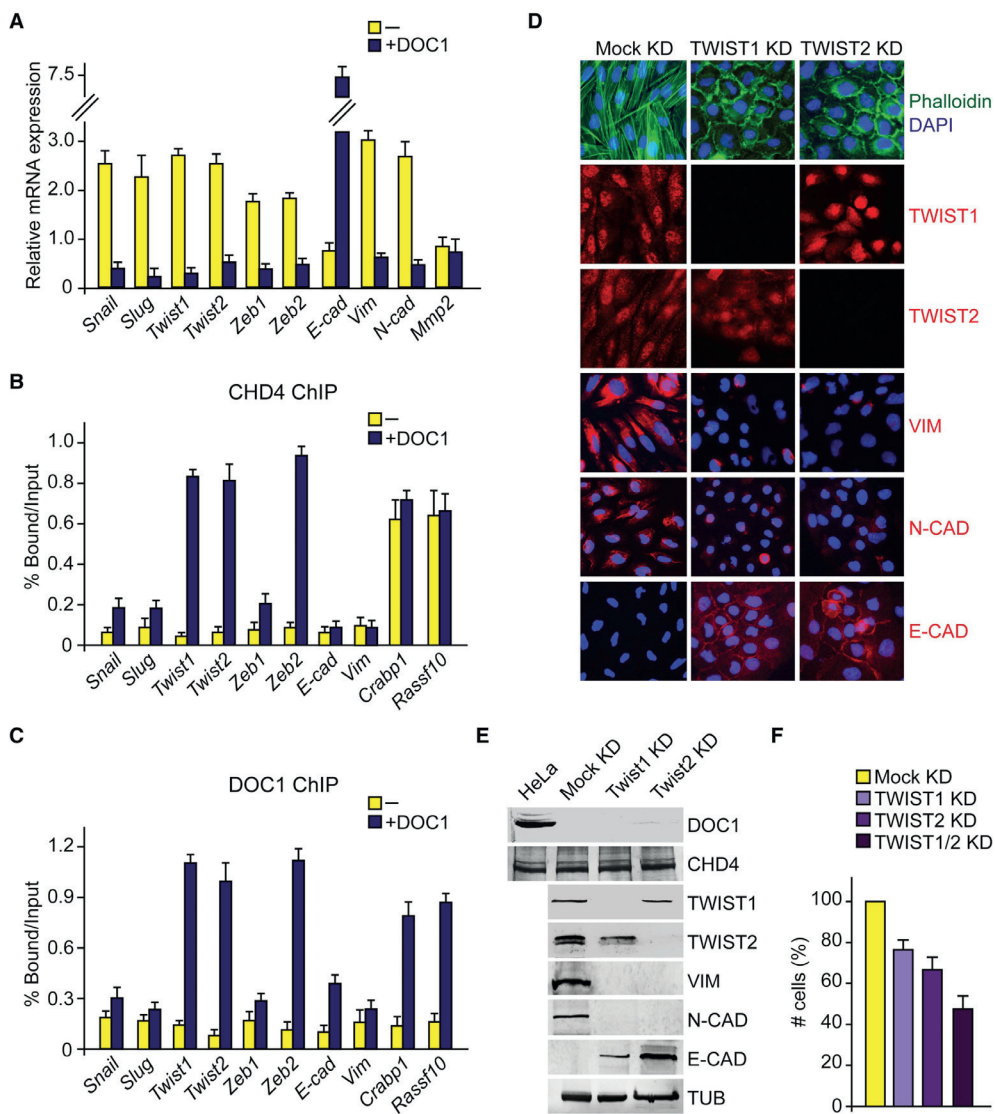
Figure 4. DOC1-mediated repression of *TWIST1/2* drives MET. (**a**) Effect of DOC1 on the expression of EMT transcription factors. mRNA was isolated from SCC9 cells that either lacked- (yellow bars) or expressed DOC1 (blue). Relative levels of mRNA were determined by RT-qPCR. *GAPDH* was used for normalization. Mean and standard deviations (SDs) were derived from three independent biological replicates. (**b**) DOC1 is required for CHD4 binding to the *Twist1*, *Twist2* and *Zeb2* promoters. ChIP-qPCR analysis of DOC1 binding to the promoters of EMT transcription factors, *E-cadherin*, *Vimentin*, *Crabp1* and *Rassf10*. Chromatin was isolated from SCC9 cells that either lacked- (yellow bars) or expressed DOC1 (blue bars). Means and SDs were derived from three independent biological replicates. (**c**) ChIP-qPCR analysis of DOC1 binding. (**d**) Depletion of TWIST1 or TWIST2 suffices for MET. Indirect IF of SCC9 cells after KD of either TWIST1 or TWIST2. Cells were stained with Phalloidin or the indicated antibodies. (**e**) Immunoblotting analysis of the effect of DOC1 on the expression of EMT markers, using antibodies against the indicated proteins. (**f**) Effect of KD of TWIST1 or TWIST2 on cell proliferation were determined 3 days after KD, as described in the legend to Figure 2A. Means and SEM were derived from three independent biological replicates.
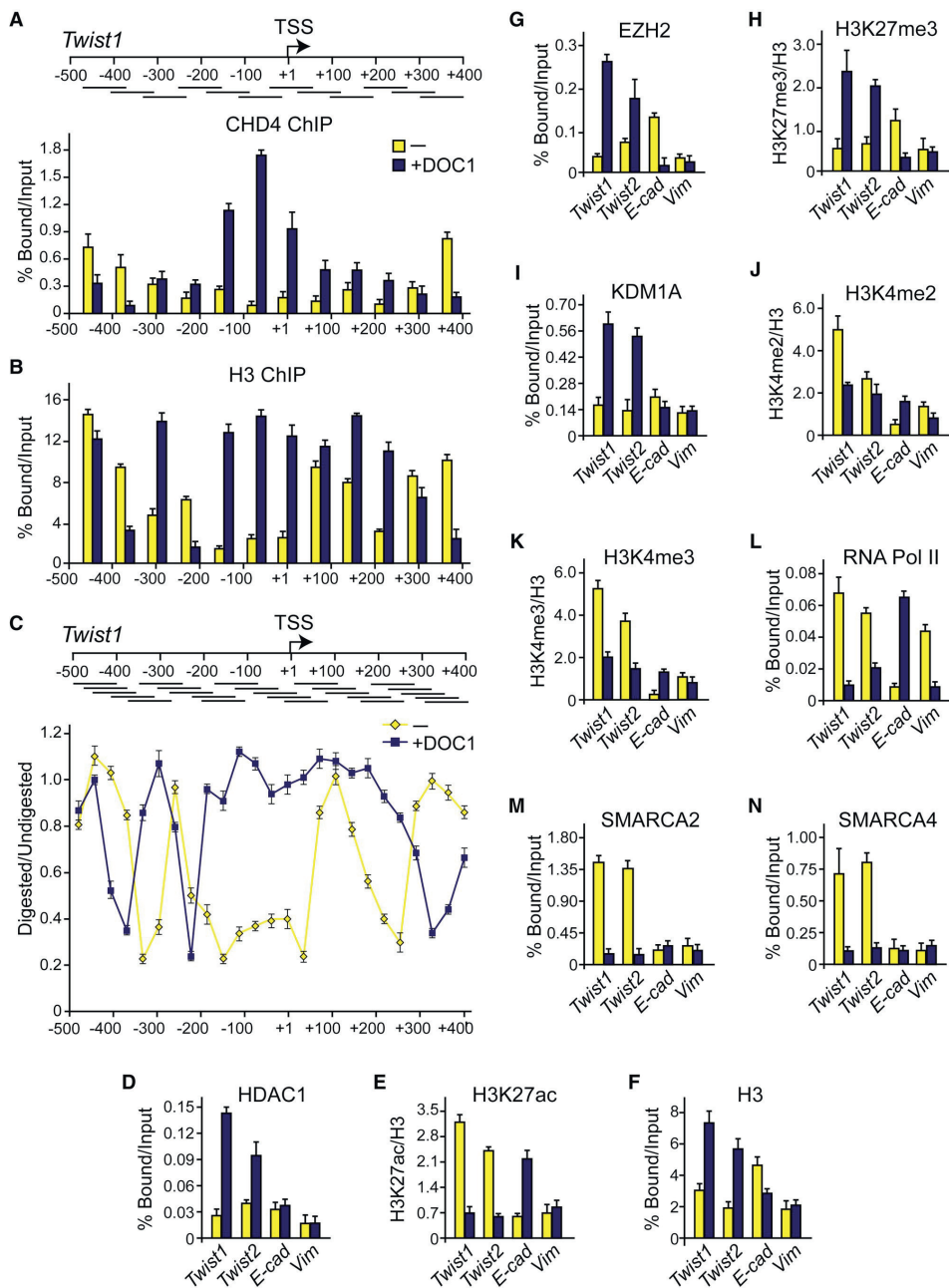
Figure 5. DOC1 directs epigenetic reprogramming of *Twist1/2*. (**a**) DOC1-dependent binding of CHD4 to the *Twist1* promoter region. ChIP-qPCR analysis of CHD4 binding to chromatin isolated from SCC9 cells that either lacked- (yellow bars) or expressed DOC1 (blue bars). The diagram depicts the PCR amplicons used covering position -480 to +400 of the *Twist1* gene. The transcription start site (TSS) is +1. (**b**) Histone H3 ChIP-qPCR. (**c**) DOC1-induced changes in nucleosome organization. High resolution MNase accessibility mapping on chromatin isolated from cells that either lacked- (yellow graph) or expressed

DOC1 (blue graph). The MNase accessibility profile was determined by normalizing the amount of digested PCR product to that of the undigested product using the delta C(t) method. Ratios were plotted against the midpoint of the corresponding PCR amplicons shown in the diagram on top. (**d-n**) ChIP-qPCR analysis of chromatin at the *Twist1*, *Twist1*, *E-cadherin* and *Vimentin* promoters. Chromatin was isolated from SCC9 cells that either lacked- (yellow bars) or expressed DOC1 (blue bars). ChIPs were performed using antibodies directed against the indicated proteins or post-translational modifications. Protein ChIP signals are presented as percentage of input chromatin. Histone modification ChIPs were normalized to H3 signals. Means and SDs for all experiments in this figure were derived from three independent biological replicates. Results for the *Zeb2* promoter are shown in Figure S4.

Previously, we reported that the SWI/SNF remodeler counteracts chromatin binding of Polycomb repressors [34]. Therefore, we wondered whether SWI/SNF might be associated with the active *Twist1/2* and *Zeb2* promoters to prevent Polycomb repression. We performed ChIPs using antibodies directed against either SMARCA4/BRG1 or SMARCA2/hBRM, the mutually exclusive ATPase subunits of SWI/SNF assemblages. Both SMARCA2 and SMARCA4 bound the active *Twist1/2* and *Zeb2* promoters, but were displaced following DOC1-driven binding of NURD (Figure 5M-N and Figure S4L-N). These observations raised the possibility that SWI/SNF and NURD act antagonistically in the control of the *Twist1/2* and *Zeb2* genes.

Loss of SWI/SNF phenocopies the effects of DOC1 re-expression

To test the idea that SWI/SNF and NURD might have opposing effects on the EMT program, we determined the consequences of SWI/SNF depletion in the absence of DOC1 induction. Depletion of either SMARCA2 or SMARCA4 had only weak effects on SCC9 cell phenotype (Figure S5A). However, knockdown of both SWI/SNF ATPases induced a strong MET. Loss of both SMARCA2 and SMARCA4 (SMARCA2/4) led to actin fiber re-organization, and a change from a fibroblast-like morphology to an epithelial cell shape (Figure 6A). We observed downregulation of VIM and N-CAD, whereas E-CAD was induced (Figure 6B and Figure S5B). Moreover, there was a loss of *Twist1/2* and *Zeb2* expression after SMARCA2/4 depletion (Figure 6C; yellow: mock, red: SMARCA2/4 knockdown). Loss of either SMARCA2 or SMARCA4 alone gave an intermediate effect, suggesting that both remodelers stimulate *Twist1/2* and *Zeb2* transcription (Figure S5C). Finally, depletion of SMARCA2/4 led to diminished cell numbers (Figure S5D). Thus, the functional consequences of SWI/SNF depletion are similar to those of DOC1 re-expression: reduced cell proliferation, attenuated expression of EMT transcription factors, and MET. Our results suggest that SWI/SNF and NURD compete for chromatin binding at *Twist1/2* and *Zeb2* promoters and generate opposite transcriptional states. To test this idea, we examined the impact of SWI/SNF depletion on chromatin organization.

Remodeler antagonism controls epigenetic reprogramming of EMT

Both SMARCA2 and SMARCA4 bind to the *Twist1/2* and *Zeb2* promoters (Figure 6D-E and Figure S6B-C). Knockdown of SMARCA2/4 caused a loss of ChIP signals, confirming the specificity of our antibodies. Following SWI/SNF depletion, the NDR disappears and the *Twist1* promoter DNA is now occluded by nucleosomes (Figure 6F, Figure S5E). The pattern of MNase accessibility after knock down of SWI/SNF is remarkably similar to that following DOC1 expression (compare Figures 5C and 6F). CHD4- and HDAC1 ChIPs showed that depletion of SWI/SNF suffices to allow NURD binding to the *Twist1/2* and *Zeb2* promoters, in spite of the absence of DOC1 (Figure 6G, Figure S5F and Figure S6D-E).

These results show that NURD devoid of DOC1 still has an intrinsic, albeit weakened, ability to bind the *Twist1/2* and *Zeb2* promoters. The chromatin changes caused by SWI/SNF depletion are remarkably similar to those observed after DOC1 re-expression (Figure 6H-J and Figure S5G-K and Figure S6F-M). Concomitant with NURD recruitment after SWI/SNF knockdown, the level of H3K27ac dropped, PRC2 binds, and H3K27ac is replaced by H3K27me3. In addition, KDM1A is recruited, accompanied by H3K4 demethylation. In agreement with repression of *Twist1/2* and *Zeb2* transcription, RNAPII is lost following the knockdown of SWI/SNF. Thus, SWI/SNF depletion in OSCC cells has similar effects on the epigenetic setting of EMT master regulators as DOC1 re-expression.

In summary, SWI/SNF prevents the binding of NURD lacking DOC1 to the *Twist1/2* and *Zeb2* promoters. Conversely, upon inclusion of DOC1 in the complex, NURD displaces SWI/SNF. The replacement of SWI/SNF by NURD results in the transition from an open- to a closed chromatin structure. Moreover, chromatin binding by PRC2 is blocked by SWI/SNF, but promoted by NURD. Thus, SWI/SNF and NURD compete for binding and generate opposite chromatin states. We propose that a disturbance in the balance between these antagonistic remodelers can set off a cascade of chromatin reprograming that promotes oncogenesis.

DOC1 assists NURD recruitment to CpG islands

To investigate the impact of DOC1 on the genome-wide binding of NURD, we performed CHD4 ChIP sequencing on chromatin from SCC9 cells. We identified 4,902 CHD4 consensus peaks in DOC1 expressing cells compared to 3,949 in cells lacking DOC1. This observation indicates that DOC1 is important for binding to a subset of NURD loci. We note that the ChIP sequencing uncovered DOC1-dependent binding to additional genes involved in EMT, as illustrated with a few examples in Figure 7A. Analysis of the genomic distribution of CHD4 revealed that about 60% (no DOC1) to 67% (+DOC1) of binding sites corresponds to genic regions, in particular promoters and introns (Figure 7B). DOC1 appears to enhance promoter binding by NURD, which increased from ~23% to ~35% of all mapped binding sites (Figure 7B-C). Strikingly, DOC1 expression led to a substantially higher proportion of CHD4 binding at CpG islands (Figure 7D). Taken together, genome-wide binding analysis confirmed that DOC1 promotes NURD binding to a subset of target loci. In particular, our results support a role for DOC1 in NURD recruitment to CpG islands.

Chapter 3
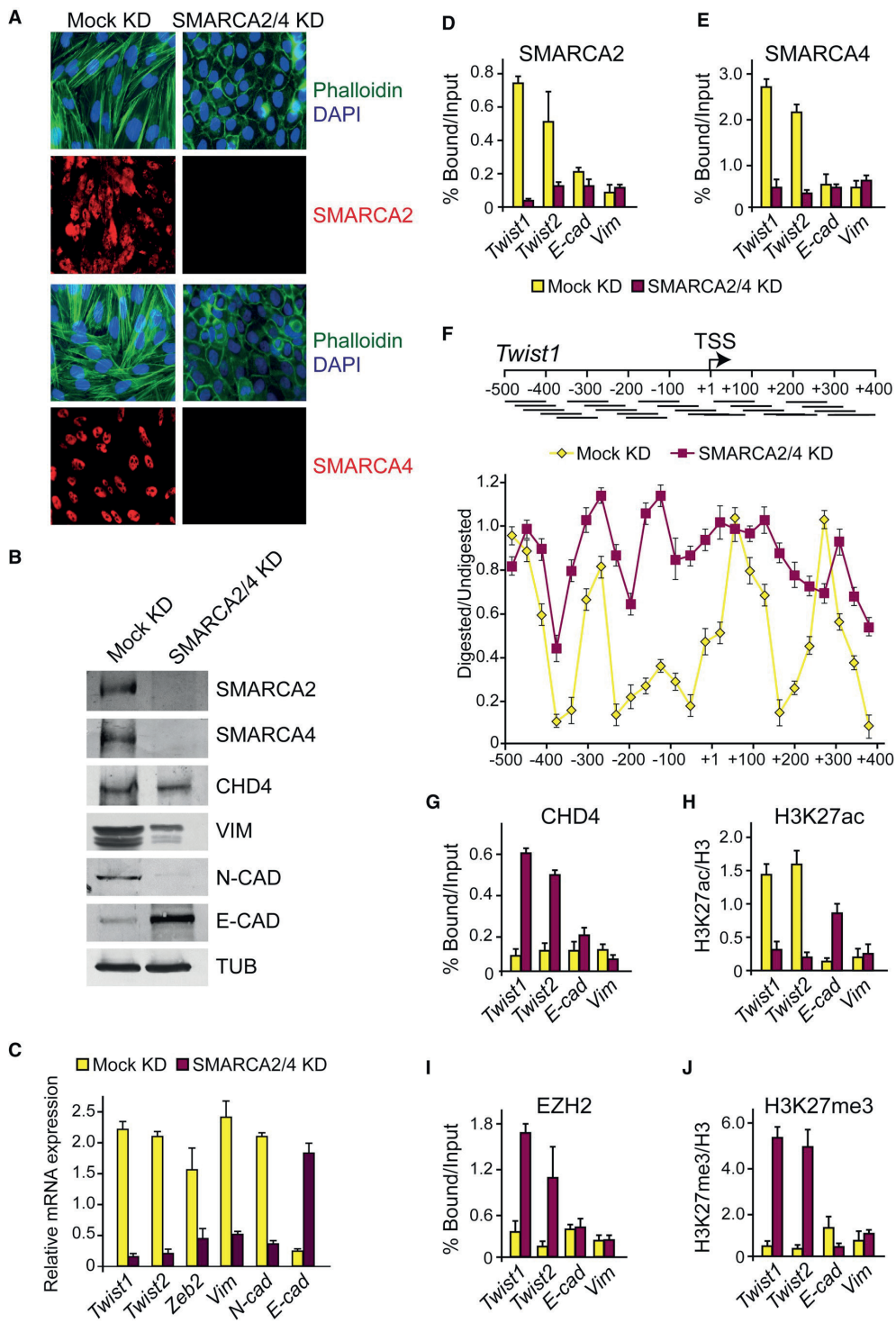
Figure 6. SWI/SNF depletion mimics the effects of DOC1 expression. (**a**) Depletion of SMARCA2 and SMARCA4 affects cell shape and actin organization. Indirect IF of SCC9 cells following either mock KD, or KD of both SMARCA2 and SMARCA4. Cells were stained with antibodies against either SMARCA2 or SMARCA4 (red) F-actin was visualized by Phalloidin staining (green). See Figure S5A for individual KDs. (**b**) Immunoblotting analysis of the effect of SMARCA2/4 KD on EMT markers. See Figure S5B for individual KDs. (**c**) Effect of SMARCA2/4 KD on the mRNA levels of *Twist1*, *Twist2, Zeb2* and markers of EMT, as determined by RT-qPCR. Mock KD: yellow bars, SMARCA2/4 KD: red bars. *GAPDH* was used for normalization. Means and SDs were derived from three independent biological replicates. See Figure S5C-D for individual KDs and effects on cell numbers. (**d-e**) ChIP-qPCR analysis of SMARCA2 and SMARCA4 binding to the *Twist1*/2 promoters following mock KD (yellow bars) or KD of both SMARCA2 and SMARCA4 (red bars). See Figure S6 for ChIP analysis of the *Zeb2* promoter. (**f**) Loss of SMARCA2/4 leads to occupation of the *Twist1* NDR. High resolution MNase accessibility mapping after SMARCA2/4 KD. See legend to Figure 5C for details. (**g-j**) ChIP-qPCR analysis of chromatin at the *Twist1*/2 promoters using antibodies directed against the indicated proteins or post-translational modifications. Protein ChIP signals are presented as percentage of input chromatin. Histone modification ChIPs were normalized to H3 signals. Means and SDs for all experiments in this figure were derived from three independent biological replicates. Additional ChIP data is presented in Figure S5. Results for the *Zeb2* promoter are presented in Figure S6. See also Figure S5 and S6.

Discussion

ATP-dependent chromatin remodelers are frequently mutated in human cancers. However, the molecular basis of the association between mutations in specific remodeler subunits and particular types of cancer is poorly understood. Here, we showed that the loss of DOC1 in oral cancer cells leads to a failure of NURD to bind and repress master transcriptional regulators of EMT. Re-expression of DOC1 in OSCC cells restores NURD recruitment to key target genes, a switch from open- to closed chromatin, transcriptional repression, and reversal of EMT (MET). Consistent with the transcriptional repression we observed after DOC1-dependent NURD recruitment, the OSCC cells we studied harbor MBD2-NURD (Figure1), the NURD variant implicated in the formation of repressivechromatin [13]. In agreement with its effects in OSCC cells, depletion of DOC1 in HaCaT keratinocytes leads to the induction of EMT, but also in decreased cell proliferation (Figure 3). Moreover, knockdown of DOC1 in primary human fibroblasts induces p53-dependent cellular senescence [35]. Thus, in spite of its role as a tumor suppressor, loss of DOC1 normally blocks- rather than stimulates cell proliferation. In all 4 OSCC cell lines we studied here, both the *p53*- and the *INK4a* tumor suppressor pathways have been compromised. We speculate that, during the development of oral cancer, DOC1 is lost after the inactivation of p53 and INK4a. The loss of DOC1 will then contribute to oncogenesis through transcriptional de-repression, EMT and further loss of proliferation control. Our genome-wide binding site analysis showed that DOC1 is crucial for NURD recruitment to a subset of target loci. In particular, these experiments suggested a role for DOC1 in NURD binding to promoter regions harboring CpG islands. We did not investigate the effect of DNA methylation, but in vitro experiments suggested that DOC1 is not directly involved in recognition of methylated CpG residues [15]. Alternatively, DOC1 may interact with specific sequence-selective transcription factors.
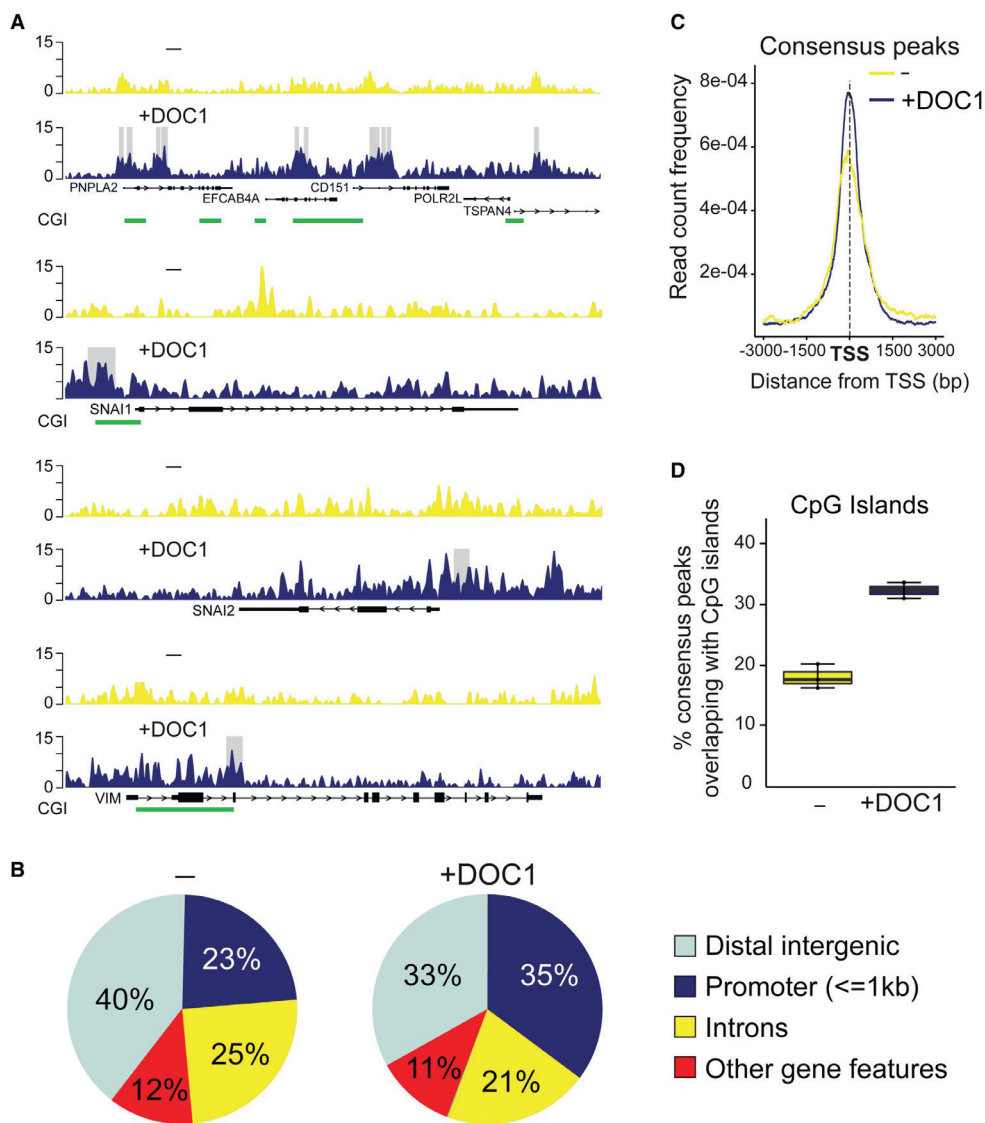
Figure 7. DOC1 promotes NURD binding to a subset of loci. (**a**) Genome browser track examples illustrating DOC1-dependent binding of CHD4 to CpG islands (CGI, green) and the *Snail* (*SNAI1*), *Slug* (*SNAI2*) and *Vimentin* genes. Read coverage of CHD4 ChIPs in the absence (yellow) or presence of DOC1 (blue). MACS2-called peaks are highlighted as gray bars. (**b**) Distribution of CHD4 consensus peaks to their nearest genomic feature. CHD4 ChIP sequencing on chromatin from SCC9 cells that either lack or express DOC1. Genomic features that corresponded to <4 percent of total peaks were aggregated into "other gene features" comprising: exons, 1-3 kb from promoter, 5' UTR, ≤3kb downstream and 3' UTR. Consensus peaks were derived from 3 (-DOC1) or 2 (+DOC1) biological replicates. (**c**) Averaged CHD4 peak density (read count frequency) around the aligned TSS of all known human genes (UCSC, hg19). –DOC1: yellow, +DOC1: blue. (**d**) Boxplots representing the relative frequency of ChIP-Seq peaks on human CpG islands.

Our results revealed that, rather than working on a naïve template, remodelers compete for access to chromatin. DOC1-mediated NURD binding to the *Twist1/2* and *Zeb2* promoters leads to eviction of SWI/SNF, and a transition from active- to repressive chromatin. This process involves nucleosome repositioning onto the NDR, histone deacetylation, recruitment of PRC2 and KDM1A with their associated histone modifications, and shut down of transcription. Remarkably, all these effects of DOC1 expression could be mimicked by SWI/SNF depletion. In the absence of SWI/SNF, the NURD complex lacking DOC1 could bind the *Twist1/2* and *Zeb2* promoters. These observations suggest that these promoters are always targeted by a remodeler. Binding of either SWI/SNF or NURD determines opposite epigenetic states, thereby committing OSCC cells to either EMT or MET.

There are interesting parallels between our results in oral cancer cells and findings in other systems. In embryonic stem cells, SWI/SNF and NURD can have reverse effects on the nucleosome organization of shared targets [36,37]. Moreover, NURD has been implicated in Polycomb repression in flies and mice [19,20,38,39]. The link between NURD and Polycomb might involve a direct molecular mechanism, e.g. H3K27 deacetylation by NURD might promote PRC2 binding [20]. Alternatively, transcriptional repression by NURD might allow the default binding of PRC2 to CpG islands of silenced genes [40]. Our results in OSCC cells emphasize the importance of the dynamic balance between NURD, Polycomb and SWI/SNF function in human cancer.

It is instructive to compare the function of DOC1 in OSCC with that of the SWI/SNF subunit SMARCB1/hSNF5 in malignant rhabdoid tumors (MRT). MRT is an extremely aggressive pediatric cancer caused by the loss of SMARCB1 [8,41]. The absence of SMARCB1 precludes SWI/SNF binding to key tumor suppressor genes, leading to a failure to block Polycomb repression [34,42]. We showed previously that re-expression of SMARCB1 in MRT cells restores SWI/SNF recruitment, causing Polycomb eviction, and activation of the *p16INK4a* and *p15INK4b* tumor suppressors [34]. Thus, in contrast to NURD, SWI/SNF antagonizes Polycomb repression. Although the loss of DOC1 in OSCC or that of SMARCB1 in MRT generates opposite epigenetic states of their target genes, in both cases this is caused by failed remodeler recruitment. The loss of a single subunit, such as DOC1 or SMARCB1, does not abrogate all other remodeler functions. For example, OSCC cells are still dependent on CHD4, MBD2 and MTA2 (Figure 3 and Figure S3) and MRT cells require SMARCA4 for survival [43].

We suggest that subunit-dependent gene-selection is a major cause of the association between the loss of specific remodeler subunits and particular types of cancer. Our results emphasize that gene control involves a dynamic equilibrium between opposing chromatin modulating enzymes rather than a static chromatin state. Disturbances in this balance can initiate a cascade of chromatin reprogramming events that drives oncogenesis. Such an intertwined system of epigenetic regulation suggests therapeutic strategies aimed at restoring the balance between antagonistic activities.

Experimental Procedures

Cell-Based Assays

Tumor analysis and IF were performed using standard procedures. FLAG-tagged DOC1 was expressed using lentiviral transduction followed by selection for expression of the

lentiviral vector with blasticidin. DOC1-expressing cells were analyzed 2-10 days after transduction, but typically at day 4. shRNAs for knockdown experiments were delivered by lentiviral transduction, cells were selected for blasticidin resistance and analyzed 4 days after transduction. For the wound healing assay, cells were plated to confluence and then a scratch was introduced with a pipette tip. Images were captured at 0 and 72 hours following scratching. Cell numbers were determined by Aqueous One Solution Cell Proliferation Assay (Promega). Means and SEMs were derived from three independent biological replicates. See the Supplemental Experimental Procedures for details, cloning, sequences and antibodies used.

Biochemical procedures

Most procedures were performed essentially as described [44]. Whole cell extracts (WCE) were prepared by sonication in RIPA buffer (50mM Tris pH 7.5, 150mM NaCl, 0.1% SDS v/v, 0.5% deoxycholate v/v, 1% NP-40 v/v, and protease inhibitors). Excess debris was removed by centrifugation. For IPs, WCE, prepared from ~10^7 cells was incubated with antibodies crosslinked to Protein A-Sepharose beads (Sigma), followed by sequential washes with HEMG/300 buffer (25mM HEPES-KOH [pH 7.6], 0.1 mM EDTA, 12.5 mM MgCl$_2$, 10% glycerol, 0.1% NP-4, 300 mM KCl and protease inhibitors), followed by washes with HEMG/600 and finally HEMG/100. Bound proteins were eluted by pH shock with Glycine buffer (100 mM glycine, 150 mM NaCl, pH 2.5). For mass spectrometric analyses, proteins were TCA precipitated, resolved by SDS-PAGE, processed and analyzed by nanoflow liquid chromatography tandem mass spectrometry as described [45]. For coIP-Western experiments, cell extracts were incubated with antibodies crosslinked to Protein A-Sepharose beads. Beads were washed with HEMG/400 mM NaCl, HEMG/200 and then bound proteins were dissolved in SDS loading buffer. Proteins were resolved by SDS-PAGE followed by immunoblotting. See the Supplemental Experimental Procedures for details and a list of antibodies used.

Chromatin analysis and RNA procedures

ChIPs were performed using standard procedures. ChIP using species- and isotype-matched immunoglobulins were used to determine background levels. qPCR analyses were performed on immunoprecipitated DNA. The enrichment of specific DNA sequences was calculated by using the ΔCT method. All ChIP data presented are the result of at least 3 biological replicate experiments and triplicate qPCR reactions. Results were averaged, and standard errors were determined. ChIPs against histone marks were normalized against histone H3. High resolution MNase mapping was performed essentially as described [46,47]. For ChIP sequencing, samples from 3 biological replicates were prepared according to the NEXTflex ChIP-Seq kit (Bioo Scientific). ChIP libraries were sequenced according to the Illumina TruSeq Rapid v2 protocol on the HiSeq2500. Trimmed ChIP-Seq reads were aligned to the human genome (hg19). Narrow peak calling was performed by MACS2 with a q-value cutoff of 0.01 using mock controls (-_IgG/+DOC1_IgG) per sample to reduce background noise and artifacts. One experiment (+DOC1, replicate # 2) was removed from further analysis due to quality concerns. Consensus peak sets per condition (-, +DOC1) were generated using DiffBind (v2.2.8). Peaks were annotated using ChIPseeker (v1.10.3) and UCSC hg19 annotations. For gene expression analysis, total RNA was isolated using the TriPure Isolation reagent (Roche Diagnostics). RT was carried out on ~1 μg of total RNA

using Superscript II RNase H-reverse transcriptase (Invitrogen) and oligo(dT)- or random hexamer primers. Quantitative real time PCR (MyIQ; Bio-Rad) was performed with GoTaq® qPCR Master Mix (Promega). *Gapdh* was used for normalization. See the Supplemental Experimental Procedures for details and a list of antibodies used.

Accession numbers: The ChIPseq data reported here has been submitted to the GEO database under accession number GSE97839.

Supplemental information: Supplemental information includes 6 figures, 1 Table and Supplemental Experimental Procedures.

Authors contributions: A.M.-S. and C.P.V. designed the research, analyzed the results and wrote the manuscript, with input from all other authors. A.M.-S. performed all molecular- and cellular assays. A.G.B. and D.Z. assisted with the IPs, IF and cell culture. K.B. and J.A.D. performed the proteomic analysis. M.T., R.F., M.J.D.H., S.M.W., R.J.B.d.J. and L.H.J.L. were responsible for the oral cancer analysis. W.F.J.v.I. and E.O. performed next generation sequencing. J.v.R. and H.J.G.v.d.W. performed analysis of ChIP-Seq data.

References

1. Luger, K.; Mader, A.W.; Richmond, R.K.; Sargent, D.F.; Richmond, T.J. Crystal structure of the nucleosome core particle at 2.8 A resolution. *Nature* **1997**, *389*, 251-260, doi:10.1038/38444.

2. Becker, P.B.; Workman, J.L. Nucleosome remodeling and epigenetics. *Cold Spring Harb Perspect Biol* **2013**, *5*, doi:10.1101/cshperspect.a017905.

3. Narlikar, G.J.; Sundaramoorthy, R.; Owen-Hughes, T. Mechanisms and functions of ATP-dependent chromatin-remodeling enzymes. *Cell* **2013**, *154*, 490-503, doi:10.1016/j.cell.2013.07.011.

4. Patel, D.J.; Wang, Z. Readout of epigenetic modifications. *Annu Rev Biochem* **2013**, *82*, 81-118, doi:10.1146/annurev-biochem-072711-165700.

5. Zentner, G.E.; Henikoff, S. Regulation of nucleosome dynamics by histone modifications. *Nat Struct Mol Biol* **2013**, *20*, 259-266, doi:10.1038/nsmb.2470.

6. Swygert, S.G.; Peterson, C.L. Chromatin dynamics: interplay between remodeling enzymes and histone modifications. *Biochim Biophys Acta* **2014**, *1839*, 728-736, doi:10.1016/j.bbagrm.2014.02.013.

7. Laugesen, A.; Helin, K. Chromatin repressive complexes in stem cells, development, and cancer. *Cell Stem Cell* **2014**, *14*, 735-751, doi:10.1016/j.stem.2014.05.006.

8. Masliah-Planchon, J.; Bieche, I.; Guinebretiere, J.M.; Bourdeaut, F.; Delattre, O. SWI/SNF chromatin remodeling and human malignancies. *Annu Rev Pathol* **2015**, *10*, 145-171, doi:10.1146/annurev-pathol-012414-040445.

9. Morgan, M.A.; Shilatifard, A. Chromatin signatures of cancer. *Genes Dev* **2015**, *29*, 238-249, doi:10.1101/gad.255182.114.

10. Kolla, V.; Naraparaju, K.; Zhuang, T.; Higashi, M.; Kolla, S.; Blobel, G.A.; Brodeur, G.M. The tumour suppressor CHD5 forms a NuRD-type chromatin remodelling complex. *Biochem J* **2015**, *468*, 345-352, doi:10.1042/BJ20150030.

11. Torchy, M.P.; Hamiche, A.; Klaholz, B.P. Structure and function insights into the NuRD chromatin remodeling complex. *Cell Mol Life Sci* **2015**, *72*, 2491-2507, doi:10.1007/s00018-015-1880-8.

12. Menafra, R.; Stunnenberg, H.G. MBD2 and MBD3: elusive functions and mechanisms. *Front Genet* **2014**, *5*, 428, doi:10.3389/fgene.2014.00428.

13. Gunther, K.; Rust, M.; Leers, J.; Boettger, T.; Scharfe, M.; Jarek, M.; Bartkuhn, M.; Renkawitz, R. Differential roles for MBD2 and MBD3 at methylated CpG islands, active promoters and binding to exon sequences. *Nucleic Acids Res* **2013**, *41*, 3010-3021, doi:10.1093/nar/gkt035.

14. Reddy, B.A.; Bajpe, P.K.; Bassett, A.; Moshkin, Y.M.; Kozhevnikova, E.; Bezstarosti, K.; Demmers, J.A.; Travers, A.A.; Verrijzer, C.P. Drosophila transcription factor Tramtrack69 binds MEP1 to recruit the chromatin remodeler NuRD. *Mol Cell Biol* **2010**, *30*, 5234-5244, doi:10.1128/MCB.00266-10.

15. Spruijt, C.G.; Bartels, S.J.; Brinkman, A.B.; Tjeertes, J.V.; Poser, I.; Stunnenberg, H.G.; Vermeulen, M. CDK2AP1/DOC-1 is a bona fide subunit of the Mi-2/NuRD complex. *Mol Biosyst* **2010**, *6*, 1700-1706, doi:10.1039/c004108d.

16. Shintani, S.; Ohyama, H.; Zhang, X.; McBride, J.; Matsuo, K.; Tsuji, T.; Hu, M.G.; Hu, G.; Kohno, Y.; Lerman, M., et al. p12(DOC-1) is a novel cyclin-dependent kinase 2-associated protein. *Mol Cell Biol* **2000**, *20*, 6300-6307, doi:10.1128/mcb.20.17.6300-6307.2000.

17. Wong, D.T.; Kim, J.J.; Khalid, O.; Sun, H.H.; Kim, Y. Double edge: CDK2AP1 in cell-cycle regulation and epigenetic regulation. *J Dent Res* **2012**, *91*, 235-241, doi:10.1177/0022034511420723.

Chapter 3

18.   Kim, Y.; McBride, J.; Kimlin, L.; Pae, E.K.; Deshpande, A.; Wong, D.T. Targeted inactivation of p12, CDK2 associating protein 1, leads to early embryonic lethality. *PLoS One* **2009**, *4*, e4518, doi:10.1371/journal.pone.0004518.

19.   Morey, L.; Brenner, C.; Fazi, F.; Villa, R.; Gutierrez, A.; Buschbeck, M.; Nervi, C.; Minucci, S.; Fuks, F.; Di Croce, L. MBD3, a component of the NuRD complex, facilitates chromatin alteration and deposition of epigenetic marks. *Mol Cell Biol* **2008**, *28*, 5912-5923, doi:10.1128/MCB.00467-08.

20.   Reynolds, N.; Salmon-Divon, M.; Dvinge, H.; Hynes-Allen, A.; Balasooriya, G.; Leaford, D.; Behrens, A.; Bertone, P.; Hendrich, B. NuRD-mediated deacetylation of H3K27 facilitates recruitment of Polycomb Repressive Complex 2 to direct gene repression. *EMBO J* **2012**, *31*, 593-605, doi:10.1038/emboj.2011.431.

21.   Whyte, W.A.; Bilodeau, S.; Orlando, D.A.; Hoke, H.A.; Frampton, G.M.; Foster, C.T.; Cowley, S.M.; Young, R.A. Enhancer decommissioning by LSD1 during embryonic stem cell differentiation. *Nature* **2012**, *482*, 221-225, doi:10.1038/nature10805.

22.   dos Santos, R.L.; Tosti, L.; Radzisheuskaya, A.; Caballero, I.M.; Kaji, K.; Hendrich, B.; Silva, J.C. MBD3/NuRD facilitates induction of pluripotency in a context-dependent manner. *Cell Stem Cell* **2014**, *15*, 102-110, doi:10.1016/j.stem.2014.04.019.

23.   Hu, G.; Wade, P.A. NuRD and pluripotency: a complex balancing act. *Cell Stem Cell* **2012**, *10*, 497-503, doi:10.1016/j.stem.2012.04.011.

24.   Lai, A.Y.; Wade, P.A. Cancer biology and NuRD: a multifaceted chromatin remodelling complex. *Nat Rev Cancer* **2011**, *11*, 588-596, doi:10.1038/nrc3091.

25.   Signolet, J.; Hendrich, B. The function of chromatin modifiers in lineage commitment and cell fate specification. *FEBS J* **2015**, *282*, 1692-1702, doi:10.1111/febs.13132.

26.   Todd, R.; McBride, J.; Tsuji, T.; Donoff, R.B.; Nagai, M.; Chou, M.Y.; Chiang, T.; Wong, D.T. Deleted in oral cancer-1 (doc-1), a novel oral tumor suppressor gene. *FASEB J* **1995**, *9*, 1362-1370, doi:10.1096/fasebj.9.13.7557027.

27.   Shintani, S.; Mihara, M.; Terakado, N.; Nakahara, Y.; Matsumura, T.; Kohno, Y.; Ohyama, H.; McBride, J.; Kent, R.; Todd, R., et al. Reduction of p12DOC-1 expression is a negative prognostic indicator in patients with surgically resected oral squamous cell carcinoma. *Clin Cancer Res* **2001**, *7*, 2776-2782.

28.   Winter, J.; Pantelis, A.; Reich, R.; Jepsen, S.; Allam, J.P.; Novak, N.; Wenghoefer, M. Risk estimation for a malignant transformation of oral lesions by S100A7 and Doc-1 gene expression. *Cancer Invest* **2011**, *29*, 478-484, doi:10.3109/07357907.2011.597813.

29.   Choi, M.G.; Sohn, T.S.; Park, S.B.; Paik, Y.H.; Noh, J.H.; Kim, K.M.; Park, C.K.; Kim, S. Decreased expression of p12 is associated with more advanced tumor invasion in human gastric cancer tissues. *Eur Surg Res* **2009**, *42*, 223-229, doi:10.1159/000208521.

30.   Hiyoshi, Y.; Watanabe, M.; Hirashima, K.; Karashima, R.; Sato, N.; Imamura, Y.; Nagai, Y.; Yoshida, N.; Toyama, E.; Hayashi, N., et al. p12CDK2-AP1 is associated with tumor progression and a poor prognosis in esophageal squamous cell carcinoma. *Oncol Rep* **2009**, *22*, 35-39, doi:10.3892/or_00000403.

31.   Wu, L.C.; Chen, Y.L.; Wu, W.R.; Li, C.F.; Huang, H.Y.; Lee, S.W.; Chang, S.L.; Lin, C.Y.; Chen, Y.H.; Hsu, H.P., et al. Expression of cyclin-dependent kinase 2-associated protein 1 confers an independent prognosticator in nasopharyngeal carcinoma: a cohort study. *J Clin Pathol* **2012**, *65*, 795-801, doi:10.1136/jclinpath-2012-200893.

32.   Puisieux, A.; Brabletz, T.; Caramel, J. Oncogenic roles of EMT-inducing transcription factors. *Nat Cell Biol* **2014**, *16*, 488-494, doi:10.1038/ncb2976.

33.   Ye, X.; Weinberg, R.A. Epithelial-Mesenchymal Plasticity: A Central Regulator of Cancer Progression. *Trends Cell Biol* **2015**, *25*, 675-686, doi:10.1016/j.tcb.2015.07.012.

34.   Kia, S.K.; Gorski, M.M.; Giannakopoulos, S.; Verrijzer, C.P. SWI/SNF mediates polycomb eviction and epigenetic reprogramming of the INK4b-ARF-INK4a locus. *Mol Cell Biol* **2008**, *28*, 3457-3464, doi:10.1128/MCB.02019-07.

35.   Alsayegh, K.N.; Gadepalli, V.S.; Iyer, S.; Rao, R.R. Knockdown of CDK2AP1 in primary human fibroblasts induces p53 dependent senescence. *PLoS One* **2015**, *10*, e0120782, doi:10.1371/journal.pone.0120782.

36.   Hainer, S.J.; Fazzio, T.G. Regulation of Nucleosome Architecture and Factor Binding Revealed by Nuclease Footprinting of the ESC Genome. *Cell Rep* **2015**, *13*, 61-69, doi:10.1016/j.celrep.2015.08.071.

37.   Yildirim, O.; Li, R.; Hung, J.H.; Chen, P.B.; Dong, X.; Ee, L.S.; Weng, Z.; Rando, O.J.; Fazzio, T.G. Mbd3/NURD complex regulates expression of 5-hydroxymethylcytosine marked genes in embryonic stem cells. *Cell* **2011**, *147*, 1498-1510, doi:10.1016/j.cell.2011.11.054.

38.   Kehle, J.; Beuchle, D.; Treuheit, S.; Christen, B.; Kennison, J.A.; Bienz, M.; Muller, J. dMi-2, a hunchback-interacting protein that functions in polycomb repression. *Science* **1998**, *282*, 1897-1900, doi:10.1126/science.282.5395.1897.

39.   Sparmann, A.; Xie, Y.; Verhoeven, E.; Vermeulen, M.; Lancini, C.; Gargiulo, G.; Hulsman, D.; Mann, M.; Knoblich, J.A.; van Lohuizen, M. The chromodomain helicase Chd4 is required for Polycomb-mediated inhibition of astroglial differentiation. *EMBO J* **2013**, *32*, 1598-1612, doi:10.1038/emboj.2013.93.

40.   Riising, E.M.; Comet, I.; Leblanc, B.; Wu, X.; Johansen, J.V.; Helin, K. Gene silencing triggers polycomb repressive complex 2 recruitment to CpG islands genome wide. *Mol Cell* **2014**, *55*, 347-360, doi:10.1016/j.molcel.2014.06.005.

41.   Wilson, B.G.; Roberts, C.W. SWI/SNF nucleosome remodellers and cancer. *Nat Rev Cancer* **2011**, *11*, 481-492, doi:10.1038/nrc3068.

42.   Wilson, B.G.; Wang, X.; Shen, X.; McKenna, E.S.; Lemieux, M.E.; Cho, Y.J.; Koellhoffer, E.C.; Pomeroy, S.L.; Orkin, S.H.; Roberts, C.W. Epigenetic antagonism between polycomb and SWI/SNF complexes during oncogenic transformation. *Cancer Cell* **2010**, *18*, 316-328, doi:10.1016/j.ccr.2010.09.006.

43.   Wang, X.; Sansam, C.G.; Thom, C.S.; Metzger, D.; Evans, J.A.; Nguyen, P.T.; Roberts, C.W. Oncogenesis caused by loss of the SNF5 tumor suppressor is dependent on activity of BRG1, the ATPase of the SWI/SNF chromatin remodeling complex. *Cancer Res* **2009**, *69*, 8094-8101, doi:10.1158/0008-5472.CAN-09-0733.

44.   Chalkley, G.E.; Verrijzer, C.P. Immuno-depletion and purification strategies to study chromatin-remodeling factors in vitro. *Methods Enzymol* **2004**, *377*, 421-442, doi:10.1016/S0076-6879(03)77028-1.

45.   Moshkin, Y.M.; Kan, T.W.; Goodfellow, H.; Bezstarosti, K.; Maeda, R.K.; Pilyugin, M.; Karch, F.; Bray, S.J.; Demmers, J.A.; Verrijzer, C.P. Histone chaperones ASF1 and NAP1 differentially modulate removal of active histone marks by LID-RPD3 complexes during NOTCH silencing. *Mol Cell* **2009**, *35*, 782-793, doi:10.1016/j.molcel.2009.07.020.

46.   Rafati, H.; Parra, M.; Hakre, S.; Moshkin, Y.; Verdin, E.; Mahmoudi, T. Repressive LTR nucleosome positioning by the BAF complex is required for HIV latency. *PLoS Biol* **2011**, *9*, e1001206, doi:10.1371/journal.pbio.1001206.

47.   Sekinger, E.A.; Moqtaderi, Z.; Struhl, K. Intrinsic histone-DNA interactions and low nucleosome density are important for preferential accessibility of promoter regions in yeast. *Mol Cell* **2005**, *18*, 735-748, doi:10.1016/j.molcel.2005.05.003.

Chapter 3

Supplementary figures
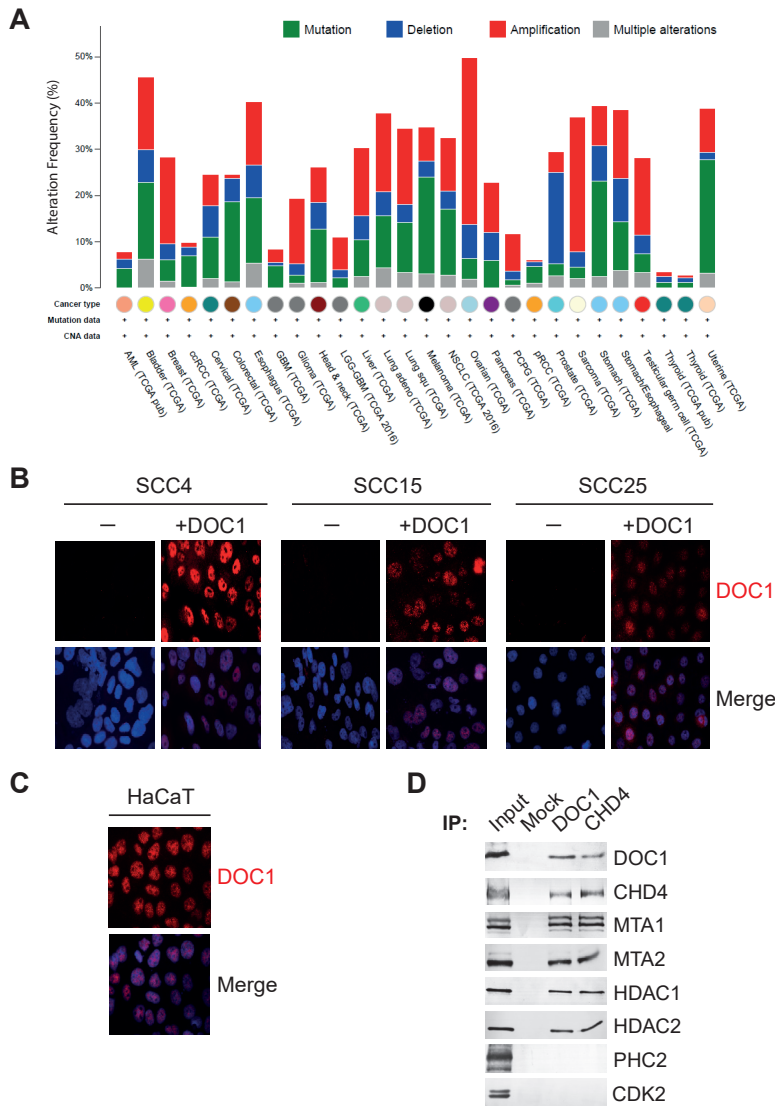
Figure S1. DOC1 is lost in OSCC cells. Related to Figure 1. (**a**) Genomic analysis of NURD alterations in human cancer. Genomic alterations in NURD subunits (CHD3/4/5, DOC1/CDK2AP1, MTA1/2/3, GATAD2A/B, HDAC1/2, RBBP4/7 and MBD2/3) in a selection of studies from The Cancer Genome Atlas network and visualized using the cBioPortal for Cancer Genomics (http://www.cbioportal.org; Cerami et al., 2012; Gao et al., 2013). Note that some cancers associate with frequent mutations in NURD, whereas in others alterations are rare. Green: mutation, blue: deletion, red: amplification and grey: multiple alterations. (**b**) DOC1 is absent in human OSCC cell lines. Indirect IF microscopy of SCC4, SCC15 and SCC25 cells transduced with lentiviruses expressing either an irrelevant control (LacZ, -) or DOC1. Cells were fixed and stained with antibodies against DOC1 (red). Nuclei were visualized by DAPI staining of DNA (blue). (**c**) Nuclear DOC1 expression in HaCaT keratinocytes. (**d**) Co-IPs of endogenous DOC1 or CHD4 from HeLa cells. Associated proteins were detected by immunoblotting with antibodies against the indicated proteins. Input represents 10% of the binding reactions.
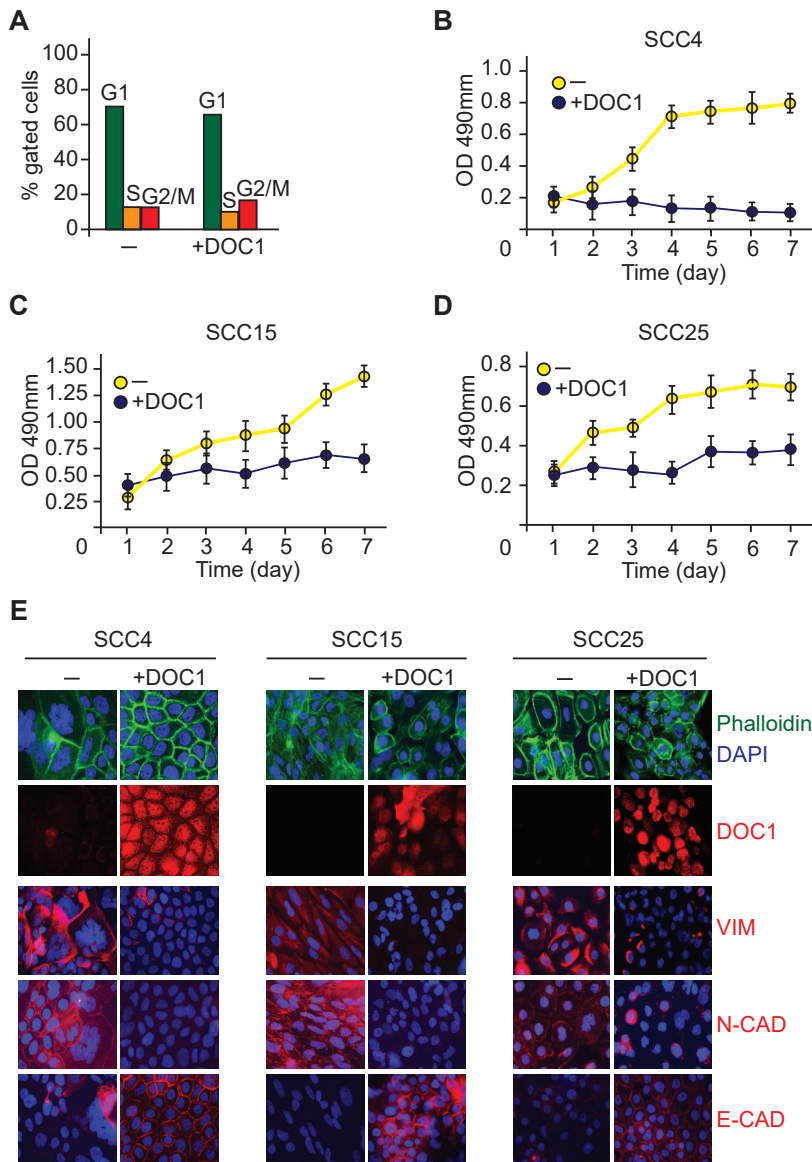
Figure S2. DOC1 expression causes MET in OSCC cells. Related to Figure 2. (**a**) Cell cycle profiles of SCC9 cells transduced with lentiviruses expressing either LacZ (yellow graph) or DOC1 (blue graph), as determined by FACS analysis. Quantification is based on gated cells. The percentage of cells in G1, S or G2/M phases and corresponding peaks are indicated. (**b-d**) Re-expression of DOC1 attenuates OSCC cell proliferation. Proliferation curves of SCC4, SCC15 and SCC25 cells transduced with lentiviruses expressing either LacZ (yellow graph) or DOC1 (blue graph), as determined by the Aqueous One Proliferation Assay (Promega). Means and standard error of mean (SEM) were derived from three independent biological replicates. (**e**) DOC1 induces MET in OSCC cells. Indirect IF microscopy of SCC4, SCC15 and SCC25 cells that either lack (-) or express DOC1. F-actin was visualized by Phalloidin staining (green). Cells were stained (red) with antibodies against Vimentin (VIM), N-cadherin (N-CAD) and E-cadherin (E-CAD). Nuclei were visualized by DAPI staining of DNA (blue).
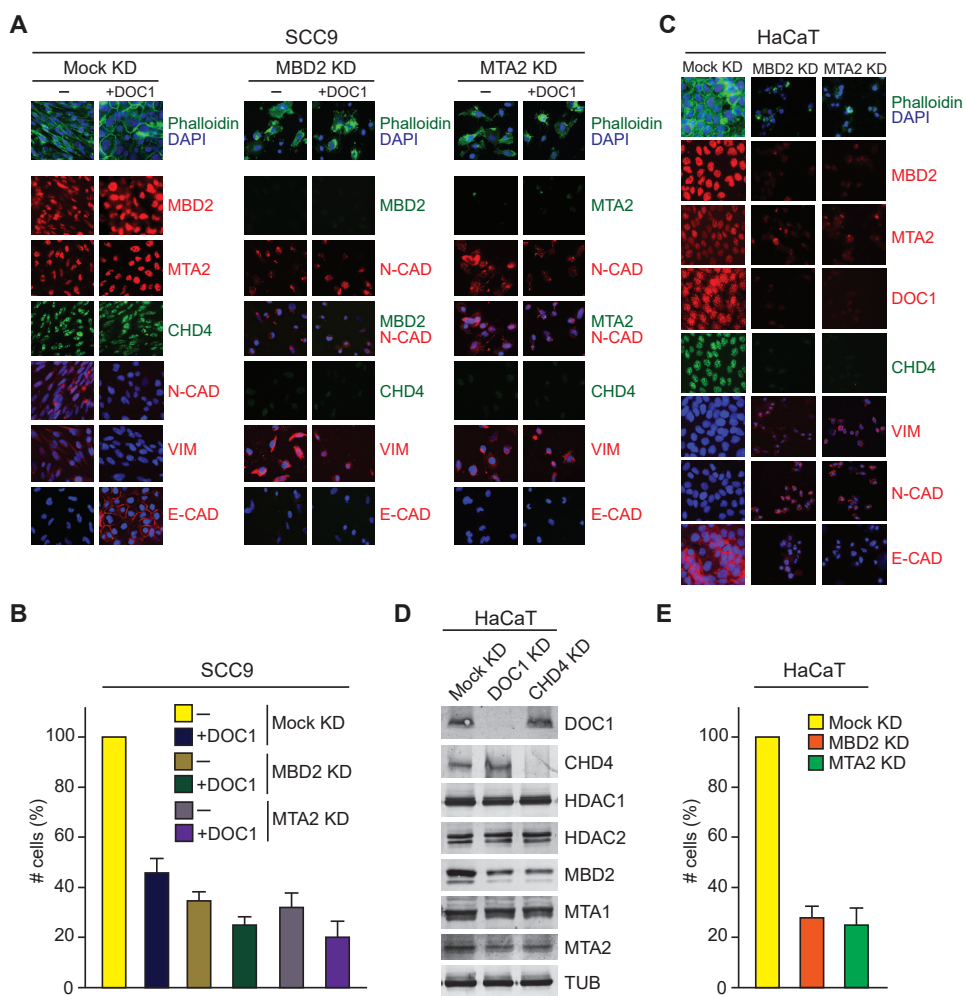
Figure S3. DOC1-induced MET depends on NURD. Related to Figure 3. (**a**) Effects of loss of MBD2 or MTA2 on cell shape and actin organization. Indirect IF of SCC9 cells that either lack or express DOC1, in combination with shRNA-mediated knockdown (KD) of MBD2 or MTA2. Cells were stained using the indicated antibodies. (**b**) Effects of DOC1 expression in combination with MBD2 or MTA2 KDs on cell proliferation were determined 3 days after KD, as described in the legend to Figure 2A. (**c**) Indirect IF of HaCaT cells after KD of MBD2 or MTA2. Cells were stained using the indicated antibodies. (**d**) Immunoblotting analysis of the effects of MBD2 or MTA2 KDs on a selection of NURD subunits. (**e**) Effects of loss of MBD2 or MTA2 on cell proliferation. HaCaT cell numbers were determined 3 days following KDs using the Aqueous One Proliferation Assay (Promega). Mock KD was used for normalization. Means and SEM were derived from three independent biological replicates.
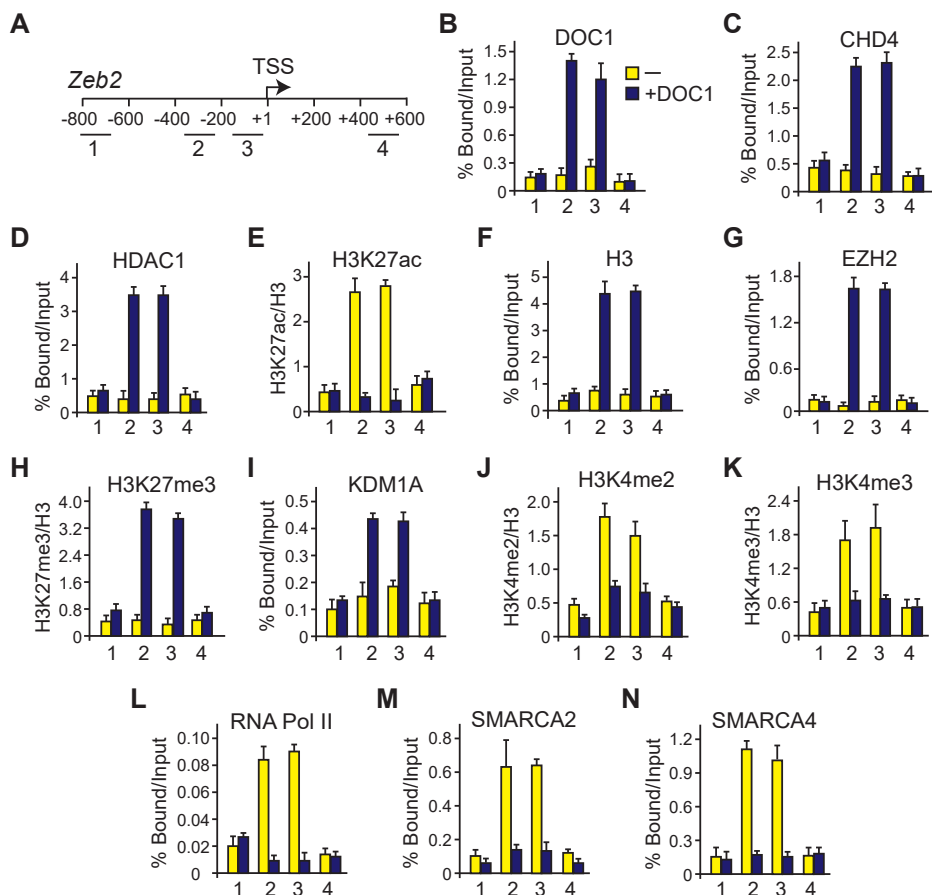
Figure S4. DOC1-dependent binding of CHD4 to the *Zeb2* promotor. Related to Figure 5. (**a**) Diagram depicting the PCR amplicons used. (**b-n**) ChIP-qPCR analysis of chromatin at the *Zeb2* promoter. Chromatin was isolated from SCC9 cells that either lacked- (yellow bars) or expressed DOC1 (blue bars). ChIPS were performed using antibodies directed against the indicated proteins or post-translational modifications. Protein ChIP signals are presented as percentage of input chromatin. Histone modification ChIPs were normalized to H3 signals. Means and SDs for all experiments in this figure were derived from three independent biological replicates.
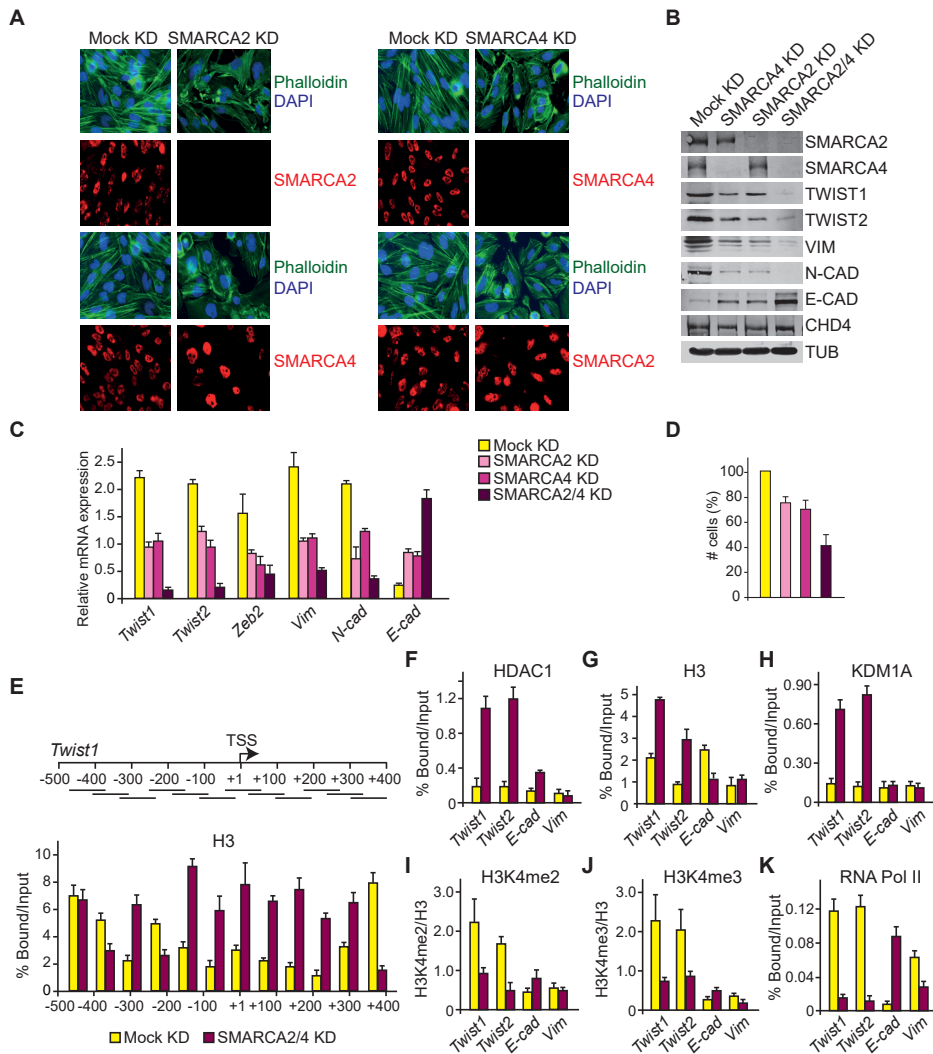
Figure S5. SWI/SNF depletion mimics the effects of DOC1 re-expression. Related to Figure 6. (**a**) Effects of loss of SMARCA2 or SMARCA4 on cell shape and actin organization. IF of SCC9 cells following KD of either SMARCA2 or SMARCA4. Cells were stained with antibodies against SMARCA2 or SMARCA4. F-actin was visualized by Phalloidin staining. (**b**) Immunoblotting analysis after depletion of SMARCA2, SMARCA4 or both SMARCA2 and SMARCA4 (SMARCA2/4), using antibodies against the indicated proteins. (**c** Effect of SMARCA2- or SMARCA4 KD on the mRNA levels of *Twist1*, *Twist2, Zeb2* and markers of EMT, as determined by RT-qPCR. *Gapdh* was used for normalization. Means and SDs were derived from three independent biological replicates. (**d**) Effects of loss of SMARCA2 or SMARCA4 on cell proliferation. Cell numbers were determined 3 days after KDs using the Aqueous One Proliferation Assay (Promega). Mock KD was used for normalization. Means and SEM were derived from three independent biological replicates. (**e**) Effect of SMARCA2/4 depletion on histone H3 occupancy, determined by ChIP- qPCR. (F-K) ChIP-qPCR analysis of chromatin at *Twist1/2* following SMARCA2/4 KD. ChIPS were performed using antibodies directed against the indicated proteins or post-translational modifications. Protein ChIP signals are presented as percentage of input chromatin. Histone modification ChIPs were normalized to H3 signals. Means and SDs for all experiments in this figure were derived from three independent biological replicates.
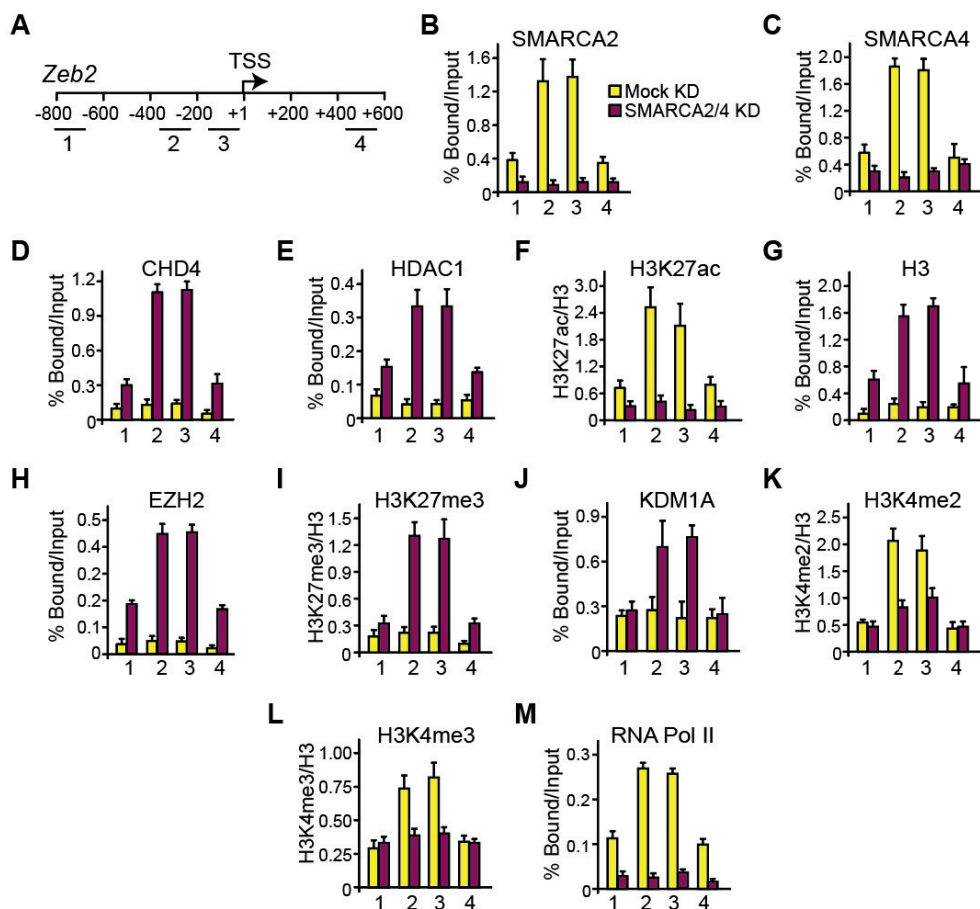
Figure S6. Effect of SWI/SNF depletion on chromatin structure at the *Zeb2* promotor. Related to Figure 6. (**a**) Diagram depicting the PCR amplicons used. (**b-m**) ChIP-qPCR analysis of chromatin at the *Zeb2* promoter. Chromatin was isolated from SCC9 cells following mock (yellow bars) or SMARCA2/4 KD (red bars). ChIPS were performed using antibodies directed against the indicated proteins or post-translational modifications. Protein ChIP signals are presented as percentage of input chromatin. Histone modification ChIPs were normalized to H3 signals. Means and SDs for all experiments in this figure were derived from three independent biological replicates.

Chapter 3

protein MW (kDa)		SCC9				SCC4				HeLa	
		DOC1 IP		CHD4 IP		DOC1 IP		CHD4 IP		DOC1 IP	CHD4 IP
		-	+DOC1	-	+DOC1	-	+DOC1	-	+DOC1		
CHD3	233	- / -	484 / 0.22	- / -	- / -	- / -	409 / 0.14	- / -	282 / 0.1	4661 / 4.06	- / -
CHD4	218	- / -	3588 / 2.44	1548 / 0.65	2089/1.38	- / -	1834 / 0.95	1174 / 0.54	1385 / 0.44	8271 / 44	4774 / 4.54
CHD5	223	- / -	- / -	- / -	- / -	- / -	- / -	- / -	- / -	1992 / 1.1	- / -
MTA1	79	- / -	136 / 0.15	77 / 0.11	186 / 0.2	- / -	177 / 0.2	54 / 0.3	70 / 0.1	2898 /13.28	260 / 0.4
MTA2	75	- / -	660 / 0.78	279 / 0.27	95 / 0.1	74 / 0.09	242 / 0.33	141 / 0.15	93 / 0.1	3153 / 20.7	1234 / 2.34
MTA3	66	- / -	- / -	- / -	- / -	- / -	- / -	- / -	- / -	2001 / 7.21	203 / 0.32
GATAD2A	68	- / -	199 / 0.36	140 / 0.27	135 / 0.17	- / -	146 / 0.29	131 / 0.37	123 / 0.19	2642 / 14.25	920 / 1.2
GATAD2B	66	- / -	468 / 0.55	80 / 0.12	99 / 0.12	- / -	452 / 0.55	60 / 0.18	142 / 0.18	2154 / 17.72	1187 / 2.1
HDAC1	55	- / -	221 / 0.38	316 / 0.68	221 / 0.48	- / -	190 / 0.3	184 / 0.38	137 / 0.21	1953 / 92.67	563 / 1.07
HDAC2	55	- / -	352 / 0.73	66 / 0.09	315 / 0.73	- / -	375 / 0.62	73 / 0.12	116 / 0.23	2028 / 146.6	725 / 1.98
RBBP4	47	49 / 0.17	331 / 0.82	324 / 0.35	322 / 0.57	137 / 0.19	329 / 0.57	241 / 0.35	252 / 0.34	1491 / 6.63	875 / 2.3
RBBP7	47	49 / -	329 / 0.69	71 / 0.13	241 / 0.36	- / -	267 / 0.46	82 / 0.12	258 / 0.45	1668 / 15.29	815 / 2.28
MBD2	43	- / -	189 / 0.18	158 / 0.18	317 / 0.51	- / -	229 / 0.39	98 / 0.15	57 / 0.09	1366 / 9.05	560 / 1.0
MBD3	33	- / -	- / -	- / -	- / -	- / -	- / -	- / -	- / -	1575 / 68.57	754 / 4.58
DOC1	12	- / -	290 / 2.98	- / -	193 / 1.29	- / -	150 / 2.92	- / -	190 / 7.4	378 / 9.16	208 / 1.19
CDK2	27	- / -	- / -	- / -	- / -	- / -	- / -	- / -	- / -	- / -	- / -
KDM1A	93	- / -	- / -	- / -	- / -	- / -	- / -	- / -	- / -	- / -	- / -

Table S1. Identification of DOC1- and CHD4 associated proteins by mass spectrometry. Related to Figure 1. DOC1 or CHD4 were immunopurified (IPed) from from whole cell extract (WCE) prepared from SCC9 or SCC4 cells transduced with lentiviruses expressing either an irrelevant control (LacZ, -) or DOC1. In addition, endogenous DOC1 and CHD4 were IPed from HeLa cells. IPs were performed using antibodies directed against either DOC1 or CHD4. Following extensive washes with a buffer containing 600 mM KCl and 0.1 % NP-40, associated factors were identified by mass spectrometric analysis. Proteins identified are shown with their mascot- and emPAI scores (mascot/emPAI).

CHAPTER IV

Phenotypic plasticity underlies local invasion and distant metastasis in colon cancer

Sacchetti A.*, Teeuwssen M.J.*, Verhagen M.*, Joosten R., Xu T., Stabile R., van der Steen B., Watson M.M., Gusinac A., Kim W.K., Ubink I., van Werken H.J.G., Fumagalli A., Paauwe M., van Rheenen J., Samsom O., Kranenburg O., Fodde R.

*equal contributions

Abstract

Phenotypic plasticity represents the most relevant hallmark of the carcinoma cell as it bestows it with the capacity of transiently altering its morphologic and functional features while *en route* to the metastatic site. However, the study of phenotypic plasticity is hindered by the rarity of these events within primary lesions and by the lack of experimental models. Here, we identified a subpopulation of phenotypic plastic colon cancer cells: EpCAM^{lo} cells are motile, invasive, chemo-resistant, and highly metastatic. EpCAM^{lo} bulk and single-cell RNAseq analysis indicated 1. enhanced Wnt/β-catenin signaling, 2. a broad spectrum of degrees of EMT activation including hybrid E/M states (partial EMT) with highly plastic features, and 3. high correlation with the CMS4 subtype, accounting for colon cancer cases with poor prognosis and a pronounced stromal component. Of note, a signature of genes specifically expressed in EpCAM^{lo} cancer cells is highly predictive of overall survival in tumors other than CMS4, thus highlighting the relevance of quasi-mesenchymal tumor cells across the spectrum of colon cancers.

Enhanced Wnt and the downstream EMT activation represent key events in eliciting phenotypic plasticity along the invasive front of primary colon carcinomas. Distinct sets of epithelial and mesenchymal genes define transcriptional trajectories through which state transitions arise. pEMT cells, often earmarked by the extracellular matrix glycoprotein SPARC together with nuclear ZEB1 and β-catenin along the invasive front of primary colon carcinomas, are predicted to represent the origin of these (de)differentiation routes through biologically-distinct cellular states, and to underlie the phenotypic plasticity of colon cancer cells.

Abstract

Introduction

Cancers of epithelial origin such as breast, prostate, pancreas, lung, and colon carcinomas are thought to develop from normal tissues through a multistep sequence of genetic events from benign precursor lesions to increasingly more malignant stages. This is exemplary illustrated by the adenoma-carcinoma sequence in colon cancer where a stepwise buildup of genetic alterations in specific oncogenes and tumor suppressor genes underlies tumor initiation and progression [1]. These alterations result in well-defined cellular changes largely reflecting the so-called 'hallmarks of cancer', which provide different selective advantages to the developing tumor and represent essential requirements for carcinoma formation at the primary site [2]. However, with regard to the capacity to disseminate through the tumor microenvironment and establish metastases in distant organ sites, epigenetic changes, rather than genetic mutations, underlie what the most clinically relevant hallmark of cancer, namely phenotypic plasticity [3,4].

Malignant cells, and in particular those responsible for local dissemination and distant metastasis, are often endowed with the capacity to undergo transient and reversible morphological and functional changes. In particular, epithelial to mesenchymal transition (EMT), i.e. the progressive loss of epithelial features and the acquirement of a more migratory and mesenchymal phenotype [5], is regarded as a crucial event in tumor cell invasion and dissemination at the primary site. EMT bestows cancer cells with stem-like plastic characteristics [6] needed to acquire quasi-mesenchymal features at the invasive front of the primary tumor, disseminate and attain therapy resistance, and to revert back to more epithelial states (MET, mesenchymal to epithelial transition) at the organ site of metastasis [7]. Epigenetic activation and silencing of EMT-inducing transcription factors (EMT-TFs) underlies the transient nature of these cellular modifications [8]. Notwithstanding these ground rules, a very broad spectrum of molecular and cellular routes underlie EMT and the resulting phenotypic plasticity in context-dependent fashion [9].

The "migrating cancer stem cell" (mCSC) model has been first proposed for colon cancer by T. Brabletz [7], also as a solution to the so-called "β-catenin paradox" [10]. In the majority of sporadic colorectal cancer cases, the rate-limiting loss of the *APC* tumor suppressor is predicted to lead to nuclear β-catenin translocation and full-blown Wnt signaling activation. Notwithstanding these predictions, tumor cells with nuclear β-catenin represent only a small minority of the primary lesion and tend to cluster non-randomly at the invasive front of colon carcinomas where they gain mesenchymal features to detach and disseminate into the adjacent stromal tissues. In view of these observations, it is plausible that cues secreted from the tumor microenvironment elicit EMT downstream of full blown Wnt signaling activation, earmarked by nuclear β-catenin, in a subset of cells located at the invasive front [7,10]. However, the molecular and cellular mechanisms underlying Wnt and EMT activation at the invasive front of colon cancers are yet largely unknown also due to a lack of robust *in vitro* and *in vivo* models.

Previously, it was shown that human immortalized breast cancer cell lines encompass different subpopulations of cells with distinct phenotypic states and functional characteristics maintained in a dynamic equilibrium through stochastic transitions between states [11]. Similar observations were made in oral squamous carcinoma cell lines where distinct CSC phenotypes are present: whereas non-EMT CSCs are proliferative and retain epithelial characteristics, the EMT-competent CSC fraction is (quasi)mesenchymal

and of increased cellular motility [12]. As such, conventional immortalized cancer cell lines may offer a valid model to elucidate the mechanisms underlying phenotypic plasticity in cancer and to identify novel EMT/CSC-related therapeutic targets.

Here, we identified and extensively characterized a subpopulation of quasi-mesenchymal colon cancer cells endowed with phenotypic plasticity that underlie local invasion and distant metastasis, and whose expression signature is predictive of reduced disease-free survival among colon cancer patients.

Results

Conventional colon cancer cell lines encompass a subpopulation of ZEB1-driven quasi-mesenchymal, highly metastatic, and chemo-resistant cells.

To assess whether, as observed for breast cancer [11], commonly employed colon cancer cell lines encompass distinct differentiated and more stem-like subpopulations of cancer cells, we first analyzed a broad panel of cell lines by FACS with antibodies directed against different (cancer) stem cell markers (CD44, CD133, CD24, ALDEFLUOR) in combination with the epithelial marker EpCAM. As shown in **Figure 1A and Figure 1-supplement 1** for HCT116 and SW480, the CD44/EpCAM combination best highlighted the presence of distinct subpopulations with a predominant CD44^{high}EpCAM^{high} cluster and a minority of CD44^{high}EpCAM^{low} cells. The same CD44^{high}EpCAM^{low} cells were identified at similarly variable percentages in other commonly employed colon cancer cell lines (**Figure 1-source data 1**). Here, we mainly focused on the HCT116 and SW480 lines as they are representative of the two main colon cancer subtypes earmarked by MIN (microsatellite instability) and CIN (chromosomal instability; also known as MSS, microsatellite stable), respectively [13]. For the sake of clarity and readability, from this point on we will refer to the CD44^{high}EpCAM^{low} and CD44^{high}EpCAM^{high} subpopulations of colon cancer cells as EpCAM^{lo} and EpCAM^{hi}, respectively.

To characterize the EpCAM^{lo} and EpCAM^{hi} colon cancer cells, they were sorted by FACS and shown to have distinct epithelial- (EpCAM^{hi}) and mesenchymal-like (EpCAM^{lo}) morphologies (**Figure 1B**). Likewise, EpCAM^{lo} cells were shown to have significantly increased migratory and invasive ability when compared with their EpCAM^{hi} counterparts (**Figure 1-supplement 2A**).

RT-qPCR analysis of the sorted subpopulations revealed differential expression of EMT-associated marker genes and transcription factors. Significantly reduced mRNA levels of *EPCAM* and E-cadherin (*CDH1*), and increased expression of vimentin (*VIM*) and of the EMT-transcription factor *ZEB1* were observed in EpCAM^{lo} cells from both lines, as also confirmed by immunofluorescence analysis (**Figure 1-supplement 2B-D**). Accordingly, knockdown of *ZEB1* expression by shRNA dramatically decreased the percentage of EpCAM^{lo} cells in both lines (**Figure 1-supplement 3A-C**).

Expression of *ZEB1* (and *ZEB2*) has been shown to be regulated by the miR-200 superfamily of micro RNAs which target specific 3'UTR sequences [14]. RT-qPCR analysis of sorted cells revealed significantly reduced expression levels of all five miR-200 members in EpCAM^{lo} cells from both cell lines (**Figure 1-supplement 3D**), i.e. in agreement with the observed increase in *ZEB1* expression. Proliferation and cell-cycle analysis indicated decreased mitotic activity in EpCAM^{lo} cells from both cell lines (**Figure 1-supplement 3E-F and Figure 1-source data 2**).
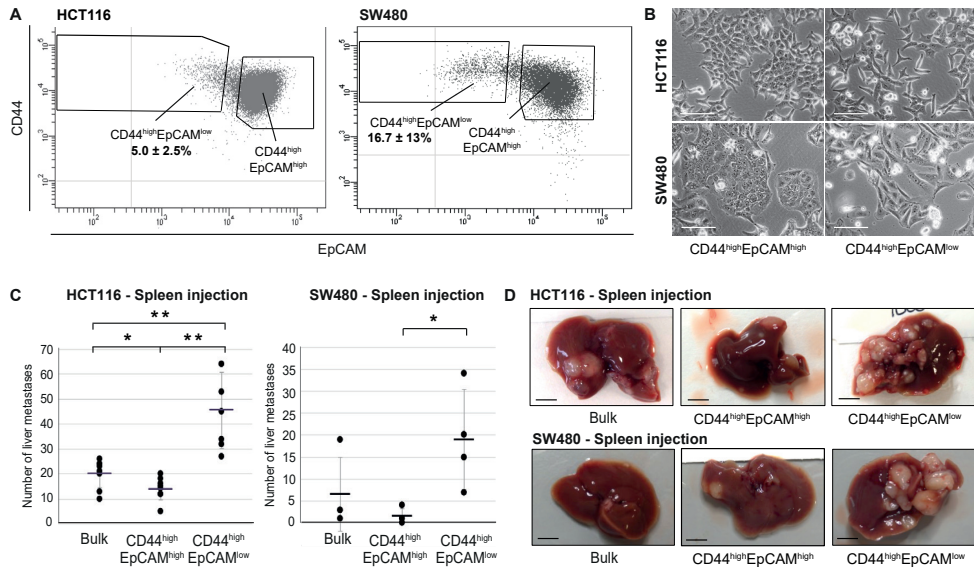
Figure 1. Identification and characterization of EpCAM^{lo} cells in colon cancer cell lines. (**a**) Flow cytometric analysis of the colon cancer cell lines HCT116 (left panel) and SW480 (right panel) with antibodies directed against CD44 and EpCAM. EpCAM/CD44 positive and negative regions were defined using multiple isotype controls, and are shown by the quadrants in the plots. Notably, both HCT116 and SW480 revealed a continuum of different EpCAM and CD44 expression levels with a large CD44^{high}EpCAM^{high} (EpCAM^{hi}) cluster followed by a tail of gradually decreasing EpCAM and increasing CD44 levels. By applying specific gates, cells were divided in a large EpCAM^{hi} cluster, together with a considerably smaller CD44^{high}EpCAM^{low} (EpCAM^{lo}) subpopulation. To ensure good separation from the large EpCAM^{hi} cluster and maximal sorting purity, EpCAM^{lo} cells were gated as CD44^{hi} events ≤60% of the EpCAM fluorescence intensity of the left border of the EpCAM^{hi} gate, and sorted from ≤50% of that value. Variable percentages of EpCAM^{lo} cells were found to feature the HCT116 (5.0±2.5%) and SW480 (16.7±13%) cell lines, respectively. For the sake of simplicity, gates are shown in the figure only if they encompass sizeable percentages of cells. Graphs show representative analysis of one experiment. (**b**) Phase contrast microscopy images of sorted EpCAM^{hi} and EpCAM^{lo} cells from HCT116 (upper images) and SW480 (lower images) cells. While EpCAM^{hi} cells formed compact colonies with characteristic epithelial morphology, EpCAM^{lo} cells showed a more spindle- and mesenchymal-like appearance Scale bar: 100 μm. (**c**) Intrasplenic injection of bulk, EpCAM^{hi}, and EpCAM^{lo} cells from HCT116 (left panel), and SW480 (right panel) in For each transplantation experiment, 2x10^4 cells were injected in the spleen of a recipient NSG mouse. Four (HCT116) and 8 (SW480) weeks after injection mice were sacrificed and individual tumors counted. Single and double asterisks indicate significant differences ($P < 0.05$ and $P < 0.01$, respectively). HCT116: bulk (n=8), EpCAM^{hi} (n=9), and EpCAM^{lo} (n=7). SW480: bulk (n=4), EpCAM^{hi} (n=4), and EpCAM^{lo} (n=4). (**d**) Images of mouse livers four (HCT116) and eight (SW480) weeks after orthotopic injection with 10^4 cells. Scale bar: 5 mm.

In view of the well-established correlation between EMT and therapy resistance [15], EpCAM^{lo} cells were cultured in the presence of oxaliplatin and 5-fluorouracil (5-FU) and their viability compared with that of EpCAM^{hi} and bulk cells by metabolic activity assay (MTT). EpCAM^{lo} cells showed increased viability at all tested oxaliplatin (**Figure 1-supplement 4A,C**, left panels) and 5-FU (**Figure 1-supplement 4B,D**, left panels) concentrations. Likewise, re-growth assays revealed that EpCAM^{lo} cells from both cell lines

Chapter 4

are able to re-enter the cell cycle at a broad range of oxaliplatin and 5-FU concentrations when compared with EpCAM^{hi} cells (**Figure 1-supplement 4**, right panels).

Last, to assess *in vivo* their capacity to form metastatic lesions in the liver, HCT116 and SW480 bulk and EpCAM$^{hi/lo}$ sorted cells were injected in the spleen of immune-incompetent recipient mice. EpCAM^{lo} cells from both lines resulted in significantly more liver metastases than with EpCAM^{hi} and bulk cells (**Figure 1C-D**). Notably, IHC analysis of the resulting liver metastases revealed a heterogeneous pattern of intracellular β-catenin, with membranous and cytoplasmic localization in cells from within the center of the lesion, and nuclear β-catenin accumulation in cells localized in the periphery, thus recapitulating what observed in primary colon carcinomas[10,16] (**Figure 1-supplement 5A**). FACS analysis of the EpCAM^{lo}-derived liver metastases revealed predominant epithelial features with a vast majority of EpCAM^{hi} cells (>99%), thus highlighting their striking plasticity and the key role played by MET in metastasis formation **(Figure 1-supplement 5B and Figure 1-source data 3).**

In order to validate the role of *ZEB1*-driven EMT in the establishment of the EpCAM^{lo} subpopulation of colon cancer cells in a cell line-unrelated *in vivo* model mimicking the course of events observed in colon cancer patients, we employed mouse intestinal organoids carrying specific mutations at the *Apc*, *Kras*, and *Tp53* genes (*Apc$^{fl/fl}$::Kras$^{G12D/+}$::Trp53$^{fl/R172H}$*; AKP) [17]. Orthotopic transplantation of AKP organoids results in the establishment of primary carcinomas in the caecum and subsequent metastasis development at distant organ sites, mainly liver and lungs [18]. We further modified the AKP organoids by tagging them with GFP and a click beetle luciferase [19], and by making them doxycycline-inducible for the expression of mouse *Zeb1* (AKP-Z) (**Figure 1-supplement 5C**). Upon orthotopic transplantation of the AKP-Z organoids and subsequent establishment of the primary tumor in the caecum, mice were administered doxycycline for one week in the drinking water to induce *Zeb1* expression. FACS analysis of the primary tumor revealed an increase in EpCAM^{lo} cells from 4.8% in the non-induced tumors up to 22-76% upon dox-induction of *Zeb1* expression (**Figure 1-supplement 5D**). As expected, only a marginal increase of lung and liver metastases was observed in AKP-Z transplanted mice upon continuous dox-administration in the drinking water for 8 weeks when compared with control (no dox) animals (**Figure 1-supplement 5E**), likely to result from the continuous induction of *Zeb1* expression and the consequent inhibition of mesenchymal-to-epithelial transitions essential for metastasis formation[7].

Overall, the results show the presence within colon cancer cell lines of EMT-driven, quasi-mesenchymal and therapy-resistant EpCAM^{lo} cells with increased invasive and metastatic capacity. *ZEB1* expression underlies *in vivo* the establishment and maintenance of the subpopulation of EpCAM^{lo} colon cancer cells, thereby contributing to increased dissemination along the invasion-metastasis cascade.

EpCAM^{lo} colon cancer cells are maintained in equilibrium with EpCAM^{hi} through stochastic state transitions

To further investigate on the plasticity of EpCAM^{lo} cancer cells, we assessed their capacity to differentiate into the more epithelial EpCAM^{hi} type and reconstitute the heterogeneous composition of the parental cell lines. Sorted EpCAM$^{lo/hi}$ cells from HCT116 and SW480 were grown separately under conventional culture conditions and analyzed

by FACS at different time points. As shown in **Figure 2A**, while the majority of EpCAM^{lo} cells from both cell lines revert to the epithelial phenotype, only a minority of EpCAM^{hi} cells switches to the more mesenchymal state. Accordingly, *CDH1* and *EPCAM* expression was significantly increased in 'late' (e.g. cultured for >60 and >100 days, respectively) vs. 'early' EpCAM^{lo} cells (e.g. collected after <7 days of culture), whereas *VIM* and *ZEB1* expression was decreased in 'late' vs. 'early' EpCAM^{lo} cells (**Figure 2-supplement 1A**). In addition, the migratory capacity of 'late' EpCAM^{lo} HCT116 cells was reduced to levels comparable with those of 'early' EpCAM^{hi} cells (**Figure 2-supplement 1B**).
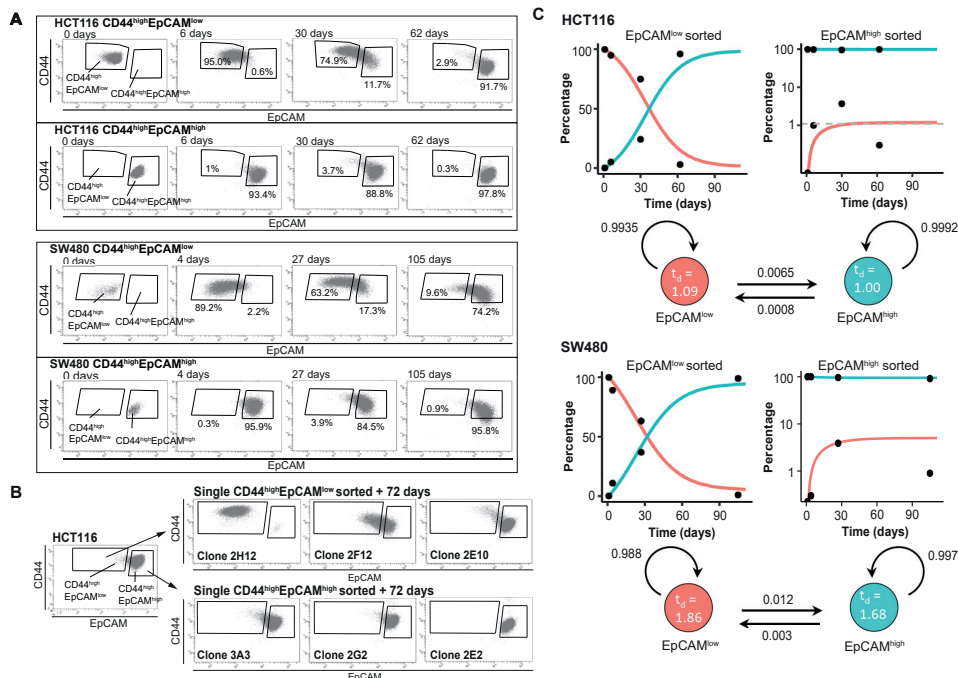
Figure 2. Phenotypic plasticity maintains EpCAM^{lo} and EpCAM^{hi} cells in a stochastic equilibrium. (**a**) Analysis of plasticity of EpCAM^{hi} and EpCAM^{lo} cells from HCT116 (upper panel) and SW480 (lower panel). EpCAM^{hi} and EpCAM^{lo} cell fractions were sorted and plated in culture. At different time points, as indicated, cells were re-analyzed by flow cytometry for their levels of CD44 (*y*-axis) and EpCAM (*x*-axis) expression. (**b**) Flow cytometric analysis of single CD44^{hi}EpCAM^{hi} and CD44^{hi}EpCAM^{lo} HCT116 cells sorted by FACS and cultured for 72 days. Three representative individual single cell clones per cell fraction are shown. (**c**) Dynamics of the EpCAM^{hi} and EpCAM^{lo} sub-populations from the HCT and SW480 cell lines as measured by FACS (% of total) over time. Under each graph, a schematic shows the estimated transition probabilities from the fitted two-state Markov Model.

To exclude cross-contamination between sub-populations, single EpCAM$^{hi/lo}$ cells from both cell lines were sorted into 96-well dishes, cultured up to 70-80 days, and analyzed by FACS at intermediate and end time points. As shown in **Figure 2B and Figure 2-source data 1**, the majority of EpCAM^{lo} single cells were capable of generating substantial percentages of EpCAM^{hi} progeny to eventually recapitulate the heterogeneous composition of the parental cell lines (e.g. **Figure 2B**, clones 2F12 and 2E10,). A minority of the cells however,

Chapter 4

appears to have lost this plasticity and retains, even after extended culture, the EpCAM[lo] phenotype (e.g. **Figure 2B**, clone 2H12). In contrast, the majority of EpCAM^{hi} single cells retained their epithelial features with <1% switching to the EpCAM[lo] state (**Figure 2B and Figure 2-source data 1**).

Based on these results, a two-state Markov model was developed to estimate the average probabilities to transition from one state to the other. First, the FACS data was employed to estimate the average doubling time of cells in both populations; slightly increased doubling times were reported for EpCAM[lo] compared to EpCAM^{hi} cells in both lines (HCT116: 1.09 vs. 1.00 days; SW480: 1.86 vs. 1.68 days). Next, we employed least square optimization to estimate the transition probabilities that best fit the observed population dynamics. The fitted model predicts that both subpopulations have a high probability to retain their cell identity, with minor though significant likelihood to transit to the other state. Of note, EpCAM^{lo} cells show a higher transition probability compared to EpCAM[hi] (8.1 and 4.0 fold in HCT116 and SW480, respectively) (**Figure 2C)**.

Due to the observed differences in doubling times between the two states, subclones with a lower EpCAM[hi>lo] transition probability will experience a slight growth advantage which will become prevalent in the long run. We ran a simulation of this effect by starting from a culture with multiple subclones having distinct transition probabilities; the results indicate that subclones with lower plasticity gain dominance within a few months (**Figure 2-supplement 2**). Consequently, especially in the long run, the percentage of EpCAM^{lo} cells will decrease as observed in late cultures (**Figure 1-source data 1**).

Overall, the above results highlight the high plasticity and stem-like features of EpCAM^{lo} cells in their ability to acquire epithelial features and reconstitute the heterogeneous composition of the parental cell line, independently of external factors other than the conventional culture conditions here employed.

Enhanced Wnt signaling activation underlies EMT and the establishment of EpCAM[lo] colon cancer cells.

In order to elucidate the mechanisms underlying plasticity and EMT in EpCAM[lo] colon cancer cells, RNAseq analysis was performed on the sorted subpopulations from the HCT116 and SW480 lines. Multidimensional scaling (MDS) showed a separation in the second dimension of EpCAM[hi] and EpCAM^{lo} cells in both cell lines (**Figure 3A**). A total of 152 and 353 differentially regulated genes were identified between the EpCAM[hi] and EpCAM^{lo} cells in HCT116 and SW480, respectively (*P. adjusted* < 0.01, when applying a Log$_2$ fold change < -1.5 and > 1.5). Among these, only relatively few (n=34) were common to both lines (**Figure 3-source data 1**). However, Ingenuity Pathway Analysis (IPA) revealed that genes differentially expressed in each cell line reflect common molecular and cellular functions including cellular motility, cellular assembly and organization, and drug metabolism (**Figure 3-supplement 1)**. Nonetheless, IPA of the combined EpCAM[lo] expression profiles highlighted significant associations with EMT regulation, Wnt/β-catenin signaling, human ESC pluripotency, IL8 signaling, and colorectal cancer metastasis (**Figure 3B and Figure 3-supplement 1**).

The activation of canonical Wnt signaling in EpCAM[lo] colon cancer cells is of interest in view of the fact that both cell lines harbor mutations (loss and gain of APC and β-catenin function in SW480 [20] and HCT116 [21], respectively) predicted to result in the constitutive

activation of the pathway. Notwithstanding the latter, Wnt appears to be increased in EpCAM^{lo} cells, possibly due to the epigenetic activation/inhibition of synergistic/antagonistic loci. In view of these observations and of the established functional link between Wnt and EMT[22,23], we evaluated whether Wnt signaling 'super-activation' in the already Wnt-ON HCT116 and SW480 cell lines could expand the relative size of the EpCAM[lo] subpopulations. Indeed, upon treatment with the glycogen synthase 3β (GSK3β) inhibitor CHIR99021 (Chiron), a robust Wnt signaling activation was observed in both cell lines by TopFLASH reporter assay (**Figure 3C**). FACS analysis of the treated cell lines showed that the enhancement of Wnt signaling led to an approx. 3-fold increase of the EpCAM[lo] population in the HCT116 cell line, though not in SW480 (**Figure 3D**). However, IF analysis showed that Chiron treatment was consistently accompanied by an increase in *ZEB1* expression in both cell lines, in agreement with the role of *ZEB1* as a downstream Wnt target [24,25] (**Figure 3E**).

To further validate the role of Wnt in the establishment of the EpCAM[lo] subpopulation, we took advantage of the recently generated isogenic subclones of the HCT116 cell line with distinct β-catenin genotypes, namely wild type (HCT116-WT), hetero- (HCT116-P), and homozygous (HCT116-MT) for the Ser45del mutant allele [26]. FACS analysis of these cell lines revealed a progressive increase in the EpCAM[lo] subpopulation from 3.9% in HCT116-WT, to 7.9% in HCT116-P, and 28.7% in HCT116-MT cells (**Figure 3F**). The observed increase in EpCAM^{lo} cells in the isogenic HCT116 lines matches their morphological features ranging from a distinct epithelial-like morphology in HCT116-WT, to a progressively increased spindle-shaped and scattered patterns in HCT116-P and -MT cells, as originally reported by Kim et al. (2019) [26].

In the majority of colon cancers, nuclear accumulation of β-catenin, is exclusively observed at the invasive front where tumor cells are more exposed to growth factors and cytokines from the stromal microenvironment likely to further enhance Wnt signaling in localized fashion thus triggering EMT, invasion, and distant metastasis [7,10]. We analyzed the invasive front of a cohort of colon carcinomas by IHC with antibodies directed against β-catenin and ZEB1 in consecutive sections. As shown in **Figure 3-supplement 2**, co-localization of nuclear β-catenin and ZEB1 expression was found in 5 out of 25 cases investigated.

Overall, the results highlight the key role played by enhanced Wnt signaling activation in establishing and maintaining the EpCAM[lo] subpopulation of colon cancer cells through *ZEB1* upregulation and EMT induction.

EpCAM^{lo} cells are associated with the CMS4 group of patients with shorter disease-free and overall survival.

Distinct recurrent gene expression patterns underlie the recently proposed classification of human colon cancers in four Consensus Molecular Subtypes (CMS1-4) [27]. Of these, the mesenchymal CMS4 subtype has the greatest propensity to form metastases.
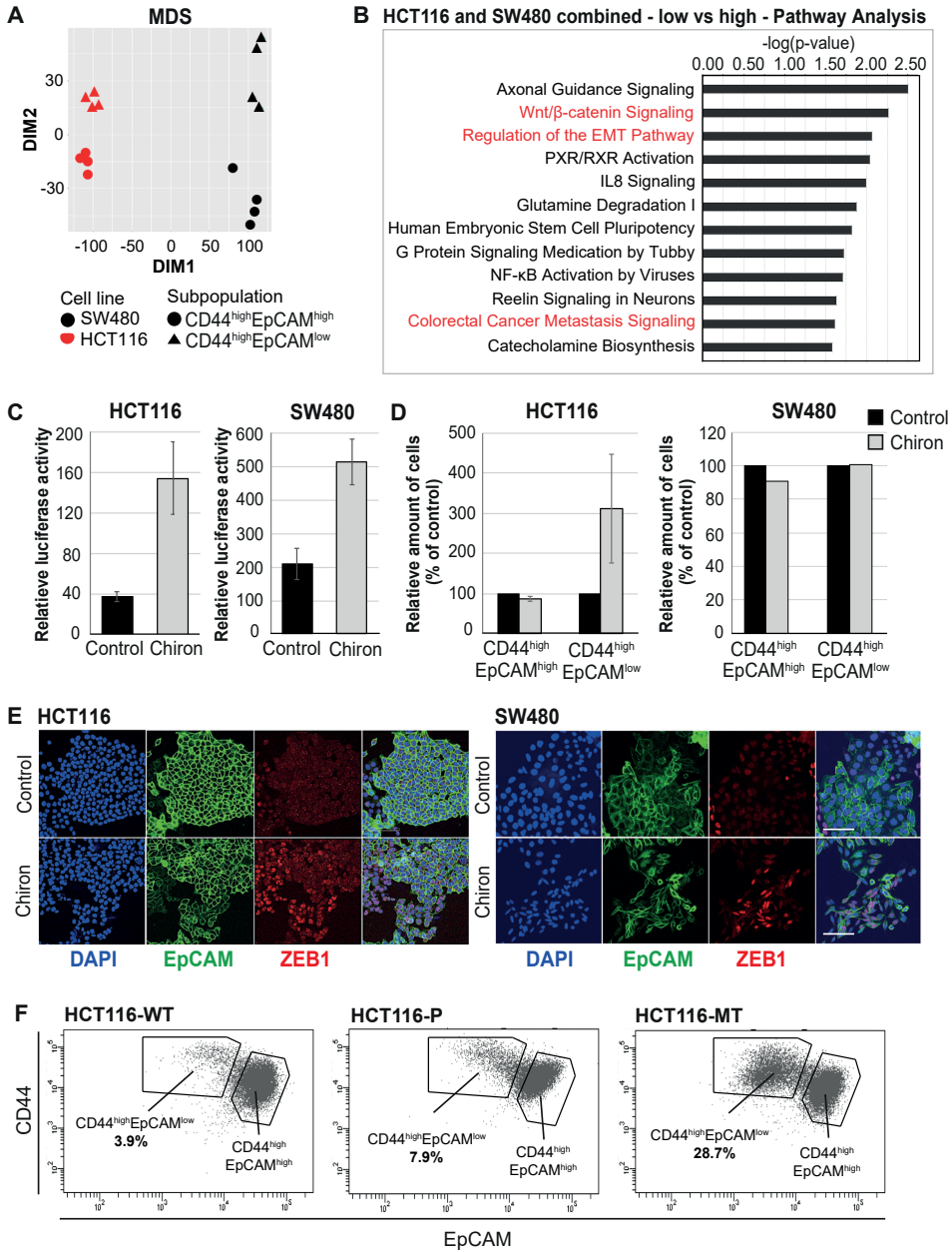
Figure 3. (opposite) RNAseq analysis reveals enhanced Wnt signaling in EpCAM^{lo} cells. (**a**) Multidimensional scaling (MDS) analysis of RNAseq profiles of EpCAM^{hi} and EpCAM^{lo} cells from the HCT116 and SW480 lines. Red: HCT116, black: SW480, circle: EpCAM^{hi}, triangle: EpCAM^{lo}. (**b**) Ingenuity Pathway Analysis (IPA) of the HCT116 and SW480 expression profiles from the multi-cell line analysis (*P. adjusted value* < 0.01; log$_2$ fold change < -1.5 and > 1.5). Red marked pathways highlight the enhanced involvement of pathways involved in EMT, Wnt signaling and the formation of colon cancer metastasis

in the EpCAM[lo] subpopulation compared to EpCAM^{hi} cells. (**c**) TOP-Flash luciferase reporter analysis of Wnt signaling activity in colon cancer cell lines HCT116 and SW480 upon treatment with 4 µM Chiron for three days. Each bar represents the mean ± SD of two independent experiments. (**d**) Flow cytometric analysis using antibodies directed against CD44 and EpCAM of control and 4 µM Chiron-supplemented HCT116 (A) and SW480 (B) cultures. Graphs show percentage of cells within the CD44^{hi}EpCAM^{hi} and CD44^{hi}EpCAM^{lo} gates relative to the control. Each bar represents the mean ± SD of two independent experiments. (**e**) Immunofluorescence analysis of control and Chiron treated HCT116 (left panel) and SW480 (right panel) cells. After three days of treatment, cells were fixed with 4% PFA and stained with antibodies against EpCAM (green) and ZEB1 (red). Nuclei were visualized by DAPI staining of DNA (blue). Scale bar: 100 µm. (**f**) Flow cytometric analysis of three HCT116 cell lines with differential -catenin mutation status, a parental HCT116 (HCT116-P) cell line harboring one WT and one mutant allele (Ser45 del), and two HCT116-WT and HCT116-MT cell lines harboring one WT or one mutant allele, respectively, generated by disruption of the other allele in the parental cell line [26].

While fibrosis is a hallmark of CMS4 and a dominant contributor of mesenchymal gene expression, the cancer cells themselves can also express genes reflecting a (quasi-) mesenchymal state. Accordingly, the CMS4 subtype was identified in tumor-derived organoids and cell lines, suggesting that CMS4 is an intrinsic property of the mesenchymal colon cancer cell [28]. Therefore, we asked whether expression of the signatures derived from the RNAseq analysis of EpCAM^{lo} cells would correlate with the CMS classification of human colon cancers and cell lines. To this end, we employed a compiled data set encompassing expression data relative to 3232 human colon cancers classified as CMS1-4 [27]. Expression of the HCT116 and SW480 signatures were highly correlated with each other (**Figure 4A**), with the CMS4 signature genes (n=143) (**Figure 4A-B**), and with the expression signature of colon cancer cell lines previously classified as mesenchymal-like (CCS3) [29] (**Figure 4-supplement 1A**).

Next, we used both HCT116 and SW480 signatures from the bulk RNAseq to generate High, Intermediate, and Low expression subgroups in the CMS cohort through k-means clustering (**Figure 4-supplement 1B**). High expression of the EpCAM[lo] signatures from both cell lines identifies a group of primary colon cancer patients with a high propensity to form metastases and with significantly shorter overall survival (**Figure 4C**).

Overall, the above data strongly link the expression of the EpCAM[lo] signatures derived from common colon cancer cell lines to the CMS4 subtype and to shorter disease-free and overall survival.

scRNAseq analysis of EpCAM[lo] colon cancer cells reveals high heterogeneity and partial EMT intermediate stages

To further elucidate the heterogeneity and molecular mechanisms underlying the phenotypic plasticity of EpCAM[lo] colon cancer cells, single cell RNA sequencing (scRNAseq) was performed using chromium controller (10X Genomics) technology on sorted subpopulations from HCT116 and SW480. More than 1000 cells were analyzed from each subpopulation and sequenced to a depth of approx. 50000 reads each with the MiSeq System (Illumina).
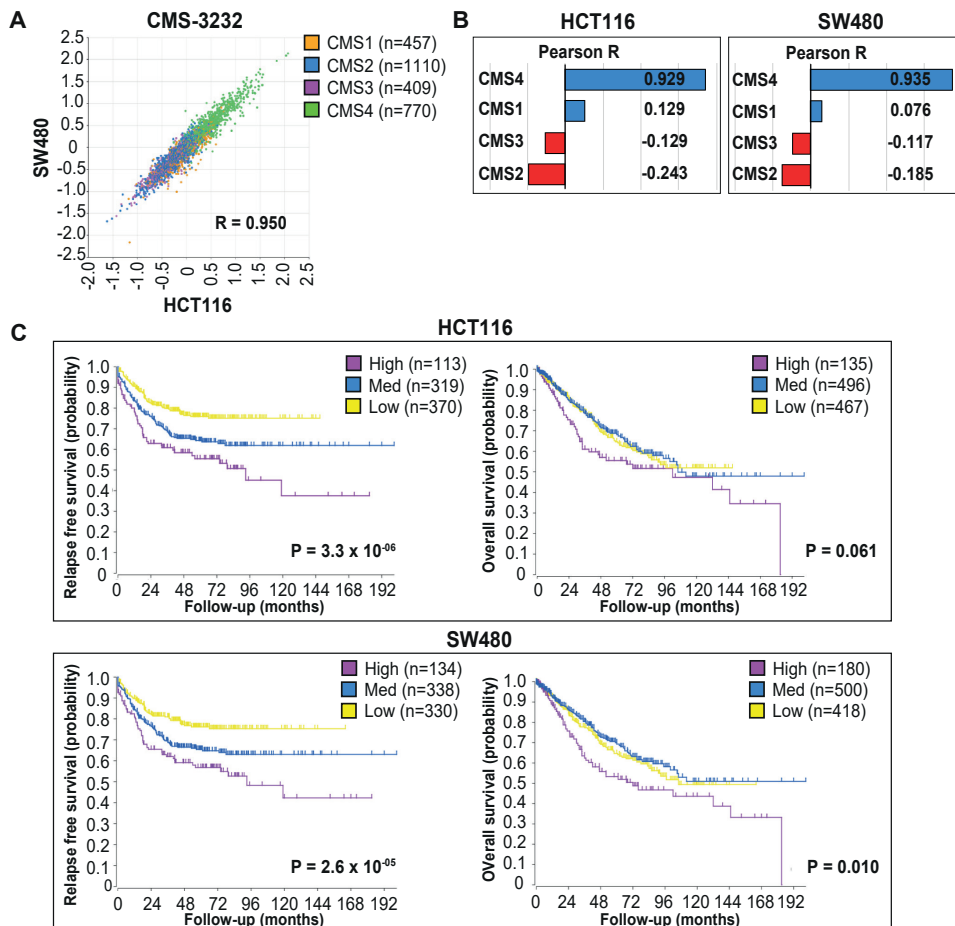
Figure 4. EpCAM^{lo} gene expression profiles correlate with CMS4 colon cancer patients with shorter disease-free and overall survival. (**a**) Correlation of meta-gene expression values of the signatures derived from EpCAM^{lo} HCT116 and SW480 cells in the CMS-3232 human colon cancer cohort [27]. (**b**) Correlation of meta-gene expression values of the signatures derived from EpCAM^{lo} HCT116 and SW480 cells with expression of CMS classifier genes positively identifying each of the four molecular subtypes. (c) Kaplan Meier analysis. The gene sets identifying the EpCAM^{lo} cells from both HCT116 and SW480 cell lines were used to cluster the tumors in the CMS3232 cohort into HIGH (purple), INTERMEDIATE (blue) and LOW (yellow) expression groups by k-means clustering. The Kaplan-Meier method was subsequently used to assess significant differences in relapse-free (left panels) and overall (right panels) survival between the generated subgroups.

After dimension reduction with tSNE, the EpCAM^{lo} and EpCAM^{hi} cells clustered in separate groups in HCT116 (**Figure 5A**), whereas the SW480 cells showed a partial overlap between the two subpopulations and a distinct EpCAM^{hi} cluster, identified as the non-adherent subpopulation within the SW480 cell line ("spheres") [30,31] (**Figure 5-supplement 1A**). Substantial overlap between the EpCAM$^{hi/lo}$ subpopulations was retained upon subsequent exclusion of the non-adherent cells in SW480, attributed to additional variance in genes independent of EpCAM$^{hi/lo}$ differences (**Figure 5-supplement 1B**). Next, the dimension reduction was repeated in supervised fashion by taking advantage of the publicly available EMT gene list from the Nanostring nCounter® PanCancer Progression Panel (n =180; 107 of which found to overlap with the scRNAseq data) (**Figure 5-source data 1**). Using this 'EMT signature', the two subpopulations were clearly resolved both in HCT116 and SW480 (**Figure 5B**).

To rank and order the cells along the E-M axis, epithelial (E; n=51) and mesenchymal (M; n=56) gene sets were defined from the EMT signature based on the provided annotations (Nanostring), and evaluated by GSVA (Gene Set Variation Analysis). Next, an EMT score was computed by subtracting the E score from the M score (EMT = M – E), while a partial EMT score was obtained based on the co-expression of the E an M gene sets (pEMT = min[E,M]). The expression of genes previously found to be differentially expressed between EpCAM$^{hi/lo}$ by bulk RNAseq was then evaluated over the course of EMT progression (**Figure 5C**). While HCT116 showed a clear transition from EpCAM^{hi} to EpCAM^{lo} with a minority of "in-between" cells earmarked by high pEMT scores, in SW480 the transition appeared to be accompanied by higher levels of inter-cellular variance. We continued to use the EMT-axis in both cell lines to study gene expression trends. As expected, epithelial expression of *EPCAM* and *CDH1* gradually decreased over the EMT-axis, while mesenchymal genes such as *ZEB1* and *VIM*, and Wnt target genes such as *AXIN2* and *DKK1*, showed opposing behavior. More generically, the level of Wnt signaling ("Wnt.score"), measured by the activation of the WNT_PATHWAY from the PID database, increased over the EMT-axis (**Figure 5D**). We evaluated the expression trends of other genes upregulated in EpCAM^{lo} cells and observed that *SPARC* (osteonectin) peaked in between the extremities of the EMT axis, indicative of a partial EMT state (**Figure 5D**).

To further characterize the transition process between EpCAM^{lo} and EpCAM^{hi}, we analyzed the HCT116 scRNAseq data by RNA velocity, an algorithm that predicts the future cell state of individual cells on a short-term timescale (usually hours), based on the ratio between spliced and unspliced mRNA. Consistent with the fitted Markov Model, the majority of cells were moving in their respective state, and both states included source and sink points that could elicit or inhibit plasticity (**Figure 2-supplement 1C**). On a population level, EpCAM^{lo} cells were more likely to transit to EpCAM^{hi} cells than vice versa (by partition-based graph abstraction or PAGA; **Figure 2-supplement 1D**). Within the EpCAM^{lo} subpopulation, *CD44* and mesenchymal genes such as *VIM* and *ZEB1* were expressed with different dynamics (**Figure 5-supplement 1C**). In fact, only a small population of cells was captured in the process of transitioning to the other identity (**Figure 5E**). This apparently plastic population, earmarked by the opposing velocity arrows, showed the highest pEMT score (**Figure 5F**), as well as high *SPARC* expression (**Figure 5G**).

Chapter 4
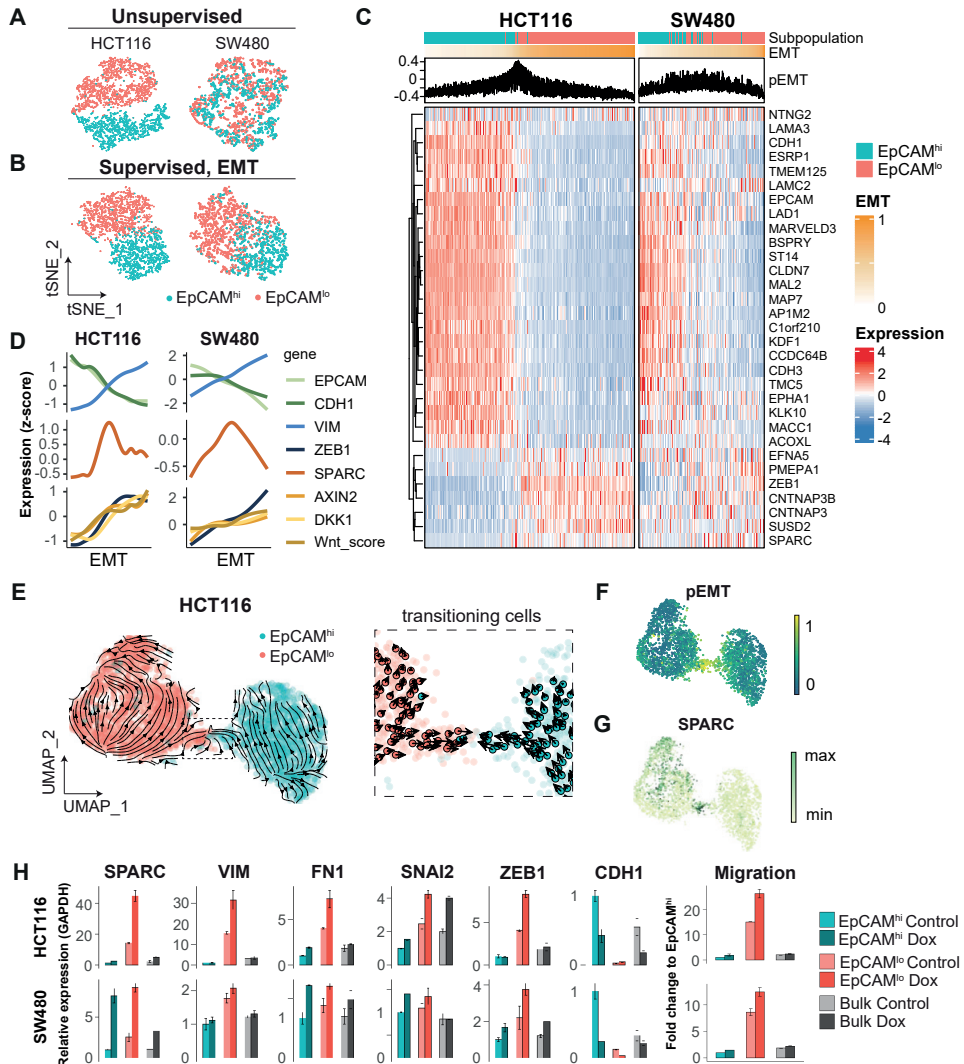
Figure 5. scRNAseq analysis of EpCAM^lo cells reveals specific markers of partial EMT cells. (**a**) tSNE of HCT116 and SW480 cells based on the variable expressed genes across EpCAM^lo and EpCAM^hi populations. (**b**) tSNE of HCT116 and SW480 cells based on genes from the EMT signature (N = 107). (**c**) Heatmap of differentially expressed genes between EpCAM^lo and EpCAM^hi populations. Cells were ranked according to their EMT score (EMT = M – E). (**d**) Gene expression trends projected over the EMT axis. Expression values were imputed with MAGIC, scaled by their z-score and smoothened by general additive models to visualize the gene expression trend. (e) RNA velocity analysis of the HCT116 scRNAseq data. Cells from both populations were moving in their respective state (left panel) with a minority population of transitioning cells (right panel). (**f**) Projection of the pEMT score on the UMAP embedding of the HCT116 cell line. (**g**) The expression of SPARC on the UMAP embedding of the HCT116 cell line. (**h**) Left panels: qPCR analysis of SPARC overexpression in the subpopulations of HCT116 and SW480. Gene expression values are relative to GAPDH and normalized to the EpCAM^hi subpopulation. Right panel: quantification of the transwell migration assay upon overexpression of SPARC.

Last, we performed cluster analysis on the HCT116 scRNAseq data. Unsupervised clustering using shared neighbor (SSN) modularity optimization revealed the presence of distinct subclusters (n=8): 3 of EpCAM^{hi} origin, and 5 EpCAM^{lo} (**Figure 5-supplement 1D**). To further investigate the gene expression patterns underlying the different EMT states, we performed a cluster analysis where the EMT signature genes are grouped with k-means according to their average expression in the unsupervised clusters (**Figure 5-supplement 1E**). This analysis revealed four sets of genes expressed in different combinations throughout the different clusters. Notably, gene set mes1, including *ZEB1, VIM* and *SNAI2,* is expressed throughout the EpCAM^{lo} clusters, while gene set mes2, including *SPARC*, *FN1* and *TWIST1* is mostly expressed in the pEMT EpCAM^{lo} cluster (#7). Of note, the partial EMT clusters #6 and #7 showed distinct expression of these gene sets indicating alternative activation of specific arrays through which partial EMT cells arise (**Figure 5-supplement 1F**).

As *SPARC* earmarks pEMT states (**Figure 5D**), we overexpressed it in the HCT116 and SW480 cell lines and observed a marked increase in the expression of EMT-TFs (*ZEB1* and *SNAI2*) and the corresponding up- and -down-regulation of mesenchymal and epithelial markers in EpCAM^{lo} cells and a corresponding increase in their motility and invasive capacity (**Figure 5H**).

Taken together, our *in silico* analysis shows substantial heterogeneity within the EpCAM^{lo} subpopulation across colon cancer cell lines. Among EpCAM^{lo} cells, a minority exhibits partial EMT and underlies the stochastic EpCAM$^{lo->hi}$ and EpCAM$^{hi->lo}$ transitions. Of note, pEMT is shown here not only as an '*in-between*' state earmarked by the co-expression of E- and M-specific genes, but also by specific genes like *SPARC* whose expression peaks at pEMT states.

Identification of EpCAM^{lo} colon cancer cells in primary colorectal tumors

As shown above, the EpCAM^{lo} gene signatures derived from both cell lines show high concordance with the CMS4 subtype, and are strongly associated with poor survival. Previously, it has been questioned to what extent the CMS4 profile reflects a *bona fide* clinical identity rather than being a representation of contamination from the tumor micro-environment [32,33].

We addressed this issue by evaluating the CMS4 signature (here referred to as "*CMS4_RF*") (**Figure 5-source data 1**) originally developed by Guinney et al. [27], and by taking advantage of a recent scRNAseq study on colon cancer resections from 29 patients [34]. Based on the latter study, as depicted in **Figure 6A**, the CMS4_RF signature shows the highest association with normal and tumor stromal cells. At the bulk RNAseq level, using the larger (n= 3232 patients) cohort of colon tumors from Guinney et al. [27], the CMS4_RF signature is clearly enriched among the CMS4 tumors (**Figure 6B**) and is likewise associated with poor survival (**Figure 6C**). Hence, the CMS4_RF signature reflects the presence of tumor-associated stromal cells, likely to be enriched in patients with decreased overall survival. To question whether the presence of a subset of *bona fide* tumor cells in quasi-mesenchymal state (EpCAM^{lo}) may also represent a feature of colon cancers with poor prognosis, we derived a distinct signature ("*CMS4_TC*") (**Figure 5-source data 1**) by selecting genes correlated (Pearson >0.3) with the CMS4_RF signature within the tumor epithelial fraction from the Lee et al. study[34].

Chapter 4
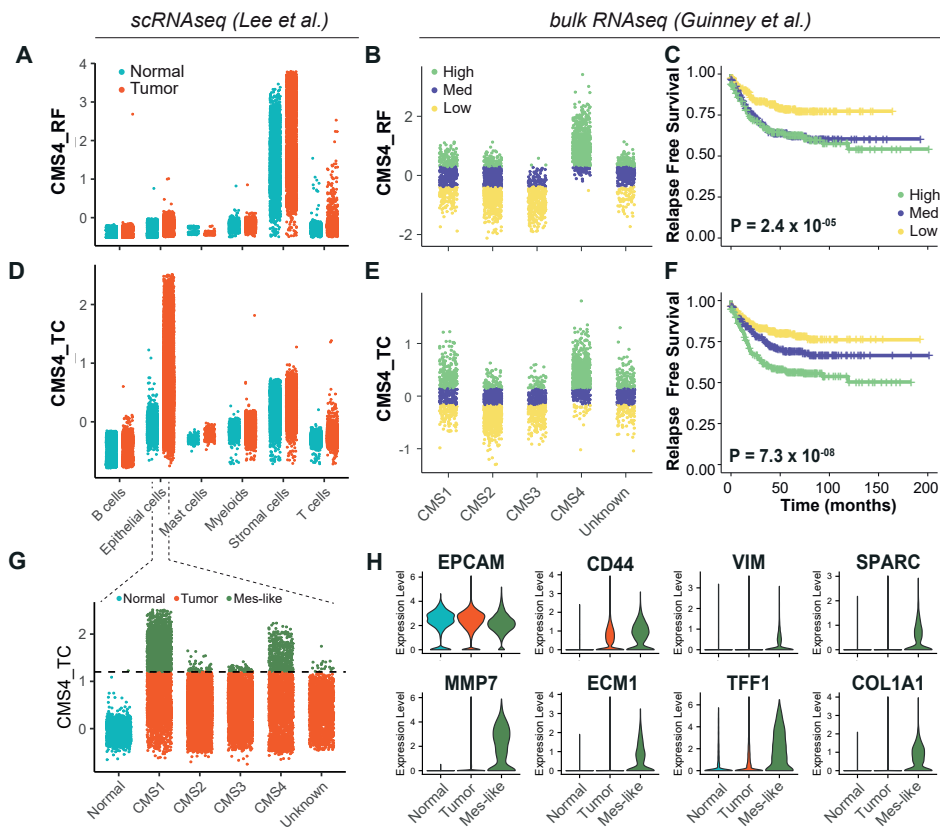
Figure 6. Identification of EpCAM^{lo} cells in primary colorectal tumors. (**a**) Expression of the CMS4_RF signature in the scRNAseq data from Lee et al. (N = 91,103 cells) indicates high association to the stromal cells. (**b**) Expression of the CMS4_RF signature in the bulk RNAseq data from Guinney et al. (N = 3232 tumors) shows association to CMS4 tumors. Tumors were grouped in 3 equal groups according to their association with the CMS4_RF signature. (c) Kaplan-Meier plot of the 3 CMS4_RF groups shows significant differences in relapse-free survival. (**d**) Expression of the CMS4_TC signature in the scRNAseq data reveals high association to the tumor epithelial cells. (**e**) Expression of the CMS4_TC signature in the bulk RNAseq data shows association to CMS1 and CMS4 tumors. Tumors were grouped in 3 equal groups according to their association with the CMS4_TC signature. (**f**) Kaplan-Meier plot of the 3 CMS4_TC groups shows significant differences in relapse-free survival. (g) Expression of the CMS4_TC signature in the fraction of epithelial cells (N = 24707 cells). Cells from CMS1 and CMS4 tumors show the highest association to the CMS4_TC signature, and were annotated as mes-like. (h) Violin plots of normal, tumor and mes-like tumor cells showing expression patterns across different genes.

Accordingly, the CMS4_TC signature shows the highest association with epithelial tumor cells (**Figure 6D**). Of note, at the bulk RNA level, the CMS4_TC signature shows increased association with both CMS1 and CMS4 tumors (**Figure 6E**), and outperforms the CMS4_RF signature in stratifying patients on survival (**Figure 6F**). The same CMS4_TC signature can clearly stratify patients from CMS groups other than CMS4, and in particular CMS1 and CMS3, on survival (**Figure 6-supplement -1**).

Finally, in order to identify EpCAM^{lo} cells in primary colorectal tumors, we took advantage of the scRNAseq data from Lee et al. [34] to annotate the tumor cells with highest association to the CMS4_TC signature as mesenchymal-like (Mes-like = 9.7% of all tumor cells) (**Figure 5-source data 1**). In agreement with the observations made at the bulk RNA level, tumor cells from CMS1 and CMS4 patients showed the highest association to the CMS4_TC signature (**Figure 6G**). Differential expression between the mesenchymal-like and bulk tumor cells revealed lower expression of *EPCAM*, while higher expression of *CD44* and mesenchymal markers such as *VIM*, *COL1A1*, *MMP7*, *ECM1*, and *SPARC* (**Figure 6H**), the latter previously identified to peak at intermediate EMT levels and predicted by RNAvelocity to earmark a subpopulation of plastic cells transitioning in between states (**Figure 5D-G**).

Discussion

The progression from primary tumor to metastasis still represents an unsolved puzzle as genomic and gene expression profiles of primary cancers and their matched metastases are in general strikingly similar [35]. Colon cancer provides a unique example for this conundrum: although it is well-established that a sequence of gene mutations underlies the adenoma-carcinoma sequence at the primary site, no alterations have been identified in genes potentially able to underlie local invasion and distant metastasis. Hence, the capacity to metastasize could already be pre-determined by specific mutations acquired by tumor cells at relatively early stages of tumorigenesis. However, this does not yet explain why and how only rare cells within the primary lesion acquire a metastatic phenotype that endows them with increased cell motility and with the capacity to invade the stromal microenvironment to eventually home at distant organ sites and form metastases. From this perspective, phenotypic plasticity likely represents a relevant mechanism for metastasizing colon carcinoma cells to transiently and reversibly change their cellular identity along the invasion-metastasis cascade [3,4].

The vast majority of colon cancers are initiated by mutations at the *APC* gene predicted to lead to constitutive Wnt signaling by β-catenin nuclear translocation. However, IHC analysis has shown that nuclear accumulation of β-catenin is exclusively observed at the invasive front where tumor cells are exposed to growth factors and cytokines secreted by the stromal microenvironment likely to further enhance Wnt signaling in localized fashion [10]. As different levels of Wnt/β-catenin signaling are associated with distinct cellular outcomes [36], it is plausible to think that the 'full-blown' activation of this pathway, earmarked by nuclear β-catenin, may trigger EMT and endow phenotypic plasticity in a minority of colon cancer cells located at the invasive front. The transient and reversible nature of these cellular modifications is likely driven by epigenetic changes at EMT-TFs.

Here, we have taken advantage of the coexistence of biologically-distinct cellular phenotypes within commonly employed colon cancer cell lines to study the cellular and molecular mechanisms which underlie phenotypic plasticity and the acquisition of invasive and metastatic capacity. While the bulk of the cancer cells have a characteristic epithelial phenotype (here referred to as EpCAM^{hi}), a minority of cells with mesenchymal morphology and plastic features (EpCAM^{lo}) coexist in a dynamic equilibrium through stochastic state transitions with their more committed counterpart. Similar observations have been previously made in breast cancer and oral squamous cell carcinoma cell lines

Chapter 4

[11,12] which underlines their relevance for the study of phenotypic plasticity in a broad spectrum of malignancies.

As predicted by their morphology, EpCAM^lo cells feature increased invasive and metastatic capacity and a distinct gene expression profile when compared to their epithelial counterpart. In particular, EMT activation resulting from enhanced Wnt signaling and *ZEB1* upregulation are distinctive features of the EpCAM^lo transcriptome. Of note, *ZEB1* plays many pleiotropic roles ranging from the modulation of oncogenic and tumor suppressive pathways, cell-fate determination, stemness, and cell plasticity [37], and is as such likely to be a determinant in colon cancer invasion and metastasis. From this perspective, the recent debate on EMT as an essential requirement for metastasis [38] likely mirrors the complexity of transcription factors and their downstream targets involved in these processes. Moreover, a recent scRNAseq comparative study of various time-course EMT models has revealed very limited overlap among differentially expressed genes indicative of the vastly context-dependent nature of these processes [9]. The here presented data emphasize the key role played by EMT and its reverse MET in colon tumor cell dissemination and distant metastasis formation.

The observed role of enhanced Wnt signaling in EpCAM^lo cells is of interest in view of the presence of *APC* and *CTNNB1* (β-catenin) gene mutations in these cell lines [20,21]. Further enhancement of Wnt signaling is likely to result in EMT activation through *ZEB1* upregulation and its conversion from a repressor to activator state [24]. On its turn, increased *ZEB1* expression was also shown to enhance Wnt, possibly in an autocrine stimulatory circuit [25]. Accordingly, Wnt 'super-activation' by GSK3β inhibition (i.e. Chiron) in the *APC/CTNNB1*-mutated colon cancer cell lines results in a significant expansion of EpCAM^lo cells and increased *ZEB1* expression. Vice versa, *ZEB1* downregulation by shRNA leads to a dramatic contraction of the EpCAM^lo subpopulation. Notably, isogenic subclones of HCT116 carrying wild type, heterozygous, and homozygous mutations at the β-catenin locus [26] show a progressive increase in the size of the EpCAM^lo subpopulation. These observations highlight the relevance of Wnt dosages in the downstream activation of EMT.

Transcriptional regulation of EMT-TFs has been shown to be controlled by miRNAs binding to specific 3'UTR sequences. In particular, members of the miR-200 family inhibit EMT and cancer cell motility by suppressing Wnt/ β-catenin signaling and by directly interfering with the expression of EMT-TFs and in particular of *ZEB1/2* [14,23]. Accordingly, we have shown that the expression of different members of the miR-200 family is downregulated in EpCAM^lo colon cancer cells when compared with their epithelial counterpart. Moreover, the RKO cell line, composed entirely of EpCAM^lo cells, was previously reported to be characterized by epigenetic downregulation of miR-200a/b/c leading to high *ZEB1* expression levels [39] in the absence of Wnt-activating mutations [40]. As the epigenetic activation/silencing of the miR-200 locus is dynamically regulated by common EMT-inducers such as TGFβ and Wnt [23,39], it is likely that phenotypic plasticity is triggered *in vivo* in cells located at the invasive front of colon carcinomas as a result of a complex interplay between their specific mutation spectra and epigenetic profiles modulated by different signaling cues from the microenvironment. The consistent presence of cells with nuclear co-localization of ZEB1 and β-catenin located at the invasive front of patient-derived colon carcinomas validates these observations. Other EMT-TFs like ZEB2 are likely to be upregulated in ZEB1-negative cases [41].

The clinical relevance of our results, originated from the analysis of immortalized cancer cell lines, came from the bioinformatic mining of bulk and scRNAseq data from patient-derived colon cancers. First, EpCAM^{lo} expression signatures are highly correlated with the CMS4 signature [27] and with shorter disease-free and overall survival. The mesenchymal CMS4 subtype accounts for approx. 25% of the cases, and is associated with the greatest propensity to form metastases. While the CMS4 signature was initially attributed to the presence of tumor-associated stroma and not to a cancer cell-intrinsic property [32,33], it has been shown that *bona fide* tumor cells from stroma-rich cancers have a markedly mesenchymal gene expression pattern [28]. By taking advantage of the Lee et al. scRNAseq study [34], we derived a tumor-specific signature (*CMS4_TC*) by selecting epithelial-specific genes from the original CMS4_RF signature, that outperforms other commonly employed prognostic and predictive markers (e.g. *BRAF* mutation and MSI; *data not shown*) in stratifying CMS1, 3, and 4 colon cancer patients based on overall survival. These results highlight the relevance of our study in the identification of a quasi-mesenchymal cellular state with plastic, invasive, and metastatic properties predictive of poor prognosis in colon cancer patients regardless of their CMS classification.

Recent studies on the role of EMT in eliciting phenotypic plasticity in cancer cells have highlighted the relevance of intermediate cellular stages co-expressing both epithelial and mesenchymal genes for tumor progression and metastasis [42-44]. These hybrid E/M or partial EMT cells are thought to be endowed with increased invasive and metastatic capacity. Our scRNAseq analysis of EpCAM^{lo} colon cancer cells has revealed not only fully mesenchymal but also hybrid E/M subclusters, the latter predicted *in silico* to underlie the observed transcriptional heterogeneity. Of note, transcriptional activation of specific arrays of E- (epi1/2) and M- (mes1/2) genes accompanies the transition between cellular states. Partial EMT cells, predicted by RNAvelocity to transit between states, are characterized not only by the co-expression of E- and M-specific genes at intermediate levels, but also by increased expression of specific genes like *SPARC* (Secreted Protein Acidic and Rich in Cysteine, also known as osteonectin), encoding for a matricellular protein involved in the modulation of cell–cell and cell–matrix interactions and known as a prognostic marker in colon cancer [45]. The role of SPARC in cancer is controversial as it has been shown to promote EMT and metastasis, but also to encompass tumor-suppressive functions in context-dependent fashion [46]. Importantly, SPARC triggers EMT through direct cell-to-cell contact and upregulation of other EMT-inducers like fibronectin (FN1) [47], reminiscent of the interactions occurring between parenchymal and stromal cells at the invasive front in colon cancer[10] where pEMT is expected to underlie plasticity and invasion through the ECM. Although SPARC is unique in its expression peaking at pEMT states and earmarking the transition between EpCAM^{lo} and EpCAM^{hi} in both cell lines, and in mes-like cells from patient-derived colon cancers, it seems unlikely that specific genes exist that can independently elicit pEMT. Instead, tumor-specific and context-dependent activation of subset of genes with distinct functions (e.g. *SPARC*, *FN1*, *MMP7*, *ZEB1*, *ECM1*) synergistically promoting, for example, collective cell migration upon interaction with the stromal microenvironment, may represent a more likely scenario.

The metastable and plastic features of EpCAM^{lo} cells was further highlighted by their striking capacity of giving rise to distant metastases reminiscent of the primary tumors both in the prevalence of EpCAM^{hi} cells and in the distinct patterns of β-catenin intracellular localization between the periphery and center of the lesions. These observations are in

agreement with the key role of MET for the onset of distant metastasis[7]. The admittedly marginal increase in liver and lung metastases upon continuous induction of *ZEB1* expression is likely to result from MET inhibition. From this perspective, our results provide support to the "migrating CSC" [7] and "β-catenin paradox" [10] models and shed light in the cellular and molecular mechanisms underlying Wnt super-activation, (p)EMT induction, and cell dissemination along the invasive front of colon carcinomas.

The characterization of the cellular and molecular mechanisms underlying phenotypic plasticity in colon cancer cells along the invasion-metastasis cascade has great relevance for the development of future diagnostic and therapeutic approaches based on circulating tumor cells (CTCs). Although current detection methodologies mainly rely on their epithelial features, more recent studies have indicated that CTCs with less pronounced epithelial characteristics are likely to underlie metastasis at distant organ sites. In breast and oral cancer, hybrid E/M tumor cells feature the highest degree of phenotypic plasticity coupling the capacity of undergoing EMT/MET with therapy resistance and other stem cells features [48,49]. Further single cell RNAseq and functional analyses of extensive cohorts of EpCAM^{lo} cells from matched primary tumors, CTCs, and the corresponding distant metastases will open new avenues for diagnostic and therapeutic applications.

Materials and Methods

Cell culture

Human colon cancer cell lines were acquired from ATCC (American Type Culture Collection) and cultured in DMEM medium (11965092, Thermo Fisher Scientific) [supplemented with 10% heat inactivated fetal bovine serum (FBS; Thermo Fisher Scientific), 1% Penicillin/Streptomycin (penicillin: 100 U/ml, streptomycin: 100 µg/ml; 15140122 Thermo Fisher Scientific)] in humidified atmosphere at 37°C and 5% CO_2. The identity of each cell line was confirmed by DNA fingerprinting with microsatellite markers (Amelogenin, CSF1PO, D13S317, D16S539, D5S818, D7S820, THO1, TPOX, vWA, D8S1179, FGA, Penta E, Penta D, D18S51, D3S1358, D21S11) and compared with the analogous data provided by ATCC, EACC, and https://web.expasy.org/cellosaurus/ (data not shown). The HCT116-P, HCT116-WT and HCT116-MT cell lines were kindly given by the laboratory of Hoguen Kim from the Yonsei University College of Medicine in Seoul, Korea.

Apc$^{fl/fl}$::Kras$^{G12D/+}$::Trp53$^{fl/R172H}$ (AKP) organoids organoids were grown in 50 µL droplets of Matrigel (Corning) covered with Advanced DMEM-F12 medium (12634028, Thermo Fisher Scientific) supplemented with 1x GlutaMAX (35050-061, Thermo Fisher Scientific), HEPES (15630-056, Thermo Fisher Scientific), gentamicin (15750060, Thermo Fisher Scientific), 100 ng/ml mEgf (PMG8041, Thermo Fisher Scientific), 2% B27 supplement (12587010, Thermo Fisher Scientific), mNoggin (self-produced according to protocol), and 100 µM Y-27632 (Y0503, Sigma Aldrich).

Chiron (CHIR99021, 4423, Tocris, dissolved at 20 mM in DMSO), 4 µM CHIR99021 was added to the culture medium every 48 hours for one week.

Flow cytometry and sorting

For flow cytometry and sorting purposes, cells were detached from the culture dishes using trypsin-EDTA (15400054, Thermo Fisher Scientific) and resuspended in staining buffer (PBS supplemented with 4% FCS). Antibody staining was performed on

ice for 30' with CD44-APC (clone IM7, 559250, BD Pharmingen) and EpCAM-FITC (ESA-214, GTX30708, GeneTex). Cells were then washed and resuspended in PBS 4% FCS. Flow cytometry analysis and cell sorting were carried out with a FACSAria III Cell Sorter (BD Biosciences). Forward-scatter height (FSC-H) versus forward-scatter width (FSC-W), and side-scatter height versus side-scatter width were employed to eliminate cell aggregates and ensure single cell sorting. Gates were defined as depicted and specified in Figure 1. The DAPI nuclear dye (D9542, Sigma-Aldrich) was used at 1 µg/ml to exclude dead cells. FITC and GFP were analyzed using 488 nm laser and 502LP and 530/30BP filters; APC and Sytox Red with a 633 nm laser and a 660/20BP filter; BV421 using a 405 nm laser and a 450/40BP filter; BV785 with a 405 nm laser and a 750LP and 780/60BP filter; PE with a 461 nm laser and a 582/15 BP filter.

For the clonogenicity assays, single cells were sorted into 96-well plates at 1 cell/well in culture medium. After sorting, the plates were checked under the microscope to confirm the presence of a single cell per well. Upon confluency, each single clone was FACS-analyzed for CD44/EpCAM at different time points.

For the flow cytometry analysis of mouse liver metastases and primary AKP-Z organoid derived tumors, freshly resected tissue samples were cut into small pieces, washed three times with ice-cold PBS, and subsequently digested in Advanced DMEM-F12 (12634028, Thermo Fisher Scientific) containing 50 mg/mL of collagenase A (11088793001, Roche) for 30' at 37°C, with vigorous pipetting every 10'. Residual tissue fragments were further treated with TrypLE Express (12605-010, Thermo Fisher Scientific), 0,25% Trypsin (Thermo Fisher Scientific) and 0.1 mg/mL DNaseI (DN25, Sigma-Aldrich) for 45' at 37°C. Samples were then washed and filtered in sequence through a 100 and 40 µm cell strainer (Corning). The HCT116 derived cells from the liver metastasis were identified and analyzed using the following antibodies for 30' on ice: HLA-A, B, C-biotin (clone W6/32, 311434, Biolegend), Streptavidin-PE-Dazzle 549 (Biolegend), rat anti-mouse CD45-BV421 (clone 30-F11, 563890, BD Biosciences), rat anti-mouse CD31-BV421 (clone 390, 563356, BD Biosciences), rat anti-mouse TER-199-BV421 (clone TER-119, 563998, BD Biosciences), CD44-APC (clone IM7, 559250, BD Pharmingen) and EpCAM-FITC (ESA-214, GTX30708, GeneTex). AKP-Z tumor derived cells were stained using the following antibodies: rat anti-mouse CD45-BV421 (clone 30-F11, 563890, BD Biosciences), rat anti-mouse CD31-BV421 (clone 390, 563356, BD Biosciences), rat anti-mouse TER-199-BV421 (clone TER-119, 563998, BD Biosciences), anti-mouse EpCAM-PE (clone G8.8, Biolegend), anti-mouse/human CD44-APC (clone !M7, BD Biosciences), and DAPI. Intrinsic GFP expression was also used to select for organoid derived cells).

Cell proliferation assay and cell cycle analysis

For proliferation assays, sorted cells were seeded in 24-well dishes (2500 cells/well) and cultured in conventional medium. Cells were harvested and counted at the indicated time points. For cell cycle analysis, sorted cells were centrifuged, fixed in 70% ethanol and stained with 50 µg/ml propidium iodide (PI) (Sigma), and 0.2 mg/ml RNAse A (10109142001, Sigma-Aldrich). The stained cells were then FACS-analyzed using a 655LP and a 695/40 BP filter.

Chapter 4

Cell viability assays

For the chemoresistance assays, cells were seeded in 96-well plates at 15000 cells/well and left overnight to adhere. Three technical replicates were plated per tested condition. Both oxaliplatin (Sigma-Aldrich) and 5-fluorouacil (5-FU; Sigma-Aldrich) were dissolved in DMSO. HCT116 cells were incubated for 3 or 5 days with 5-FU and oxaliplatin, respectively, whereas SW480 cells were treated with 5-FU or oxaliplatin for 7 days (calibrated on the response of the parental line in terms of viability). After removal of the chemotherapeutic drug, cells were washed with PBS and left to re-grow in standard culture medium. Cell viability was assessed using the MTT (3-(4,5-dimethylthiazol-2-yl)-2,5-diphenyltetrazolium bromide; Sigma-Aldrich) assay at time zero, i.e. upon removal of the drug, and after re-growth (range 1-36 days). Briefly, cells were incubated at 37°C, 5% CO_2 for 3 hrs. in culture medium supplemented with 0.45 mg/mL MTT. The 96-well plates were then centrifuged at 1,000 rpm for 5' and the culture medium removed. MTT formazan precipitates were solubilized with DMSO. O.D. reading was performed at 595 nm with a Microplate Reader (Model 550, Bio-Rad). Background measurements were subtracted from each data point. MTT-based results were also validated by manual count of trypan blue positive cells, using cells harvested from additional 96 wells. At least two biological experiments were performed for each individual cell line and drug.

Selection of oxaliplatin and 5-FU concentrations and administration times for chemo-resistance assays was as follows. In a pre-defined range of concentrations (1.5 -100 g/ml for 5-FU, and 0.6-50 □g/ml for oxaliplatin) based on previous data, the maximal concentration and length of treatment was selected as the combination able to induce cell death in approx. 80% of EpCAM^{lo} cells. From that concentration, the curve was scaled down by 50% at least three times to reach the lowest concentration to be tested. The minimal treatment length was 72 hrs, while the maximal duration was 1 week. Oxaliplatin was considerably slower than 5-FU in its cytotoxicity with HCT116 cells. The difference was less relevant in SW480 cells where numerous cells, although irreversibly damaged, remained viable for several days. For the latter reason, treatment was longer in SW480 cells.

Migration and invasion assays

For the 'transwell' (modified Boyden chamber) migration and invasion assays, cells were starved for 24 hrs. in DMEM supplemented with 1% FBS. For each tested subpopulation, 1.0×10^6 cells were harvested, resuspended in 1% FBS medium and plated in transwell tissue culture inserts (8 μm polycarbonate membrane, 24 well, 3428; Corning). For the invasion assays 1.5 μg/ml Matrigel dissolved in serum-free medium was pipetted on top of the transwell membrane and left to set at 37°C for several hours before plating the cells. DMEM medium with 10% FBS was then placed in the lower compartment of the transwell chamber. For both assays three technical replicates were plated for each subpopulation. Plates were incubated for 24 hrs. at 37°C/5% CO_2, after which the cells and membranes were fixed in methanol and stained with crystal violet. The non-migrated cells on the upper surface of the membrane were removed with a cotton-wool bud and the cells migrated to the lower surface of the membrane counted. For both assays two independent experiments were performed.

RNA isolation and qRT-PCR

RNA was isolated from cells using TRIzol™ Reagent (15596018, ThermoFisher Scientific) according to the manufacturer's instructions. RNA concentration was measured by NanoDrop. Subsequently, reverse transcription into cDNA was conducted using the High-Capacity cDNA Reverse Transcription Kit (4368814, Life Technologies) according to the manufacturer's instructions. RT-qPCR was performed with Fast SYBR Green Master Mix (4385617; ThermoFisher Scientific). PCR amplification and detection were implemented with the 7400 Fast Real-Time PCR System. Expression levels were normalized for the endogenous *GAPDH* reference gene. All PCR primers here employed are listed here below:

GENE	FORWARD PRIMER	REVERSE PRIMER
GAPDH	5'-ACCCAGAAGACTGTGGATGG-3'	5'-TCTAGACGGCAGGTCAGGTC-3'
EPCAM	5'-GCAGCTCAGGAAGAATGTG-3'	5'-CAGCCAGCTTTGAGCAAATGAC-3'
CDH1	5'-TGCCCAGAAAATGAAAAAGG-3'	5'-GTGTATGTGGCAATGCGTTC-3'
VIM	5'-GAGAACTTTGCCGTTGAAGC-3'	5'-GCTTCCTGTAGGTGGCAATC-3'
CDH2	5'-CAACTTGCCAGAAAACTCCAGG-3'	5'-ATGAAACCGGGCTATCTGCTC-3'
FN1	5'-CAGTGGGAGACCTCGAGAAG-3'	5'-TCCCTCGGAACATCAGAAAC-3'
ZEB1	5'-GCACAACCAAGTGCAGAAGA-3'	5'-CATTTGCAGATTGAGGCTGA-3'
ZEB2	5'-TTCCTGGGCTACGACCATAC-3'	5'-TGTGCTCCATCAAGCAATTC-3'
TWIST1	5'-GTCCGCAGTCTTACGAGGAG-3'	5'-GCTTGAGGGTCTGAATCTTGCT-3'
SNAI1	5'-GCGAGCTGCAGGACTCTAAT-3'	5'-CCACTGTCCTCATCTGACA-3'
SNAI2	5'-GGGGAGAAGCCTTTTTCTTG-3'	5'-TCCTCATGTTTGTGCAGGAG-3'
FOXC2	5'-GCCTAAGGACCTGGTGAAGC-3'	5'-TTGACGAAGCACTCGTTGAG-3'

miRNA

For miRNA experiments, sorted cell populations from HCT116 and SW480 cell lines were cultured up till 70% confluency in 6 well-multiwell plates. Total RNA was then isolated using the Trizol™ (Ambion) protocol. For *miR-200-family (miR-200a, miR-200b, miR-200c, miR-141, miR-429)*, reverse transcription was performed using the TaqMan MicroRNA RT Kit (Applied Biosystem), followed by qRT-PCR using TaqMan MicroRNA assay (Thermo Fisher scientific). *U6* snRNA was used as tanendogenous control. The expression of *miR-200-family* was analyzed by the ΔCT method. The experiment was repeated three times.

shRNA

in order to knock-down *ZEB1* expression, lentiviral inducible shRNA vectors encompassing control or *ZEB1* sequences were developed. *Cloning was performed according to the manufacturer's instructions[50]. Briefly,* Tet-pLKO-puro (gift from D. Wiederschain, Addgene plasmid # 21915) was digested with AgeI and EcoRI and isolated by gel purification (QIAEX II Gel Extraction Kit, Qiagen). The sequences of the control and *ZEB1 shRNA were as follows:* shRNA control (shCT) (Addgene sequence #1864): top 5'-CCGGCC TAAGGTTAAGTCGCCCTCGCTCGAGCGAGGGCGACTTAACCTTAGGTTTTTTG-3', bottom: 5'-AATTCAAAAAACCTAAGGTTAAGTCGCCCTCGCTCGAGCGAGGGCGACTTAACCTTAGG-3', shZEB1-A: target sequence (Broad Institute): 5'-GCTGCCAATAAGCAAACGATT-3'; oligo sequence: top: 5'-CCGGGCTGCCAATAAGCAAACGATTCTCGAGAATCGTTTGCTTATTGG CAGCTTTTT-3', bottom: 5'-AATTAAAAAGCTGCCAATAAGCAAACGATTCTCGAGAATCG

TTTGCTTATTGGCAGC-3', shZEB1-B: target sequence (Broad Institute): 5'-GTCTGGGT GTAATCGTAAATT-3' oligo sequence: top 5'-CCGGGTCTGGGTGTAATCGTAAATTCTCGAG AATTTACGATTACACCCAGACTTTTT-3', bottom 5'- AATTAAAAAGTCTGGGTGTAATCGTA AATTCTCGAGAATTTACGATTACACCCAGAC-3'. *The "top" and "bottom" labels indicate the oligonucleotide that were annealed in 0.1 M NaCl, 10 mM TrisHCl, pH 7.4, after incubation at 95°C followed by a cooling down step until room temperature is reached.* The digested vector (200 ng) was ligated with 1 μL of the oligonucleotides (0.45nmol/μl) using T4 DNA ligase (Promega) for 3 hrs. at room temperature. "One Shot Stbl3" chemically competent E. coli (Thermo Fisher Scientific) were transformed with the ligation product. Individual colonies were inoculated for mini-prep cultures and the presence of the insert was checked using the restriction enzyme XhoI and by sequencing.

For lentivirus production, the shCT or the pool of the two *ZEB1* shRNA constructs were packaged into second generation virus particles using psPAX2 (Addgene plasmid # 12260; gift from dr. Didier Trono), pMD2.G (Addgene plasmid # 12259) into HEK293T. Virus particles were titrated with the HCT116 cell line and a MOI of 0.5 was employed to produce the shRNA inducible HCT116 and SW480 cell lines. Lentivirus-infected cells were selected in medium containing 1 μg/mL puromycin (Dulbecco). shRNA induction was implemented by using 1 μg/mL doxycycline for 72 hrs. The extent of *ZEB1* downregulation was assessed by RT-qPCR.

Construction of Zeb1 inducible vector

A pORF mZeb1 plasmid (Cat, no. ORF062179) encompassing the cDNA of the *Zeb1* gene was employed for the construction of the lentiviral vector. The *Zeb1* gene was cloned into the pEN_TmiRc3 plasmid, gift from Iain Fraser (California Institute of Technology, CA). The *Zeb1* insert was transferred into a pSLIK-Hygro plasmid (#25737; Addgene, USA) by Gateway technology. All newly generated plasmids were sequence-verified by LGC Genomics (LGC Genomics GmbH, Germany). The pSLIK-Hygro plasmid was transiently transfected by Fugene HD (Promega) in HEK293T cells together with the VSV-G, MD and REV packaging plasmids. After 2 days, the culture medium was collected and viral particles were concentrated by ultracentrifugation. AKP organoids were transduced with the concentrated virus. After 24 hours, the transduced cells were selected by hygromycin B (Thermo Fisher Scientific, The Netherlands) (60 μg/mL) for7 days. Expression of *Zeb1* was confirmed by qRT–PCR upon stimulation with doxycycline hyclate.

Animal experiments

All protocols involving animals were approved by the Dutch Animal Experimental Committee and were conformed to the Code of Practice for Animal Experiments in Cancer Research established by the Netherlands Inspectorate for Health Protections, Commodities and Veterinary Public health (The Hague, the Netherlands, 1999). Animals were bred and maintained in the Erasmus MC animal facility (EDC) under conventional specific pathogen-free (SPF) conditions.

Spleen transplantation assays were implemented on 6 to 8 week-old NOD.Cg-*Prkdc^scid^ Il2rg^tm1Wjl^*/SzJ (NSG) male and female mice anesthetized intraperitoneally with ketamine (Ketalin®, 0.12 mg/ml) and xylazine (Rompun®, 0.61 mg/ml). Carpofen (Rimadyl®, 5 mg/ml) was given subcutaneously as analgesia. The spleen was exteriorized through a left lateral flank incision and $2.5x10^4$ HCT116 and SW480 cells, resuspended in 50 μl of PBS,

were injected into the spleen parenchyma using an insulin syringe. Fifteen minutes after injection, a splenectomy was performed with a fine tip cautery pen in order to remove spilled cells and ensure hemostasis. The peritoneum and skin were then sutured in two layers. Mice injected with HCT116 cells were sacrificed 4 weeks after injection for tumor collection; mice injected with SW480 cells were killed 8 weeks after spleen transplantation. Upon liver resection, individual macroscopic metastatic lesions were counted, dissected, and fixed in 4% paraformaldehyde (4% PFA). Residual liver tissue and the lungs were also fixed in 4% PFA for further immunohistochemical analyses.

Orthotopic transplantation of intestinal mouse organoids was performed as previously described[18]. In brief, the day before transplantation AKP-Zeb1 organoids containing a GFP and click beetle luciferase vector (ATG-1929, a gift from Keith Wood, Addgene plasmid #108712) were collected and mechanically dissociated into small clumps. About 100.000 cells were plated in 10 μL drops neutralized Rat Tail High Concentrate Type I Collagen (Corning, cat. No. 354249) and let to recover overnight at 37°C in Advanced DMEM-F12 medium (12634028, Thermo Fisher Scientific) 100 ng/mL mEgf (PMG8041, Thermo Fisher), 2% B27 supplement (12587010, Thermo Fisher), mNoggin (self-produced according to protocol), 100 μM Y-27632 (Y0503, Sigma Aldrich). Caecum transplantation assays were implemented on 6 to 8-week-old male NOD.Cg-*Prkdc^{scid} Il2rg^{tm1Wjl}*/SzJ (NSG) mice anesthetized intraperitoneally with ketamine (Ketalin®, 0.12 mg/ml) and xylazine (Rompun®, 0.61 mg/ml). Carpofen (Rimadyl®, 5 mg/ml) was given subcutaneously as analgesia. The caecum was exposed through a midline abdominal incision and a collagen drop containing tumor cells was surgically transplanted in the caecal submucosa. The peritoneum and skin were then sutured in two layers. Tumor growth was monitored by abdominal palpation. Mice were sacrificed 6-8 weeks after transplantation. Upon collection, primary caecal tumors were single cell digested and further analyzed by FACS. Mice used for quantification of liver and lung metastases were injected with Luciferin-D and imaged with an IVIS® Spectrum imaging system (Caliper Life Sciences, Hopkinton, MA, USA). After imaging tissues were fixed and cut into 500-micron slices using a Fibrotome, processed for IHC, stained for β-catenin visualize tumor cells, scanned using a NanoZoomer, and counted using NDP view software.

Immunofluorescence (IF) analysis

Coverslips containing a monolayer of cancer cells were fixed for 30' in 4% PFA at 37 °C and washed twice with PBS. Cells were first permeabilised for 15 minutes at room temperature with 0.2% of Triton X-100 and then incubated in blocking buffer (5% milk powder in PBS-Tween) for 1 hour at room temperature. Cells were then exposed overnight at 4 °C to primary antibodies against EpCAM (mouse, 1:250; sc-66020; Santa Cruz Biotechnology) and ZEB1 (rabbit, 1:200; sc-25388, Santa Cruz Biotechnology). After washing twice with PBS-Tween, coverslips were incubated for 1 hour at room temperature in blocking buffer containing the following secondary antibodies: Goat anti-Rabbit Alexa Fluor® 594 conjugate (1:250, #A-11037, Life Technologies) and Donkey anti-Mouse Alexa Fluor® 488 conjugate (1:250, #A-21202, Life Technologies). Cells were counterstained with DAPI to visualize the nuclei. Coverslips were mounted in VECTAHIELD HardSet Antifade Mounting Medium (#H-1400, Vector Labs) and imaged with a Zeiss LSM-700 confocal

microscope. Images were processed with ImageJ (U.S. National Institutes of Health, Bethesda, MD, USA).

Immunohistochemistry (IHC) analysis

Tissues from animal experiments were fixed overnight in 4% PFA and embedded in paraffin. Paraffin blocks containing human colon cancer tissue were obtained from the department of Pathology at the Erasmus Medical Center in Rotterdam. Four μm sections were mounted on slides. Immunohistochemistry was performed using the EnVision Plus-HRP system (Dako) and antibodies directed against β-catenin (1:200, 610154, BD Biosciences) and ZEB1 (1:200, HPA027524, Sigma-Aldrich). Briefly, paraffin embedded sections were dewaxed with Xylene and hydrated in 100% and 70% ethanol. Antigen retrieval was performed using pressure cooker pretreatment in a citrate buffer (pH 6.0) for ZEB1 and in a Tris-EDTA buffer (pH 9.0) for the anti-human-mitochondria and anti-β-catenin antibodies. Subsequently, slides were incubated at room temperature in 3% hydrogen peroxidase for 15' to block endogenous peroxidase activity. Tissue sections were washed and blocked with 5% BSA in PBS-Tween for 1 hour to then be incubated with the primary antibodies overnight at 4 °C. Slides were washed twice with PBS-Tween and incubated with Rabbit EnVision+ System-HRP (K4001, Dako) or Mouse EnVision+ System-HRP (K4007, Dako) for 30'. Subsequently, signal detection was and tissues were counterstained with Mayer's Hematoxylin. Dehydration was performed by incubation in 70% and 100% ethanol followed by Xylene before sleds were mounted using Pertex (00811, Histolab).

TOP-Flash reporter assay

For the β-catenin/TCF reporter assay (TOP-Flash reporter assay), cells were plated on 48-well dishes and cultured in medium with or without 4 μM CHIR99021. After 48 hrs., when 70% confluence was reached, cells were transfected by Fugene HD (Promega) with 125 ng of the TOP-Flash or FOP-Flash reporter constructs together with 25 ng of the Renilla luciferase vector for normalization purposes. Luciferase activity was measured using the Dual-Luciferase Reporter Assay System (Promega) 24 hrs. post-transfection. Luminesence was measured using a GloMax Luminometer.

Next Generation Sequencing (NGS): RNAseq

RNA quality and quantity was evaluated on a 2100 Bio-analyzer (Agilent) using the Agilent RNA 6000 Pico Kit. RNA samples were further processes according to the TruSeq Sample Preparation v.2 Guide (Illumina) and paired end-sequenced on the HiSeq 2500 (Illumina).

Illlumina paired-end reads of 76 bases were trimmed by removing the TrueSeq adapter sequences using Trimmomatic (v.0.33)[51]. Subsequently, the reads were mapped in a two-pass procedure to the human reference genome build hg38 with the RNA-seq aligner STAR (v2.4.2a)[52] and the Homo sapiens GENCODE v23 annotation[53]. Raw counts were summed with the summarize overlaps function with union mode from the Bioconductor Genomic Alignments package[54] (v1.14.0). Genes were called differentially expressed with a generalized linear model using a negative binomial distribution with correcting for cell lines in multi-cell line comparisons. DESeq2 (v1.16.1) was used to perform these calculations[55]. We applied a Wald-test to identify statistical significant

differently expressed genes. *P*-values were adjusted using the Benjamini-Hochberg[56] correction based on which a threshold value was set at < 0.01. Multidimensional scaling was performed after the read counts were normalized with blind variance stabilizing log2 transformation function of DESeq2. Gene Ontology (GO) and Kyoto Encyclopedia of Genes and Genomes (KEGG) gene enrichment analyses were carried out as described previously[57]. R (v 3.4.0) (R Core Team, 2017; https://www.R-project.org/) was employed for statistical analysis and visualization of the data.

Bioinformatics analysis bulk RNAseq

For pathway analysis generated RNAseq datasets were uploaded into Ingenuity Pathway Analysis software (Qiagen). For other bioinformatics analyses, the generated datasets were uploaded into the R2 Genomics Analysis and Visualization Platform (http://r2.amc.nl). First, we used the 'differential expression between groups' option to identify the hundred genes with highest expression in the EpCAM^{lo} fraction in both the HCT116 and SW480 cells. These genes were saved as separate gene sets. Expression values of all genes in both gene sets was then assessed in the CMS-3232 composite cohort[27], as well as in a large cohort of profiled cell lines originating from the Broad institute. This yielded single meta-gene expression values per tumor or cell line. These gene set expression values were then stored as separate tracks and compared using the 'relate 2 tracks' option, yielding Pearson R values and accompanying p values.

The 'relate 2 tracks' option was also used to compare the 2 gene sets identifying the EpCAM^{lo} cells with gene sets positively identifying the 4 different molecular subtypes within the published 273-gene CMS classifier, again yielding r values and corresponding p-values.

The gene sets identifying the EpCAM^{lo} cells from both cell lines were also used to cluster the tumors in the CMS3232 cohort into low, intermediate and high expression groups by k-means clustering. The Kaplan-Meier method was subsequently used to assess significant differences in survival between the generated subgroups. As all tumors in this cohort had previously been assigned to specific CMS subgroups, we then analyzed the contribution of each CMS subtype to each of the generated low, intermediate, high expression subgroups.

Single cell RNA seq

Cell lines were brought to 60-70% confluency before the start of the experiment. For each sample, between $5x10^4$ and $1x10^5$ EpCAM^{lo} and EpCAM^{hi} cells were FACS sorted and processed using the 10X Genomics Chromium Single Cell Controller. Samples were deep-sequenced (Illumina) to a depth ranging 49k-65k reads/cells. Gene-cell matrices were obtained by conversion of the raw data using the Cell Ranger pipeline. Filtered gene-cell matrices were merged in R, and processed for downstream analysis using the Seurat package. Dimension reduction was performed using PCA, tSNE and UMAP. Epithelial and mesenchymal scores were computed using the Rmagic (imputation) and GSVA (scoring) packages. RNA velocity analysis was done in Python using Velocyto and scVelo packages.

Data accessibility

The RNA-sequencing data from this study have been submitted to the Gene Expression Omnibus (GEO)[58] database under the accession number GSE154927 and GSE154930 for

Chapter 4

the bulk and single-cell RNAseq data, respectively. Other dataset referenced in this study are publicly available and can be accessed with GSE144735 and GSE132465 (Lee et al.), and at Synapse with syn2623706 (Guinney et al.).

Statistical analysis

For each experiment, data are shown as mean ±SD. IBM SPSS Statistics software was used for data analysis. The Mann-Whitney U test was used to analyze the difference between two groups of quantitative variables; α-value was set at 5%.

Competing Interests Statement

The authors of this manuscript do not have any competing financial interests in relation to the work described.

References

1. Fearon, E.R.; Vogelstein, B. A genetic model for colorectal tumorigenesis. *Cell* **1990**, *61*, 759-767, doi:10.1016/0092-8674(90)90186-i.

2. Hanahan, D.; Weinberg, R.A. The hallmarks of cancer. *Cell* **2000**, *100*, 57-70, doi:10.1016/s0092-8674(00)81683-9.

3. Varga, J.; Greten, F.R. Cell plasticity in epithelial homeostasis and tumorigenesis. *Nature cell biology* **2017**, *19*, 1133-1141.

4. Teeuwssen, M.; Fodde, R. Cell Heterogeneity and Phenotypic Plasticity in Metastasis Formation: The Case of Colon Cancer. *Cancers (Basel)* **2019**, *11*, doi:10.3390/cancers11091368.

5. Nieto, M.A.; Huang, R.Y.; Jackson, R.A.; Thiery, J.P. Emt: 2016. *Cell* **2016**, *166*, 21-45.

6. Mani, S.A.; Guo, W.; Liao, M.J.; Eaton, E.N.; Ayyanan, A.; Zhou, A.Y.; Brooks, M.; Reinhard, F.; Zhang, C.C.; Shipitsin, M.; et al. The epithelial-mesenchymal transition generates cells with properties of stem cells. *Cell* **2008**, *133*, 704-715.

7. Brabletz, T.; Jung, A.; Spaderna, S.; Hlubek, F.; Kirchner, T. Opinion: migrating cancer stem cells - an integrated concept of malignant tumour progression. *Nature reviews* **2005**, *5*, 744-749.

8. Skrypek, N.; Goossens, S.; De Smedt, E.; Vandamme, N.; Berx, G. Epithelial-to-Mesenchymal Transition: Epigenetic Reprogramming Driving Cellular Plasticity. *Trends Genet* **2017**, *33*, 943-959.

9. Cook, D.P.; Vanderhyden, B.C. Context specificity of the EMT transcriptional response. *Nat Commun* **2020**, *11*, 2142, doi:10.1038/s41467-020-16066-2.

10. Fodde, R.; Brabletz, T. Wnt/beta-catenin signaling in cancer stemness and malignant behavior. *Current opinion in cell biology* **2007**, *19*, 150-158.

11. Gupta, P.B.; Fillmore, C.M.; Jiang, G.; Shapira, S.D.; Tao, K.; Kuperwasser, C.; Lander, E.S. Stochastic state transitions give rise to phenotypic equilibrium in populations of cancer cells. *Cell* **2011**, *146*, 633-644, doi:10.1016/j.cell.2011.07.026.

12. Biddle, A.; Liang, X.; Gammon, L.; Fazil, B.; Harper, L.J.; Emich, H.; Costea, D.E.; Mackenzie, I.C. Cancer stem cells in squamous cell carcinoma switch between two distinct phenotypes that are preferentially migratory or proliferative. *Cancer Res* **2011**, *71*, 5317-5326, doi:10.1158/0008-5472.CAN-11-1059.

13. Lengauer, C.; Kinzler, K.W.; Vogelstein, B. Genetic instability in colorectal cancers. *Nature* **1997**, *386*, 623-627, doi:10.1038/386623a0.

14. Brabletz, S.; Brabletz, T. The ZEB/miR-200 feedback loop--a motor of cellular plasticity in development and cancer? *EMBO Rep* **2010**, *11*, 670-677, doi:10.1038/embor.2010.117.

15. Dean, M.; Fojo, T.; Bates, S. Tumour stem cells and drug resistance. *Nat Rev Cancer* **2005**, *5*, 275-284, doi:10.1038/nrc1590.

16. Kirchner, T.; Brabletz, T. Patterning and nuclear beta-catenin expression in the colonic adenoma-carcinoma sequence. Analogies with embryonic gastrulation. *Am J Pathol* **2000**, *157*, 1113-1121, doi:10.1016/s0002-9440(10)64626-3.

17. Fumagalli, A.; Drost, J.; Suijkerbuijk, S.J.; van Boxtel, R.; de Ligt, J.; Offerhaus, G.J.; Begthel, H.; Beerling, E.; Tan, E.H.; Sansom, O.J.; et al. Genetic dissection of colorectal cancer progression by orthotopic transplantation of engineered cancer organoids. *Proc Natl Acad Sci U S A* **2017**, *114*, E2357-E2364, doi:10.1073/pnas.1701219114.

Chapter 4

18. Fumagalli, A.; Suijkerbuijk, S.J.E.; Begthel, H.; Beerling, E.; Oost, K.C.; Snippert, H.J.; van Rheenen, J.; Drost, J. A surgical orthotopic organoid transplantation approach in mice to visualize and study colorectal cancer progression. *Nat Protoc* **2018**, *13*, 235-247, doi:10.1038/nprot.2017.137.

19. Hall, M.P.; Woodroofe, C.C.; Wood, M.G.; Que, I.; Van't Root, M.; Ridwan, Y.; Shi, C.; Kirkland, T.A.; Encell, L.P.; Wood, K.V.; et al. Click beetle luciferase mutant and near infrared naphthyl-luciferins for improved bioluminescence imaging. *Nat Commun* **2018**, *9*, 132, doi:10.1038/s41467-017-02542-9.

20. Nishisho, I.; Nakamura, Y.; Miyoshi, Y.; Miki, Y.; Ando, H.; Horii, A.; Koyama, K.; Utsunomiya, J.; Baba, S.; Hedge, P. Mutations of chromosome 5q21 genes in FAP and colorectal cancer patients. *Science* **1991**, *253*, 665-669, doi:10.1126/science.1651563.

21. Ilyas, M.; Tomlinson, I.P.; Rowan, A.; Pignatelli, M.; Bodmer, W.F. Beta-catenin mutations in cell lines established from human colorectal cancers. *Proc Natl Acad Sci U S A* **1997**, *94*, 10330-10334, doi:10.1073/pnas.94.19.10330.

22. Lamouille, S.; Xu, J.; Derynck, R. Molecular mechanisms of epithelial-mesenchymal transition. *Nat Rev Mol Cell Biol* **2014**, *15*, 178-196.

23. Ghahhari, N.M.; Babashah, S. Interplay between microRNAs and WNT/beta-catenin signalling pathway regulates epithelial-mesenchymal transition in cancer. *Eur J Cancer* **2015**, *51*, 1638-1649, doi:10.1016/j.ejca.2015.04.021.

24. Sanchez-Tillo, E.; de Barrios, O.; Siles, L.; Cuatrecasas, M.; Castells, A.; Postigo, A. beta-catenin/TCF4 complex induces the epithelial-to-mesenchymal transition (EMT)-activator ZEB1 to regulate tumor invasiveness. *Proc Natl Acad Sci U S A* **2011**, *108*, 19204-19209, doi:10.1073/pnas.1108977108.

25. Sanchez-Tillo, E.; de Barrios, O.; Valls, E.; Darling, D.S.; Castells, A.; Postigo, A. ZEB1 and TCF4 reciprocally modulate their transcriptional activities to regulate Wnt target gene expression. *Oncogene* **2015**, *34*, 5760-5770, doi:10.1038/onc.2015.352.

26. Kim, W.K.; Kwon, Y.; Jang, M.; Park, M.; Kim, J.; Cho, S.; Jang, D.G.; Lee, W.B.; Jung, S.H.; Choi, H.J.; et al. beta-catenin activation down-regulates cell-cell junction-related genes and induces epithelial-to-mesenchymal transition in colorectal cancers. *Sci Rep* **2019**, *9*, 18440, doi:10.1038/s41598-019-54890-9.

27. Guinney, J.; Dienstmann, R.; Wang, X.; de Reynies, A.; Schlicker, A.; Soneson, C.; Marisa, L.; Roepman, P.; Nyamundanda, G.; Angelino, P.; et al. The consensus molecular subtypes of colorectal cancer. *Nat Med* **2015**, *21*, 1350-1356, doi:10.1038/nm.3967.

28. Vellinga, T.T.; den Uil, S.; Rinkes, I.H.; Marvin, D.; Ponsioen, B.; Alvarez-Varela, A.; Fatrai, S.; Scheele, C.; Zwijnenburg, D.A.; Snippert, H.; et al. Collagen-rich stroma in aggressive colon tumors induces mesenchymal gene expression and tumor cell invasion. *Oncogene* **2016**, *35*, 5263-5271, doi:10.1038/onc.2016.60.

29. De Sousa, E.M.F.; Wang, X.; Jansen, M.; Fessler, E.; Trinh, A.; de Rooij, L.P.; de Jong, J.H.; de Boer, O.J.; van Leersum, R.; Bijlsma, M.F.; et al. Poor-prognosis colon cancer is defined by a molecularly distinct subtype and develops from serrated precursor lesions. *Nat Med* **2013**, *19*, 614-618, doi:10.1038/nm.3174.

30. Hirsch, D.; Barker, N.; McNeil, N.; Hu, Y.; Camps, J.; McKinnon, K.; Clevers, H.; Ried, T.; Gaiser, T. LGR5 positivity defines stem-like cells in colorectal cancer. *Carcinogenesis* **2014**, *35*, 849-858, doi:10.1093/carcin/bgt377.

31. Yi, H.; Li, G.; Long, Y.; Liang, W.; Cui, H.; Zhang, B.; Tan, Y.; Li, Y.; Shen, L.; Deng, D.; et al. Integrative multi-omics analysis of a colon cancer cell line with heterogeneous Wnt activity revealed RUNX2 as an epigenetic regulator of EMT. *Oncogene* **2020**, *39*, 5152-5164, doi:10.1038/s41388-020-1351-z.

32. Calon, A.; Lonardo, E.; Berenguer-Llergo, A.; Espinet, E.; Hernando-Momblona, X.; Iglesias, M.; Sevillano, M.; Palomo-Ponce, S.; Tauriello, D.V.; Byrom, D.; et al. Stromal gene expression defines poor-prognosis subtypes in colorectal cancer. *Nat Genet* **2015**, *47*, 320-329, doi:10.1038/ng.3225.

33. Isella, C.; Terrasi, A.; Bellomo, S.E.; Petti, C.; Galatola, G.; Muratore, A.; Mellano, A.; Senetta, R.; Cassenti, A.; Sonetto, C.; et al. Stromal contribution to the colorectal cancer transcriptome. *Nat Genet* **2015**, *47*, 312-319, doi:10.1038/ng.3224.

34. Lee, H.O.; Hong, Y.; Etlioglu, H.E.; Cho, Y.B.; Pomella, V.; Van den Bosch, B.; Vanhecke, J.; Verbandt, S.; Hong, H.; Min, J.W.; et al. Lineage-dependent gene expression programs influence the immune landscape of colorectal cancer. *Nat Genet* **2020**, *52*, 594-603, doi:10.1038/s41588-020-0636-z.

35. Bernards, R.; Weinberg, R.A. A progression puzzle. *Nature* **2002**, *418*, 823.

36. Gaspar, C.; Fodde, R. APC dosage effects in tumorigenesis and stem cell differentiation. *The International journal of developmental biology* **2004**, *48*, 377-386.

37. Caramel, J.; Ligier, M.; Puisieux, A. Pleiotropic Roles for ZEB1 in Cancer. *Cancer Res* **2017**, *78*, 30-35.

38. Maheswaran, S.; Haber, D.A. Cell fate: Transition loses its invasive edge. *Nature* **2015**, *527*, 452-453, doi:10.1038/nature16313.

39. Davalos, V.; Moutinho, C.; Villanueva, A.; Boque, R.; Silva, P.; Carneiro, F.; Esteller, M. Dynamic epigenetic regulation of the microRNA-200 family mediates epithelial and mesenchymal transitions in human tumorigenesis. *Oncogene* **2012**, *31*, 2062-2074, doi:10.1038/onc.2011.383.

40. Sparks, A.B.; Morin, P.J.; Vogelstein, B.; Kinzler, K.W. Mutational analysis of the APC/beta-catenin/Tcf pathway in colorectal cancer. *Cancer Res* **1998**, *58*, 1130-1134.

41. Kahlert, C.; Lahes, S.; Radhakrishnan, P.; Dutta, S.; Mogler, C.; Herpel, E.; Brand, K.; Steinert, G.; Schneider, M.; Mollenhauer, M.; et al. Overexpression of ZEB2 at the invasion front of colorectal cancer is an independent prognostic marker and regulates tumor invasion in vitro. *Clin Cancer Res* **2011**, *17*, 7654-7663.

42. Jolly, M.K.; Boareto, M.; Huang, B.; Jia, D.; Lu, M.; Ben-Jacob, E.; Onuchic, J.N.; Levine, H. Implications of the Hybrid Epithelial/Mesenchymal Phenotype in Metastasis. *Frontiers in oncology* **2015**, *5*, 155.

43. Aiello, N.M.; Maddipati, R.; Norgard, R.J.; Balli, D.; Li, J.; Yuan, S.; Yamazoe, T.; Black, T.; Sahmoud, A.; Furth, E.E.; et al. EMT Subtype Influences Epithelial Plasticity and Mode of Cell Migration. *Developmental cell* **2018**, *45*, 681-695 e684.

44. Pastushenko, I.; Brisebarre, A.; Sifrim, A.; Fioramonti, M.; Revenco, T.; Boumahdi, S.; Van Keymeulen, A.; Brown, D.; Moers, V.; Lemaire, S.; et al. Identification of the tumour transition states occurring during EMT. *Nature* **2018**, *556*, 463-468.

45. Kim, J.Y.; Jeong, D.; Ahn, T.S.; Kim, H.J.; Park, D.S.; Park, S.Y.; Bae, S.B.; Lee, S.; Lee, S.S.; Lee, M.S.; et al. Expression of Secreted Protein Acidic and Rich in Cysteine in the Stroma of a Colorectal Carcinoma is Associated With Patient Prognosis. *Ann Coloproctol* **2013**, *29*, 93-99, doi:10.3393/ac.2013.29.3.93.

Chapter 4

46. Podhajcer, O.L.; Benedetti, L.G.; Girotti, M.R.; Prada, F.; Salvatierra, E.; Llera, A.S. The role of the matricellular protein SPARC in the dynamic interaction between the tumor and the host. *Cancer Metastasis Rev* **2008**, *27*, 691-705, doi:10.1007/s10555-008-9146-7.

47. Takigawa, H.; Kitadai, Y.; Shinagawa, K.; Yuge, R.; Higashi, Y.; Tanaka, S.; Yasui, W.; Chayama, K. Mesenchymal Stem Cells Induce Epithelial to Mesenchymal Transition in Colon Cancer Cells through Direct Cell-to-Cell Contact. *Neoplasia* **2017**, *19*, 429-438, doi:10.1016/j.neo.2017.02.010.

48. Yu, M.; Bardia, A.; Wittner, B.S.; Stott, S.L.; Smas, M.E.; Ting, D.T.; Isakoff, S.J.; Ciciliano, J.C.; Wells, M.N.; Shah, A.M.; et al. Circulating breast tumor cells exhibit dynamic changes in epithelial and mesenchymal composition. *Science* **2013**, *339*, 580-584, doi:339/6119/580 [pii]

10.1126/science.1228522.

49. Biddle, A.; Gammon, L.; Liang, X.; Costea, D.E.; Mackenzie, I.C. Phenotypic Plasticity Determines Cancer Stem Cell Therapeutic Resistance in Oral Squamous Cell Carcinoma. *EBioMedicine* **2016**, *4*, 138-145, doi:10.1016/j.ebiom.2016.01.007

S2352-3964(16)30005-6 [pii].

50. Wiederschain, D.; Wee, S.; Chen, L.; Loo, A.; Yang, G.; Huang, A.; Chen, Y.; Caponigro, G.; Yao, Y.M.; Lengauer, C.; et al. Single-vector inducible lentiviral RNAi system for oncology target validation. *Cell cycle (Georgetown, Tex* **2009**, *8*, 498-504.

51. Bolger, A.M.; Lohse, M.; Usadel, B. Trimmomatic: a flexible trimmer for Illumina sequence data. *Bioinformatics (Oxford, England)* **2014**, *30*, 2114-2120.

52. Dobin, A.; Davis, C.A.; Schlesinger, F.; Drenkow, J.; Zaleski, C.; Jha, S.; Batut, P.; Chaisson, M.; Gingeras, T.R. STAR: ultrafast universal RNA-seq aligner. *Bioinformatics (Oxford, England)* **2013**, *29*, 15-21, doi:bts635 [pii] 10.1093/bioinformatics/bts635.

53. Harrow, J.; Frankish, A.; Gonzalez, J.M.; Tapanari, E.; Diekhans, M.; Kokocinski, F.; Aken, B.L.; Barrell, D.; Zadissa, A.; Searle, S.; et al. GENCODE: the reference human genome annotation for The ENCODE Project. *Genome Res* **2012**, *22*, 1760-1774, doi:22/9/1760 [pii] 10.1101/gr.135350.111.

54. Gentleman, R.C.; Carey, V.J.; Bates, D.M.; Bolstad, B.; Dettling, M.; Dudoit, S.; Ellis, B.; Gautier, L.; Ge, Y.; Gentry, J.; et al. Bioconductor: open software development for computational biology and bioinformatics. *Genome Biol* **2004**, *5*, R80, doi:gb-2004-5-10-r80 [pii] 10.1186/gb-2004-5-10-r80.

55. Love, M.I.; Huber, W.; Anders, S. Moderated estimation of fold change and dispersion for RNA-seq data with DESeq2. *Genome Biol* **2014**, *15*, 550, doi:s13059-014-0550-8 [pii] 10.1186/s13059-014-0550-8.

56. Benjamini, Y.; Hochberg, Y. Controlling the False Discovery Rate: A Practical and Powerful Approach to Multiple Controlling the False Discovery Rate. . *Journal of the Royal Statistical Society.* **1995**, *57*, 289-3000, doi:https://doi.org/10.2307/2346101.

57. Meinders, M.; Kulu, D.I.; van de Werken, H.J.; Hoogenboezem, M.; Janssen, H.; Brouwer, R.W.; van Ijcken, W.F.; Rijkers, E.J.; Demmers, J.A.; Kruger, I.; et al. Sp1/Sp3 transcription factors regulate hallmarks of megakaryocyte maturation and platelet formation and function. *Blood* **2015**, *125*, 1957-1967, doi:blood-2014-08-593343 [pii] 10.1182/blood-2014-08-593343.

58. Edgar, R.; Domrachev, M.; Lash, A.E. Gene Expression Omnibus: NCBI gene expression and hybridization array data repository. *Nucleic Acids Res* **2002**, *30*, 207-210.

Supplementary figures
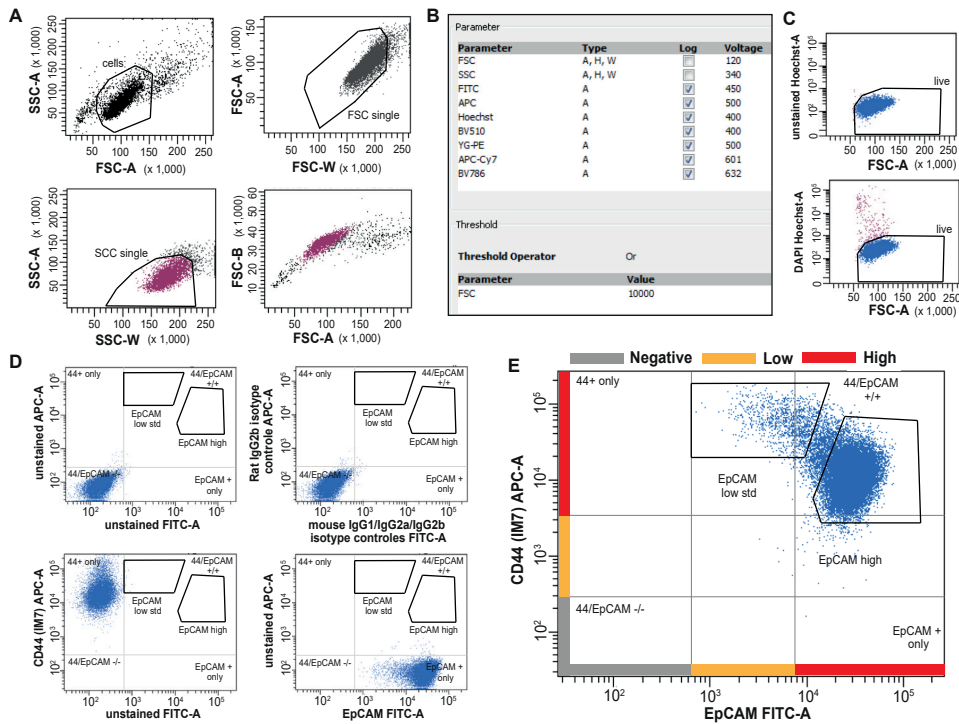
Figure 1 – supplement 1. Further characterization of EpCAM^{lo} cells in colon cancer cell lines: FACS analysis. (**a**) FSC-A/SSC–A, FSC-W/FSC-A, and SSC-W/SSC-A single cell gates (confirmed by gating on FSC-A/FSC-H). Purity of sorted single cells was confirmed by microscopy. (**b**) Acquisition parameters used for FACS analysis. (**c**) Gating strategy employed to select for live cells by DAPI staining (top: unstained cells; bottom: after DAPI staining). (d) Top: unstained and isotype controls, showing absence of relevant unspecific antibody binding. Bottom: Fluorescence Minus One (FMO) samples, showing the absence of uncompensated spillover between fluorescence channels. For the sake of clarity, a quadrant is placed to show the relative position of unstained and single stains in both cells lines. For the EpCAM-FITC antibody, a mouse IgG1-FITC isotype control S. Cruz sc-2855 was used; for the CD44-APC antibody, a Rat IgG2a-APC isotype control S. Cruz sc-2895 was used. Similar results were obtained with SW480 cells (not shown). (e) Full EpCAM/CD44 staining, also showing the rationale behind the definition of high and low referred to EpCAM and CD44 levels. Despite the differences in CD44 levels between EpCAM^{hi} and EpCAM^{lo} cells, for the sake of simplicity the populations were defined "low" for a defined marker if they were mainly covering a region within the 1st log above the negative gate, high if they were above the 1st log.
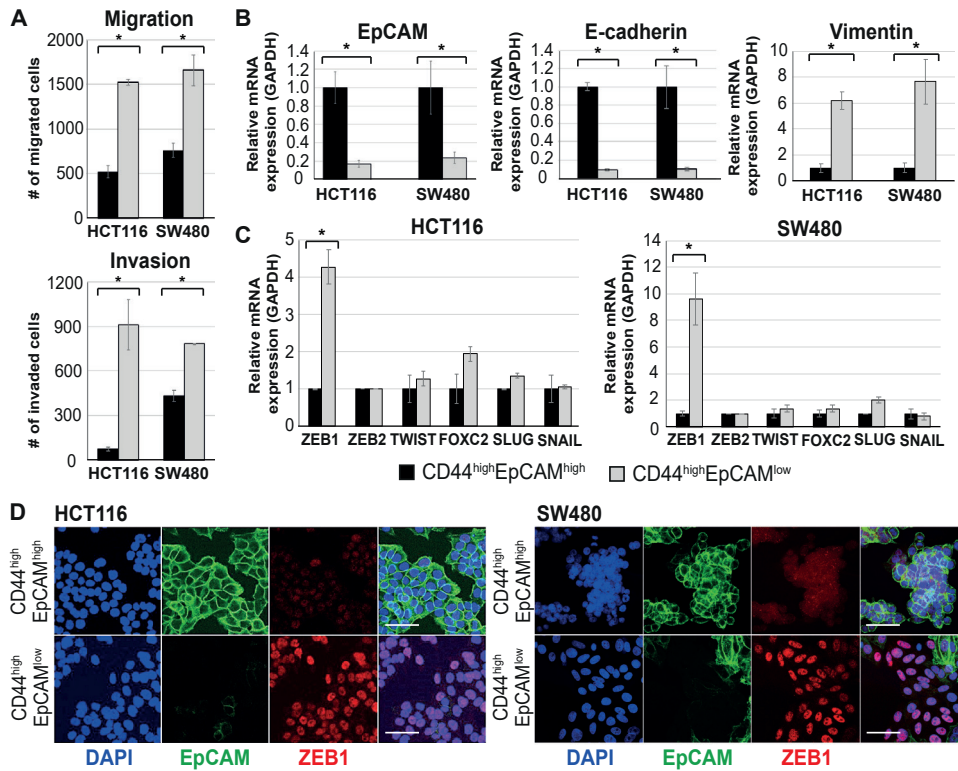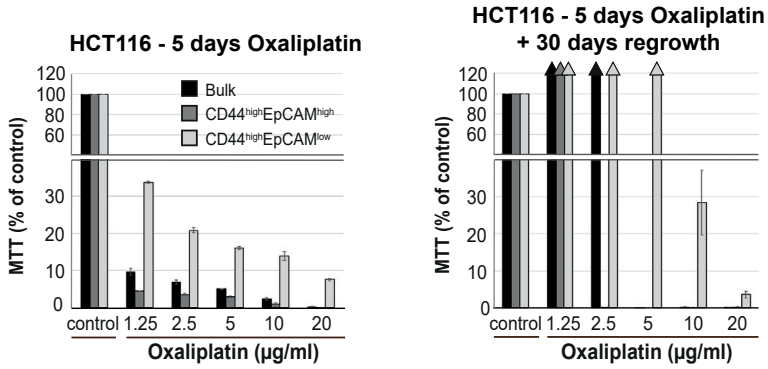
Figure 1- supplement 2. Further characterization of EpCAM^{lo} cells in colon cancer cell lines: migration/invasion and EMT analysis. (**a**) Top panel: transwell migration assay of EpCAM[hi] (black bar) and EpCAM[lo] (grey bar) cells from the HCT116 and SW480 lines. 10^5 cells were plated on TC-coated membrane in triplicate and left overnight before counting the number of migrated cells on the bottom side of the membrane. Each bar represents the mean ± SD of two independent experiments. Asterisks indicate significant differences ($P < 0.05$). Bottom panel: invasion assay of EpCAM[hi] (black bar) and EpCAM[lo] (grey bar) cells from the HCT116 and SW480 lines. 10^5 cells were plated in triplicate on top of an extracellular matrix-coated coated membrane and left overnight before counting the number of cells migrated to other side of the membrane. Each bar represents the mean ±SD of two independent experiments. Asterisks indicate significant differences ($P < 0.05$). (b) RT-qPCR expression analysis of epithelial (*EPCAM* and *CDH1*) and mesenchymal (*VIM*) markers in sorted EpCAM[hi] (black bars) and EpCAM[lo] (grey bars) from the HCT116 and SW480 lines. *GAPDH* was employed for normalization purposes. Each bar represents the mean ±SD of three independent experiments. Asterisks indicate significant differences ($P < 0.05$). (**c**) RT-qPCR expression analysis of EMT transcription factors (*ZEB1, ZEB2, TWIST, FOXC2, SLUG* and *SNAIL*) in EpCAM[hi] (black bars) and EpCAM[lo] (grey bars) cells. Left panel: HCT116. Right panel: SW480. *GAPDH* was employed for normalization. Each bar represents the mean ± SD of three independent experiments. Asterisks indicate significant differences ($P < 0.05$). (d) Immunofluorescence (IF) analysis of EpCAM[hi] and EpCAM^{lo} cells. Cells were sorted and directed plated on cover slips. After four days cells were fixed with 4% PFA and stained with antibodies against EpCAM (green) and ZEB1 (red). Nuclei were visualized by DAPI staining of DNA (blue). Scale bar: 50 μm.
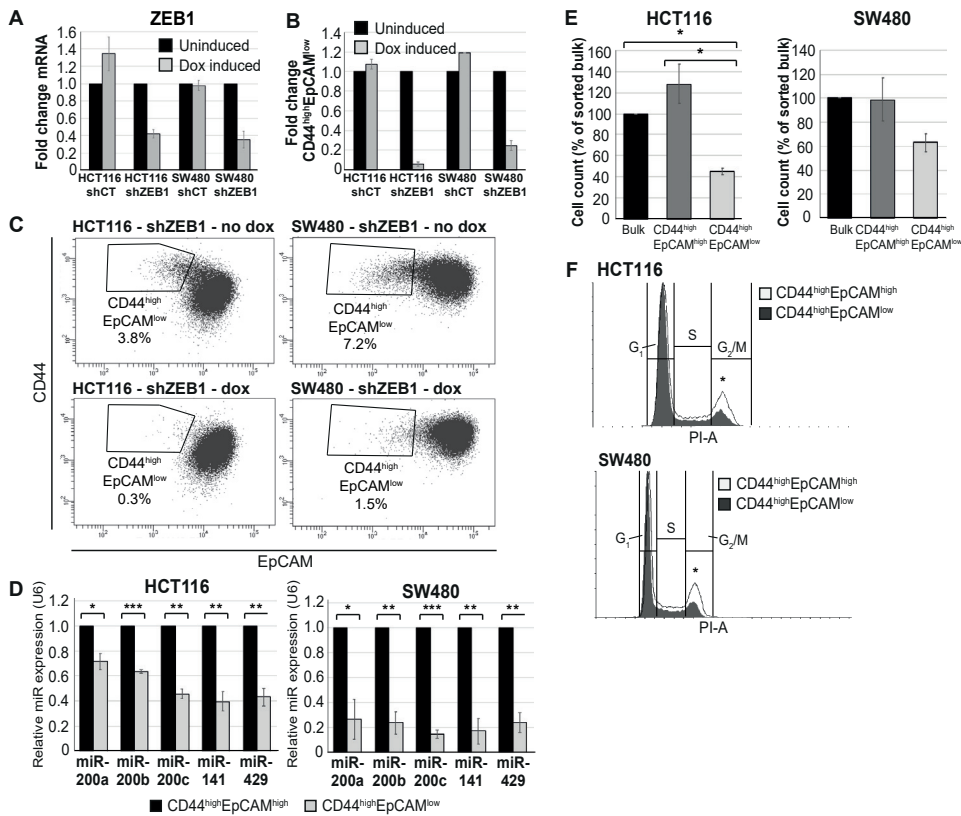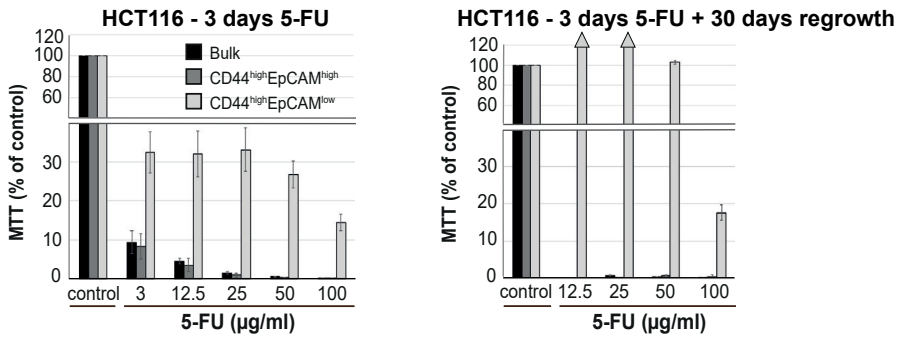
Figure 1- supplement 3. Further characterization of EpCAM^lo cells in colon cancer cell lines: EMT analysis and cell cycle analysis. (**a**) qRT-PCR expression analysis of *ZEB1* in HCT116 and SW480 transduced with an inducible control (shCT) or ZEB1-shRNA (shZEB1) construct. shRNA expression was induced with 1 μg/mL of doxycycline. Each bar represents the mean ± SD of three independent experiments. (b) Bar graph of flow cytometric analysis (see b. here below). Each bar represents the relative mean ± SD of three independent experiments. (c) Representative analysis of the flow cytometric analysis of the shCT- and shZEB1-transfected HCT116 and SW480 cell lines using antibodies against CD44 and EpCAM. Cells were induced with 1 μg/mL doxycycline for 72 hrs. before analysis. (**d**) RT-qPCR expression analysis of the members of the miRNA 200 family (miR-200a, miR-200b, miR-200c, miR-141 and miR-429) in EpCAM^hi (black bars) and EpCAM^lo (grey bars) cells. Upper panel: HCT116. Bottom panel: SW480. *U6* was employed for normalization. Each bar represents the mean ± SD of three independent experiments. Single asterisks indicate significant differences of $P < 0.05$, double asterisks of $P < 0.01$, and triple asterisks of $P < 0.001$. (**e**) Cell proliferation assay. Sorted bulk, EpCAM^hi and EpCAM^lo cells were seeded in triplicate in plates and cultured in conventional medium. HCT116 and SW480 cells were harvested and number of cells was counted at 4 and 11 days, respectively. Each bar represents the mean ± SD three independent experiments. (**f**) Cell cycle analysis of EpCAM^hi and EpCAM^lo cells in HCT116 (upper panel) and SW480 (lower panel). Cells fractions were sorted and plated in culture. After 72 hours cells were fixed and stained with propidium iodide. Cell cycle distribution was assayed by flow cytometry. Graphs show representative analysis of one experiment. Tables demonstrate average and standard deviation of three independent experiments. White graph: EpCAM^hi, grey graph: EpCAM^lo. Asterisks show the significant ($P < 0.05$) differences between EpCAM^hi and EpCAM^lo cells in G_1 and G_2M-phases.

A

HCT116 - 5 days Oxaliplatin

HCT116 - 5 days Oxaliplatin
+ 30 days regrowth

B

HCT116 - 3 days 5-FU

HCT116 - 3 days 5-FU + 30 days regrowth

C

SW480 - 7 days Oxaliplatin

SW480 - 7 days Oxaliplatin + 14 days regrowth

D

SW480 - 7 days 5-FU

SW480 - 7 days 5-FU + 14 days regrowth
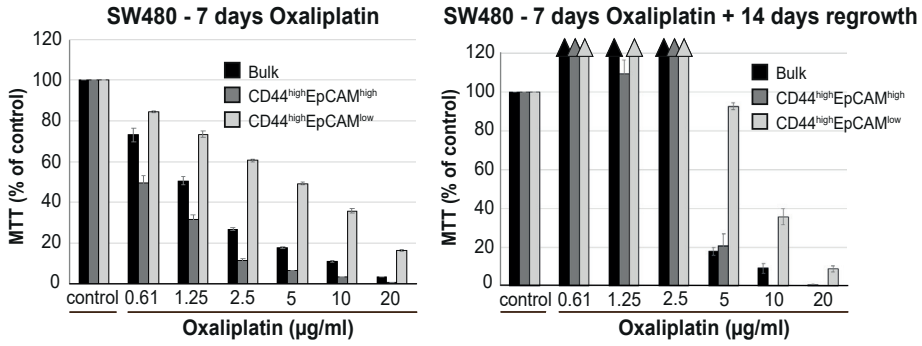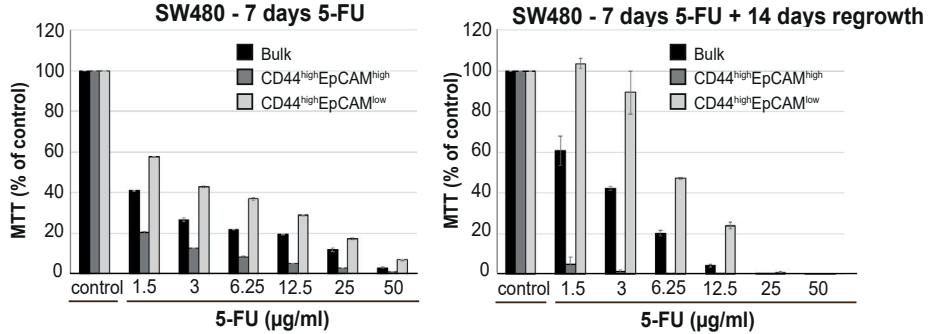
Figure 1- supplement 4. (opposite) Further characterization of EpCAM^{lo} cells in colon cancer cell lines: chemoresistance. Bulk, EpCAM[hi] and EpCAM[lo] HCT116 and SW480 cells were sorted and plated to recover and expand for four days. 10^5 cells per well were plated in in triplicate in a 96-well plate and left to attach. After 24 h, standard cell culture medium was changed for medium containing chemotherapeutic drug oxaliplatin or 5-FU. HCT116 cells were left with 5-FU and oxaliplatin for respectively 3 and 5 days. For each drug SW480 cells were treated for 7 days. After removal of the chemotherapeutic drug, cells were washed with PBS and left to re-grow in standard culture medium. Cell viability was assessed using the MTT upon removal of the drug, and after re-growth (ranging 13-30 days). O.D. reading was performed at 595 nm with a Microplate Reader. Background measurements were subtracted from each data point. All experiments were performed at least in duplicate for each individual cell line and drug. (**a-b**) Chemo sensitivity assays using oxaliplatin (**a**) or 5-FU (**b**) in bulk (black bars), EpCAM[hi] (dark grey bars) and EpCAM[lo] (light grey bars) HCT116 cells. Bars represent the average ± SD of the O.D. corrected for the background measurements. (**c-d**) Chemo sensitivity assays using oxaliplatin (**c**) or 5-FU (**d**) in bulk (black bars), EpCAM[hi] (dark grey bars) and EpCAM[lo] (light grey bars) SW480 cells. Bars represent the average ± SD of the O.D. corrected for the background measurements.

Chapter 4

A

HE — anti-β-catenin

HCT116

SW480

B

BULK - meta 1 — EpCAM^{hi} - meta 1 — EpCAM^{lo} - meta 1

EpCAM^{lo} 0.1% — EpCAM^{lo} 0.0% — EpCAM^{lo} 1.2%

BULK - meta 2 — EpCAM^{hi} - meta 2 — EpCAM^{lo} - meta 2

EpCAM^{lo} 1.0% — EpCAM^{lo} 1,2% — EpCAM^{lo} 0.2%

CD44

EpCAM

C

Zeb1

Relative mRNA expression (Gapdh)

*

AKP   AKP-Zeb1

■ no dox   ▨ dox

D

no DOX

CD44^{high}EpCAM^{low} 4.8%

DOX

CD44^{high}EpCAM^{low} 22.3%

DOX

CD44^{high}EpCAM^{low} 76%

CD44

EpCAM

E

AKP-Zeb1 - liver

# of liver metastases per cm^2

no dox   dox

AKP-Zeb1 - lung

# of lung metastases per cm^2

no dox   dox

Figure 1- supplement 5. (opposite) Further characterization of EpCAM^lo cells in colon cancer cell lines: invasive and metastatic behaviour. (**a**) Hematoxylin and eosin (H&E; first two panels) and IHC with antibody directed against β-catenin (third and fourth panel) in liver metastasis obtained four or eight weeks after intrasplenic injection with HCT116 (upper panels) and SW480 (lower panels) cells, respectively. Second and fourth panels show zoom of the marked area in respectively first and third panel. Scale bar first and third panels: 100 µm. Scale bar second and fourth panel: 50 µm. (b) FACS analysis of liver metastases obtained by spleen injection of HCT116 bulk, EpCAM^hi, and EpCAM^lo cells. Upper panel: representative FACS plots. (c) Microscopic (top, left panel) analysis of AKP-Z organoids tagged with GFP and click beetle luciferase. The graph (bottom, left panel) shows the RT-qPCR expression analysis of *Zeb1* in AKP (left) and AKP-Z (right) organoids upon *in vitro* doxycycline treatment for 48 hrs. Black bars: no doxycycline treatment; grey bars: 1 µg/mL doxycycline. Each bar represents the mean ± SD of three independent experiments. (d) Upon establishment of a primary tumor in the caecum, transplanted mice were administered doxycycline in the drinking water to induce Zeb1 expression. FACS analysis of the primary tumor was performed one week after the start of the doxycycline. The panels show representative FACS plots of a control and two dox-treated primary tumors. (**e**) Quantification of the number of lung and liver metastases in uninduced (black; n=4) and dox-induced (grey; n=5) AKP-Z transplanted mice. Liver tissue was cut into 500-micron slices, processed for IHC, stained for β-catenin to visualize tumor cells, scanned using a NanoZoomer, and counted using NDP view software. The area of tissue analyzed was used to normalize the data.
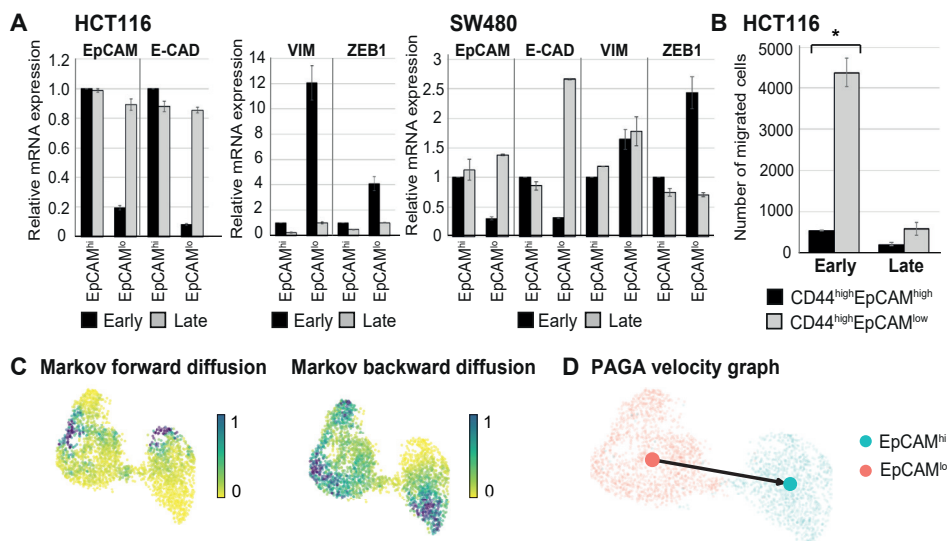
Figure 2 - supplement 1. Further characterization of phenotypic plasticity in EpCAM^lo and EpCAM^hi cells. (**a**) RT-qPCR expression analysis of *EPCAM*, *CDH1*, *VIM*, and *ZEB1* in 'early' (e.g. cells that were used shortly after FACS sorting) and 'late' (e.g. cells that were cultured for an extended period of time before performing the experiment) sorted EpCAM^hi and EpCAM^lo cell from HCT116 and SW480 cell lines. *GAPDH* was employed for normalization purposes. Each bar represents the mean ± SD of two independent experiments. (**b**) Transwell migration assay of 'early' and 'late' EpCAM^hi (black bar) and EpCAM^lo (grey bar) cultures in HCT116. 10^5 cells were plated in triplicate on TC-coated membrane and left overnight before counting the number of migrated cells on the bottom side of the membrane. Each bar represents the mean ± SD of two independent experiments. Asterisks indicate significant differences ($P < 0.05$). (**c**) Analysis of the HCT116 scRNAseq data as a Markov diffusion process. Markov forward (left) and backward (right) diffusion indicating the presence of sink and source points in both EpCAM^hi and EpCAM^lo populations. (**d**) Partition-based graph abstraction (PAGA) velocity graph mapping out the direction of velocity on a subpopulation level in HCT116.
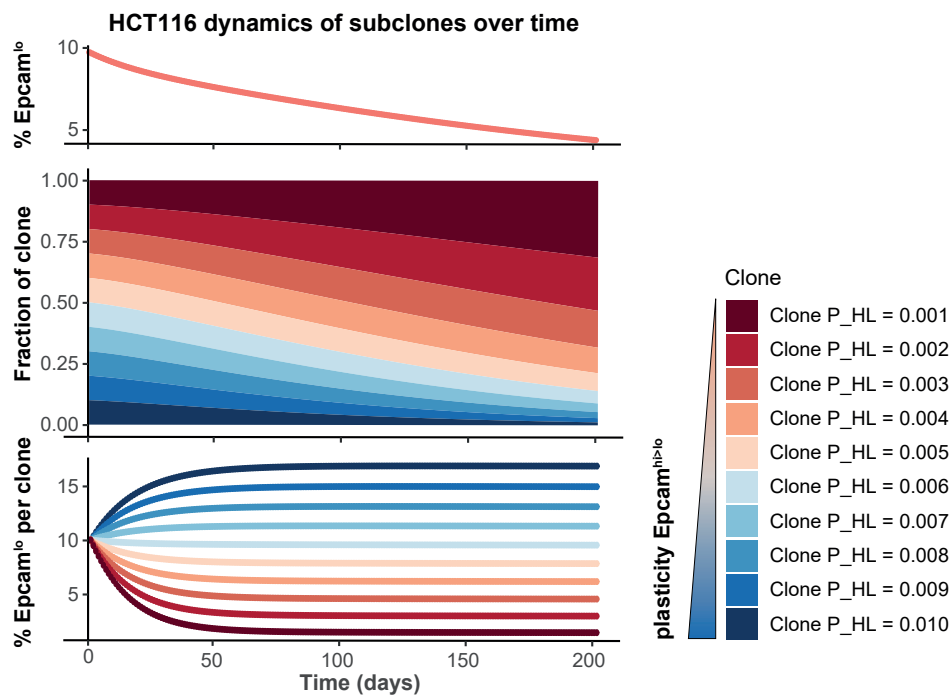
Figure 2 - supplement. Simulation of the HCT116 two-state Markov model with a non-homogenous starting population. The starting population was defined as ten subclones with varying transition probability P_HL at equal proportion. The Markov Model was run till day 200 and shows that the total EpCAM^{lo} population decreases over time (top panel), because clones with lower plasticity will gain dominance in the long run (lower panels).

HCT116 - Molecular and Cellular Functions
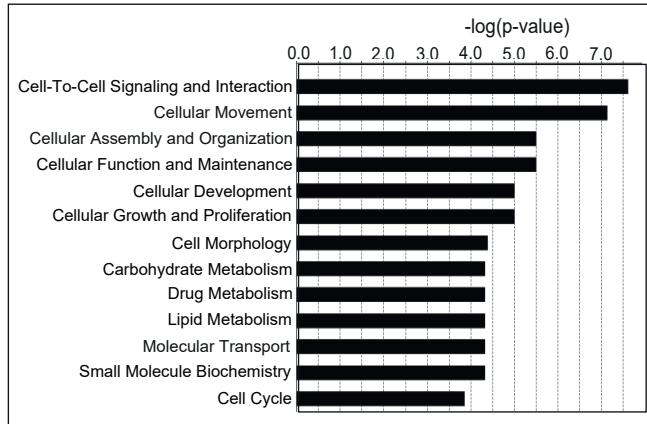
SW480 - Molecular and Cellular Functions
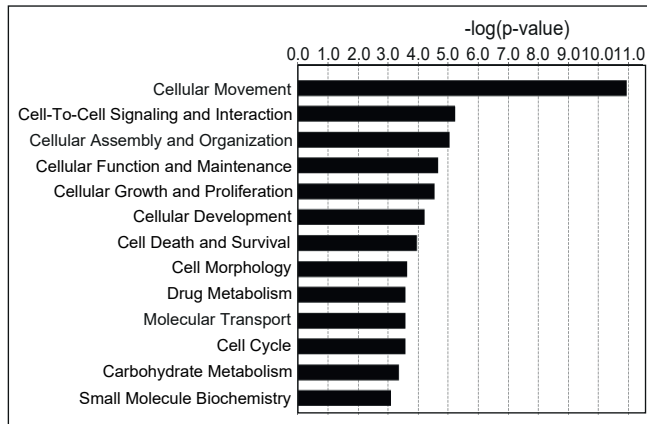
HCT116 and SW480 - Molecular and Cellular Functions
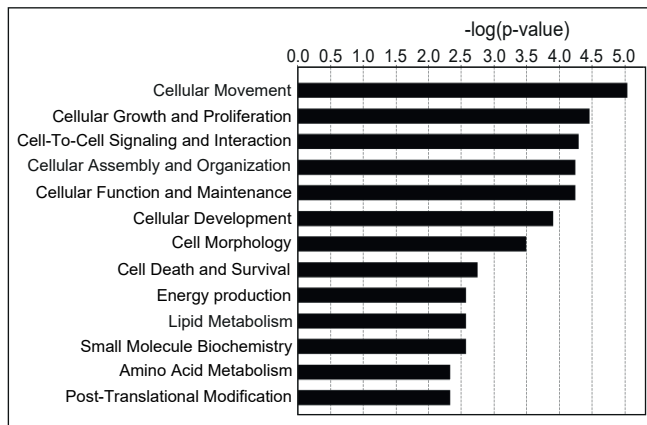
Figure 3 - supplement 1. Gene ontology (GO) of molecular and cellular functions in HCT116 (upper left panel), SW480 (upper right panel) and the combined (bottom panel) gene lists.
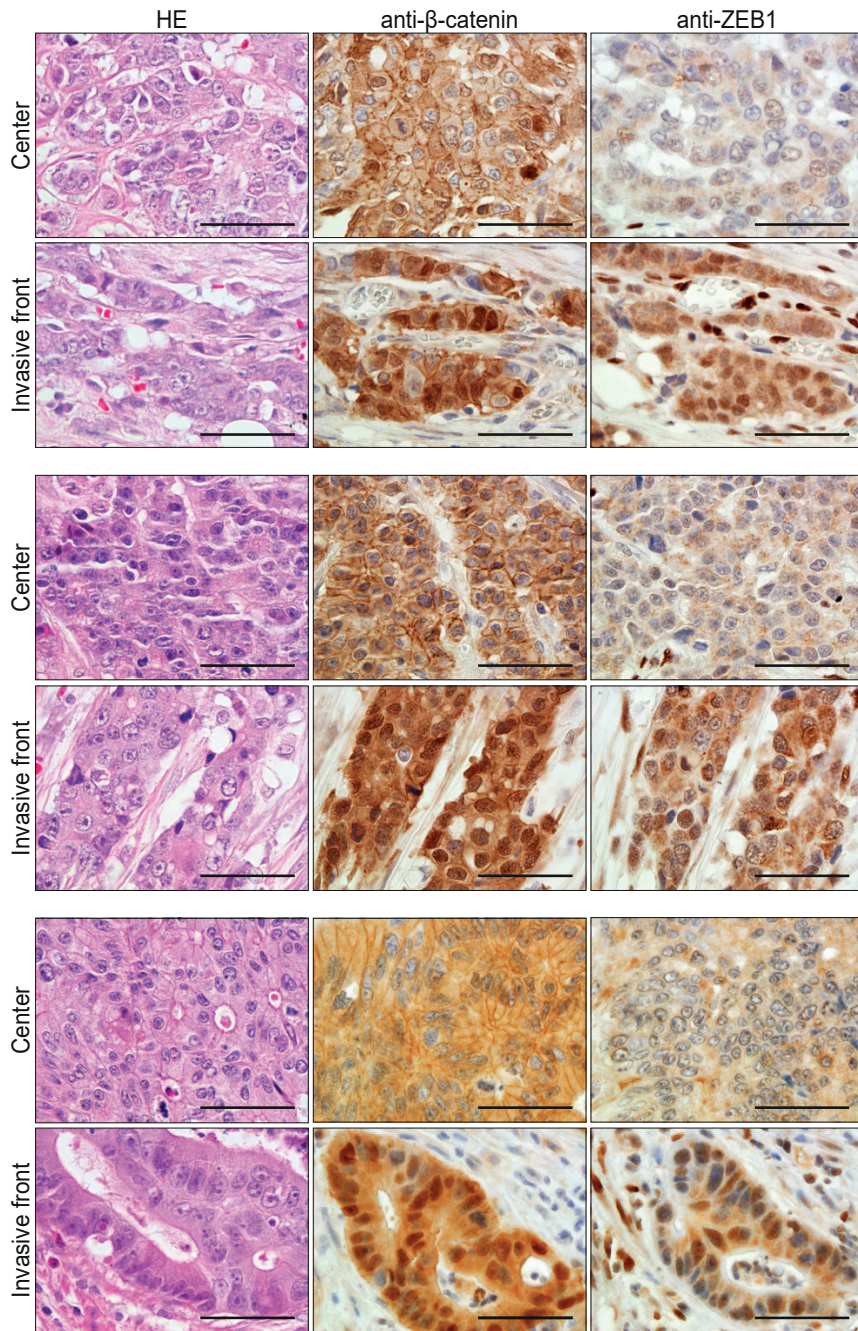
Figure 3 - supplement 2. Hematoxylin and eosin (H&E) and IHC analyses with antibodies directed against β-catenin and ZEB1 in consecutive sections of colon cancers from three unrelated patients with sporadic colon cancer. For each case, areas from the tumor center and the invasive front are shown. Co-localization of nuclear β-catenin and ZEB1 expression was found in 5 out of 25 cases investigated. Scale bar: 50 μm.

A

B
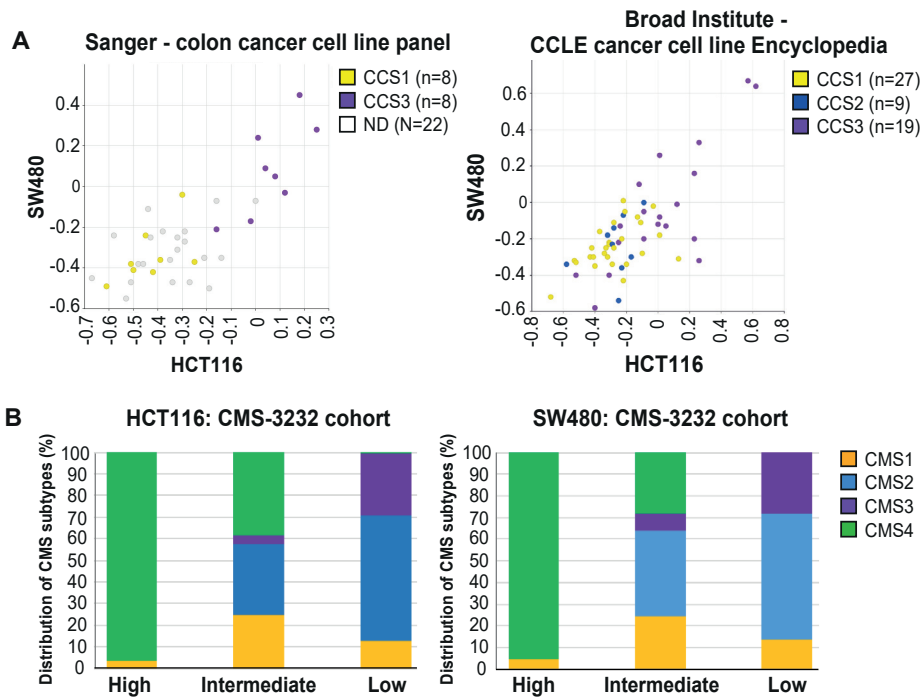
Figure 4 - supplement 1. EpCAM[lo] expression signatures correlate with CCS3 cell lines and CMS4 colon cancer patients. (**a**) Correlation of meta-gene expression values of the signatures derived from EpCAM[lo] HCT116 and SW480 cells in two cohorts of colon cancer cell lines in the absence of a stromal component. CCS1: epithelial-like tumor lines; CCS2: tumor lines with microsatellite instability. CCS3: mesenchymal-like tumor cell lines [29]. (**b**) The gene sets identifying the EpCAM^{lo} cells from both HCT116 and SW480 were used to cluster the tumors in the CMS3232 cohort into High, Intermediate, and Low expression groups by k-means clustering. As all tumors in this cohort had previously been assigned to specific CMS subgroups, and then analyzed the contribution of each CMS subtype to each of the generated High, Intermediate, and Low expression subgroups.

Chapter 4
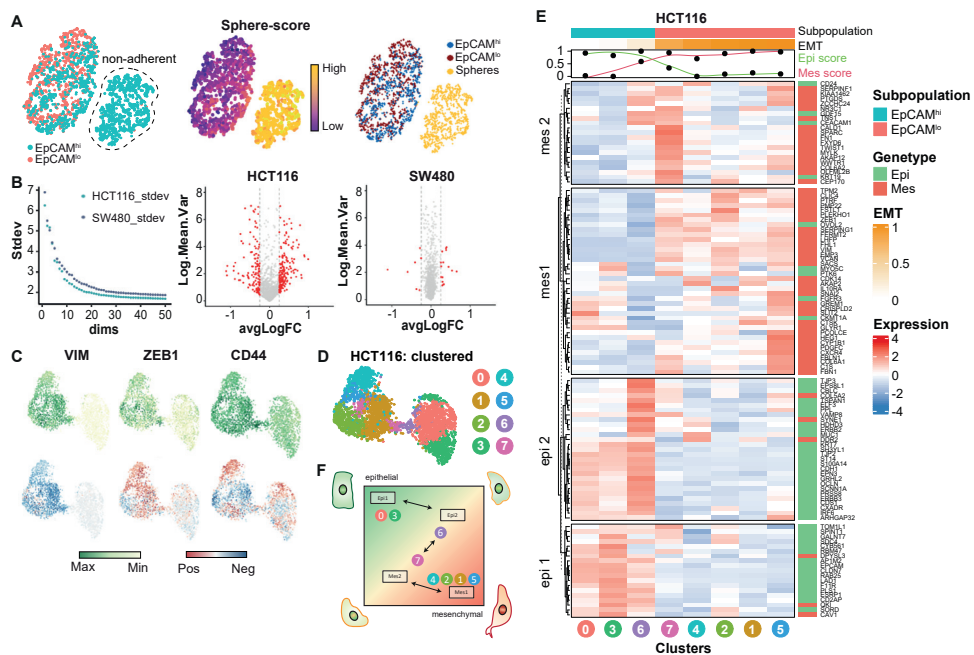
Figure 5 - supplement 1. Further scRNAseq analysis of EpCAM^{lo} cells: EMT/MET transcriptional trajectory. (**a**) tSNE of the SW480 cell line indicating an additional subpopulation in the EpCAM[hi] population (left panel). Using a signature derived from the bulk RNAseq, this population was identified as the "sphere" population (middle panel) and annotated to be excluded for further analysis (right panel). (**b**) Left panel: the SW480 cell line, after exclusion of the "sphere" population, contains slightly higher variability compared to the HCT116 cell line, as evidenced by the variance of the top-50 principal components. Right panel: while in HCT116, most of the variable expressed genes are differentially expressed between the EpCAM[hi] and EpCAM[lo] population, this is not the case in SW480, where most of the highly variable genes do not differ between the two populations. (**c**) Top panels: expression values of *VIM*, *ZEB1* and *CD44* on the UMAP embedding of the HCT116 cell line. Lower panels: projection of the RNA velocity direction of the same genes. (**d**) HCT116 UMAP embedding annotated with the eight unsupervised clusters. (**e**) Heatmap of HCT116 with expression values of the EMT signature averaged by the eight clusters. Clusters were ranked according to their EMT score and genes were clustered in four distinct gene sets using k-means clustering. (**f**) Schematic diagram showing a transcriptional trajectory with distinct gene arrays through which pEMT cells arise.
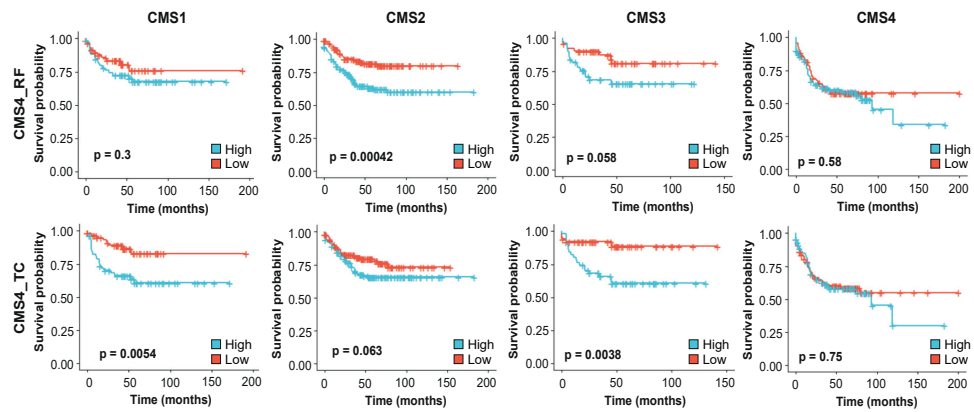
Figure 6 - supplement 1. Survival analysis of the CMS4_RF (top panels) and CMS4_TC (lower panels) signatures across the different consensus molecular subtypes. Patients were divided into 2 equal groups based on their association to the signatures and Kaplan-Meier plots were made based on relapse-free survival.

CHAPTER V

Wnt signalling in ovarian cancer stemness, EMT, and therapy resistance

Teeuwssen M.J. and Fodde R.

Abstract

Ovarian cancers represent the deadliest among gynecologic malignancies and are characterized by a hierarchical structure with cancer stem cells (CSCs) endowed with self-renewal and the capacity to differentiate. The Wnt/β-catenin signaling pathway, known to regulate stemness in a broad spectrum of stem cell niches including the ovary, is thought to play an important role in ovarian cancer. Importantly, Wnt activity was shown to correlate with grade, epithelial to mesenchymal transition, chemotherapy resistance, and poor prognosis in ovarian cancer. This review will discuss the current knowledge of the role of Wnt signaling in ovarian cancer stemness, epithelial to mesenchymal transition (EMT), and therapy resistance. In addition, the alleged role of exosomes in the paracrine activation of Wnt signaling and pre-metastatic niche formation will be reviewed. Finally, novel potential treatment options based on Wnt inhibition will be highlighted.

Keywords: Ovarian cancer; Wnt signaling; cancer stem cells; tumor progression; therapy resistance; exosomes

Abstract

1. Introduction

Epithelial ovarian cancer (EOC) represents the deadliest among gynecologic malignancies [1]. This is mainly due to the fact that up to 80% of ovarian cancer patients present with symptoms and are subsequently diagnosed only at late disease stages, i.e., when metastases have already spread to pelvic organs (stage II), the abdomen (stage III), or beyond the peritoneal cavity (stage IV) [2].

EOC is an extremely heterogeneous disease. Multiple (epi)genetic alterations at a broad spectrum of oncogenes and tumor suppressor genes have been observed in ovarian cancer leading to deregulation of signal transduction pathways whose functions ranges from DNA repair, cell proliferation, apoptosis, cell adhesion, and motility. Based on these molecular alterations, ovarian cancer has been subdivided in two major type I and type II classes of tumors [3]. Type I tumors are slow growing, mostly restricted to the ovary, and develop from well-established precursor lesions called "borderline" tumors. Type I tumors comprise of four different subtypes, namely low-grade serous, mucinous, clear cell, and endometrioid cancers. The histological composition of these four types resemble normal cells present in the fallopian tube and/or ovarian surface epithelium, endocervix, vagina, and endometrium, respectively, thus suggesting different cells of origin for the different histotypes [3]. Type I lesions frequently carry mutations in *KRAS*, *BRAF*, *PTEN*, and *CTNNB1* (β-catenin), and often show a relatively stable karyotype.

Type II ovarian cancers include high-grade serous (HGS) and undifferentiated carcinomas, the vast majority of which characterized by *TP53* alterations and pronounced genomic instability [3]. Of note, inherited and somatic *BRCA1* and *BRCA2* mutations are usually found in type II tumors. It is under debate whether HGS ovarian cancers originate from the fimbria of the fallopian tube or from the ovarian surface epithelium (OSE) [4].

Ovarian cancers are thought, because of their distinctive progression and recurrence patterns, to be characterized by a hierarchical structure with cancer stem cells (CSCs) endowed with self-renewal and the capacity to differentiate, which continuously fuel the growth of the tumor mass and coexist with more committed cell types [5,6]. Notably, the Wnt/β-catenin signaling pathway, known to regulate stemness in a broad spectrum of stem cell niches including the ovary, is thought to play an important role in ovarian cancer. First, 16–54% of endometrioid ovarian cancers are characterized by mutations in β-catenin or, though at a considerably less frequency, in other members of the Wnt cascade such as *APC*, *AXIN1*, and *AXIN2* [7,8]. Second, other histotypes, and in particular serous ovarian carcinomas where mutations in Wnt-related genes are relatively uncommon, are characterized by constitutive Wnt signaling activation as indicated by alterations in β-catenin subcellular localization (i.e., nuclear and cytoplastic vs. membrane-bound) [9–12]. Importantly, Wnt activity was shown to correlate with grade [12], epithelial to mesenchymal transition (EMT) [7], chemo-resistance [13], and poor prognosis [14] in patients with ovarian carcinomas.

Here, we will review the current knowledge of the role of Wnt signaling in ovarian cancer stemness, EMT, and therapy resistance. The alleged role of exosomes in the paracrine activation of Wnt signaling, and novel potential treatment options based on Wnt inhibition will also be highlighted.

Chapter 5

2. The Wnt/β-Catenin Signaling Pathway

Stem cells are distinguished from other somatic cells by their ability to self-renew and to give rise to distinct differentiated cell types throughout their lifetime [6]. The canonical Wnt signaling program plays a central role in controlling the balance between stemness and differentiation in several adult stem cell niches [15], including the ovary [7]. Accordingly, aberrant Wnt signaling is associated with pathological conditions like cancer [15].

Wnt proteins comprise a group of evolutionary conserved, lipid-modified glycoproteins [16] that operate at both short and long distances in order to regulate programs involved in proliferation, differentiation and stemness [15,17]. In absence of canonical Wnt ligands, intracellular β-catenin levels are regulated by the formation of a multiprotein "destruction complex" encompassing protein phosphatase 2A (PP2a), glycogen synthase kinase 3 (GSK3β) and casein kinase 1α (CK1α), and the scaffold proteins adenomatous polyposis coli (APC), and AXIN1/2. The destruction complex binds and phosphorylates β-catenin at specific serine and threonine residues, thereby targeting it for ubiquitination and subsequent degradation by the proteasome (Figure 1a). Instead, in the presence of Wnt ligands, co-activation of the Frizzled and LRP5/6 (low-density lipoprotein receptor-related proteins) receptors prevents the formation of the destruction complex, thereby stabilizing intracellular β-catenin and eventually leading to its translocation from the cytoplasm to the nucleus. Here, β-catenin interacts with members of the T-cell specific transcription factor/lymphoid enhancer binding factor (TCF/LEF) family of transcription factors and modulates the expression of a broad spectrum of Wnt downstream target genes regulating stemness, proliferation, and differentiation [15] (Figure 1b).

An illustrative example of the relevance of a tightly controlled Wnt signal regulation is provided by the intestinal stem cell niche, i.e., the crypt of Lieberkühn. At the bottom of the crypt, where the highly proliferative intestinal stem cells (ISC) reside, Wnt signaling is highly active due to signals from the surrounding stromal compartment [18], as also shown by nuclear β-catenin localization in both ISCs and the intercalating Paneth cells.

Moving up along the crypt-villus axis, Wnt becomes progressively less active, following a signaling gradient inversely proportional to the differentiation grade of the epithelial lining [19]. In accordance with the central role played by this Wnt gradient, loss of function mutations at the tumor suppressor gene *APC* or gain of function mutations in the β-catenin (*CTNNB1*) oncogene leading to ligand-independent (i.e., constitutive) Wnt activation represent the main initiating events in the vast majority of sporadic colon cancer cases. Hence, the disruption of the homeostatic equilibrium among stemness, differentiation, and proliferation along the crypt-villus axis brought about by constitutive Wnt activation is sufficient to trigger colon cancer development [20].

The functional relevance of the Wnt pathway in controlling stemness, proliferation, and differentiation in organ-specific adult stem cell niches other than the intestinal tract is reflected by the broad spectrum of cancer where its deregulation contributes to tumor initiation and/or progression. Accordingly, there is ample evidence from the scientific literature supporting an important role for Wnt signaling in both the onset and progression of ovarian cancer [7].
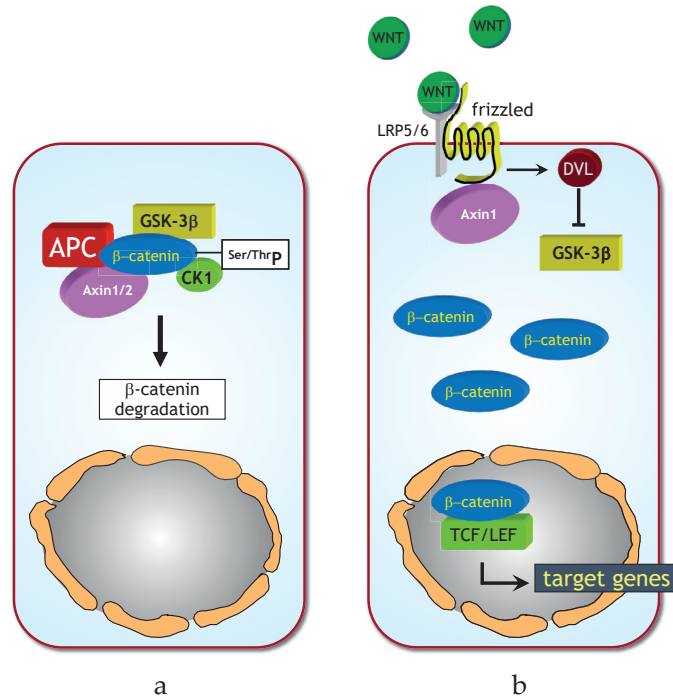
Figure 1. The Wnt/β-catenin signal transduction pathway in homeostasis. (**a**) In the absence of Wnt ligands, intracellular β-catenin levels are controlled by a destruction complex encompassing protein phosphatase 2A (PP2a), glycogen synthase kinase 3 (GSK3β) and casein kinase 1α (CK1α), adenomatous polyposis coli (APC), and AXIN1/2. This complex binds and phosphorylates β-catenin at serine and threonine residues, thereby targeting it for ubiquitination and proteolytic degradation by the proteasome. (**b**) In presence of Wnt, co-activation of the Frizzled and low-density lipoprotein receptor-related protein 5/6 (LRP5/6) (low-density lipoprotein receptor-related proteins) receptors prevents the formation of the destruction complex leading to the stabilization and consequent translocation of β-catenin from the cytoplasm to the nucleus. Here, β-catenin interacts with members of the T-cell specific transcription factor/lymphoid enhancer binding factor (TCF/LEF) family of transcription factors and modulates the expression of a broad spectrum of Wnt downstream target genes. DVL – disheveled. Adapted from [21].

3. Wnt Signaling in Ovarian Development and Tissue Homeostasis

Mammalian sex determination is a developmental process consisting of two distinct antagonistic genetic pathways allowing XX or XY undifferentiated gonads to differentiate into two different organs, namely the testis and the ovary [22]. The SRY-SOX9-FGF9 pathway supports testis development, while the RSPO1-Wnt-β-catenin-FOXL2 network promotes ovarian determination [22] (Figure 2).
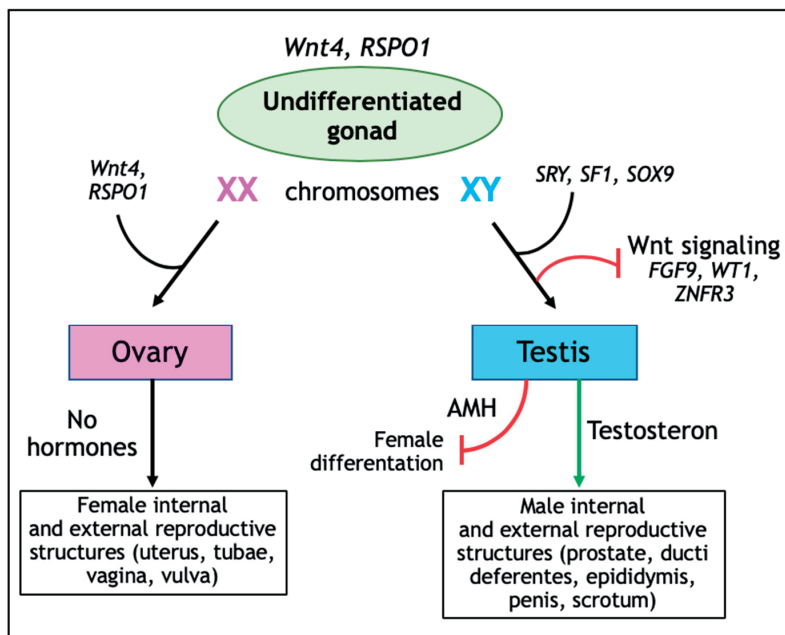
Before sex determination, the undifferentiated gonad is composed of the coelomic epithelium, together with germ and mesenchymal cells. Here, both the Wnt signaling activators Wnt4 and R-spondin 1 (RPSO1) are important regulators of proliferation of

the coelomic epithelium, as indicated by ablation of both *Rspo1* and *Wnt4* leading to reduced numbers of coelomic epithelial cells in XX and XY gonads and, consequently, to hypoplastic testis in XY mutant gonads [23].

During XY sex determination, the transcription factor sex-determining region Y (SRY) together with Splicing factor 1 (SF1) upregulate SRY-Box 9 (*SOX9*) gene expression. Subsequently, *SOX9* upregulation leads to the differentiation of coelomic epithelium into anti-Müllerian hormone producing Sertoli cells, thereby stimulating testis development [24]. Sertoli cells also secrete FGF9 (Fibroblast Growth Factor 9) thus inhibiting the pro-ovarian Wnt signaling pathway [25]. Furthermore, WT1 (Wilms Tumor 1) and ZNFR3 (Zinc Finger 3) also have been shown to downregulate Wnt signaling during male sexual differentiation [26,27]. Accordingly, genetic ablation of *Znrf3* leads to ectopic Wnt signaling in XY gonads and consequentially in the presentation of a female phenotype [27].

In females, both granulosa cells and ovarian surface epithelium (OSE) are derived from the coelomic epithelium. During fetal stages, *Rspo1* is expressed in the mesothelial lining of the coelomic cavity and within the fetal ovary [28], whereas *Wnt4* expression is localized to the gonad medulla and mesonephros between the gonad and the Müllerian duct [29]. Wnt4 and RSPO1 are essential for ovarian differentiation and oogenesis as they suppress *Sox9* expression, stimulate granulosa cell differentiation, and promote female sexual development by sustaining Müllerian duct differentiation [28,30,31]. Genetic ablation of *Wnt4, Rspo1,* or *Ctnnb1* in XX gonads lead to premature differentiation of granulosa cells in fetal stages and consequentially to the abrogation of ovary development at perinatal stages [32].

Ng et al. (2014) [33] provided additional evidence highlighting the significance of the role played by Wnt during ovarian development and tissue maintenance and regeneration in adulthood. In this study, *Lgr5*, the marker of the above-mentioned and Wnt-driven intestinal stem cells, was shown to be broadly expressed during ovarian organogenesis, whereas it was restricted to the OSE in neonatal life. Using in vivo lineage tracing, $Lgr5^+$ cells were identified as stem or progenitor cells, able to contribute to the development of the OSE cell lineage, the mesovarian ligament, and the fimbriae. In adult ovaries, $Lgr5^+$ cells were restricted to the proliferative regions of the OSE and the mesovarian-fimbria junctional epithelium. In the OSE, $Lgr5^+$ cells are thought to preserve homeostasis and to underlie repair of the epithelial damage after ovulation [33]. Indeed, using a Wnt-reporter mouse model, the complete coelomic epithelium overlying the undifferentiated gonad displayed β-catenin/Tcf mediated LacZ expression gradually reduced to smaller populations during postnatal, pre-puberal, and adult life [34]. Of note, the $LacZ^+$ OSE cells were enriched in SP (side population) positive cells, a sub-population of stem-like cells identified by their capacity to efflux the dye Hoechst 33342 by ATP-binding cassette super-family G member 2 (ABCG2) transporter pumps [34], a clinically relevant feature acquired by chemotherapy resistant ovarian CSCs.

Figure 2. Schematic view of sex determination. In the undifferentiated gonad both Wnt4 and RSPO1 (R-spondin 1) are important regulators in particular for the proliferation of the coelomic epithelium. In XX gonads, expression of Wnt4, and RSPO1 leads to ovarian differentiation and oogenesis as they suppress *Sox9* expression, stimulate granulosa cell differentiation, and promote female sexual development by sustaining Müllerian duct differentiation. In XY gonads male reproductive organs are determined by the expression of sex-determining region Y (SRY) together with Splicing factor 1 (SF1) leading to upregulation of *Sox9* gene expression. In addition, Fibroblast Growth Factor 9 (FGF9), Wilms Tumor 1 (WT1), and Zinc Finger 3 (ZNFR3) inhibit the pro-ovarian Wnt signaling pathway. Also, anti-Müllerian hormone (AMH) prevents the development of the Müllerian duct into female reproductive organs.

Apart from its role during embryonic development of the ovary, Wnt signaling was also shown to be an essential regulator of ovarian homeostasis, fertility, and tumorigenesis. Knock-out of *APC2*, a homologue of the *APC* tumor suppressor gene [35], resulted in the activation of ovarian Wnt signaling and in sub-fertility. The latter was due to disturbed follicular growth and the consequent reduced ovulation rate and corpora lutea formation [36]. Notably, aged *APC2*$^{-/-}$ mice developed granulosa cell tumors (GCT) with comparable histological features and molecular signatures to those of the corresponding human GCTs [36].

Overall, the central role played by Wnt in regulating the delicate balance between stemness, proliferation, and differentiation to ensure ovarian tissue homeostasis is reflected by its causal association with ovarian cancer onset and/or progression as discussed in the next section.

Chapter 5

4. Wnt Signaling in Ovarian Cancer

As mentioned above, *CTNNB1* (β-catenin) mutations are found in 16–54% of endometrioid ovarian cancer cases. Likewise, genetic alterations in other members of the Wnt cascade, such as *APC*, *AXIN1*, and *AXIN2*, have also been detected in this specific ovarian cancer histotype [7,8]. In a conditional *APC* knock-out mouse model, it was shown that constitutive activation of Wnt/β-signaling in Müllerian duct-derived organs (i.e., fallopian tubes, uterus, cervix, and the upper two thirds of the vagina) results in the formation of endometrioid tumors in the oviduct, reminiscent of the corresponding histotype in man. Of note, in the same study the ovarian surface epithelium was unaffected, thus suggesting that the oviduct, rather than the OSE, encompasses the cell of origin of (endometrioid) ovarian cancer [37].

In addition to endometrioid ovarian carcinomas, mutations in *CTNNB1* are also found in rare cases of mucinous ovarian cancer [38]. Moreover, both *CTNNB1* and *APC* mutations have also been detected in non-epithelial microcystic stromal tumors (MSTs) of the ovary [39–41]. Accordingly, an increased incidence of MSTs has also been reported among patients affected by familial adenomatous polyposis (FAP) due to germline mutations in *APC* [40,41]

Yet, it should be clearly stated that endometrioid tumors represent a notable exception as mutations in Wnt-related genes are in general extremely rare in any other ovarian cancer histotype [7]. However, even in the absence of specific mutations, Wnt signaling has been reported to be frequently activated in the more common serous histotype as indicated by nuclear and cytoplasmic β-catenin subcellular localization [9–12]. In addition, expression profiling data have confirmed the frequent activation of Wnt signaling in ovarian cancer at large [42,43]. In particular, transcriptome analysis of ascites-derived ovarian cancer cells and tumor-associated macrophages (TAMs) has revealed that both canonical and non-canonical Wnt ligands (i.e., *WNT7A*, *WNT2A*, *WNT5A*, *WNT9A*) are expressed in tumor cells, whereas *LRP* and *FZD* are common to both tumor cells and TAMs [43].

Pangon et al. (2016) took advantage of the Cancer Genome Atlas (TCGA) to show that the oncogene *JRK* (jerky) is overexpressed in 15% of ovarian cancers in association with increased expression of canonical Wnt target genes [44]. JRK directly interacts with the β-catenin transcriptional complex, thereby stabilizing the β-catenin/TCF complex and ultimately resulting in increased β-catenin transcriptional activity and cell proliferation. Consistent with this, depletion of JRK in cancer cell lines repressed expression of β-catenin target genes and reduced cell proliferation [44].

More recently, noncoding RNAs (ncRNAs) have emerged as important post-translational regulators of Wnt-associated gene expression in ovarian cancer (Table 1). By using orthotopic mouse models of ovarian cancer, it was demonstrated that β-catenin plays a key role in the formation of metastasis by controlling the endoribonuclease Dicer, a key component of the microRNA (miR)-processing machinery. β-catenin directly targets Dicer, thereby downregulating multiple miRNAs including the miR-29 family known for its role as a negative EMT regulator. Silencing of β-catenin or overexpression of Dicer or mi-R29 in metastatic ovarian cancer cells reduced their migratory capacity, and attenuated metastasis formation upon β-catenin knockdown in orthotopic mouse models [45]. Of note, reduced expression of miR-29 is associated with ovarian cancer progression and strongly correlated with poor survival [46].

Several other miRs have been demonstrated to impact migration, invasion, and cancer progression via Wnt signaling in ovarian cancer [47–59]. Interestingly, miR-939 has been suggested to function as a tumor promotor by regulating Wnt signaling through direct suppression of the previously discussed *APC2* tumor suppressor [48].

Next to miRs, several long non-coding RNAs (lncRNAs) have been described to play a causative role in Wnt-associated cell proliferation, EMT, and chemotherapy resistance in ovarian cancer [60–65]. Table 1 summarizes the data relative to gene and non-coding RNA alterations leading to Wnt signaling activation in ovarian cancer.

Table 1. Gene and non-coding RNA alterations leading to Wnt signaling activation in ovarian cancers.

Gene/ncRNA	Ovarian cancer histotype*	Mechanism/Target	Reference
CTNNB1	Endometrioid.	Oncogenic activation.	[8,38,66–70]
CTNNB1	Mucinous.	Oncogenic activation.	[38]
CTNNB1	Microcystic Stromal Tumors (MST).	Oncogenic activation.	[39]
APC	Endometrioid.	Loss of tumor suppressor function.	[8]
APC	Microcystic Stromal Tumors (MST).	Loss of tumor suppressor function.	[40,41]
AXIN1	Endometrioid.	Loss of tumor suppressor function.	[8]
AXIN2	Endometrioid.	Loss of tumor suppressor function.	[8]
microRNA (miR)-10a	Granulosa cell tumor.	miR-10a targets *PTEN* and indirectly activates Wnt (and AKT) signaling. Oncogenic activation.	[54]
miR-15b	Epithelial ovarian cancer*.	miR-15b targets *WNT7A* 3'-untranslated region (3'-UTR) and thus inhibits Wnt signaling. Loss of tumor suppressor function.	[50]
miR-16	Epithelial ovarian cancer*.	miR-16 target(s) yet unknown; it inhibits Wnt signaling. Loss of tumor suppressor function.	[56]
miR-21	Epithelial ovarian cancer*.	miR-21 target(s) yet unknown; it activates Wnt signaling. Oncogenic activation.	[57]
miR-27a	Epithelial ovarian cancer*.	mir-27 targets the Wnt antagonist *FOXO1*. Oncogenic activation.	[55]
miR-29	Serous, mucinous, and clear cell ovarian cancer.	miR-29 target(s) yet unknown; it activates Wnt signaling. Oncogenic activation.	[45,46]
miR-92a-1	Epithelial ovarian cancer*.	miR-92a-1 targets the Wnt antagonist Dickkopf 1 *(DKK1)*. Oncogenic activation.	[51]
miR-200c	Epithelial ovarian cancer*.	miR-200c target(s) yet unknown; it inhibits Wnt signaling. Loss of tumor suppressor function.	[47]
miR-214	Epithelial ovarian cancer*.	miR-214 target(s) yet unknown; it inhibits Wnt signaling. Loss of tumor suppressor function.	[53]
miR-219-5p	Epithelial ovarian cancer*.	miR-219-5p targets the EMT transcription factor *TWIST* and inhibits Wnt signaling. Loss of tumor suppressor function.	[52]
miR-654-5p	Epithelial ovarian cancer*.	miR-654-5p targets *CDCP1* and *PLAGL2*. Loss of tumor suppressor function.	[58]
miR-939	Epithelial ovarian cancer*.	miR-939 targets *APC2*. Loss of tumor suppressor function.	[48]
miR-1180	Epithelial ovarian cancer*.	miR-1180 targets *SFRP1*. Loss of tumor suppressor function.	[59]
miR-1207	Epithelial ovarian cancer*	miR-1207 targets *SFRP1*, *AXIN2*, and *ICAT*. Loss of tumor suppressor function.	[49]

Chapter 5

Gene/ncRNA	Ovarian cancer histotype[*]	Mechanism/Target	Reference
HOTAIR [1]	Epithelial ovarian cancer*.	HOTAIR target(s) unknown; Wnt agonist. Oncogenic activation.	[60]
SNHG20 [2]	Epithelial ovarian cancer*.	SNHG20 target(s) unknown; Wnt agonist. Oncogenic activation.	[61]
HOXD-AS1 [3]	Epithelial ovarian cancer*.	HOXD-AS1 targets the Wnt antagonist miR-133a-3p. Oncogenic activation.	[62]
CCAT2 [4]	Epithelial ovarian cancer*.	Targets unknown; EMT and Wnt agonist. Oncogenic activation.	[63]
MALAT1 [5]	Epithelial ovarian cancer*.	Targets unknown; Wnt agonist. Oncogenic activation.	[64]
AWPPH [6]	Epithelial ovarian cancer*.	Targets unknown; Wnt agonist. Oncogenic activation.	[65]
HOXB-AS3 [7]	Serous ovarian cancer samples; other histotypes.	Targets unknown; Wnt agonist. Oncogenic activation.	[71]

*, histotype not characterized; [1,] HOTAIR—HOX antisense intergenic RNA; [2,] SNHG20—small nucleolar RNA host gene 20; [3,] HOXD-AS1—HOXD cluster antisense RNA 1; [4,] CCAT2—colon cancer-associated transcript 2; [5,] MALAT1—metastasis associated lung adenocarcinoma 1; [6,] AWPPH—associated with poor prognosis of hepatocellular carcinoma; [7,] HOXB-AS3—HOXD cluster antisense RNA 3.

Apart from the above alterations in genes and non-coding RNAs, Wnt signaling activation in ovarian cancer might result from additional alternative epigenetic mechanisms, either cell-autonomous or induced by the tumor microenvironment. Epigenetic alterations leading to autocrine overexpression of Wnt ligands [72,73], receptors [74], and/or of other Wnt agonists like *FRAT1* [12] or *PYGO2* [75], or to the inhibition of antagonists such as the secreted frizzled receptors proteins (sFRP) and Dickkopf (DKK1) [14,76–78] have been reported in the literature. Likewise, paracrine secretion of Wnt-activating cues was observed from either the stroma surrounding the primary ovarian cancer, or from ascites in the case of late-stage disease. Several components of ovarian cancer ascites, known to be associated with shorter progression free survival [79,80], have been previously implicated in promoting Wnt signaling: leptin [81,82], urokinase-type plasminogen activator receptor (uPAR) [83], and macrophage migrating inhibitory factor (MIF) [84]. These soluble factors may act by activating the Wnt pathway in disseminated ovarian cancer cells present in ascites. Two additional ascites factors, namely osteoprotegerin (OPG) [85] and interleukin 8 (IL-8) [86], are in fact downstream Wnt targets and could serve as markers of Wnt signaling activity in ascites. In addition, β-1 integrin-mediated adhesion to the peritoneal mesothelium, a key step in the route to ovarian cancer metastasis, activates β-catenin signaling [87]. Of note, it has recently been shown that extracellular vesicles such as exosomes play a critical role in long-distance transmission of morphogens and in particular in Wnt signaling [88]. In the context of ovarian cancer ascites, exosomes may represent a stable source of paracrine Wnt signals [89]. The role of exosomes will be discussed at more length later on in this review.

5. Wnt Signaling in Ovarian Cancer Stem Cells, EMT, and Therapy Resistance

After diagnosis, tumor debulking surgery followed by carboplatin- and paclitaxel-based chemotherapy represent the standard first line therapy for high grade serous ovarian cancer patients. Although at this stage the primary response to chemotherapy

is extremely efficient, most patients relapse and develop metastases locally and at distant organ sites [90]. This is mainly due to sub-populations of tumor cells likely to have acquired stem cell features (CSCs) through EMT and, consequently, the EMT-associated chemo-resistance [5]. In 2005, it was shown for the first time that the aggressiveness of human ovarian cancer results from alterations in stem and progenitor-like cells in the ovary [91]. Moreover, this study demonstrated that the small subpopulation of stem-like, tumor-propagating ovarian cancer cells were earmarked by expression of cluster of differentiation 44 (CD44) and other stem cell and EMT markers such as *KIT* (CD117), *SCF* (stem cell factor), *SLUG* (*SNAIL2*), and *VIM* (vimentin) [91]. After this initial report, several cell surface antigen markers have been identified which allow enrichment of ovarian CSCs from immortalized cell lines, primary tumors, and ascitic fluids: CD133, CD24, CD44, CD177, aldehyde dehydrogenase 1 (ALDH1), and SP [5]. Ovarian cancer follows a unique pattern of metastasis formation where, unlike many other cancer types, no anatomical barrier exists between the primary site and the abdominal cavity, thus greatly facilitating the dissemination of exfoliated malignant cells. In particular, disseminated ovarian cancer cells secrete vascular permeability factors and can block lymphatic drainage leading to accumulation of ascites fluid within the peritoneal cavity [94]. These malignant ascites provide a favorable tumor microenvironment (TME) enriched in secreted inflammatory cytokines [79], growth factors [95], and extracellular macromolecules (collagen, fibronectin, and laminin) [96]. In this environment, tumor cells form multicellular aggregates enriched in cancer stem/progenitor cells, the so-called 'spheroids', which eventually implant on the mesothelial lining of the peritoneum [97] (Figure 3). The attachment of these floating spheroids to the peritoneal lining and associated organs represents the major route for metastasis formation in ovarian cancer [98] where, as observed in other epithelial cancers, EMT was shown to play a key role [99]. Interestingly, although hematogenous spread is generally thought to play a relatively minor role in metastasis formation in ovarian cancer, it has recently been demonstrated in a parabiosis mouse model [100]. In this study, two mice, one of which intraperitoneal transplanted with ovarian cancer cells, were surgically connected to share blood supply. The development of ovarian cancer in the cancer-free animal likely results from hematogenous spread [100]. Likewise, circulating tumor cells have been identified in peripheral blood from ovarian cancer patients [101].

Overall, the naturally occurring spheroids in ascites are likely to underlie metastatic disease in ovarian cancer patients. In the next sections, we will discuss the current experimental evidence on the role of Wnt signaling in eliciting EMT and chemo-resistance in high grade serous ovarian cancer.

5.1. Wnt Signaling and EMT in Ovarian Cancer

EMT is a reversible developmental program exploited by cancer cells to reversibly switch from an epithelial phenotype with apical-basal polarity and cell–cell adhesions, to a more motile mesenchymal state with spindle like morphology and front-back-end polarity [102]. Next to the motility and invasive features characteristic of the mesenchymal state, EMT is functionally associated with the acquirement of stem-like features, resistance to therapy, and immune suppression [103–105]. Last, the capacity of cells undergoing EMT to revert to an epithelial state by mesenchymal-to-epithelial transition (MET) is rate-limiting to allow the stem- and mesenchymal-like migrating CSCs to regain proliferative and epithelial features essential to colonize the metastatic site [102,106]. Various signaling

pathways are involved in EMT, including transforming growth factor β (TGF-β), Notch, and Wnt/β-catenin. Activation of the Wnt/β-catenin pathway has been shown to be an important regulator of EMT in many different types of cancers [106–108], including ovarian cancer [109–112]. In this context, ovarian cancer cell lines with a high SNAIL to E-cadherin ratio, are characterized by enhanced CSC-like, motile, and therapy-resistant features when compared with epithelial ovarian cancer cell lines. Accordingly, *SNAIL* knockdown reversed the malignant properties and tumor burden of the more mesenchymal ovarian cancer cell lines in xenograft models [111]. *SNAIL* and other EMT transcription factors (EMT-TFs) have been shown to activate expression of the *GOLPH3* (Golgi phosphoprotein 3) gene, encoding for an oncoprotein frequently upregulated in ovarian cancer tissues and cell lines, through Wnt/β-catenin signaling activation [112]. Induction of EMT and the consequent acquisition of migratory and invasive cellular features downstream of Wnt activation have also been demonstrated in ovarian carcinomas where *IQGAP2*, a Wnt antagonist, is frequently silenced by DNA methylation [110]. Last, cyclin G2, an unconventional cyclin that opposes cell cycle progression and inhibits EMT, acts as a tumor suppressor in ovarian cancer by inhibiting Wnt/β-catenin signaling [109].

More recently, it has been suggested that, rather than being a binary process with fully opposing epithelial and mesenchymal phenotypes, EMT generates hybrid E/M cancer cells displaying both epithelial and mesenchymal characteristics [113,114]. Indeed, similar to the normal ovarian surface epithelial (OSE) cells previously shown to display both epithelial and mesenchymal characteristics and a remarkable phenotypic plasticity during post-ovulatory repair, double positive E-cadherin and vimentin cells have been observed in ovarian cancers [115]. Accordingly, different intermediate EMT states have been identified in ovarian cancer cell lines [116] and ascites-derived spheroids [117]. Here, ovarian cancer cells in hybrid E/M states were shown to exhibit stem-like features, anoikis resistance, and increased migration and invasion when compared with the fully epithelial and mesenchymal states [116–118].

Overall, it is yet unclear whether the hybrid E/M cells represent a 'metastable' cell population or are cells captured in a time frame during the transition between the epithelial to mesenchymal states. The elucidation of the complex network of intrinsic and extrinsic mechanisms underlying EMT during metastasis formation and the role of Wnt signaling therein represents an important future research challenge. In the next section, the current knowledge on the role of Wnt signaling in resistance to chemotherapy in ovarian cancer will be discussed.

5.2. Wnt Signaling and Therapy Resistance in Ovarian Cancer

As mentioned above, chemotherapy is extremely efficient in the first-line treatment of primary ovarian cancers although it inevitably leaves behind chemo-resistant CSCs likely to underlie relapse and metastasis in distant organ sites [90]. Wnt signaling has been associated with resistance to chemotherapy in different tumor types including ovarian cancer [119].
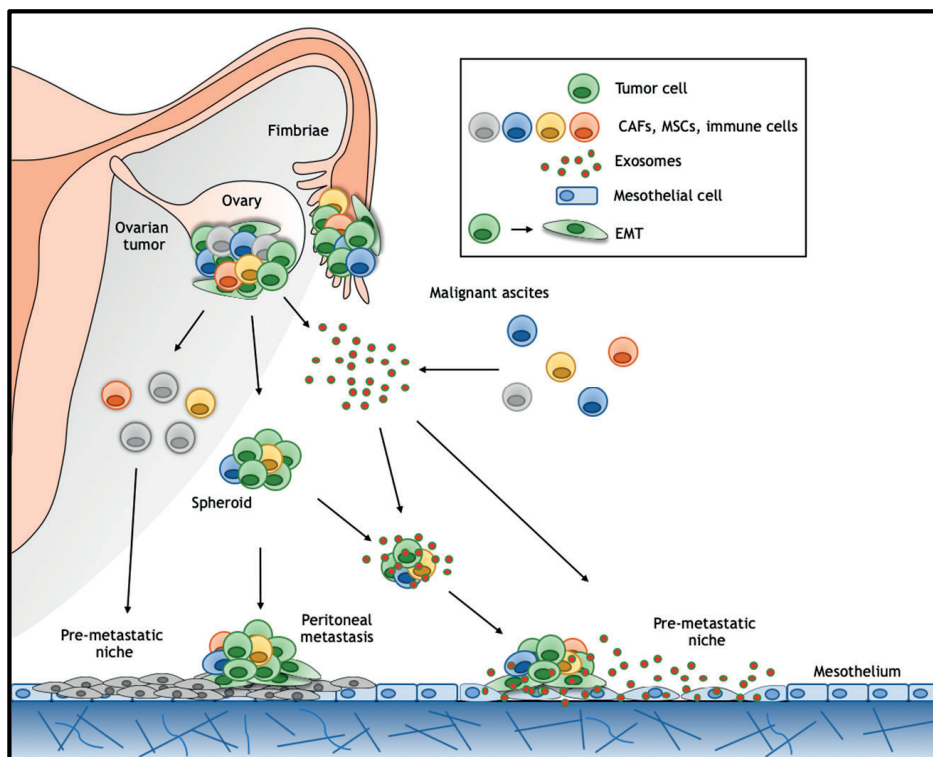
Figure 3. Model for peritoneal metastasis formation in ovarian cancer. Ovarian cancer follows a unique pattern of metastasis formation, where no anatomical barrier exists between the primary site and the abdominal cavity. Multicellular aggregates enriched in cancer stem/progenitor cells, the so-called spheroids, detach from the primary tumor and eventually implant on the mesothelial lining of the peritoneum. EMT was shown to play a key role facilitating the acquisition of stem-like features, anoikis resistance, and increased migration and invasion. The establishment of premetastatic niches composed of several cell populations, including tumor-associated neutrophils, is thought to be required for disseminating carcinoma cells to engraft at the distant site. Exosomes in ovarian cancer ascites have been proposed as a putative mechanism to facilitate long-range distance cell–cell communication thereby establishing both pre-metastatic niches in the peritoneal cavity and preserving stemness in disseminated cancer cells. CAFs: cancer associated fibroblasts; MSCs: mesenchymal stem cells.

Chemo-resistance can be acquired through a broad spectrum of molecular and cellular mechanisms such as the upregulation of ATP-binding cassette (ABC) transporter pumps, the activation of EMT, and the exosome-mediated transport of molecules controlling a broad spectrum of pathways underlying drug resistance [120]. ABC transporters have indeed been shown to be expressed in ovarian cancer usually in association with cancer stemness and poor prognosis [121,122]. Notably, upregulation of the ABCG2 transporter pump and Wnt signaling activation downstream of cKIT mediate the onset of resistance to cisplatin and paclitaxel in ovarian CSCs [13]. In the same study, *ABCG2* expression and chemo-resistance to both cisplatin and paclitaxel could be reversed by β-catenin siRNA

knockdown, once again highlighting the central role of Wnt signaling in these processes [13].

Another well-established mechanism underlying therapy resistance in ovarian cancer, as also mentioned in the previous section, is represented by EMT [99]. Su et al. (2010) showed that *SFRP5* (secreted frizzled-related protein 5), a well-known Wnt and EMT antagonist, is frequently downregulated in ovarian cancer by epigenetic silencing through promoter hypermethylation [123]. Accordingly, restoration of *SFRP5* expression inhibits Wnt signaling and EMT thus sensitizing ovarian cancer cells to chemotherapy. Activation of the EMT-TF *TWIST* and of *AKT2* signaling play key roles downstream of *SFRP5* silencing [123].

In addition to the above-mentioned cell-autonomous mechanisms, ascites also forms a unique tumor microenvironment likely to contribute to therapy resistance [124]. Malignant ascites provides a favorable tumor microenvironment consisting of cellular and non-cellular components, each likely to play a role in the development of resistance to carboplatin- and paclitaxel-based therapy. Among these, cancer associated fibroblasts (CAFs) represent an important component of ovarian cancer ascites [124]. CAFs are a subpopulation of fibroblasts capable of affecting tumor progression, dissemination, and therapy response through signaling to tumor cells and/or remodeling of the extracellular matrix (ECM) [125]. Recently, Ferrari et al. (2019) demonstrated that Dickkopf-3 (DKK3), the stromal expression of which is strongly associated with aggressive ovarian cancer, promotes CAFs' aggressive behavior by enhancing Yes-associated protein/transcriptional co-activator with PDZ-binding motif (YAP/TAZ) activity through Wnt/β-catenin signaling [126]. From a mechanistic perspective, DKK3 destabilizes the Wnt-antagonist Kremen, leading to increased LRP6 localization at the cell membrane. This in turn stabilizes YAP/TAZ and β-catenin levels leading to more global gene expression changes enhancing cancer stemness, malignant progression, and metastasis [126]. Other ascites cellular components such as macrophages have also been shown to take part in tumor progression and the development of therapy resistance. Ragahvan et al. (2019) showed that Wnt signaling participates in a bidirectional ovarian CSC-macrophage interaction [92]. By taking advantage of hetero-spheroids composed of macrophages and ovarian cancer cells in close contact with each other, it was shown that Wnt signaling, activated by secretion of the Wnt5b ligand from macrophages, led to an increase of the ovarian CSC compartment (ALDH$^+$) and to the enhancement of the immune-suppressive characteristics of the macrophages. Likewise, Wnt5b knockdown in macrophages resulted in a loss of the ALDH$^+$ ovarian CSC fraction. Most importantly, the hetero-spheroids were less sensitive to chemotherapeutics and were more invasive in in vitro assays [92]. Hence, macrophage-initiated Wnt activation is likely to play a central role in ovarian cancer stemness maintenance and in therapy resistance.

Notwithstanding more recent advances in chemotherapy (e.g., intraperitoneal delivery of cytotoxic drugs and the introduction of novel, more targeted agents such as bevacizumab and imatinib) [127–129], less than 30% of advanced ovarian cancer patients survive longer than five years after diagnosis [1]. Therefore, there is urgent need for novel therapeutic strategies based on improved understanding of the molecular and cellular mechanisms underlying dissemination and metastasis formation by ovarian cancer cells in the peritoneal cavity and their acquisition of dormant and chemo-resistant properties. Recently, the role played by extracellular vesicles and in particular by exosomes in tumor

progression, dissemination, and resistance to therapy has opened new avenues in basic and translational cancer research. In the next section we will present and discuss the current knowledge on exosomes in ovarian cancer, especially in the context of intra-abdominal ascites and of long-range Wnt signaling activation.

6. Exosomes and Wnt Signaling in Ovarian Cancer Ascites

Malignant ascites provides a favorable tumor microenvironment and consists of a heterogeneous mixture of cells and secreted factors that modulate cancer cell behavior during tumor progression, metastasis formation, and acquirement of chemo-resistance. As mentioned, Wnt ligands are modified lipids and are therefore highly hydrophobic, thereby limiting their ability for extracellular diffusion [16]. Recently however, studies have shown that Wnts can be transported across tissues by exosomes [88,130]. In the following paragraphs we will highlight the current knowledge on the role played by exosomes in ovarian cancer ascites as a putative mechanism to activate Wnt signaling over long-range distances both in establishing pre-metastatic niches in the peritoneal cavity and in preserving stemness in disseminated cancer cells.

6.1. Exosomes
Exosomes are small extracellular vesicles ranging in diameter from 30 to 100 nm that are secreted by most eukaryotic cells. Secreted exosomes are important mediators in cell–cell communication as they carry molecules such as microRNAs, mRNAs, and both membrane-bound and secreted proteins [131]. Exosomes are thought to facilitate tumor survival and progression by stimulating angiogenesis and tumor growth, suppressing immune responses, remodeling of the extracellular matrix, promoting metastasis formation either directly and/or through the establishment of premetastatic niches [131] (Figure 3). Numerous studies have demonstrated the presence of exosomes in ovarian cancer cell line cultures, and in patient-derived serum and ascites [132–135]. Notably, it has been shown that active Wg (Wingless) and Wnt3a ligands are membrane-bound in exosomes from Drosophila and human cells, respectively [88]. Moreover, macrophage-derived and exosome-packaged Wnts are rate-limiting for the regenerative response of intestine intestinal stem cells after radiation [130]. In relation to cancer, fibroblast-derived exosomes carrying Wnt ligands increase cell migration and metastasis formation in breast cancer [136]. Hu et al. (2019) recently found that exosomes derived from stromal fibroblasts contain Wnt ligands capable of eliciting the de-differentiation of colon cancer cells into therapy resistant CSCs [137]. Alternatively, activation of Wnt signaling in target cells has been shown to occur by exosomes encompassing β-catenin in their cargo. Here, both 14-3-3 proteins and β-catenin were encompassed in the extracellular vesicles. 14-3-3 proteins bind to dishevelled segment polarity protein 2 (Dvl-2) and GSK3β thereby interfering with β-catenin phosphorylation and stimulating Wnt signaling [138].

Although to date no evidence has been presented supporting the presence of exosomes encompassing active Wnt ligands in ovarian cancer ascites, differential expression analysis of ovarian cancer exosomes compared with those from normal OSE cells indicate a potential involvement of miRNAs known to target the Wnt signal transduction pathway [139]. Moreover, recently it has been demonstrated that exosomes isolated from a highly invasive ovarian cancer cell line promote metastasis in vivo compared to exosomes from

Chapter 5

cells with low invasive capacity [140]. Quantitative proteomic analysis of tumor tissues of the mice treated with exosomes derived from these two different cell lines revealed a potential role for Wnt signaling in the role played by exosomes in tumor growth and metastasis in vivo [140]. Also, as discussed here below, ovarian cancer exosomes containing the Wnt target and transmembrane protein CD44 have been shown to participate in the formation of pre-metastatic niches [141].

6.2. Pre-Metastatic Niche

Ovarian carcinomas spread through the shedding of clusters of tumor cells from the primary lesion into the peritoneal cavity. In this context, the key event in metastatic seeding is the mesothelial adhesion of ovarian cancer cells in the intraperitoneal cavity. The establishment of premetastatic niches is thought to be required for disseminating cancer cells to engraft at the distant site [142]. Premetastatic niches comprise of a specialized and favorable micro-environment that facilitates colonization and promotes survival and outgrowth of disseminated tumor cells [142] (Figure 3). The relevance of the formation of pre-metastatic niches in ovarian cancer has been proposed by several studies [141,143]. Lee et al. (2019) demonstrated that inflammatory factors secreted by ovarian cancer cells mobilize neutrophils and stimulate them to create chromatin webs called 'neutrophil extracellular traps' (NETs) in the omentum in both tumor-bearing mice (before metastasis occurs) and in early-stage ovarian cancer patients. The NETs can sequentially capture ovarian cancer cells and thereby promote metastasis formation. Reversely, inhibiting NET formation abrogated omental colonization [143].

Next to NETs, ovarian cancer exosomes have also been shown to participate in the establishment of a pre-metastatic niche by alternative mechanisms. First, *MMP1* mRNA has been found in extracellular vesicles derived from ovarian cancer cell lines and ascites from ovarian cancer patients that promotes apoptotic cell death of the mesothelial cells, thus resulting in the destruction of the peritoneal barrier [144]. In addition, ovarian cancer cells' exosomes encompassing the cell-surface glycoprotein CD44 can transfer it to peritoneal mesothelial cells and induce their reprogramming by EMT activation. The modified mesothelium facilitates ovarian cancer invasion and metastasis formation [141]. Of note, CD44 is a major Wnt target gene in the intestinal epithelium [145] and is essential for Wnt induction during colon cancer progression [146], thus suggesting yet another functional link between Wnt signaling and ovarian cancer exosomes in pre-metastatic niche formation.

To interfere with the interaction between disseminated ovarian cancer cells and the exosome-receiving mesothelial cells, De la Fuente et al. (2015) developed a metastatic trap (M-Trap) [147]. By embedding exosomes purified from ovarian cancer patient ascites on a 3D scaffold, the authors showed that the M-Trap device was able to capture ovarian cancer cells in a mouse model of ovarian cancer. This led to a more focalized disease and an increase in survival rate [147]. These results lay the foundation for future clinical approaches to improve treatment of ovarian cancer patients with malignant ascites [147].
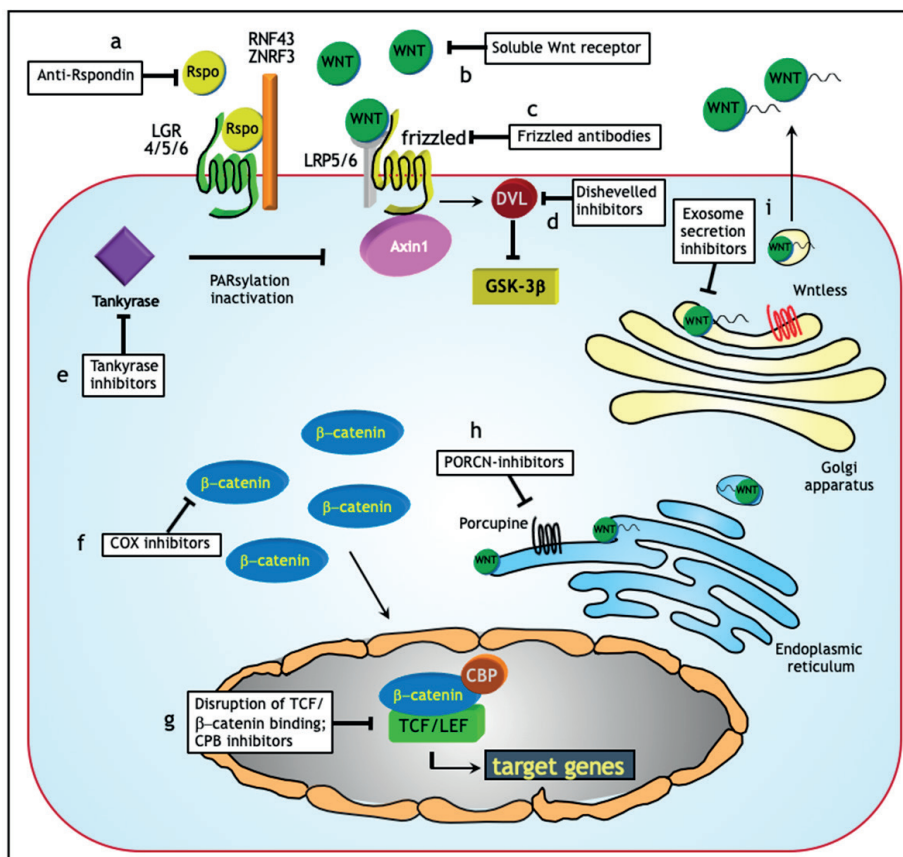
Figure 4. Therapeutic targets for the inhibition of Wnt signaling. (a, b, c) Wnt soluble receptors, anti-R-spondin antibodies, and antibodies directed against Frizzled receptors impair the ligand/receptor interaction and prevent downstream signaling. (d) Disheveled inhibitors block Wnt signaling by interfering with the Frizzled/Disheveled interaction. (e) Tankyrase activates Axin through PARsylation. Tankyrase inhibition increases Axin levels thus stimulating the formation of the β-catenin destruction complex and reducing the intracellular β-catenin pool. (f) cyclooxygenase (COX) inhibitors increase ubiquitination and proteasomal degradation of β-catenin. Next, COX2 inhibition leads to reduced levels of prostaglandin E2 (PGE2) known to positively affect Wnt signaling. (g) Disruption of its interaction with TCF inhibits β-catenin-mediated transcriptional activity. CREB-binding protein (CBP) inhibitors instead interfere with the interaction between TCF/LEF and CBP thereby reducing transcriptional activity. (h) *PORCN*-inhibitors hamper the palmitoylation of Wnt before its extracellular release. (i) Exosome secretion inhibitors reduce the transport of biomolecules like active Wnt ligands, RNAs and proteases that contribute to angiogenesis, tumor growth, immune response suppression, the remodeling and degradation of the extracellular matrix (ECM). Additional abbreviatons: RNF43 = RING finger 43; LGR4/5/6 = Leucine-rich repeat-containing G-protein coupled receptor 4/5/6; RSPO = R-spondin; ZRNF3 = Zinc RING finger 3; GSK3β = glycogen synthase kinase 3β; LRP5/6 = LDL Receptor Related Protein 5/6; TCF/LEF = T-cell specific transcription factor/lymphoid enhancer binding factor.

Overall, notwithstanding that treatment of advanced stage ovarian cancer patients still represents a major clinical challenge, recent advances in our understanding of the mechanisms underlying ovarian cancer ascites formation and the role they play in metastasis formation in the peritoneal cavity are of good auspices for the future. Exosomes in particular, may represent powerful tools in early diagnosis and treatment [135]. As for the latter, targeted exosome ablation or inhibition of exosome secretion may affect tumor progression or therapy resistance (Figure 4). In this scenario, the Wnt signaling pathway may also represent a relevant therapeutic target. In the next paragraph, treatment options based on targeting of Wnt signaling in ovarian cancer will be discussed.

7. Targeting Wnt in Ovarian Cancer: Opportunities for Treatment?

During the last decade, the therapeutic response rate of ovarian cancer patients has improved through optimization of chemotherapy strategies, their intraperitoneal administration, and the introduction of targeted therapies [127–129]. However, despite these developments, the overall survival of ovarian cancer patients has not significantly improved [1]. Because of the role played in cancer stemness and in therapy resistance, the Wnt signaling pathway forms a candidate target for therapeutic intervention as different segment of this cascade are suitable for therapeutic targeting **(Figure 4; Table 2**).

Although R-spondins (RSPO) are unable to initiate Wnt signaling, they can, by binding to leucine-rich repeat-containing G-protein coupled receptors (LGR) enhance responses to low-dose Wnt proteins [148]. Functional RSPOs have been found in multiple human tumor types and anti-RSPO monoclonal antibodies shown to reduce the tumorigenicity of cancer cells in patient-derived tumor xenograft models of several malignancies including ovarian cancer [149]. Porcupine (PORCN) inhibitors form another relevant target to inhibit Wnt signaling. The acetyltransferase PORCN is responsible for

post-translational modifications of Wnt proteins essential for the transport, secretion, and activity of the ligands. WNT974 is a selective PORCN inhibitor that has been shown to exert cytostatic effects on ascites-derived ovarian cancer cells as a consequence of Wnt signaling inhibition [150]. When combined with the conventional chemotherapeutic drug carboplatin, WNT974 administration led to increased cytotoxic effects and cell cycle arrest in ascites samples when compared with single drug treatments [150].

The FDA (Food and Drug Administration)-approved anti-helminth compound niclosamide represents yet another powerful Wnt inhibitor shown to repress ovarian CSC growth through downregulation of both the disheveled protein DVL2 and the surface receptor LRP6 [151]. Next to Wnt, niclosamide targets additional signaling pathways known to play a role in cancer stemness, including Notch, mTORC1, and Stat3 [152].

Besides the above mentioned Wnt targets and inhibitory compounds, inhibition of Wnt ligands secretion, inactivation of the extracellular portion of Frizzled receptors, and interference with the TCF/β-catenin complex represent additional and presently under investigation strategies [153] (Figure 4; Table 2).

Currently, different Wnt inhibitors are being evaluated in clinical trials for different cancer types including ovarian cancer. As a notable example, Ipafricept is a recombinant fusion protein that competes with the FZD8 receptor for its ligand thereby antagonizing Wnt signaling. Ipafricept reduces cancer stem cells, promotes differentiation, and synergizes with taxanes in ovarian cancer xenografts. More recently, a phase 1B trial was

conducted with ipafricept in combination with carboplatin and paclitaxel in patients with recurrent platinum-sensitive ovarian cancer [154]. Unfortunately, although generally well-tolerated by patients, bone toxicity at efficacy doses limited ipafricept treatment [154]. Nonetheless, other Wnt inhibitors targeting PORCN and β-catenin are now being tested in clinical trials in different tumor types [155].

8. Conclusive Remarks

In conclusion, a considerable body of evidence supports the relevance of the role played by Wnt signaling in ovarian cancer stemness, progression to malignancy, and resistance to chemotherapy. Notwithstanding the potential and innovative therapeutic strategies currently in development to specifically target the Wnt pathway, plasticity of cancer cells still represents an escape mechanism leading to therapy resistance. Moreover, because of Wnt's essential role in tissue homeostasis and regeneration upon damage, its inhibition is likely to result in adverse events. Therefore, the identification and elucidation of the complex network of intrinsic and extrinsic mechanisms driving ovarian cancer progression and therapy resistance represent the major future research challenge in the translation of the fundamental understanding of metastasis and therapy.

Table 2. Wnt inhibitors in ovarian cancer.

Molecular targets	Inhibitors	Activity	Reference
Extracellular targeting	Anti-Rspondin	anti-RSPO monoclonal antibodies reduce tumorigenicity of cancer cells in patient-derived ovarian tumor xenograft models.	[149]
	Ipafricept (OMP54F28)	Recombinant fusion protein that competes with the membrane-bound Frizzled 8 (FZD8) receptor for its ligand; leads to tumor regression in combination with taxane in ovarian xenograft models; currently under clinical trial.	[154]
LRP6 inactivation	Salinomycin	Small molecule blocking Wnt induced LRP6 phosphorylation and induces its degradation; leads to repression of EMT in epithelial ovarian cancer.	[156,157]
Dishevelled	3289–8625	Small molecule disrupting the frizzled-disheveled interaction by targeting the PDZ domain; chemo-sensitizes paclitaxel-resistant ovarian cancer cells.	[158]
PORCN	WNT974	Small molecule inhibitors of Wnt acetyltransferase porcupine; increases cytostatic effects on ascites-derived ovarian cancer cells.	[150]
CK1α activation	Pyrvinium	Small molecule that selectively potentiates CK1α kinase activity leading to increased β-catenin phosphorylation; enhances sensitivity to chemotherapy of ovarian cancer cells.	[159,160]
Non-specific or Overlapping targets	Niclosamide	Small molecule inhibitor promoting FZD1 endocytosis and suppressing LRP6 expression; inhibits growth and increases cell death in ovarian cancer.	[161–163]

Chapter 5

COX-inhibitors	Aspirin lowers the risk of ovarian cancer development; in case of ovarian cancer underlying mechanism yet unknown.	[164]

Conflicts of Interest: The authors declare no conflict of interest.

References

1. Siegel, R.L.; Miller, K.D.; Jemal, A. Cancer statistics, 2018. *CA Cancer J. Clin.* **2018**, *68*, 7–30, doi:10.3322/caac.21442.
2. Bast, R.C., Jr.; Hennessy, B.; Mills, G.B. The biology of ovarian cancer: New opportunities for translation. *Nat. Rev. Cancer* **2009**, *9*, 415–428, doi:10.1038/nrc2644.
3. Kurman, R.J.; Shih Ie, M. Pathogenesis of ovarian cancer: Lessons from morphology and molecular biology and their clinical implications. *Int. J. Gynecol. Pathol.* **2008**, *27*, 151–160, doi:10.1097/PGP.0b013e318161e4f5.
4. Kurman, R.J.; Shih Ie, M. The origin and pathogenesis of epithelial ovarian cancer: A proposed unifying theory. *Am. J. Surg. Pathol.* **2010**, *34*, 433–443, doi:10.1097/PAS.0b013e3181cf3d79.
5. Foster, R.; Buckanovich, R.J.; Rueda, B.R. Ovarian cancer stem cells: Working towards the root of stemness. *Cancer Lett.* **2013**, *338*, 147–157, doi:10.1016/j.canlet.2012.10.023.
6. Reya, T.; Morrison, S.J.; Clarke, M.F.; Weissman, I.L. Stem cells, cancer, and cancer stem cells. *Nature* **2001**, *414*, 105–111.
7. Arend, R.C.; Londono-Joshi, A.I.; Straughn, J.M., Jr.; Buchsbaum, D.J. The Wnt/beta-catenin pathway in ovarian cancer: A review. *Gynecol. Oncol.* **2013**, *131*, 772–779, doi:10.1016/j.ygyno.2013.09.034.
8. Wu, R.; Zhai, Y.; Fearon, E.R.; Cho, K.R. Diverse mechanisms of beta-catenin deregulation in ovarian endometrioid adenocarcinomas. *Cancer Res.* **2001**, *61*, 8247–8255.
9. Kildal, W.; Risberg, B.; Abeler, V.M.; Kristensen, G.B.; Sudbo, J.; Nesland, J.M.; Danielsen, H.E. beta-catenin expression, DNA ploidy and clinicopathological features in ovarian cancer: A study in 253 patients. *Eur. J. Cancer* **2005**, *41*, 1127–1134, doi:10.1016/j.ejca.2005.01.022.
10. Lee, C.M.; Shvartsman, H.; Deavers, M.T.; Wang, S.C.; Xia, W.; Schmandt, R.; Bodurka, D.C.; Atkinson, E.N.; Malpica, A.; Gershenson, D.M., et al. beta-catenin nuclear localization is associated with grade in ovarian serous carcinoma. *Gynecol. Oncol.* **2003**, *88*, 363–368.
11. Rask, K.; Nilsson, A.; Brannstrom, M.; Carlsson, P.; Hellberg, P.; Janson, P.O.; Hedin, L.; Sundfeldt, K. Wnt-signalling pathway in ovarian epithelial tumours: Increased expression of beta-catenin and GSK3beta. *Br. J. Cancer* **2003**, *89*, 1298–1304, doi:10.1038/sj.bjc.6601265.
12. Wang, Y.; Hewitt, S.M.; Liu, S.; Zhou, X.; Zhu, H.; Zhou, C.; Zhang, G.; Quan, L.; Bai, J.; Xu, N. Tissue microarray analysis of human FRAT1 expression and its correlation with the subcellular localisation of beta-catenin in ovarian tumours. *Br. J. Cancer* **2006**, *94*, 686–691, doi:10.1038/sj.bjc.6602988.
13. Chau, W.K.; Ip, C.K.; Mak, A.S.; Lai, H.C.; Wong, A.S. c-Kit mediates chemoresistance and tumor-initiating capacity of ovarian cancer cells through activation of Wnt/beta-catenin-ATP-binding cassette G2 signaling. *Oncogene* **2013**, *32*, 2767–2781, doi:10.1038/onc.2012.290.
14. Jacob, F.; Ukegjini, K.; Nixdorf, S.; Ford, C.E.; Olivier, J.; Caduff, R.; Scurry, J.P.; Guertler, R.; Hornung, D.; Mueller, R., et al. Loss of secreted frizzled-related protein 4 correlates with an aggressive phenotype and predicts poor outcome in ovarian cancer patients. *PLoS One* **2012**, *7*, e31885, doi:10.1371/journal.pone.0031885.
15. Reya, T.; Clevers, H. Wnt signalling in stem cells and cancer. *Nature* **2005**, *434*, 843–850, doi:10.1038/nature03319.
16. Willert, K.; Brown, J.D.; Danenberg, E.; Duncan, A.W.; Weissman, I.L.; Reya, T.; Yates, J.R., 3rd; Nusse, R. Wnt proteins are lipid-modified and can act as stem cell growth factors. *Nature* **2003**, *423*, 448–452, doi:10.1038/nature01611.

Chapter 5

17. Zecca, M.; Basler, K.; Struhl, G. Direct and long-range action of a wingless morphogen gradient. *Cell* **1996**, *87*, 833–844, doi:10.1016/s0092-8674(00)81991-1.

18. Shoshkes-Carmel, M.; Wang, Y.J.; Wangensteen, K.J.; Toth, B.; Kondo, A.; Massasa, E.E.; Itzkovitz, S.; Kaestner, K.H. Subepithelial telocytes are an important source of Wnts that supports intestinal crypts. *Nature* **2018**, *557*, 242–246, doi:10.1038/s41586-018-0084-4.

19. Gregorieff, A.; Clevers, H. Wnt signaling in the intestinal epithelium: From endoderm to cancer. *Genes Dev.* **2005**, *19*, 877–890, doi:10.1101/gad.1295405.

20. Fodde, R.; Smits, R.; Clevers, H. APC, signal transduction and genetic instability in colorectal cancer. *Nat. Rev. Cancer* **2001**, *1*, 55–67.

21. Fodde, R.; Brabletz, T. Wnt/beta-catenin signaling in cancer stemness and malignant behavior. *Curr Opin Cell Biol* **2007**, *19*, 150–158.

22. Biason-Lauber, A.; Chaboissier, M.C. Ovarian development and disease: The known and the unexpected. *Semin. Cell Dev. Biol.* **2015**, *45*, 59–67, doi:10.1016/j.semcdb.2015.10.021.

23. Chassot, A.A.; Bradford, S.T.; Auguste, A.; Gregoire, E.P.; Pailhoux, E.; de Rooij, D.G.; Schedl, A.; Chaboissier, M.C. WNT4 and RSPO1 together are required for cell proliferation in the early mouse gonad. *Development* **2012**, *139*, 4461–4472, doi:10.1242/dev.078972.

24. Sekido, R.; Lovell-Badge, R. Sex determination involves synergistic action of SRY and SF1 on a specific Sox9 enhancer. *Nature* **2008**, *453*, 930–934, doi:10.1038/nature06944.

25. Jameson, S.A.; Lin, Y.T.; Capel, B. Testis development requires the repression of Wnt4 by Fgf signaling. *Dev. Biol.* **2012**, *370*, 24–32, doi:10.1016/j.ydbio.2012.06.009.

26. Chang, H.; Gao, F.; Guillou, F.; Taketo, M.M.; Huff, V.; Behringer, R.R. Wt1 negatively regulates beta-catenin signaling during testis development. *Development* **2008**, *135*, 1875–1885, doi:10.1242/dev.018572.

27. Harris, A.; Siggers, P.; Corrochano, S.; Warr, N.; Sagar, D.; Grimes, D.T.; Suzuki, M.; Burdine, R.D.; Cong, F.; Koo, B.K., et al. ZNRF3 functions in mammalian sex determination by inhibiting canonical WNT signaling. *Proc. Natl. Acad. Sci. U S A* **2018**, *115*, 5474–5479, doi:10.1073/pnas.1801223115.

28. Parma, P.; Radi, O.; Vidal, V.; Chaboissier, M.C.; Dellambra, E.; Valentini, S.; Guerra, L.; Schedl, A.; Camerino, G. R-spondin1 is essential in sex determination, skin differentiation and malignancy. *Nat. Genet.* **2006**, *38*, 1304–1309, doi:10.1038/ng1907.

29. Kim, Y.; Kobayashi, A.; Sekido, R.; DiNapoli, L.; Brennan, J.; Chaboissier, M.C.; Poulat, F.; Behringer, R.R.; Lovell-Badge, R.; Capel, B. Fgf9 and Wnt4 act as antagonistic signals to regulate mammalian sex determination. *PLoS Biol.* **2006**, *4*, e187, doi:10.1371/journal.pbio.0040187.

30. Chassot, A.A.; Ranc, F.; Gregoire, E.P.; Roepers-Gajadien, H.L.; Taketo, M.M.; Camerino, G.; de Rooij, D.G.; Schedl, A.; Chaboissier, M.C. Activation of beta-catenin signaling by Rspo1 controls differentiation of the mammalian ovary. *Hum. Mol. Genet.* **2008**, *17*, 1264–1277, doi:10.1093/hmg/ddn016.

31. Vainio, S.; Heikkila, M.; Kispert, A.; Chin, N.; McMahon, A.P. Female development in mammals is regulated by Wnt-4 signalling. *Nature* **1999**, *397*, 405–409, doi:10.1038/17068.

32. Chassot, A.A.; Gillot, I.; Chaboissier, M.C. R-spondin1, WNT4, and the CTNNB1 signaling pathway: Strict control over ovarian differentiation. *Reproduction* **2014**, *148*, R97-110, doi:10.1530/REP-14-0177.

33. Ng, A.; Tan, S.; Singh, G.; Rizk, P.; Swathi, Y.; Tan, T.Z.; Huang, R.Y.; Leushacke, M.; Barker, N. Lgr5 marks stem/progenitor cells in ovary and tubal epithelia. *Nat. Cell. Biol.* **2014**, *16*, 745–757, doi:10.1038/ncb3000.

34. Usongo, M.; Farookhi, R. beta-catenin/Tcf-signaling appears to establish the murine ovarian surface epithelium (OSE) and remains active in selected postnatal OSE cells. *BMC Dev. Biol.* **2012**, *12*, 17, doi:10.1186/1471-213X-12-17.

35. van Es, J.H.; Kirkpatrick, C.; van de Wetering, M.; Molenaar, M.; Miles, A.; Kuipers, J.; Destree, O.; Peifer, M.; Clevers, H. Identification of APC2, a homologue of the adenomatous polyposis coli tumour suppressor. *Curr. Biol.* **1999**, *9*, 105–108, doi:10.1016/s0960-9822(99)80024-4.

36. Mohamed, N.E.; Hay, T.; Reed, K.R.; Smalley, M.J.; Clarke, A.R. APC2 is critical for ovarian WNT signalling control, fertility and tumour suppression. *BMC Cancer* **2019**, *19*, 677, doi:10.1186/s12885-019-5867-y.

37. van der Horst, P.H.; van der Zee, M.; Heijmans-Antonissen, C.; Jia, Y.; DeMayo, F.J.; Lydon, J.P.; van Deurzen, C.H.; Ewing, P.C.; Burger, C.W.; Blok, L.J. A mouse model for endometrioid ovarian cancer arising from the distal oviduct. *Int. J. Cancer* **2014**, *135*, 1028–1037, doi:10.1002/ijc.28746.

38. Sagae, S.; Kobayashi, K.; Nishioka, Y.; Sugimura, M.; Ishioka, S.; Nagata, M.; Terasawa, K.; Tokino, T.; Kudo, R. Mutational analysis of beta-catenin gene in Japanese ovarian carcinomas: Frequent mutations in endometrioid carcinomas. *Jpn. J. Cancer Res.* **1999**, *90*, 510–515, doi:10.1111/j.1349-7006.1999.tb00777.x.

39. Lee, J.H.; Kim, H.S.; Cho, N.H.; Lee, J.Y.; Kim, S.; Kim, S.W.; Kim, Y.T.; Nam, E.J. Genetic analysis of ovarian microcystic stromal tumor. *Obstet. Gynecol. Sci.* **2016**, *59*, 157–162, doi:10.5468/ogs.2016.59.2.157.

40. Liu, C.; Gallagher, R.L.; Price, G.R.; Bolton, E.; Joy, C.; Harraway, J.; Venter, D.J.; Armes, J.E. Ovarian Microcystic Stromal Tumor: A Rare Clinical Manifestation of Familial Adenomatous Polyposis. *Int J Gynecol Pathol* **2016**, *35*, 561–565, doi:10.1097/PGP.0000000000000289.

41. Lee, S.H.; Koh, Y.W.; Roh, H.J.; Cha, H.J.; Kwon, Y.S. Ovarian microcystic stromal tumor: A novel extracolonic tumor in familial adenomatous polyposis. *Genes Chromosomes Cancer* **2015**, *54*, 353–360, doi:10.1002/gcc.22233.

42. Marchion, D.C.; Xiong, Y.; Chon, H.S.; Al Sawah, E.; Bou Zgheib, N.; Ramirez, I.J.; Abbasi, F.; Stickles, X.B.; Judson, P.L.; Hakam, A., et al. Gene expression data reveal common pathways that characterize the unifocal nature of ovarian cancer. *Am. J. Obstet. Gynecol.* **2013**, *209*, 576 e571-576 e516, doi:10.1016/j.ajog.2013.08.004.

43. Reinartz, S.; Finkernagel, F.; Adhikary, T.; Rohnalter, V.; Schumann, T.; Schober, Y.; Nockher, W.A.; Nist, A.; Stiewe, T.; Jansen, J.M., et al. A transcriptome-based global map of signaling pathways in the ovarian cancer microenvironment associated with clinical outcome. *Genome Biol.* **2016**, *17*, 108, doi:10.1186/s13059-016-0956-6.

44. Pangon, L.; Ng, I.; Giry-Laterriere, M.; Currey, N.; Morgan, A.; Benthani, F.; Tran, P.N.; Al-Sohaily, S.; Segelov, E.; Parker, B.L., et al. JRK is a positive regulator of beta-catenin transcriptional activity commonly overexpressed in colon, breast and ovarian cancer. *Oncogene* **2016**, *35*, 2834–2841, doi:10.1038/onc.2015.347.

45. To, S.K.Y.; Mak, A.S.C.; Eva Fung, Y.M.; Che, C.M.; Li, S.S.; Deng, W.; Ru, B.; Zhang, J.; Wong, A.S.T. beta-catenin downregulates Dicer to promote ovarian cancer metastasis. *Oncogene* **2017**, *36*, 5927–5938, doi:10.1038/onc.2017.185.

46. Dai, F.; Zhang, Y.; Chen, Y. Involvement of miR-29b signaling in the sensitivity to chemotherapy in patients with ovarian carcinoma. *Hum. Pathol.* **2014**, *45*, 1285–1293, doi:10.1016/j.humpath.2014.02.008.

Chapter 5

47. Zhang, Y.; Wang, J.; Wu, D.; Li, M.; Zhao, F.; Ren, M.; Cai, Y.; Dou, J. IL-21-secreting hUCMSCs combined with miR-200c inhibit tumor growth and metastasis via repression of Wnt/beta-catenin signaling and epithelial-mesenchymal transition in epithelial ovarian cancer. *Onco. Targets Ther.* **2018**, *11*, 2037–2050, doi:10.2147/OTT.S147855.

48. Ying, X.; Li-ya, Q.; Feng, Z.; Yin, W.; Ji-hong, L. MiR-939 promotes the proliferation of human ovarian cancer cells by repressing APC2 expression. *Biomed. Pharmacother.* **2015**, *71*, 64–69, doi:10.1016/j.biopha.2015.02.020.

49. Wu, G.; Liu, A.; Zhu, J.; Lei, F.; Wu, S.; Zhang, X.; Ye, L.; Cao, L.; He, S. MiR-1207 overexpression promotes cancer stem cell-like traits in ovarian cancer by activating the Wnt/beta-catenin signaling pathway. *Oncotarget* **2015**, *6*, 28882–28894, doi:10.18632/oncotarget.4921.

50. MacLean, J.A., 2nd; King, M.L.; Okuda, H.; Hayashi, K. WNT7A Regulation by miR-15b in Ovarian Cancer. *PLoS One* **2016**, *11*, e0156109, doi:10.1371/journal.pone.0156109.

51. Chen, M.W.; Yang, S.T.; Chien, M.H.; Hua, K.T.; Wu, C.J.; Hsiao, S.M.; Lin, H.; Hsiao, M.; Su, J.L.; Wei, L.H. The STAT3-miRNA-92-Wnt Signaling Pathway Regulates Spheroid Formation and Malignant Progression in Ovarian Cancer. *Cancer Res.* **2017**, *77*, 1955–1967, doi:10.1158/0008-5472.CAN-16-1115.

52. Wei, C.; Zhang, X.; He, S.; Liu, B.; Han, H.; Sun, X. MicroRNA-219-5p inhibits the proliferation, migration, and invasion of epithelial ovarian cancer cells by targeting the Twist/Wnt/beta-catenin signaling pathway. *Gene* **2017**, *637*, 25–32, doi:10.1016/j.gene.2017.09.012.

53. Liu, Y.; Lin, J.; Zhai, S.; Sun, C.; Xu, C.; Zhou, H.; Liu, H. MicroRNA-214 Suppresses Ovarian Cancer by Targeting beta-Catenin. *Cell Physiol. Biochem.* **2018**, *45*, 1654–1662, doi:10.1159/000487733.

54. Tu, J.; Cheung, H.H.; Lu, G.; Chen, Z.; Chan, W.Y. MicroRNA-10a promotes granulosa cells tumor development via PTEN-AKT/Wnt regulatory axis. *Cell Death Dis.* **2018**, *9*, 1076, doi:10.1038/s41419-018-1117-5.

55. Zhang, L.Y.; Chen, Y.; Jia, J.; Zhu, X.; He, Y.; Wu, L.M. MiR-27a promotes EMT in ovarian cancer through active Wnt/-catenin signalling by targeting FOXO1. *Cancer Biomark.* **2019**, *24*, 31–42, doi:10.3233/CBM-181229.

56. Li, N.; Yang, L.; Sun, Y.; Wu, X. MicroRNA-16 inhibits migration and invasion via regulation of the Wnt/beta-catenin signaling pathway in ovarian cancer. *Oncol. Lett.* **2019**, *17*, 2631–2638, doi:10.3892/ol.2019.9923.

57. Wang, Y.; Yang, X.; Yuan, M.; Xian, S.; Zhang, L.; Yang, D.; Cheng, Y. Promotion of ovarian cancer cell invasion, migration and colony formation by the miR21/Wnt/CD44v6 pathway. *Oncol. Rep.* **2019**, *42*, 91–102, doi:10.3892/or.2019.7153.

58. Majem, B.; Parrilla, A.; Jimenez, C.; Suarez-Cabrera, L.; Barber, M.; Marin, A.; Castellvi, J.; Tamayo, G.; Moreno-Bueno, G.; Ponce, J., et al. MicroRNA-654-5p suppresses ovarian cancer development impacting on MYC, WNT and AKT pathways. *Oncogene* **2019**, *38*, 6035–6050, doi:10.1038/s41388-019-0860-0.

59. Hu, J.; Zhao, W.; Huang, Y.; Wang, Z.; Jiang, T.; Wang, L. MiR-1180 from bone marrow MSCs promotes cell proliferation and glycolysis in ovarian cancer cells via SFRP1/Wnt pathway. *Cancer Cell Int.* **2019**, *19*, 66, doi:10.1186/s12935-019-0751-z.

60. Li, J.; Yang, S.; Su, N.; Wang, Y.; Yu, J.; Qiu, H.; He, X. Overexpression of long non-coding RNA HOTAIR leads to chemoresistance by activating the Wnt/beta-catenin pathway in human ovarian cancer. *Tumour Biol.* **2016**, *37*, 2057–2065, doi:10.1007/s13277-015-3998-6.

61. He, S.; Zhao, Y.; Wang, X.; Deng, Y.; Wan, Z.; Yao, S.; Shen, H. Up-regulation of long non-coding RNA SNHG20 promotes ovarian cancer progression via Wnt/beta-catenin signaling. *Biosci. Rep.* **2018**, *38*, doi:10.1042/BSR20170681.

62. Zhang, Y.; Dun, Y.; Zhou, S.; Huang, X.H. LncRNA HOXD-AS1 promotes epithelial ovarian cancer cells proliferation and invasion by targeting miR-133a-3p and activating Wnt/beta-catenin signaling pathway. *Biomed. Pharmacother.* **2017**, *96*, 1216–1221, doi:10.1016/j. biopha.2017.11.096.

63. Wang, B.; Liu, M.; Zhuang, R.; Jiang, J.; Gao, J.; Wang, H.; Chen, H.; Zhang, Z.; Kuang, Y.; Li, P. Long non-coding RNA CCAT2 promotes epithelial-mesenchymal transition involving Wnt/ beta-catenin pathway in epithelial ovarian carcinoma cells. *Oncol. Lett.* **2018**, *15*, 3369–3375, doi:10.3892/ol.2017.7669.

64. Guo, C.; Wang, X.; Chen, L.P.; Li, M.; Li, M.; Hu, Y.H.; Ding, W.H.; Wang, X. Long non-coding RNA MALAT1 regulates ovarian cancer cell proliferation, migration and apoptosis through Wnt/beta-catenin signaling pathway. *Eur. Rev. Med. Pharmacol. Sci.* **2018**, *22*, 3703–3712, doi:10.26355/ eurrev_201806_15249.

65. Yu, G.; Wang, W.; Deng, J.; Dong, S. LncRNA AWPPH promotes the proliferation, migration and invasion of ovarian carcinoma cells via activation of the Wnt/betacatenin signaling pathway. *Mol. Med. Rep.* **2019**, *19*, 3615–3621, doi:10.3892/mmr.2019.10029.

66. Saegusa, M.; Okayasu, I. Frequent nuclear beta-catenin accumulation and associated mutations in endometrioid-type endometrial and ovarian carcinomas with squamous differentiation. *J. Pathol.* **2001**, *194*, 59–67, doi:10.1002/path.856.

67. Moreno-Bueno, G.; Gamallo, C.; Perez-Gallego, L.; de Mora, J.C.; Suarez, A.; Palacios, J. beta-Catenin expression pattern, beta-catenin gene mutations, and microsatellite instability in endometrioid ovarian carcinomas and synchronous endometrial carcinomas. *Diagn. Mol. Pathol.* **2001**, *10*, 116–122.

68. Wright, K.; Wilson, P.; Morland, S.; Campbell, I.; Walsh, M.; Hurst, T.; Ward, B.; Cummings, M.; Chenevix-Trench, G. beta-catenin mutation and expression analysis in ovarian cancer: Exon 3 mutations and nuclear translocation in 16% of endometrioid tumours. *Int. J. Cancer* **1999**, *82*, 625–629, doi:10.1002/(sici)1097-0215(19990827)82:5<625::aid-ijc1>3.0.co;2-2.

69. Gamallo, C.; Palacios, J.; Moreno, G.; Calvo de Mora, J.; Suarez, A.; Armas, A. beta-catenin expression pattern in stage I and II ovarian carcinomas : Relationship with beta-catenin gene mutations, clinicopathological features, and clinical outcome. *Am. J. Pathol.* **1999**, *155*, 527–536, doi:10.1016/s0002-9440(10)65148-6.

70. Palacios, J.; Gamallo, C. Mutations in the beta-catenin gene (CTNNB1) in endometrioid ovarian carcinomas. *Cancer Res.* **1998**, *58*, 1344–1347.

71. Zhuang, X.H.; Liu, Y.; Li, J.L. Overexpression of long noncoding RNA HOXB-AS3 indicates an unfavorable prognosis and promotes tumorigenesis in epithelial ovarian cancer via Wnt/beta-catenin signaling pathway. *Biosci. Rep.* **2019**, *39*, doi:10.1042/BSR20190906.

72. Ricken, A.; Lochhead, P.; Kontogiannea, M.; Farookhi, R. Wnt signaling in the ovary: Identification and compartmentalized expression of wnt-2, wnt-2b, and frizzled-4 mRNAs. *Endocrinology* **2002**, *143*, 2741–2749, doi:10.1210/endo.143.7.8908.

73. Tothill, R.W.; Tinker, A.V.; George, J.; Brown, R.; Fox, S.B.; Lade, S.; Johnson, D.S.; Trivett, M.K.; Etemadmoghadam, D.; Locandro, B., et al. Novel molecular subtypes of serous and endometrioid ovarian cancer linked to clinical outcome. *Clin. Cancer Res.* **2008**, *14*, 5198–5208, doi:10.1158/1078-0432.CCR-08-0196.

74. Badiglian Filho, L.; Oshima, C.T.; De Oliveira Lima, F.; De Oliveira Costa, H.; De Sousa Damiao, R.; Gomes, T.S.; Goncalves, W.J. Canonical and noncanonical Wnt pathway: A comparison among normal ovary, benign ovarian tumor and ovarian cancer. *Oncol. Rep.* **2009**, *21*, 313–320.

Chapter 5

75. Popadiuk, C.M.; Xiong, J.; Wells, M.G.; Andrews, P.G.; Dankwa, K.; Hirasawa, K.; Lake, B.B.; Kao, K.R. Antisense suppression of pygopus2 results in growth arrest of epithelial ovarian cancer. *Clin. Cancer Res.* **2006**, *12*, 2216–2223, doi:10.1158/1078-0432.CCR-05-2433.

76. Duan, H.; Yan, Z.; Chen, W.; Wu, Y.; Han, J.; Guo, H.; Qiao, J. TET1 inhibits EMT of ovarian cancer cells through activating Wnt/beta-catenin signaling inhibitors DKK1 and SFRP2. *Gynecol Oncol* **2017**, *147*, 408–417, doi:10.1016/j.ygyno.2017.08.010.

77. Gray, J.W.; Suzuki, S.; Kuo, W.L.; Polikoff, D.; Deavers, M.; Smith-McCune, K.; Berchuck, A.; Pinkel, D.; Albertson, D.; Mills, G.B. Specific keynote: Genome copy number abnormalities in ovarian cancer. *Gynecol. Oncol.* **2003**, *88*, S16–S21. discussion S22-14.

78. Takada, T.; Yagi, Y.; Maekita, T.; Imura, M.; Nakagawa, S.; Tsao, S.W.; Miyamoto, K.; Yoshino, O.; Yasugi, T.; Taketani, Y., et al. Methylation-associated silencing of the Wnt antagonist SFRP1 gene in human ovarian cancers. *Cancer Sci.* **2004**, *95*, 741–744, doi:10.1111/j.1349-7006.2004.tb03255.x.

79. Matte, I.; Lane, D.; Laplante, C.; Rancourt, C.; Piche, A. Profiling of cytokines in human epithelial ovarian cancer ascites. *Am. J. Cancer Res.* **2012**, *2*, 566–580.

80. Thibault, B.; Castells, M.; Delord, J.P.; Couderc, B. Ovarian cancer microenvironment: Implications for cancer dissemination and chemoresistance acquisition. *Cancer Metastasis Rev.* **2014**, *33*, 17–39, doi:10.1007/s10555-013-9456-2.

81. Endo, H.; Hosono, K.; Uchiyama, T.; Sakai, E.; Sugiyama, M.; Takahashi, H.; Nakajima, N.; Wada, K.; Takeda, K.; Nakagama, H., et al. Leptin acts as a growth factor for colorectal tumours at stages subsequent to tumour initiation in murine colon carcinogenesis. *Gut* **2011**, *60*, 1363–1371, doi:10.1136/gut.2010.235754.

82. Yan, D.; Avtanski, D.; Saxena, N.K.; Sharma, D. Leptin-induced epithelial-mesenchymal transition in breast cancer cells requires beta-catenin activation via Akt/GSK3- and MTA1/Wnt1 protein-dependent pathways. *J. Biol. Chem.* **2012**, *287*, 8598–8612, doi:10.1074/jbc.M111.322800.

83. Asuthkar, S.; Gondi, C.S.; Nalla, A.K.; Velpula, K.K.; Gorantla, B.; Rao, J.S. Urokinase-type plasminogen activator receptor (uPAR)-mediated regulation of WNT/beta-catenin signaling is enhanced in irradiated medulloblastoma cells. *J. Biol. Chem.* **2012**, *287*, 20576–20589, doi:10.1074/jbc.M112.348888.

84. Zhang, X.; Chen, L.; Wang, Y.; Ding, Y.; Peng, Z.; Duan, L.; Ju, G.; Ren, Y.; Wang, X. Macrophage migration inhibitory factor promotes proliferation and neuronal differentiation of neural stem/precursor cells through Wnt/beta-catenin signal pathway. *Int. J. Biol. Sci.* **2013**, *9*, 1108–1120, doi:10.7150/ijbs.7232.

85. Glass, D.A., 2nd; Bialek, P.; Ahn, J.D.; Starbuck, M.; Patel, M.S.; Clevers, H.; Taketo, M.M.; Long, F.; McMahon, A.P.; Lang, R.A., et al. Canonical Wnt signaling in differentiated osteoblasts controls osteoclast differentiation. *Dev. Cell* **2005**, *8*, 751–764, doi:10.1016/j.devcel.2005.02.017.

86. Masckauchan, T.N.; Shawber, C.J.; Funahashi, Y.; Li, C.M.; Kitajewski, J. Wnt/beta-catenin signaling induces proliferation, survival and interleukin-8 in human endothelial cells. *Angiogenesis* **2005**, *8*, 43–51, doi:10.1007/s10456-005-5612-9.

87. Burkhalter, R.J.; Symowicz, J.; Hudson, L.G.; Gottardi, C.J.; Stack, M.S. Integrin regulation of beta-catenin signaling in ovarian carcinoma. *J Biol Chem* **2011**, *286*, 23467–23475, doi:10.1074/jbc.M110.199539.

88. Gross, J.C.; Chaudhary, V.; Bartscherer, K.; Boutros, M. Active Wnt proteins are secreted on exosomes. *Nat Cell Biol.* **2012**, *14*, 1036–1045, doi:10.1038/ncb2574.

89. Beach, A.; Zhang, H.G.; Ratajczak, M.Z.; Kakar, S.S. Exosomes: An overview of biogenesis, composition and role in ovarian cancer. *J. Ovarian Res.* **2014**, *7*, 14, doi:10.1186/1757-2215-7-14.

90. Latifi, A.; Abubaker, K.; Castrechini, N.; Ward, A.C.; Liongue, C.; Dobill, F.; Kumar, J.; Thompson, E.W.; Quinn, M.A.; Findlay, J.K., et al. Cisplatin treatment of primary and metastatic epithelial ovarian carcinomas generates residual cells with mesenchymal stem cell-like profile. *J. Cell Biochem.* **2011**, *112*, 2850–2864, doi:10.1002/jcb.23199.

91. Bapat, S.A.; Mali, A.M.; Koppikar, C.B.; Kurrey, N.K. Stem and progenitor-like cells contribute to the aggressive behavior of human epithelial ovarian cancer. *Cancer Res.* **2005**, *65*, 3025–3029, doi:10.1158/0008-5472.CAN-04-3931.

92. Raghavan, S.; Mehta, P.; Xie, Y.; Lei, Y.L.; Mehta, G. Ovarian cancer stem cells and macrophages reciprocally interact through the WNT pathway to promote pro-tumoral and malignant phenotypes in 3D engineered microenvironments. *J. Immunother. Cancer* **2019**, *7*, 190, doi:10.1186/s40425-019-0666-1.

93. Ruan, X.; Liu, A.; Zhong, M.; Wei, J.; Zhang, W.; Rong, Y.; Liu, W.; Li, M.; Qing, X.; Chen, G., et al. Silencing LGR6 Attenuates Stemness and Chemoresistance via Inhibiting Wnt/beta-Catenin Signaling in Ovarian Cancer. *Mol. Ther. Oncolytics* **2019**, *14*, 94–106, doi:10.1016/j.omto.2019.04.002.

94. Ahmed, N.; Stenvers, K.L. Getting to know ovarian cancer ascites: Opportunities for targeted therapy-based translational research. *Front Oncol* **2013**, *3*, 256, doi:10.3389/fonc.2013.00256.

95. Mills, G.B.; May, C.; Hill, M.; Campbell, S.; Shaw, P.; Marks, A. Ascitic fluid from human ovarian cancer patients contains growth factors necessary for intraperitoneal growth of human ovarian adenocarcinoma cells. *J. Clin. Invest.* **1990**, *86*, 851–855, doi:10.1172/JCI114784.

96. Burleson, K.M.; Casey, R.C.; Skubitz, K.M.; Pambuccian, S.E.; Oegema, T.R., Jr.; Skubitz, A.P. Ovarian carcinoma ascites spheroids adhere to extracellular matrix components and mesothelial cell monolayers. *Gynecol. Oncol.* **2004**, *93*, 170–181, doi:10.1016/j.ygyno.2003.12.034.

97. Shield, K.; Ackland, M.L.; Ahmed, N.; Rice, G.E. Multicellular spheroids in ovarian cancer metastases: Biology and pathology. *Gynecol. Oncol.* **2009**, *113*, 143–148, doi:10.1016/j.ygyno.2008.11.032.

98. Naora, H.; Montell, D.J. Ovarian cancer metastasis: Integrating insights from disparate model organisms. *Nat. Rev. Cancer* **2005**, *5*, 355–366, doi:10.1038/nrc1611.

99. Loret, N.; Denys, H.; Tummers, P.; Berx, G. The Role of Epithelial-to-Mesenchymal Plasticity in Ovarian Cancer Progression and Therapy Resistance. *Cancers (Basel)* **2019**, *11*, doi:10.3390/cancers11060838.

100. Pradeep, S.; Kim, S.W.; Wu, S.Y.; Nishimura, M.; Chaluvally-Raghavan, P.; Miyake, T.; Pecot, C.V.; Kim, S.J.; Choi, H.J.; Bischoff, F.Z., et al. Hematogenous metastasis of ovarian cancer: Rethinking mode of spread. *Cancer Cell* **2014**, *26*, 77–91, doi:10.1016/j.ccr.2014.05.002.

101. Kuhlmann, J.D.; Wimberger, P.; Bankfalvi, A.; Keller, T.; Scholer, S.; Aktas, B.; Buderath, P.; Hauch, S.; Otterbach, F.; Kimmig, R., et al. ERCC1-positive circulating tumor cells in the blood of ovarian cancer patients as a predictive biomarker for platinum resistance. *Clin. Chem.* **2014**, *60*, 1282–1289, doi:10.1373/clinchem.2014.224808.

102. Nieto, M.A.; Huang, R.Y.; Jackson, R.A.; Thiery, J.P. Emt: 2016. *Cell* **2016**, *166*, 21–45.

103. Dongre, A.; Rashidian, M.; Reinhardt, F.; Bagnato, A.; Keckesova, Z.; Ploegh, H.L.; Weinberg, R.A. Epithelial-to-Mesenchymal Transition Contributes to Immunosuppression in Breast Carcinomas. *Cancer Res.* **2017**, *77*, 3982–3989.

104. Mani, S.A.; Guo, W.; Liao, M.J.; Eaton, E.N.; Ayyanan, A.; Zhou, A.Y.; Brooks, M.; Reinhard, F.; Zhang, C.C.; Shipitsin, M., et al. The epithelial-mesenchymal transition generates cells with properties of stem cells. *Cell* **2008**, *133*, 704–715.

Chapter 5

105. Smith, B.N.; Bhowmick, N.A. Role of EMT in Metastasis and Therapy Resistance. *J. Clin. Med.* **2016**, *5*, doi:10.3390/jcm5020017.

106. Brabletz, T.; Jung, A.; Spaderna, S.; Hlubek, F.; Kirchner, T. Opinion: Migrating cancer stem cells - an integrated concept of malignant tumour progression. *Nat. Rev. Cancer* **2005**, *5*, 744–749.

107. Wu, Z.Q.; Li, X.Y.; Hu, C.Y.; Ford, M.; Kleer, C.G.; Weiss, S.J. Canonical Wnt signaling regulates Slug activity and links epithelial-mesenchymal transition with epigenetic Breast Cancer 1, Early Onset (BRCA1) repression. *Proc. Natl. Acad. Sci. U S A* **2012**, *109*, 16654–16659.

108. Yook, J.I.; Li, X.Y.; Ota, I.; Fearon, E.R.; Weiss, S.J. Wnt-dependent regulation of the E-cadherin repressor snail. *J. Biol. Chem.* **2005**, *280*, 11740–11748.

109. Bernaudo, S.; Salem, M.; Qi, X.; Zhou, W.; Zhang, C.; Yang, W.; Rosman, D.; Deng, Z.; Ye, G.; Yang, B.B., et al. Cyclin G2 inhibits epithelial-to-mesenchymal transition by disrupting Wnt/beta-catenin signaling. *Oncogene* **2016**, *35*, 4816–4827, doi:10.1038/onc.2016.15.

110. Deng, Z.; Wang, L.; Hou, H.; Zhou, J.; Li, X. Epigenetic regulation of IQGAP2 promotes ovarian cancer progression via activating Wnt/beta-catenin signaling. *Int. J. Oncol.* **2016**, *48*, 153–160, doi:10.3892/ijo.2015.3228.

111. Hojo, N.; Huisken, A.L.; Wang, H.; Chirshev, E.; Kim, N.S.; Nguyen, S.M.; Campos, H.; Glackin, C.A.; Ioffe, Y.J.; Unternaehrer, J.J. Snail knockdown reverses stemness and inhibits tumour growth in ovarian cancer. *Sci. Rep.* **2018**, *8*, 8704, doi:10.1038/s41598-018-27021-z.

112. Sun, J.; Yang, X.; Zhang, R.; Liu, S.; Gan, X.; Xi, X.; Zhang, Z.; Feng, Y.; Sun, Y. GOLPH3 induces epithelial-mesenchymal transition via Wnt/beta-catenin signaling pathway in epithelial ovarian cancer. *Cancer Med.* **2017**, *6*, 834–844, doi:10.1002/cam4.1040.

113. Aiello, N.M.; Maddipati, R.; Norgard, R.J.; Balli, D.; Li, J.; Yuan, S.; Yamazoe, T.; Black, T.; Sahmoud, A.; Furth, E.E., et al. EMT Subtype Influences Epithelial Plasticity and Mode of Cell Migration. *Dev. Cell* **2018**, *45*, 681–695 e684.

114. Pastushenko, I.; Brisebarre, A.; Sifrim, A.; Fioramonti, M.; Revenco, T.; Boumahdi, S.; Van Keymeulen, A.; Brown, D.; Moers, V.; Lemaire, S., et al. Identification of the tumour transition states occurring during EMT. *Nature* **2018**, *556*, 463–468.

115. Hudson, L.G.; Zeineldin, R.; Stack, M.S. Phenotypic plasticity of neoplastic ovarian epithelium: Unique cadherin profiles in tumor progression. *Clin. Exp. Metastasis* **2008**, *25*, 643–655, doi:10.1007/s10585-008-9171-5.

116. Huang, R.Y.; Wong, M.K.; Tan, T.Z.; Kuay, K.T.; Ng, A.H.; Chung, V.Y.; Chu, Y.S.; Matsumura, N.; Lai, H.C.; Lee, Y.F., et al. An EMT spectrum defines an anoikis-resistant and spheroidogenic intermediate mesenchymal state that is sensitive to e-cadherin restoration by a src-kinase inhibitor, saracatinib (AZD0530). *Cell Death Dis.* **2013**, *4*, e915, doi:10.1038/cddis.2013.442.

117. Klymenko, Y.; Johnson, J.; Bos, B.; Lombard, R.; Campbell, L.; Loughran, E.; Stack, M.S. Heterogeneous Cadherin Expression and Multicellular Aggregate Dynamics in Ovarian Cancer Dissemination. *Neoplasia* **2017**, *19*, 549–563, doi:10.1016/j.neo.2017.04.002.

118. Strauss, R.; Li, Z.Y.; Liu, Y.; Beyer, I.; Persson, J.; Sova, P.; Moller, T.; Pesonen, S.; Hemminki, A.; Hamerlik, P., et al. Analysis of epithelial and mesenchymal markers in ovarian cancer reveals phenotypic heterogeneity and plasticity. *PLoS One* **2011**, *6*, e16186, doi:10.1371/journal.pone.0016186.

119. Chikazawa, N.; Tanaka, H.; Tasaka, T.; Nakamura, M.; Tanaka, M.; Onishi, H.; Katano, M. Inhibition of Wnt signaling pathway decreases chemotherapy-resistant side-population colon cancer cells. *Anticancer Res.* **2010**, *30*, 2041–2048.

120. Zheng, H.C. The molecular mechanisms of chemoresistance in cancers. *Oncotarget* **2017**, *8*, 59950–59964, doi:10.18632/oncotarget.19048.

121. Eyre, R.; Harvey, I.; Stemke-Hale, K.; Lennard, T.W.; Tyson-Capper, A.; Meeson, A.P. Reversing paclitaxel resistance in ovarian cancer cells via inhibition of the ABCB1 expressing side population. *Tumour Biol.* **2014**, *35*, 9879–9892, doi:10.1007/s13277-014-2277-2.

122. Hu, L.; McArthur, C.; Jaffe, R.B. Ovarian cancer stem-like side-population cells are tumourigenic and chemoresistant. *Br. J. Cancer* **2010**, *102*, 1276–1283, doi:10.1038/sj.bjc.6605626.

123. Su, H.Y.; Lai, H.C.; Lin, Y.W.; Liu, C.Y.; Chen, C.K.; Chou, Y.C.; Lin, S.P.; Lin, W.C.; Lee, H.Y.; Yu, M.H. Epigenetic silencing of SFRP5 is related to malignant phenotype and chemoresistance of ovarian cancer through Wnt signaling pathway. *Int. J. Cancer* **2010**, *127*, 555–567, doi:10.1002/ijc.25083.

124. Zhang, B.; Chen, F.; Xu, Q.; Han, L.; Xu, J.; Gao, L.; Sun, X.; Li, Y.; Li, Y.; Qian, M., et al. Revisiting ovarian cancer microenvironment: A friend or a foe? *Protein Cell* **2018**, *9*, 674–692, doi:10.1007/s13238-017-0466-7.

125. Shiga, K.; Hara, M.; Nagasaki, T.; Sato, T.; Takahashi, H.; Takeyama, H. Cancer-Associated Fibroblasts: Their Characteristics and Their Roles in Tumor Growth. *Cancers (Basel)* **2015**, *7*, 2443–2458, doi:10.3390/cancers7040902.

126. Ferrari, N.; Ranftl, R.; Chicherova, I.; Slaven, N.D.; Moeendarbary, E.; Farrugia, A.J.; Lam, M.; Semiannikova, M.; Westergaard, M.C.W.; Tchou, J., et al. Dickkopf-3 links HSF1 and YAP/TAZ signalling to control aggressive behaviours in cancer-associated fibroblasts. *Nat. Commun.* **2019**, *10*, 130, doi:10.1038/s41467-018-07987-0.

127. Armstrong, D.K.; Bundy, B.; Wenzel, L.; Huang, H.Q.; Baergen, R.; Lele, S.; Copeland, L.J.; Walker, J.L.; Burger, R.A.; Gynecologic Oncology, G. Intraperitoneal cisplatin and paclitaxel in ovarian cancer. *N Engl. J. Med.* **2006**, *354*, 34–43, doi:10.1056/NEJMoa052985.

128. Burger, R.A.; Brady, M.F.; Bookman, M.A.; Fleming, G.F.; Monk, B.J.; Huang, H.; Mannel, R.S.; Homesley, H.D.; Fowler, J.; Greer, B.E., et al. Incorporation of bevacizumab in the primary treatment of ovarian cancer. *N Engl. J. Med.* **2011**, *365*, 2473–2483, doi:10.1056/NEJMoa1104390.

129. Katsumata, N.; Yasuda, M.; Takahashi, F.; Isonishi, S.; Jobo, T.; Aoki, D.; Tsuda, H.; Sugiyama, T.; Kodama, S.; Kimura, E., et al. Dose-dense paclitaxel once a week in combination with carboplatin every 3 weeks for advanced ovarian cancer: A phase 3, open-label, randomised controlled trial. *Lancet* **2009**, *374*, 1331–1338, doi:10.1016/S0140-6736(09)61157-0.

130. Saha, S.; Aranda, E.; Hayakawa, Y.; Bhanja, P.; Atay, S.; Brodin, N.P.; Li, J.; Asfaha, S.; Liu, L.; Tailor, Y., et al. Macrophage-derived extracellular vesicle-packaged WNTs rescue intestinal stem cells and enhance survival after radiation injury. *Nat. Commun.* **2016**, *7*, 13096, doi:10.1038/ncomms13096.

131. Azmi, A.S.; Bao, B.; Sarkar, F.H. Exosomes in cancer development, metastasis, and drug resistance: A comprehensive review. *Cancer Metastasis Rev.* **2013**, *32*, 623–642, doi:10.1007/s10555-013-9441-9.

132. Keller, S.; Konig, A.K.; Marme, F.; Runz, S.; Wolterink, S.; Koensgen, D.; Mustea, A.; Sehouli, J.; Altevogt, P. Systemic presence and tumor-growth promoting effect of ovarian carcinoma released exosomes. *Cancer Lett.* **2009**, *278*, 73–81, doi:10.1016/j.canlet.2008.12.028.

133. Liang, B.; Peng, P.; Chen, S.; Li, L.; Zhang, M.; Cao, D.; Yang, J.; Li, H.; Gui, T.; Li, X., et al. Characterization and proteomic analysis of ovarian cancer-derived exosomes. *J. Proteomics* **2013**, *80*, 171–182, doi:10.1016/j.jprot.2012.12.029.

134. Runz, S.; Keller, S.; Rupp, C.; Stoeck, A.; Issa, Y.; Koensgen, D.; Mustea, A.; Sehouli, J.; Kristiansen, G.; Altevogt, P. Malignant ascites-derived exosomes of ovarian carcinoma patients contain CD24 and EpCAM. *Gynecol. Oncol.* **2007**, *107*, 563–571, doi:10.1016/j.ygyno.2007.08.064.

Chapter 5

135. Taylor, D.D.; Gercel-Taylor, C. MicroRNA signatures of tumor-derived exosomes as diagnostic biomarkers of ovarian cancer. *Gynecol. Oncol.* **2008**, *110*, 13–21, doi:10.1016/j.ygyno.2008.04.033.

136. Luga, V.; Zhang, L.; Viloria-Petit, A.M.; Ogunjimi, A.A.; Inanlou, M.R.; Chiu, E.; Buchanan, M.; Hosein, A.N.; Basik, M.; Wrana, J.L. Exosomes mediate stromal mobilization of autocrine Wnt-PCP signaling in breast cancer cell migration. *Cell* **2012**, *151*, 1542–1556, doi:10.1016/j.cell.2012.11.024.

137. Hu, Y.B.; Yan, C.; Mu, L.; Mi, Y.L.; Zhao, H.; Hu, H.; Li, X.L.; Tao, D.D.; Wu, Y.Q.; Gong, J.P., et al. Exosomal Wnt-induced dedifferentiation of colorectal cancer cells contributes to chemotherapy resistance. *Oncogene* **2019**, *38*, 1951–1965, doi:10.1038/s41388-018-0557-9.

138. Dovrat, S.; Caspi, M.; Zilberberg, A.; Lahav, L.; Firsow, A.; Gur, H.; Rosin-Arbesfeld, R. 14-3-3 and beta-catenin are secreted on extracellular vesicles to activate the oncogenic Wnt pathway. *Mol. Oncol.* **2014**, *8*, 894–911, doi:10.1016/j.molonc.2014.03.011.

139. Zhang, S.; Zhang, X.; Fu, X.; Li, W.; Xing, S.; Yang, Y. Identification of common differentially-expressed miRNAs in ovarian cancer cells and their exosomes compared with normal ovarian surface epithelial cell cells. *Oncol. Lett.* **2018**, *16*, 2391–2401, doi:10.3892/ol.2018.8954.

140. Alharbi, M.; Lai, A.; Guanzon, D.; Palma, C.; Zuniga, F.; Perrin, L.; He, Y.; Hooper, J.D.; Salomon, C. Ovarian cancer-derived exosomes promote tumour metastasis in vivo: An effect modulated by the invasiveness capacity of their originating cells. *Clin. Sci. (Lond)* **2019**, *133*, 1401–1419, doi:10.1042/CS20190082.

141. Nakamura, K.; Sawada, K.; Kinose, Y.; Yoshimura, A.; Toda, A.; Nakatsuka, E.; Hashimoto, K.; Mabuchi, S.; Morishige, K.I.; Kurachi, H., et al. Exosomes Promote Ovarian Cancer Cell Invasion through Transfer of CD44 to Peritoneal Mesothelial Cells. *Mol. Cancer Res.* **2017**, *15*, 78–92, doi:10.1158/1541-7786.MCR-16-0191.

142. Liu, Y.; Cao, X. Characteristics and Significance of the Pre-metastatic Niche. *Cancer Cell* **2016**, *30*, 668–681.

143. Lee, W.; Ko, S.Y.; Mohamed, M.S.; Kenny, H.A.; Lengyel, E.; Naora, H. Neutrophils facilitate ovarian cancer premetastatic niche formation in the omentum. *J. Exp. Med.* **2019**, *216*, 176–194, doi:10.1084/jem.20181170.

144. Yokoi, A.; Yoshioka, Y.; Yamamoto, Y.; Ishikawa, M.; Ikeda, S.I.; Kato, T.; Kiyono, T.; Takeshita, F.; Kajiyama, H.; Kikkawa, F., et al. Malignant extracellular vesicles carrying MMP1 mRNA facilitate peritoneal dissemination in ovarian cancer. *Nat. Commun.* **2017**, *8*, 14470, doi:10.1038/ncomms14470.

145. Wielenga, V.J.; Smits, R.; Korinek, V.; Smit, L.; Kielman, M.; Fodde, R.; Clevers, H.; Pals, S.T. Expression of CD44 in Apc and Tcf mutant mice implies regulation by the WNT pathway. *Am. J. Pathol.* **1999**, *154*, 515–523, doi:10.1016/S0002-9440(10)65297-2.

146. Schmitt, M.; Metzger, M.; Gradl, D.; Davidson, G.; Orian-Rousseau, V. CD44 functions in Wnt signaling by regulating LRP6 localization and activation. *Cell Death Differ.* **2015**, *22*, 677–689, doi:10.1038/cdd.2014.156.

147. de la Fuente, A.; Alonso-Alconada, L.; Costa, C.; Cueva, J.; Garcia-Caballero, T.; Lopez-Lopez, R.; Abal, M. M-Trap: Exosome-Based Capture of Tumor Cells as a New Technology in Peritoneal Metastasis. *J. Natl. Cancer Inst.* **2015**, *107*, doi:10.1093/jnci/djv184.

148. de Lau, W.B.; Snel, B.; Clevers, H.C. The R-spondin protein family. *Genome Biol.* **2012**, *13*, 242, doi:10.1186/gb-2012-13-3-242.

149. Chartier, C.; Raval, J.; Axelrod, F.; Bond, C.; Cain, J.; Dee-Hoskins, C.; Ma, S.; Fischer, M.M.; Shah, J.; Wei, J., et al. Therapeutic Targeting of Tumor-Derived R-Spondin Attenuates beta-Catenin Signaling and Tumorigenesis in Multiple Cancer Types. *Cancer Res.* **2016**, *76*, 713–723, doi:10.1158/0008-5472.CAN-15-0561.

150. Boone, J.D.; Arend, R.C.; Johnston, B.E.; Cooper, S.J.; Gilchrist, S.A.; Oelschlager, D.K.; Grizzle, W.E.; McGwin, G., Jr.; Gangrade, A.; Straughn, J.M., Jr., et al. Targeting the Wnt/beta-catenin pathway in primary ovarian cancer with the porcupine inhibitor WNT974. *Lab. Invest.* **2016**, *96*, 249–259, doi:10.1038/labinvest.2015.150.

151. Yo, Y.T.; Lin, Y.W.; Wang, Y.C.; Balch, C.; Huang, R.L.; Chan, M.W.; Sytwu, H.K.; Chen, C.K.; Chang, C.C.; Nephew, K.P., et al. Growth inhibition of ovarian tumor-initiating cells by niclosamide. *Mol. Cancer Ther.* **2012**, *11*, 1703–1712, doi:10.1158/1535-7163.MCT-12-0002.

152. Li, Y.; Li, P.K.; Roberts, M.J.; Arend, R.C.; Samant, R.S.; Buchsbaum, D.J. Multi-targeted therapy of cancer by niclosamide: A new application for an old drug. *Cancer Lett.* **2014**, *349*, 8–14, doi:10.1016/j.canlet.2014.04.003.

153. Yang, K.; Wang, X.; Zhang, H.; Wang, Z.; Nan, G.; Li, Y.; Zhang, F.; Mohammed, M.K.; Haydon, R.C.; Luu, H.H., et al. The evolving roles of canonical WNT signaling in stem cells and tumorigenesis: Implications in targeted cancer therapies. *Lab. Invest.* **2016**, *96*, 116–136, doi:10.1038/labinvest.2015.144.

154. Moore, K.N.; Gunderson, C.C.; Sabbatini, P.; McMeekin, D.S.; Mantia-Smaldone, G.; Burger, R.A.; Morgan, M.A.; Kapoun, A.M.; Brachmann, R.K.; Stagg, R., et al. A phase 1b dose escalation study of ipafricept (OMP54F28) in combination with paclitaxel and carboplatin in patients with recurrent platinum-sensitive ovarian cancer. *Gynecol. Oncol.* **2019**, *154*, 294–301, doi:10.1016/j.ygyno.2019.04.001.

155. Harb, J.; Lin, P.J.; Hao, J. Recent Development of Wnt Signaling Pathway Inhibitors for Cancer Therapeutics. *Curr. Oncol. Rep.* **2019**, *21*, 12, doi:10.1007/s11912-019-0763-9.

156. Li, R.; Dong, T.; Hu, C.; Lu, J.; Dai, J.; Liu, P. Salinomycin repressed the epithelial-mesenchymal transition of epithelial ovarian cancer cells via downregulating Wnt/beta-catenin pathway. *Onco. Targets Ther.* **2017**, *10*, 1317–1325, doi:10.2147/OTT.S126463.

157. Baryawno, N.; Sveinbjornsson, B.; Eksborg, S.; Chen, C.S.; Kogner, P.; Johnsen, J.I. Small-molecule inhibitors of phosphatidylinositol 3-kinase/Akt signaling inhibit Wnt/beta-catenin pathway cross-talk and suppress medulloblastoma growth. *Cancer Res.* **2010**, *70*, 266–276, doi:10.1158/0008-5472.CAN-09-0578.

158. Zhang, K.; Song, H.; Yang, P.; Dai, X.; Li, Y.; Wang, L.; Du, J.; Pan, K.; Zhang, T. Silencing dishevelled-1 sensitizes paclitaxel-resistant human ovarian cancer cells via AKT/GSK-3beta/beta-catenin signalling. *Cell Prolif.* **2015**, *48*, 249–258, doi:10.1111/cpr.12161.

159. Zhang, C.; Zhang, Z.; Zhang, S.; Wang, W.; Hu, P. Targeting of Wnt/beta-Catenin by Anthelmintic Drug Pyrvinium Enhances Sensitivity of Ovarian Cancer Cells to Chemotherapy. *Med. Sci. Monit.* **2017**, *23*, 266–275, doi:10.12659/msm.901667.

160. Thorne, C.A.; Hanson, A.J.; Schneider, J.; Tahinci, E.; Orton, D.; Cselenyi, C.S.; Jernigan, K.K.; Meyers, K.C.; Hang, B.I.; Waterson, A.G., et al. Small-molecule inhibition of Wnt signaling through activation of casein kinase 1alpha. *Nat. Chem. Biol.* **2010**, *6*, 829–836, doi:10.1038/nchembio.453.

161. Arend, R.C.; Londono-Joshi, A.I.; Gangrade, A.; Katre, A.A.; Kurpad, C.; Li, Y.; Samant, R.S.; Li, P.K.; Landen, C.N.; Yang, E.S., et al. Niclosamide and its analogs are potent inhibitors of Wnt/beta-catenin, mTOR and STAT3 signaling in ovarian cancer. *Oncotarget* **2016**, *7*, 86803–86815, doi:10.18632/oncotarget.13466.

Chapter 5

162. Arend, R.C.; Londono-Joshi, A.I.; Samant, R.S.; Li, Y.; Conner, M.; Hidalgo, B.; Alvarez, R.D.; Landen, C.N.; Straughn, J.M.; Buchsbaum, D.J. Inhibition of Wnt/beta-catenin pathway by niclosamide: A therapeutic target for ovarian cancer. *Gynecol. Oncol.* **2014**, *134*, 112–120, doi:10.1016/j.ygyno.2014.04.005.

163. King, M.L.; Lindberg, M.E.; Stodden, G.R.; Okuda, H.; Ebers, S.D.; Johnson, A.; Montag, A.; Lengyel, E.; MacLean Ii, J.A.; Hayashi, K. WNT7A/beta-catenin signaling induces FGF1 and influences sensitivity to niclosamide in ovarian cancer. *Oncogene* **2015**, *34*, 3452–3462, doi:10.1038/onc.2014.277.

164. Barnard, M.E.; Poole, E.M.; Curhan, G.C.; Eliassen, A.H.; Rosner, B.A.; Terry, K.L.; Tworoger, S.S. Association of Analgesic Use With Risk of Ovarian Cancer in the Nurses' Health Studies. *JAMA Oncol.* **2018**, *4*, 1675–1682, doi:10.1001/jamaoncol.2018.4149.

CHAPTER VI

RNAseq analysis of epithelial and quasi-mesenchymal cells in ovarian cancer

Teeuwssen M.J., Verhagen M., Joosten R., Saccetti A., and Fodde R.

Abstract

Recently, we identified a subpolulation of quasi-mesenchymal (EpCAM^{lo}) colon cancer cells endowed with phenotypic plasticity, i.e. the capacity to transiently and reversibly alter their morphological and functional features along the invasion-metastasis cascade. Accordingly, these cells are highly invasive and metastatic both *in vitro* and *in vivo* and their expression signatures are predictive of reduced disease-free survival among colon cancer patients.

Here, we show that a similar dichotomy between epithelial and quasi-mesenchymal subpopulations of cancer cells exists in ovarian cancer. As shown by RT-qPCR and RNAseq analysis of EpCAM$^{hi/lo}$ subpopulations sorted by FACS from ovarian cancer cell lines, EpCAM^{lo} cells are earmarked by increased expression of the EMT transcription factor *ZEB1*, and the consequent up- and down-regulation of mesenchymal and epithelial markers, respectively. Moreover, they are resistant to cytotoxic drugs commonly employed in the treatment of ovarian cancer, such as cisplatin and paclitaxel. Accordingly, patients with ovarian cancers characterized by increased *ZEB1* expression are usually associated with worse progression-free and overall survival. However, intratumor heterogeneity still represents a major obstacle in the positive identification of subpopulations of quasi-mesenchymal ovarian cancer cells in patient-derived material. By taking advantage of an EMT signature derived from the RNAseq data we here showed the presence of quasi-mesenchymal cells in ovarian cancer tumors.

Keywords: ovarian cancer, EMT, ZEB1

Abstract

Introduction

High grade serous (HGS) ovarian cancers feature a metastatic spread pattern characterized by direct extension to adjacent organs, via lymphatics, and by dissemination of clonogenic cancer cells into the peritoneal cavity [1,2]. Blood-born metastases are less common [3]. After diagnosis, tumor debulking surgery followed by carboplatin- and paclitaxel-based chemotherapy represent the standard first line therapy for HGS ovarian cancer patients. Although at this stage the primary response to chemotherapy is extremely efficient, most patients relapse and develop metastases locally and at distant organ sites [4]. This is mainly due to sub-populations of tumor cells likely to have acquired stem cell features (CSCs) through epithelial-mesenchymal transition (EMT) and, consequently, the EMT-associated chemo-resistance [5].

EMT is a developmental program exploited by malignant cells to reversibly shift from an epithelial state with apical-basal polarity and pronounced cell–cell adhesions, to a more motile mesenchymal phenotype with spindle-like morphology and front-back-end polarity [6]. In addition to the motile and invasive characteristics of the mesenchymal state, EMT is functionally linked to the acquirement of stem-like features, resistance to therapy, and immune suppression [7-9]. The reversible nature of EMT is crucial as mesenchymal-to-epithelial transitions (MET) allow metastasizing cancer (stem-like) cells to regain proliferative and epithelial characteristics essential to colonize distant organ sites [6,10].

Recently, we reported on the identification and extensive functional characterization of a subpolulation of quasi-mesenchymal (EpCAM^{lo}) colon cancer cells endowed with phenotypic plasticity, e.g. the cell's capacity to transiently and reversibly alter its morphological and functional features along the invasion-metastasis cascade [11]. Expression of a EpCAM^{lo}-specific signature is indicative of the presence of these cells in patient-derived tumors, where they are usually found along the invasion front, and is predictive of reduced disease-free survival in colon cancer. Here, we show that, similar to colon cancer, HGS ovarian cancer encompass a EpCAM^{lo} subpopulation. Ovarian EpCAM^{lo} cancer cells show increased motility and resistance to chemotherapy. Expression of the EMT transcription factor *ZEB1* underlies the quasi-mesenchymal phenotype of EpCAM^{lo} ovarian cancer cells. Of note, comparison of the genome-wide expression profiles between ovarian and colon EpCAM^{lo} cells indicate that, although the differentially expressed genes are distinct due to the individual lineage identities, the overall functional pathways are conserved. *ZEB1* RNA levels can be used to stratify patients into groups with different survival probabilities with a significant correlation between high expression and poor clinical outcome. Similarly, the EpCAM^{lo} signature derived from the RNAseq analysis of ovarian cancer cell lines can be used to identify mesenchymal-like cells in patient-derived ovarian cancers, despite their relatively low abundance within the bulk of EpCAM^{hi} cells.

Chapter 6

Results

A subpopulation of quasi-mesenchymal, migratory, and chemo-resistant cells coexist with epithelial cells within HGS ovarian cancer cell lines.

By following a similar approach to that previously applied for the analysis of colon cancer cell lines [11], FACS analysis of the HGS ovarian cancer cell lines OV90, SKOV3, COV504 and CAOV3, revealed the presence of distinct $CD44^{hi}EpCAM^{hi}$ ($EpCAM^{hi}$) and $CD44^{hi}EpCAM^{lo}$ ($EpCAM^{lo}$) subpopulations at different percentages (**Figure 1A**). Upon sorting, $EpCAM^{hi}$ and $EpCAM^{lo}$ cells revealed distinct epithelial- and mesenchymal-like morphologies, respectively (**Figure 1B**). Accordingly, trans-well assays showed that $EpCAM^{lo}$ cells have enhanced capability to migrate and invade when compared with the $EpCAM^{hi}$ counterparts (**Figure 1C**).

RT-qPCR analysis of the sorted subpopulations showed differential expression of EMT marker related transcription factors and genes. In particular, in $EpCAM^{lo}$ cells from all four cell lines a significant reduction was observed in *EPCAM* and E-cadherin (*CDH1*) mRNA levels, whereas expression of vimentin (*VIM*) and of the EMT-transcription factor *ZEB1* was increased, as also validated by immunofluorescence analysis of OV90 cells (**Figure 1-supplement 1A-B; Figure 1–supplement 2**). Hence, *ZEB1* knockdown by shRNA significantly reduced the percentage of $EpCAM^{lo}$ cells in OV90, SKOV3 and COV504 cell lines (**Figure 1-supplement 1C-D**).

Transcriptional regulation of *ZEB1* (and *ZEB2*) has been shown to be controlled by the miR-200 superfamily of microRNAs (miR-200a, miR-200b, miR-200c, miR-141, miR-429) which bind to particular 3'UTR seed sequences resulting in a decreased expression and consequently EMT inhibition [12]. RT-qPCR analysis of sorted OV90 and CAOV3 cells revealed reduced expression levels of all five miR-200 members in $EpCAM^{lo}$ cells (**Figure 1-supplement 1E**).

Last, because of the recognized correlation between EMT and therapy resistance [9], OV90 and CAOV3 $EpCAM^{lo}$ cells were cultured in the presence of two chemotherapeutic agents commonly employed in the treatment of ovarian cancer, i.e cisplatin and paclitaxel, and their viability compared with that of $EpCAM^{hi}$ and bulk cells by metabolic activity assay (MTT). Both OV90 and CAOV3 $EpCAM^{lo}$ cells showed increased viability at all examined cisplatin (**Figure 1-supplement 3A and C**, left panels) and paclitaxel (**Figure 1-supplement 3A and C**, right panels) concentrations. Likewise, the re-growth assay revealed that the chemo-resistant $EpCAM^{lo}$ cells from the OV90 cell line were capable to re-enter the cell cycle at a wide spectrum of cisplatin and paclitaxel concentrations when evaluated against $EpCAM^{hi}$ cells (**Figure 1-supplement 3B**). Similar observations were obtained in CAOV3 cells for paclitaxel (**Figure 1-supplement 3D**, right panel), though the same was not true for cisplatin (**Figure 1-supplement 3D**, left panel).

Overall, these results show that, similar to our previous analysis of colon cancer cell lines, a subpopulation of EMT-driven, quasi-mesenchymal, motile, and therapy-resistant $EpCAM^{lo}$ cells characterizes HGS ovarian cancer cell lines.
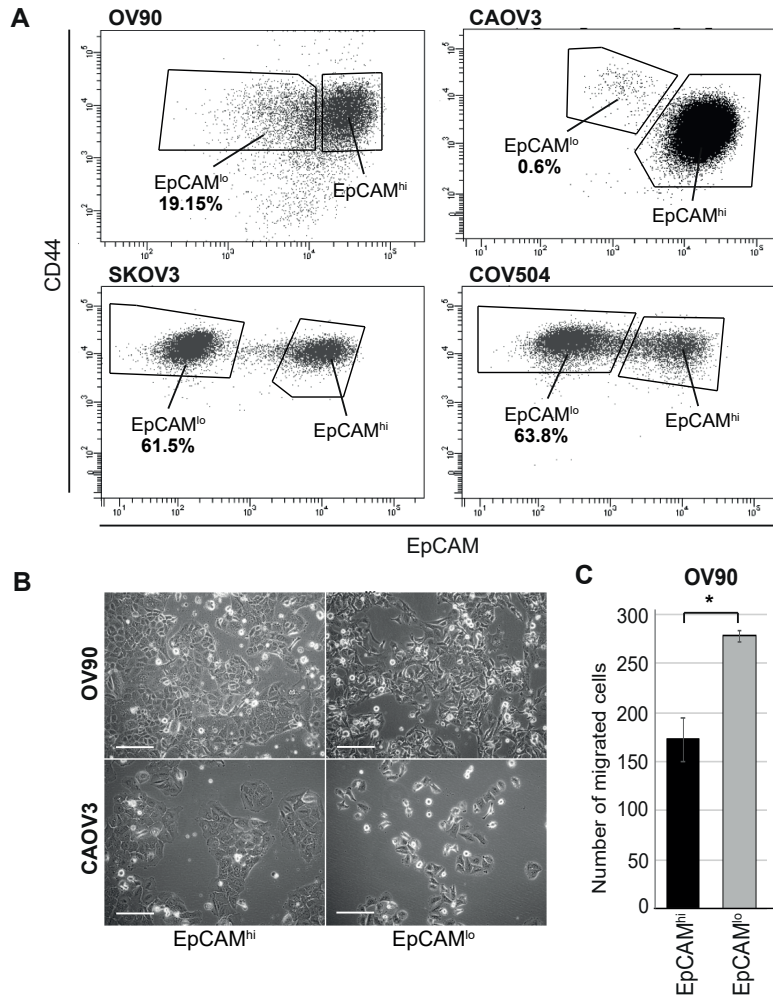
Figure 1. (**a**) Flow cytometric analysis of the ovarian cancer cell OV90 (upper left panel), CAOV3 (upper right panel, SKOV4 (bottom left panel) and COV504 (bottom right panel) with antibodies aimed against CD44 and EpCAM. EpCAM/CD44 positive and negative areas were identified using multiple isotype controls. Using specific gates, cells were separated in a CD44highEpCAMhigh group, together with a CD44highEpCAMlow subpopulation. To guarantee good separation from the large EpCAMhigh cluster and maximal sorting purity, EpCAMlow cells were gated as CD44high events ≤60% of the EpCAM fluorescence intensity of the left border of the CD44highEpCAMhigh gate, and sorted from ≤50% of that value. The percentages of CD44highEpCAMlow cells within each cell line are revealed. For the sake of simplicity, gates are shown in the figure only if they contain substantial percentages of cells. (**b**) Phase contrast microscopy illustrations of sorted EpCAMhi and EpCAMlo cells from OV90 (upper images) and CAOV3 (lower images) cells. Scale bar: 100 μm. (**c**) Transwell migration assay of EpCAMhi (black bar) and EpCAMlo (grey bar) cells from the OV90 cell line. 10^5 cells were plated on TC-coated membrane and left overnight before counting the number of migrated cells on the bottom side of the membrane. Each bar symbolizes the mean ± SD. Asterisks indicate significant differences ($P < 0.05$

Genetic profiles of EpCAM^{lo} populations of distinct cancer cell lines are different, yet the overall functional outcome is similar

In order to elucidate the global molecular and cellular mechanisms underlying the EpCAM^{lo} subpopulation of ovarian cancer cells, RNAseq analysis was carried out on the separated EpCAM subpopulations from the OV90 and CAOV3 lines. Principal component analysis (PCA) by multidimensional scaling (MDS) revealed a separation in the second dimension of EpCAM^{hi} and EpCAM^{lo} cells in the two ovarian cancer cell lines (**Figure 2A**). Totally 509 and 778 differentially expressed genes (DEGs) were discovered among the EpCAM^{hi} and EpCAM^{lo}/bulk cells in OV90 and CAOV3, respectively (*P. adjusted* < 0.01, when applying a Log$_2$ fold change < -1.5 and > 1.5). Between these, 110 were equal to both lines (**Figure 2B**). More specifically, 17 genes were upregulated in both cell lines, whereas 93 genes were downregulated in both OV90 and CAOV3 cell lines (**Figure 2C**). Interestingly, by comparing DEGs between the ovarian and colon EpCAM^{lo} populations [11], 19 genes were common to all four cell lines. Of these, *ZEB1* was the only upregulated gene (**Figure 2B**), whereas the remaining 18 were downregulated in all four cell lines (**Figure 2C**).

Pathway analysis (PA) using the EpCAM^{lo} expression profiles of ovarian cancer cell lines OV90 and CAOV3 highlighted significant associations with '*Epithelial Mesenchymal Transition*', '*TNF-α signaling via NF- κB*', '*Inflammatory response*', '*Apoptosis*', '*KRAS signaling up*' and '*Angiogenesis*' (**Figure 2D**). Further comparison of the EpCAM^{hi/lo} RNAseq profiles of the colon and ovarian cell lines by PCA (**Figure 2-supplement 2A**) as well as by PA using Gene Set Variation Analysis (**Figure 2-supplement 2B**), showed no significant overlap. However, cell line centered pathway analysis exposed that genes differentially expressed in each cell line reflect general molecular and cellular functions consisting of '*Epithelial Mesenchymal Transition*' and '*TNF-α signaling via NF-κB*' (**Figure 2D**). Hence, although the genetic profiles of each EpCAM^{lo} population are different among the four cell lines, the overall functional outcome appears to be similar.

Mesenchymal-like cells predict shorter progression-free and overall survival in ovarian cancer patients

To validate the clinical relevance of our cell line-based RNAseq analysis of EpCAM^{lo} cells, we further analyzed the expression of *ZEB1* in ovarian cancers using the GSE14764 dataset containing expression data with clinical follow up of 614 patients [13]. The Kaplan-Meier method was applied to evaluate differences in progression-free and overall survival between patients with high and low *ZEB1* expression levels. As show in **Figure 3A**, increased *ZEB1* expression was associated with worse progression-free (hazard ratio: 1.6 (1.3-1.97; P=7.1x10^{-6})) and overall survival (hazard ration: 1.6 (1.28-1.99; P=2.2x10^{-5})) in the ovarian cancer dataset.

Next, in order to identify mesenchymal-like cells in ovarian cancer tumors, we analyzed cancer cells from 4 ovarian cancer patients using publicity available scRNAseq data [14]. After dimension reduction with tSNE individual cells were clustered in separate groups by tumor site (**Figure 3-supplement 1A**) or patient (**Figure 3-supplement 1B**). We next developed an EMT signature representing the EpCAM^{lo} identity, using genes previously identified in the bulk RNAseq of EpCAM^{lo} cells (**Figure 2-supplement 1**).
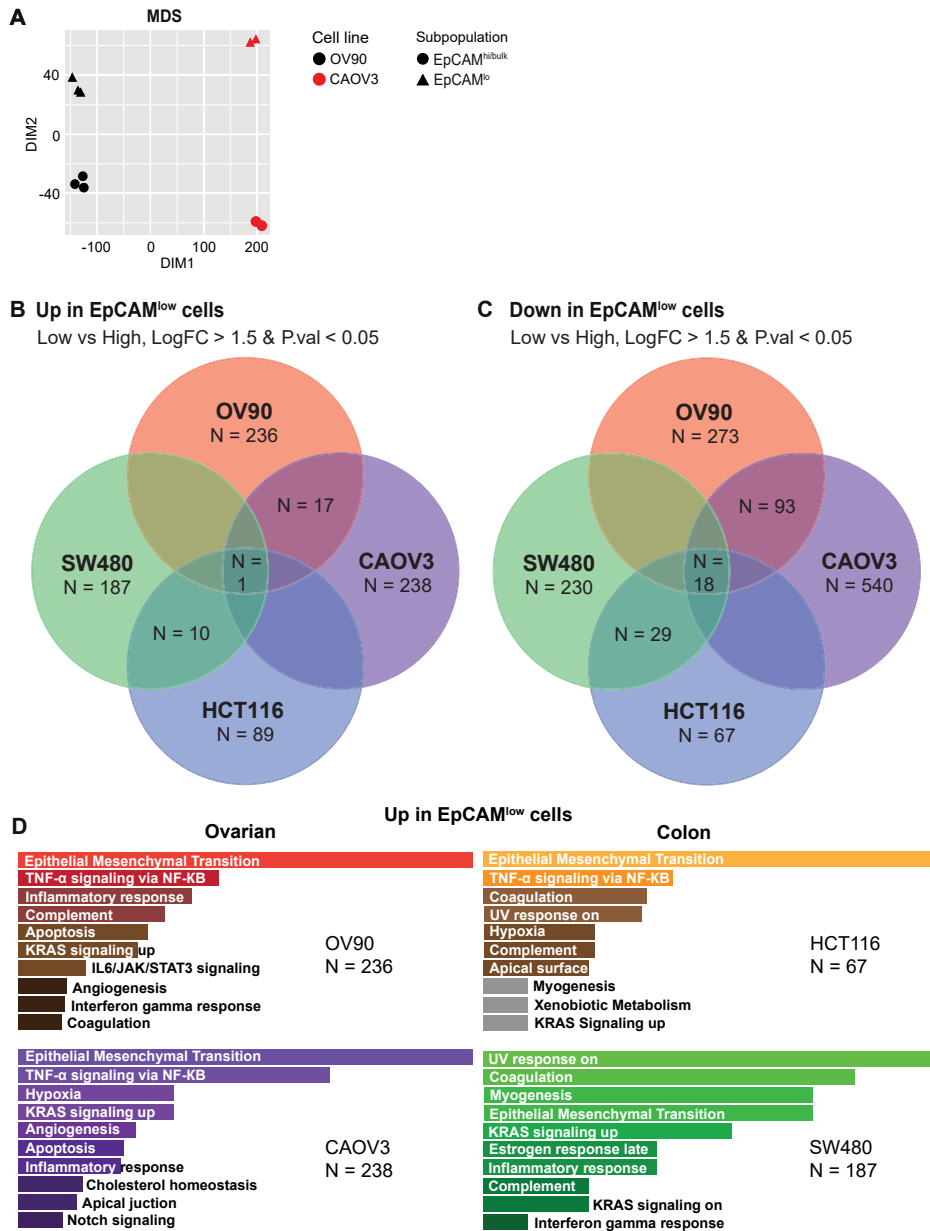
Figure 2. (**a**) Multidimensional scaling (MDS) analysis of RNAseq profiles of EpCAM^{hi} and EpCAM^{lo} cells from the OV90 and CAOV3 lines. Black: OV90, red: CAOV3, circle: EpCAM^{hi}, triangle: EpCAM^{lo}. (**b-c**) Differentially expressed genes that are upregulated (**b**) or downregulated (**c**) in the ovarian and colon EpCAM^{lo} compared with EpCAM^{hi} populations. (**d**) Cell line centered gene ontology (GO) of molecular and cellular functions in HCT116 (orange), SW480 (green), OV90 (red) and CAOV 3 (purple).

Chapter 6
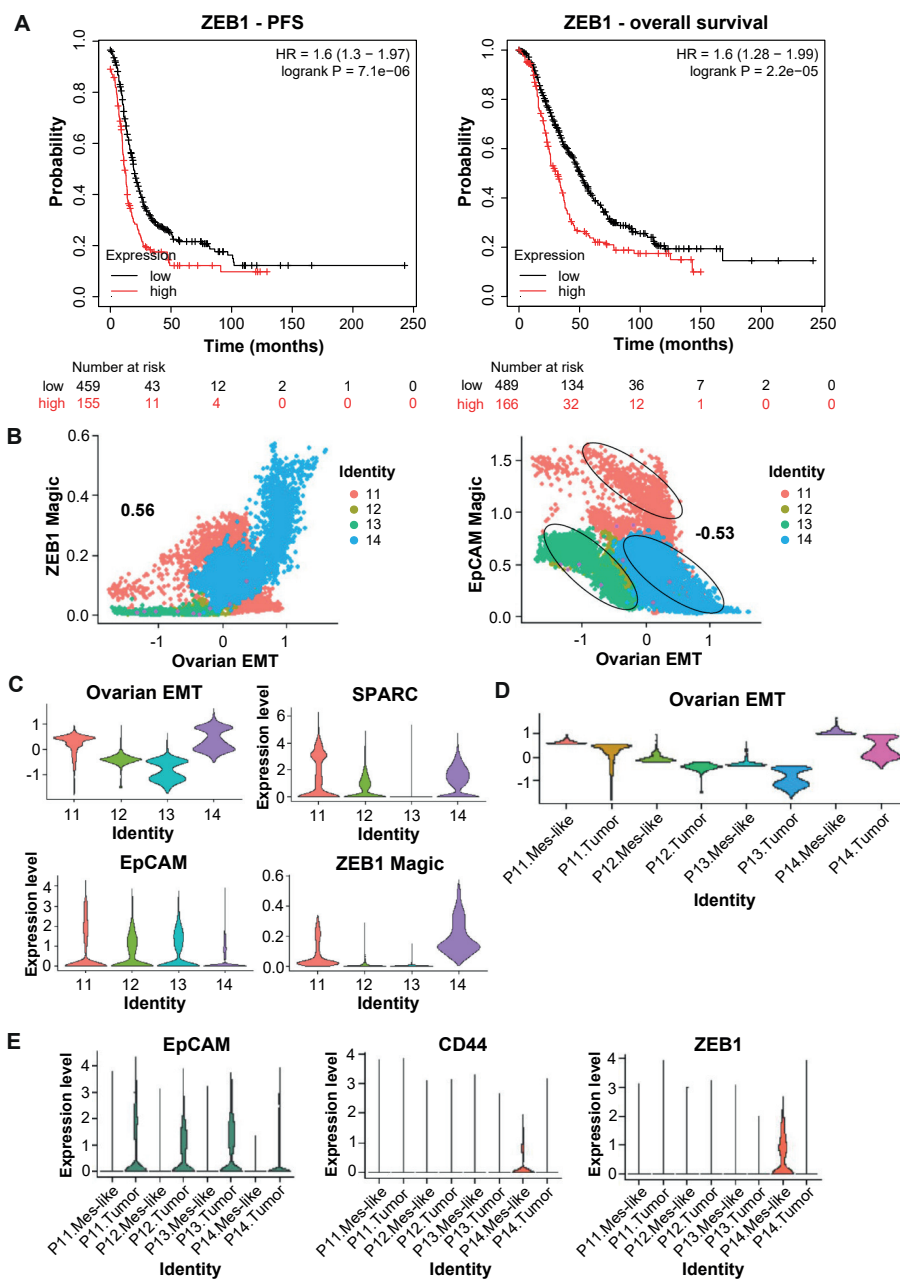
Figure 3. (**a**) Kaplan Meier analysis. *ZEB1* was used to cluster the tumors from the GSE14764 dataset in patients with high or low *ZEB1* expression. The Kaplan-Meier method was subsequently used to assess significant differences in progression-free (left panel) and overall (right panel) survival between the generated subgroups. (**b**) Correlation of ZEB1 (left panel) and EpCAM (right panel) expression (y-axis) in single ovarian cancer cells projected over the EMT signature obtained from the bulk RNA sequencing of ovarian cancer cell lines OV90 and CAOV3 (y-axis). Each color represents an individual patient. (**c**) Violin plot tumor cells from different ovarian cancer patients showing expression patterns across different

genes. (**d**) Obtaining a mesenchymal-like subcluster of individual tumor cells from individual ovarian cancer patients by taking 10% of the tumor cells that contain the highest EMT score (EMT signature derived from the ovarian RNA sequencing). (**e**) Violin plots of tumor and mesenchymal-like tumor cells (obtained from figure 4D) showing expression patterns across different genes.

An EMT signature score was computed by averaging upregulated the genes in ovarian EpCAM^{lo} cells and subtracting the average of the genes downregulated in EpCAM^{lo} cells. As expected, the EMT signature showed a positive correlation with *ZEB1* (Pearson's r = 0.56) (**Figure 3B**) and a negative correlation with *EPCAM* (Pearson's r = -0.53) (**Figure 3C**) within the collection of ovarian cancer cells. Next, we evaluated the distribution of the EMT signature across the 4 ovarian cancer patients (**Figure 3C**). Of note, the four patients showed distinct distributions, with 'patient 13' showing the overall lowest association to the EMT signature and 'patient 14' the highest. This observation was supported by their distinct expression levels of *EPCAM* and EpCAM^{lo} genes (e.g. *ZEB1, SPARC*) (**Figure 3C**). Following this, we questioned whether the EMT signature could be used to select quasi-mesenchymal tumor cells within the different patients. For each patient we selected the epithelial cancer cells with the highest association to the EMT signature (top 10%), and annotated these cells as Mes-like (**Figure 3D**). Notably, while expression of *EPCAM* was reduced in the Mes-like cells across the four patients, elevated expression of EpCAM^{lo} genes, like *CD44* and *ZEB1*, was solely observed in 'patient 14' (**Figure 3E**). Differential expression analysis of the Mes-like cancer cells versus the remaining tumor bulk revealed a heterogenous pattern across patients. *ZEB1* and collagens were selectively upregulated in 'patient 14', *SPARC* and *FN1* expression was observed in the Mes-like cells from 'patient 14' and 'patient 11', and downregulation of epithelial gene expression (e.g. *EPCAM*, keratins) was observed in all patients (**Figure 3-supplement 2**).

Taken together, while we observed notable differences in the level of EMT across patients, analysis within the same tumors revealed considerable intratumor heterogeneity. Similar to our results in ovarian cancer cell lines, the repression of epithelial gene expression is similar across patients, while upregulation of quasi-mesenchymal genes follows a more heterogenous pattern.

Discussion

Phenotypic plasticity, defined as the ability of one genotype to produce more than one phenotype when exposed to different environments, is regarded as the most clinically relevant among the cancer's hallmarks as it allows the carcinoma cell to detach from the primary tumor and undergo transient and reversible morphologic and functional modifications along the multiple steps of the invasion-metastasis cascade. However, the study of phenotypic plasticity is often hampered by the rarity of these events, often restricted to a minor subgroup of cells within primary cancers and by the lack of suitable experimental models. Over 10 years ago, Gupta et al. demonstrated that immortalized breast cancer cell lines contain different subpopulations of tumor cells with specific phenotypic states preserved in a dynamic equilibrium through stochastic state transitions [15]. These findings were subsequently confirmed in oral [16] and colon [11] cancer cell lines. In the latter study, we identified a minority subpopulations of quasi-mesenchymal EpCAM^{lo} (CD44^{hi}/EpCAM^{lo}) cells resulting from EMT activation and earmarked by phenotypic plasticity and highly invasive and metastatic capacity [11]. Of note, specific

gene signatures derived from the RNAseq analysis of the cell line-derived EpCAM^{lo} cells allow the identification of the analogous cells in patient-derived colon cancers and outperforms previous classifiers in predicting survival and overall outcome. In the present study, we have followed a similar approach for the analysis of HGS ovarian cancer cell lines where, analogous to breast, oral, and colon cancer cell lines, the dichotomy of epithelial (EpCAM^{hi}) and quasi-mesenchymal (EpCAM^{lo}) subpopulations also exists.

Genome-wide expression analysis of the ovarian EpCAM$^{hi/lo}$ subpopulations of ovarian cancer cells by RNAseq revealed that, when compared with their epithelial counterparts, EpCAM^{lo} cells are characterized by the differential expression of genes involved in EMT, inflammation, angiogenesis, apoptosis, and KRAS-signaling. However, although more than 500 genes were found to be differentially expressed in the individual cell lines (n=509 in OV90 and n=778 in CAOV3), a relatively small percentage of them was shared by both (n=110). Likewise, when compared with the profiles of EpCAM^{lo} cells derived from colon cancer cell lines, although the individual DEGs are different (only 19 common genes, 1 up- and 18 downregulated), the functional pathways underlying the establishment and maintenance of quasi-mesenchymal subpopulations appear to be conserved. As expected from the increased *ZEB1* expression in EpCAM^{lo} cells, notably the only upregulated gene common to all four cell lines, and the differential expression of several epithelial and mesenchymal markers, EMT/MET was confirmed to play a central role in the dynamic equilibrium between the two subpopulations. Moreover, activation of the TNFa and NFkB signaling pathways and of the overall response to inflammation seem to earmark the transcriptome of quasi-mesenchymal ovarian and colon cancer cells. These observations suggest that the fundamental molecular and cellular mechanisms underlying phenotypic plasticity in different types of cancer follow the same ground rules yet by modulating the expression of distinct gene modules. Central to these processes, *ZEB1* controls a broad spectrum of intracellular processes key to malignancy including EMT and MET, stemness and differentiation, cell proliferation and senescence, and survival and apoptosis [17]. Moreover, enhanced *ZEB1* expression underlies resistance to therapy [18-20] and is correlated with a poor recurrence/progression-free survival (RFS) in patients with epithelial ovarian cancer [21]. Our findings also indicate that the decreased *ZEB1* expression in EpCAM^{hi} cells is likely to result from the activation of several members of the miR-200 family, previously shown to suppress EMT by silencing both *ZEB1* and *ZEB2* because of the presence of their seed target sequences in their 3' UTR's [22]. Reciprocally, ZEB1 binds to and represses the promotor of the three co-regulated mir-200B/A/429 [23] thus establishing a double negative feedback loop with three miR-200 members and exerting opposite effects on EMT [12]. Accordingly, the miR-200 family appears to play an important role in ovarian cancer: its expression is correlated with an overall favorable prognosis, and the expression the miR-200 family is associated with a favorable response to chemotherapeutic drugs [24-27].

The role of EMT in metastasis has recently been the object of a debate based on two studies based on the analysis of individual EMT-transcription factors and downstream targets in specific lung and pancreas cancer models [28,29]. However, EMT is a complex and highly context-dependent cellular process with several transcription factors known to cooperate in eliciting it and in controlling the extension of the execution of the trans-differentiation program [30]. As such individual genes cannot be used to discard EMT's

role in metastasis against an overwhelming body of experimental evidence from the scientific literature [31].

On top of this heterogeneity of EMT molecular programs that makes a single and unifying molecular definition of EMT and its role in metastasis simply not feasible, primary carcinomas originating in different organs often follow different routes to and cellular strategies to locally invade, metastasize, and evade therapy. Ovarian and colon cancers, because of the very different anatomical localization of the primary lesions, metastasize distant organs (liver and abdominal cavity, respectively) with very different modalities, namely blood-born versus peritoneal dissemination [1,2,32]. This is likely to be reflected by the differences found between the EpCAM^{lo} RNAseq profiles between colon and ovarian cancer. The development of hematogenous metastases follow the invasion-metastasis cascade: (1) local invasion of the surrounding stroma, (2) intravasation into the vasculature, (3) survival in the circulatory system, (4) extravasation into the parenchyma of the distant organ, (5) colonization into a distal organ, and (6) re-initiation of proliferation to form macroscopic metastases [33]. Whereas peritoneal metastases arise by detachment of tumor cells from the primary tumor (step 1), anoikis evasion (step 2), adherence to the peritoneal surface (step 3), invasion into the peritoneum (step 4), and proliferation and formation of the peritoneal metastasis (step 5) [34]. During hematogenous spread, circulating tumor cells (CTCs) are chemically and mechanically surrounded and protected by neutrophils and platelets that help CTCs to avoid shear stress, protect them from immune attacks by natural killer cells and support them in adherence to the endothelium and extravasation [35]. However, during peritoneal spread, cancer cells cluster to escape anoikis and in addition continue to proliferate [36]. In addition, recent studies have indicated that adhesion molecules important for tumor cells during the attachment to their target organ differ between hematogenous and peritoneal metastases. In hematogenous spread the binding of CD44 to hyaluronan, the blood group antigens sLea and sLex to selectins and mucins binding to ECM molecules has shown to be required for cancer cell dissemination [37]. In peritoneal metastases, however, an important role for integrins, proteoglycans, members of the immunoglobulin superfamily, mucins, and the epithelial cell adhesion molecule (EpCAM) have been suggested [34]. Lastly, the tumor microenvironment is also involved in all stages of tumor proliferation in both types of dissemination. Differences in immune cells, soluble factors, and the ECM may be involved in these different processes [38]. However, more experimental and clinical studies is needed that could contribute in the clarification of the genetic and epigenetic differences between similar metastatic populations. Better understanding of these mechanisms will help to provide specific targets for therapeutic interventions in the future.

Materials and Methods

Cell culture
CAOV3, SKOV3, COV504, HEK293T, Wnt3a producing L cells (gift from R. Nusse, Stanford University), and control (i.e. non-Wnt3a producing) cell lines were cultured in DMEM medium (11965092, Thermo Fisher Scientific) supplemented with 10% heat inactivated fetal bovine serum (FBS; Thermo Fisher Scientific), 2 mM L-glutamin (200 mM; 25030081; Thermo Fisher Scientific), and 1% Penicillin/Streptomycin (Pen/Strep; penicillin: 100 U/ml, streptomycin: 100 µg/ml; 15140122 Thermo Fisher Scientific). OV90 was cultured in

a 1:1 mixture of MCDB 105 medium (M6395; Sigma Aldrich containing 1.5 g/L sodium bicarbonate) and Medium 199 (31150022; Thermo Fisher Scientific containing 2.2 g/L sodium bicarbonate) supplemented with 15% heat inactivated fetal bovine serum (FBS; Thermo Fisher Scientific) and 1% Penicillin/Streptomycin (Pen/Strep).

Flow cytometry and sorting

For flow cytometry and sorting purposes, cells were detached from the culture dishes using trypsin-EDTA (15400054, Thermo Fisher Scientific) and resuspended in staining buffer (PBS supplemented with 4% FCS). Antibody staining was performed on ice for 30′ with CD44-APC (clone IM7, 559250, BD Pharmingen) and EpCAM-FITC (ESA-214, GTX30708, GeneTex). Cells were then washed and resuspended in PBS 4% FCS. Flow cytometry analysis and cell sorting were conducted by a FACSAria III Cell Sorter (BD Biosciences). Forward-scatter height (FSC-H) versus forward-scatter width (FSC-W), and side-scatter height versus side-scatter width were used to eliminate cell aggregates and guarantee single cell sorting. Gates were defined as illustrated and specified in Figure 1. The DAPI nuclear dye (D9542, Sigma-Aldrich) was used at 1 µg/ml to exclude dead cells. FITC and GFP were analyzed using 488 nm laser and 502LP and 530/30BP filters; APC and Sytox Red with a 633 nm laser and a 660/20BP filter; BV421 using a 405 nm laser and a 450/40BP filter; BV785 with a 405 nm laser and a 750LP and 780/60BP filter; PE with a 461 nm laser and a 582/15 BP filter.

Cell viability assays

For the chemoresistance assays, cells were plated in 96-well plates at 15000 cells/well and left overnight to adhere. Three technical replicates were seeded per tested condition. Both cisplatin (Sigma-Aldrich) and paclitaxal (Sigma-Aldrich) were dissolved in DMSO. OV90 cells were incubated for 72 hours with cisplatin or paclitaxel. CAOV3 were treated with cisplatin or paclitaxal for 96 or 72 hours respectively (adjusted on the response of the parental line regarding viability). Upon removal of the chemotherapeutic drug, cells were washed with PBS and left to re-grow in standard culture medium. Cell viability was measured using the MTT (3-(4,5-dimethylthiazol-2-yl)-2,5-diphenyltetrazolium bromide; Sigma-Aldrich) assay at time zero, i.e. upon removal of the drug, and after re-growth (range 18-35 days). Briefly, cells were incubated at 37°C, 5% CO_2 for 3 hrs. in culture medium augmented with 0.45 mg/mL MTT. The 96-well plates were then centrifuged at 1,000 rpm for 5′ and the culture medium removed. MTT formazan precipitates were solubilized with DMSO. O.D. reading was completed at 595 nm with a Microplate Reader (Model 550, Bio-Rad). Background measurements were subtracted from each data point. MTT-based outcomes were also confirmed by manual count of trypan blue positive cells, using cells collected from additional 96 wells. At least two biological experiments were performed for each individual cell line and drug.

The choise of cisplatin and paclitaxal concentrations and administration times for chemo-resistance tests was as follows. In a pre-defined range of concentrations (3.125-50 µM for cisplatin, and 3.125-100 nM for paclitaxal based on previous data, the maximal concentration and length of treatment was chosen as the combination capable to cause cell death in approx. 80% of EpCAM^{lo} cells. From that concentration, the curve was scaled down by 50% at least three times to reach the lowest concentration to be tested.

Migration and invasion assays

For the 'transwell' (modified Boyden chamber) migration and invasion assays, cells were starved for 24 hrs. in DMEM supplemented with 1% FBS. For every analysed subpopulation, 1.0 x 10^6 cells were collected, resuspended in 1% FBS medium and plated in transwell tissue culture inserts (8 µm polycarbonate membrane, 24 well, 3428; Corning). DMEM medium with 10% FBS was then pipetted in the bottom compartment of the transwell chamber. For both assays three technical replicates were plated for each subpopulation. Plates were incubated for 24 hrs. at 37°C/5% CO_2, after which the cells and membranes were fixed in methanol and stained with crystal violet. The non-migrated cells on the upper surface of the membrane were removed with a cotton-wool bud and the cells migrated to the lower surface of the membrane counted. For both assays two independent experiments were performed.

RNA isolation and qRT-PCR

RNA was obtained from cells using TRIzol™ Reagent (15596018, ThermoFisher Scientific) corresponding to the manufacturer's instructions. RNA concentration was determined by NanoDrop. Subsequently, reverse transcription into cDNA was performed using the High-Capacity cDNA Reverse Transcription Kit (4368814, Life Technologies) according to the manufacturer's instructions. RT-qPCR was accomplished with Fast SYBR Green Master Mix (4385617; ThermoFisher Scientific). PCR amplification and detection were executed with the 7400 Fast Real-Time PCR System. Expression levels were normalized for the endogenous *GAPDH* reference gene. All PCR primers here used are listed here below:

GENE	FORWARD PRIMER	REVERSE PRIMER
GAPDH	5'-ACCCAGAAGACTGTGGATGG-3'	5'-TCTAGACGGCAGGTCAGGTC-3'
EPCAM	5'-GCAGCTCAGGAAGAATGTG-3'	5'-CAGCCAGCTTTGAGCAAATGAC-3'
CDH1	5'-TGCCCAGAAAATGAAAAAGG-3'	5'-GTGTATGTGGCAATGCGTTC-3'
VIM	5'-GAGAACTTTGCCGTTGAAGC-3'	5'-GCTTCCTGTAGGTGGCAATC-3'
ZEB1	5'-GCACAACCAAGTGCAGAAGA-3'	5'-CATTTGCAGATTGAGGCTGA-3'
ZEB2	5'-TTCCTGGGCTACGACCATAC-3'	5'-TGTGCTCCATCAAGCAATTC-3'
TWIST1	5'-GTCCGCAGTCTTACGAGGAG-3'	5'-GCTTGAGGGTCTGAATCTTGCT-3'
SNAI1	5'-GCGAGCTGCAGGACTCTAAT-3'	5'-CCACTGTCCTCATCTGACA-3'
SNAI2	5'-GGGGAGAAGCCTTTTTCTTG-3'	5'-TCCTCATGTTTGTGCAGGAG-3'

miRNA

For miRNA experiments, sorted cell populations from OV90, CAOV3, COV504 and SKOV3 cell lines were cultured up till 70% confluency in 6 well-multiwell plates. Total RNA was then isolated using the Trizol™ (Ambion) protocol. For *miR-200-family (miR-200a, miR-200b, miR-200c, miR-141, miR-429)*, reverse transcription was achieved using the TaqMan MicroRNA RT Kit (Applied Biosystem), followed by qRT-PCR using TaqMan MicroRNA assay (Thermo Fisher scientific). *U6* snRNA was used as tanendogenous control. The expression of *miR-200-family* was analyzed by the ΔCT method. The experiment was repeated three times.

Chapter 6

shRNA

in order to knock-down *ZEB1* expression, lentiviral inducible shRNA vectors encompassing control or *ZEB1* sequences were established. *Cloning was accomplished according to the manufacturer's guidelines (Wiederschain et al). Briefly,* Tet-pLKO-puro (gift from D. Wiederschain, Addgene plasmid # 21915) was digested with AgeI and EcoRI and isolated by gel purification (QIAEX II Gel Extraction Kit, Qiagen). The sequences of the control and *ZEB1 shRNA were as follows:* shRNA control (shCT) (Addgene sequence #1864): top 5'-CCGGCCTAAGGTTAAGTCGCCCTCGCTCGAGCGAGGGCGACTTAACCTTAGG TTTTTTG-3', bottom: 5'-AATTCAAAAAACCTAAGGTTAAGTCGCCCTCGCTCGAGCGAGGGCG ACTTAACCTTAGG-3', shZEB1-A: target sequence (Broad Institute): 5'-GCTGCCAATAAGC AAACGATT-3'; oligo sequence: top: 5'-CCGGGCTGCCAATAAGCAAACGATTCTCGAGAAT CGTTTGCTTATTGGCAGCTTTTT-3', bottom: 5'-AATTAAAAAGCTGCCAATAAGCAAACGA TTCTCGAGAATCGTTTGCTTATTGGCAGC-3', shZEB1-B: target sequence (Broad Institute): 5'-GTCTGGGTGTAATCGTAAATT-3' oligo sequence: top 5'-CCGGGTCTGGGTGTAATCGT AAATTCTCGAGAATTTACGATTACACCCAGACTTTTT-3', bottom 5'- AATTAAAAAGTCTGGG TGTAATCGTAAATTCTCGAGAATTTACGATTACACCCAGAC-3'. *The "top" and "bottom" labels indicate the oligonucleotide that were annealed in 0.1 M NaCl, 10 mM TrisHCl, pH 7.4, after incubation at 95℃ followed by a cooling down step until room temperature is reached.* The digested vector (200 ng) was ligated with 1 µL of the oligonucleotides (0.45nmol/µl) using T4 DNA ligase (Promega) for 3 hrs. at room temperature. "One Shot Stbl3" chemically competent E. coli (Thermo Fisher Scientific) were transformed with the ligation product. Individual colonies were inoculated for mini-prep cultures and the presence of the insert was checked using the restriction enzyme XhoI and by sequencing.

For lentivirus production, the shCT or the pool of the two *ZEB1* shRNA constructs were packaged into second generation virus particles using psPAX2 (Addgene plasmid # 12260; gift from dr. Didier Trono), pMD2.G (Addgene plasmid # 12259) into HEK293T. Virus particles were titrated with the OV90 cell line and a MOI of 0.5 was employed to produce the shRNA inducible OV90, COV504 and SKOV3 cell lines. Lentivirus-infected cells were selected in medium containing 1 µg/mL puromycin (Dulbecco). shRNA induction was implemented by using 1 µg/mL doxycycline for 72 hrs. The extent of *ZEB1* downregulation was assessed by RT-qPCR.

Immunofluorescence (IF) analysis

Coverslips containing a monolayer of cancer cells were fixed for 30' in 4% PFA at 37 ℃ and washed twice with PBS. Cells were first permeabilised for 15 minutes at room temperature with 0.2% of Triton X-100 and then incubated in blocking buffer (5% milk powder in PBS-Tween) for 1 hour at room temperature. Cells were then exposed overnight at 4 ℃ to primary antibodies against EpCAM (mouse, 1:250; sc-66020; Santa Cruz Biotechnology), E-cadherin (rabbit, 1:200; Santa Cruz), Vimentin (mouse, 1:200, Santa Cruz) and ZEB1 (rabbit, 1:200; sc-25388, Santa Cruz Biotechnology). After washing twice with PBS-Tween, coverslips were incubated for 1 hour at room temperature in blocking buffer containing the following secondary antibodies: Goat anti-Rabbit Alexa Fluor® 594 conjugate (1:250, #A-11037, Life Technologies) and Donkey anti-Mouse Alexa Fluor® 488 conjugate (1:250, #A-21202, Life Technologies). Cells were counterstained with DAPI to visualize the nuclei. Coverslips were mounted in VECTAHIELD HardSet Antifade Mounting Medium (#H-1400, Vector Labs) and imaged with a Zeiss LSM-700 confocal microscope.

Images were processed with ImageJ (U.S. National Institutes of Health, Bethesda, MD, USA).

Next Generation Sequencing (NGS): RNAseq

RNA quality and quantity was evaluated on a 2100 Bio-analyzer (Agilent) using the Agilent RNA 6000 Pico Kit. RNA samples were further processes according to the TruSeq Sample Preparation v.2 Guide (Illumina) and paired end-sequenced on the HiSeq 2500 (Illumina).

Illlumina paired-end reads of 76 bases were trimmed by removing the TrueSeq adapter sequences using Trimmomatic (v.0.33) [39]. Subsequently, the reads were mapped in a two-pass procedure to the human reference genome build hg38 with the RNA-seq aligner STAR (v2.4.2a) [40] and the Homo sapiens GENCODE v23 annotation [41]. Raw counts were summed with the summarize overlaps function with union mode from the Bioconductor Genomic Alignments package [42] (v1.14.0). Genes were called differentially expressed with a generalized linear model using a negative binomial distribution with correcting for cell lines in multi-cell line comparisons. DESeq2 (v1.16.1) was used to perform these calculations [43]. We applied a Wald-test to identify statistical significant differently expressed genes. *P*-values were adjusted using the Benjamini-Hochberg [44] correction based on which a threshold value was set at < 0.01. Multidimensional scaling was performed after the read counts were normalized with blind variance stabilizing log2 transformation function of DESeq2. Gene Ontology (GO) and Kyoto Encyclopedia of Genes and Genomes (KEGG) gene enrichment analyses were carried out as described previously [45]. R (v 3.4.0) (R Core Team, 2017; https://www.R-project.org/) was employed for statistical analysis and visualization of the data.

Bioinformatics analysis bulk RNAseq

For other bioinformatics analyses, the generated datasets were uploaded into the R2 Genomics Analysis and Visualization Platform (http://r2.amc.nl). First, we used the 'differential expression between groups' option to identify the hundred genes with highest expression in the EpCAM^{lo} fraction in both the OV90 and COAV3 cells. These genes were saved as separate gene sets. Expression values of all genes in both gene sets was then assessed in the GSE14764 dataset containing expression data with clinical follow up of 614 patients [13]. The Kaplan-Meier method was used to assess differences in progression-free and overall survival, yielding Pearson R values and accompanying p values.

In order to identify mesenchymal-like cells in ovarian cancer tumors, we analyzed cancer cells from 4 ovarian cancer patients using publicly available scRNAseq data [14]. An EMT signature score was computed by averaging upregulated the genes in ovarian EpCAM^{lo} cells and subtracting the average of the genes downregulated in EpCAM^{lo} cells. The distribution of the EMT signature was evaluated across the 4 ovarian cancer patients.

Data accessibility

The RNA-sequencing data from this study have been submitted to the Gene Expression Omnibus (GEO)[46] database under the accession number GSE154927 and GSE192920 for the bulk colon and ovarian cancer cell line RNAseq data, respectively. Other dataset referenced in this study are publicly available and can be accessed with GSE144735 and GSE132465 (Lee et al.), and at Synapse with syn2623706 (Guinney et al.).

Chapter 6

Statistical analysis

For each experiment, data are shown as mean ±SD. IBM SPSS Statistics software was used for data analysis; α-value was set at 5%.

Funding

Competing Interests Statement

The authors of this manuscript do not have any competing financial interests in relation to the work described.

References

1. Adam, R.A.; Adam, Y.G. Malignant ascites: past, present, and future. *J Am Coll Surg* **2004**, *198*, 999-1011, doi:10.1016/j.jamcollsurg.2004.01.035.
2. Feldman, G.B.; Knapp, R.C.; Order, S.E.; Hellman, S. The role of lymphatic obstruction in the formation of ascites in a murine ovarian carcinoma. *Cancer Res* **1972**, *32*, 1663-1666.
3. Tarin, D.; Price, J.E.; Kettlewell, M.G.; Souter, R.G.; Vass, A.C.; Crossley, B. Mechanisms of human tumor metastasis studied in patients with peritoneovenous shunts. *Cancer Res* **1984**, *44*, 3584-3592.
4. Latifi, A.; Abubaker, K.; Castrechini, N.; Ward, A.C.; Liongue, C.; Dobill, F.; Kumar, J.; Thompson, E.W.; Quinn, M.A.; Findlay, J.K.; et al. Cisplatin treatment of primary and metastatic epithelial ovarian carcinomas generates residual cells with mesenchymal stem cell-like profile. *J Cell Biochem* **2011**, *112*, 2850-2864, doi:10.1002/jcb.23199.
5. Foster, R.; Buckanovich, R.J.; Rueda, B.R. Ovarian cancer stem cells: working towards the root of stemness. *Cancer Lett* **2013**, *338*, 147-157, doi:10.1016/j.canlet.2012.10.023.
6. Nieto, M.A.; Huang, R.Y.; Jackson, R.A.; Thiery, J.P. Emt: 2016. *Cell* **2016**, *166*, 21-45.
7. Dongre, A.; Rashidian, M.; Reinhardt, F.; Bagnato, A.; Keckesova, Z.; Ploegh, H.L.; Weinberg, R.A. Epithelial-to-Mesenchymal Transition Contributes to Immunosuppression in Breast Carcinomas. *Cancer Res* **2017**, *77*, 3982-3989.
8. Mani, S.A.; Guo, W.; Liao, M.J.; Eaton, E.N.; Ayyanan, A.; Zhou, A.Y.; Brooks, M.; Reinhard, F.; Zhang, C.C.; Shipitsin, M.; et al. The epithelial-mesenchymal transition generates cells with properties of stem cells. *Cell* **2008**, *133*, 704-715.
9. Smith, B.N.; Bhowmick, N.A. Role of EMT in Metastasis and Therapy Resistance. *J Clin Med* **2016**, *5*, doi:10.3390/jcm5020017.
10. Brabletz, T.; Jung, A.; Spaderna, S.; Hlubek, F.; Kirchner, T. Opinion: migrating cancer stem cells - an integrated concept of malignant tumour progression. *Nat Rev Cancer* **2005**, *5*, 744-749.
11. Sacchetti, A.; Teeuwssen, M.; Verhagen, M.; Joosten, R.; Xu, T.; Stabile, R.; van der Steen, B.; Watson, M.M.; Gusinac, A.; Kim, W.K.; et al. Phenotypic plasticity underlies local invasion and distant metastasis in colon cancer. *Elife* **2021**, *10*, doi:10.7554/eLife.61461.
12. Brabletz, S.; Brabletz, T. The ZEB/miR-200 feedback loop--a motor of cellular plasticity in development and cancer? *EMBO Rep* **2010**, *11*, 670-677, doi:10.1038/embor.2010.117.
13. Gyorffy, B.; Lanczky, A.; Szallasi, Z. Implementing an online tool for genome-wide validation of survival-associated biomarkers in ovarian-cancer using microarray data from 1287 patients. *Endocr Relat Cancer* **2012**, *19*, 197-208, doi:10.1530/ERC-11-0329.
14. Qian, J.; Olbrecht, S.; Boeckx, B.; Vos, H.; Laoui, D.; Etlioglu, E.; Wauters, E.; Pomella, V.; Verbandt, S.; Busschaert, P.; et al. A pan-cancer blueprint of the heterogeneous tumor microenvironment revealed by single-cell profiling. *Cell Res* **2020**, *30*, 745-762, doi:10.1038/s41422-020-0355-0.
15. Gupta, P.B.; Fillmore, C.M.; Jiang, G.; Shapira, S.D.; Tao, K.; Kuperwasser, C.; Lander, E.S. Stochastic state transitions give rise to phenotypic equilibrium in populations of cancer cells. *Cell* **2011**, *146*, 633-644, doi:10.1016/j.cell.2011.07.026.
16. Biddle, A.; Liang, X.; Gammon, L.; Fazil, B.; Harper, L.J.; Emich, H.; Costea, D.E.; Mackenzie, I.C. Cancer stem cells in squamous cell carcinoma switch between two distinct phenotypes that are preferentially migratory or proliferative. *Cancer Res* **2011**, *71*, 5317-5326, doi:10.1158/0008-5472.CAN-11-1059.
17. Caramel, J.; Ligier, M.; Puisieux, A. Pleiotropic Roles for ZEB1 in Cancer. *Cancer Res* **2018**, *78*, 30-35, doi:10.1158/0008-5472.CAN-17-2476.

Chapter 6

18. Arumugam, T.; Ramachandran, V.; Fournier, K.F.; Wang, H.; Marquis, L.; Abbruzzese, J.L.; Gallick, G.E.; Logsdon, C.D.; McConkey, D.J.; Choi, W. Epithelial to mesenchymal transition contributes to drug resistance in pancreatic cancer. *Cancer Res* **2009**, *69*, 5820-5828, doi:10.1158/0008-5472.CAN-08-2819.

19. Ren, J.; Chen, Y.; Song, H.; Chen, L.; Wang, R. Inhibition of ZEB1 reverses EMT and chemoresistance in docetaxel-resistant human lung adenocarcinoma cell line. *J Cell Biochem* **2013**, *114*, 1395-1403, doi:10.1002/jcb.24481.

20. Siebzehnrubl, F.A.; Silver, D.J.; Tugertimur, B.; Deleyrolle, L.P.; Siebzehnrubl, D.; Sarkisian, M.R.; Devers, K.G.; Yachnis, A.T.; Kupper, M.D.; Neal, D.; et al. The ZEB1 pathway links glioblastoma initiation, invasion and chemoresistance. *EMBO Mol Med* **2013**, *5*, 1196-1212, doi:10.1002/emmm.201302827.

21. Sakata, J.; Kajiyama, H.; Suzuki, S.; Utsumi, F.; Niimi, K.; Sekiya, R.; Shibata, K.; Senga, T.; Kikkawa, F. Impact of positive ZEB1 expression in patients with epithelial ovarian carcinoma as an oncologic outcome-predicting indicator. *Oncol Lett* **2017**, *14*, 4287-4293, doi:10.3892/ol.2017.6658.

22. Gregory, P.A.; Bert, A.G.; Paterson, E.L.; Barry, S.C.; Tsykin, A.; Farshid, G.; Vadas, M.A.; Khew-Goodall, Y.; Goodall, G.J. The miR-200 family and miR-205 regulate epithelial to mesenchymal transition by targeting ZEB1 and SIP1. *Nat Cell Biol* **2008**, *10*, 593-601, doi:10.1038/ncb1722.

23. Bracken, C.P.; Gregory, P.A.; Kolesnikoff, N.; Bert, A.G.; Wang, J.; Shannon, M.F.; Goodall, G.J. A double-negative feedback loop between ZEB1-SIP1 and the microRNA-200 family regulates epithelial-mesenchymal transition. *Cancer Res* **2008**, *68*, 7846-7854, doi:10.1158/0008-5472.CAN-08-1942.

24. Cittelly, D.M.; Dimitrova, I.; Howe, E.N.; Cochrane, D.R.; Jean, A.; Spoelstra, N.S.; Post, M.D.; Lu, X.; Broaddus, R.R.; Spillman, M.A.; et al. Restoration of miR-200c to ovarian cancer reduces tumor burden and increases sensitivity to paclitaxel. *Mol Cancer Ther* **2012**, *11*, 2556-2565, doi:10.1158/1535-7163.MCT-12-0463.

25. Cochrane, D.R.; Spoelstra, N.S.; Howe, E.N.; Nordeen, S.K.; Richer, J.K. MicroRNA-200c mitigates invasiveness and restores sensitivity to microtubule-targeting chemotherapeutic agents. *Mol Cancer Ther* **2009**, *8*, 1055-1066, doi:10.1158/1535-7163.MCT-08-1046.

26. Hu, X.; Macdonald, D.M.; Huettner, P.C.; Feng, Z.; El Naqa, I.M.; Schwarz, J.K.; Mutch, D.G.; Grigsby, P.W.; Powell, S.N.; Wang, X. A miR-200 microRNA cluster as prognostic marker in advanced ovarian cancer. *Gynecol Oncol* **2009**, *114*, 457-464, doi:10.1016/j.ygyno.2009.05.022.

27. Leskela, S.; Leandro-Garcia, L.J.; Mendiola, M.; Barriuso, J.; Inglada-Perez, L.; Munoz, I.; Martinez-Delgado, B.; Redondo, A.; de Santiago, J.; Robledo, M.; et al. The miR-200 family controls beta-tubulin III expression and is associated with paclitaxel-based treatment response and progression-free survival in ovarian cancer patients. *Endocr Relat Cancer* **2011**, *18*, 85-95, doi:10.1677/ERC-10-0148.

28. Fischer, K.R.; Durrans, A.; Lee, S.; Sheng, J.; Li, F.; Wong, S.T.; Choi, H.; El Rayes, T.; Ryu, S.; Troeger, J.; et al. Epithelial-to-mesenchymal transition is not required for lung metastasis but contributes to chemoresistance. *Nature* **2015**, *527*, 472-476, doi:10.1038/nature15748.

29. Zheng, X.; Carstens, J.L.; Kim, J.; Scheible, M.; Kaye, J.; Sugimoto, H.; Wu, C.C.; LeBleu, V.S.; Kalluri, R. Epithelial-to-mesenchymal transition is dispensable for metastasis but induces chemoresistance in pancreatic cancer. *Nature* **2015**, *527*, 525-530.

30. Cook, D.P.; Vanderhyden, B.C. Context specificity of the EMT transcriptional response. *Nat Commun* **2020**, *11*, 2142, doi:10.1038/s41467-020-16066-2.

31. Teeuwssen, M.; Fodde, R. Cell Heterogeneity and Phenotypic Plasticity in Metastasis Formation: The Case of Colon Cancer. *Cancers (Basel)* **2019**, *11*, doi:10.3390/cancers11091368.

32. Hanahan, D.; Weinberg, R.A. Hallmarks of cancer: the next generation. *Cell* **2011**, *144*, 646-674.

33. Fidler, I.J. The pathogenesis of cancer metastasis: the 'seed and soil' hypothesis revisited. *Nat Rev Cancer* **2003**, *3*, 453-458.

34. Sluiter, N.; de Cuba, E.; Kwakman, R.; Kazemier, G.; Meijer, G.; Te Velde, E.A. Adhesion molecules in peritoneal dissemination: function, prognostic relevance and therapeutic options. *Clin Exp Metastasis* **2016**, *33*, 401-416, doi:10.1007/s10585-016-9791-0.

35. Lambert, A.W.; Pattabiraman, D.R.; Weinberg, R.A. Emerging Biological Principles of Metastasis. *Cell* **2017**, *168*, 670-691.

36. Cai, Q.; Yan, L.; Xu, Y. Anoikis resistance is a critical feature of highly aggressive ovarian cancer cells. *Oncogene* **2015**, *34*, 3315-3324, doi:10.1038/onc.2014.264.

37. Bird, N.C.; Mangnall, D.; Majeed, A.W. Biology of colorectal liver metastases: A review. *J Surg Oncol* **2006**, *94*, 68-80, doi:10.1002/jso.20558.

38. Pretzsch, E.; Bosch, F.; Neumann, J.; Ganschow, P.; Bazhin, A.; Guba, M.; Werner, J.; Angele, M. Mechanisms of Metastasis in Colorectal Cancer and Metastatic Organotropism: Hematogenous versus Peritoneal Spread. *J Oncol* **2019**, *2019*, 7407190, doi:10.1155/2019/7407190.

39. Bolger, A.M.; Lohse, M.; Usadel, B. Trimmomatic: a flexible trimmer for Illumina sequence data. *Bioinformatics (Oxford, England)* **2014**, *30*, 2114-2120.

40. Dobin, A.; Davis, C.A.; Schlesinger, F.; Drenkow, J.; Zaleski, C.; Jha, S.; Batut, P.; Chaisson, M.; Gingeras, T.R. STAR: ultrafast universal RNA-seq aligner. *Bioinformatics (Oxford, England)* **2013**, *29*, 15-21, doi:bts635 [pii] 10.1093/bioinformatics/bts635.

41.. Harrow, J.; Frankish, A.; Gonzalez, J.M.; Tapanari, E.; Diekhans, M.; Kokocinski, F.; Aken, B.L.; Barrell, D.; Zadissa, A.; Searle, S.; et al. GENCODE: the reference human genome annotation for The ENCODE Project. *Genome Res* **2012**, *22*, 1760-1774, doi:22/9/1760 [pii] 10.1101/gr.135350.111.

42. Gentleman, R.C.; Carey, V.J.; Bates, D.M.; Bolstad, B.; Dettling, M.; Dudoit, S.; Ellis, B.; Gautier, L.; Ge, Y.; Gentry, J.; et al. Bioconductor: open software development for computational biology and bioinformatics. *Genome Biol* **2004**, *5*, R80, doi:gb-2004-5-10-r80 [pii] 10.1186/gb-2004-5-10-r80.

43. Love, M.I.; Huber, W.; Anders, S. Moderated estimation of fold change and dispersion for RNA-seq data with DESeq2. *Genome Biol* **2014**, *15*, 550, doi:s13059-014-0550-8 [pii] 10.1186/s13059-014-0550-8.

44. Benjamini, Y.; Hochberg, Y. Controlling the False Discovery Rate: A Practical and Powerful Approach to Multiple Controlling the False Discovery Rate. . *Journal of the Royal Statistical Society.* **1995**, *57*, 289-3000, doi:https://doi.org/10.2307/2346101.

45. Meinders, M.; Kulu, D.I.; van de Werken, H.J.; Hoogenboezem, M.; Janssen, H.; Brouwer, R.W.; van Ijcken, W.F.; Rijkers, E.J.; Demmers, J.A.; Kruger, I.; et al. Sp1/Sp3 transcription factors regulate hallmarks of megakaryocyte maturation and platelet formation and function. *Blood* **2015**, *125*, 1957-1967, doi:blood-2014-08-593343 [pii]

Chapter 6

Supplementary figures
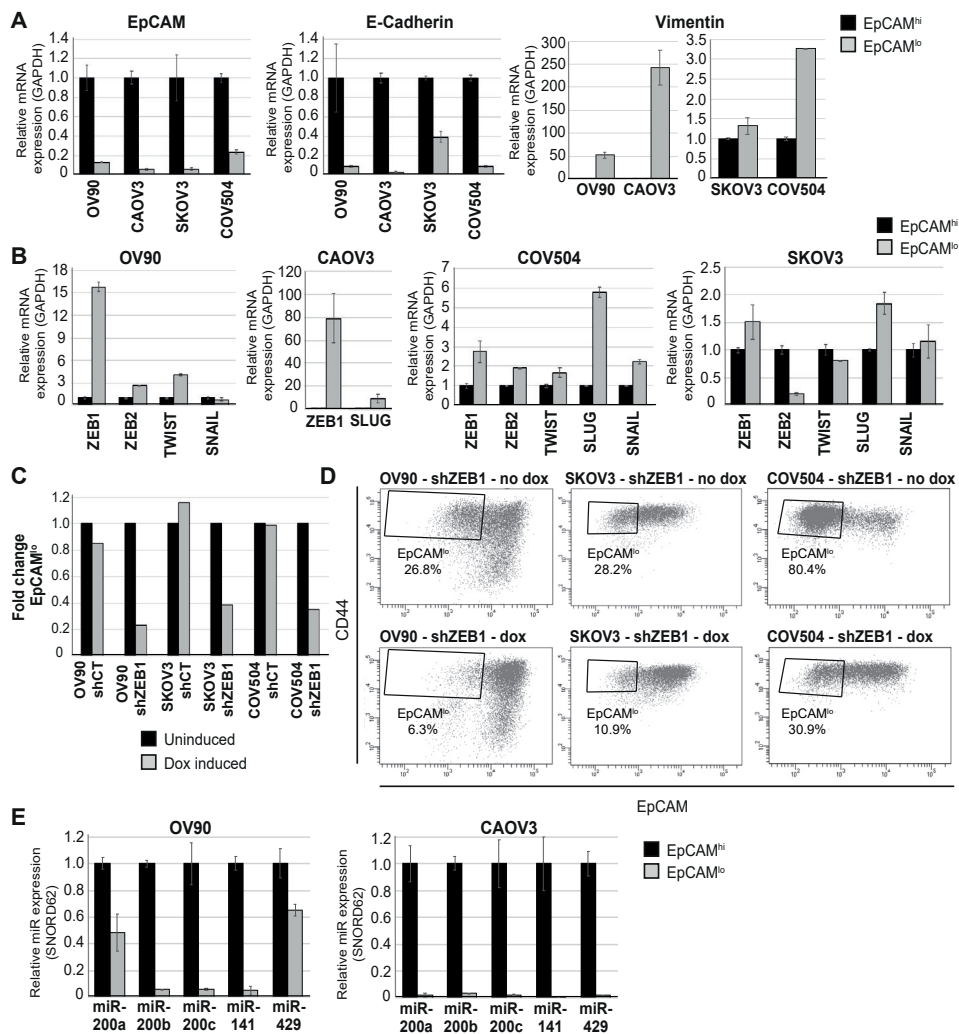
Figure 1 – supplement 1. (**a**) RT-qPCR expression analysis of epithelial (*EPCAM* and *CDH1*) and mesenchymal (*VIM*) markers in sorted EpCAM^hi (black bars) and EpCAM^lo (grey bars) from the OV90, CAOV3, SKOV3 and COV504 lines. *GAPDH* was employed for normalization purposes. Each bar represents the mean ± SD. (**b**) RT-qPCR expression analysis of EMT transcription factors (*ZEB1, ZEB2, TWIST, SLUG* and *SNAIL*) in EpCAM^hi (black bars) EpCAM^lo (grey bars) cells. *GAPDH* was employed for normalization. Each bar represents the mean ± SD. (**c**) qRT-PCR expression analysis of *ZEB1* in OV90, SKOV3 and COV504 transduced with an inducible control (shCT) or ZEB1-shRNA (shZEB1) construct. shRNA expression was induced with 1 µg/mL of doxycycline. Each bar represents the mean ± SD. (**d**) Flow cytometric analysis of OV90, SKOV3 and COV504 shCT- and shZEB1-transfected cell lines using antibodies against CD44 and EpCAM. Cells were induced with 1 µg/mL doxycycline for 72 hrs. before analysis. (**e**) RT-qPCR expression analysis of the members of the miRNA 200 family (miR-200a, miR-200b, miR-200c, miR-141 and miR-429) in EpCAM^hi (black bars) and EpCAM^lo (grey bars) cells. Left panel: OV90. Right panel: SW480. *U6* was employed for normalization. Each bar represents the mean ± SD.
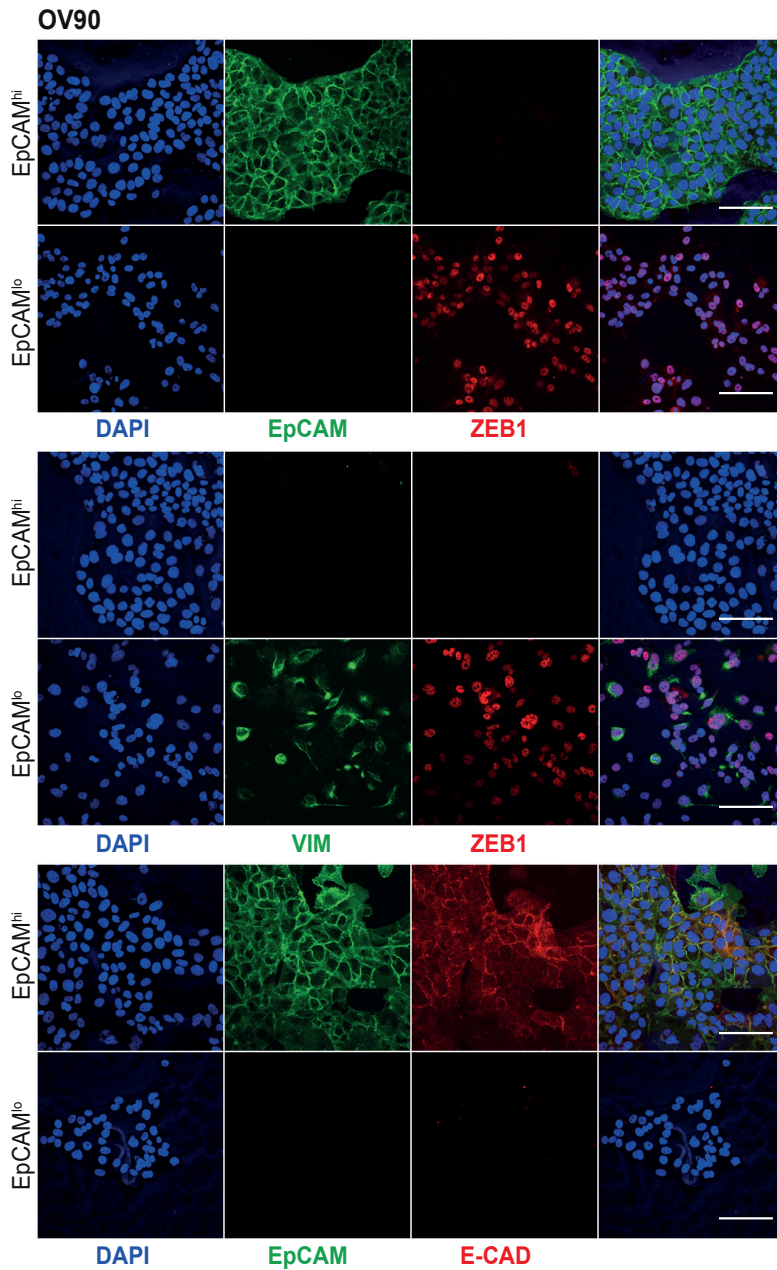
Figure 1 – supplement 2. Immunofluorescence (IF) analysis EpCAM^{hi} and EpCAM^{lo} cells. Cells were sorted and directed plated on cover slips. After four days cells were fixed with 4% PFA and stained with antibodies against EpCAM (green) and ZEB1 (red; upper panel), Vimentin (green) and ZEB1 (red; middle panel), and EpCAM (green) and E-cadherin (red; lower panel). Nuclei were visualized by DAPI staining of DNA (blue). Scale bar: 50 µm.
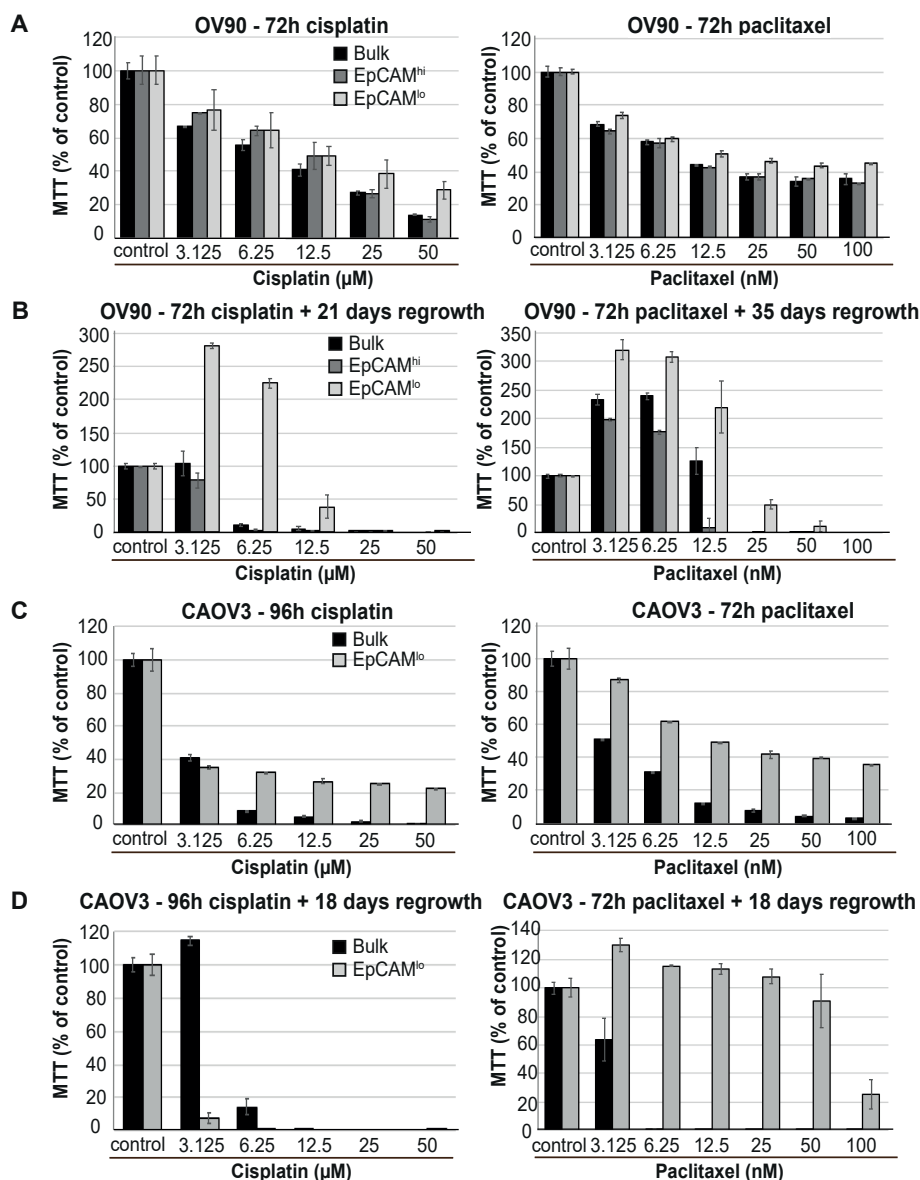
Figure 1 – supplement 3. (**a-d**) Bulk, EpCAM[hi] and EpCAM[lo] OV90 and bulk and EpCAM^{lo} CAOV3 cells were sorted and plated to recover and expand for four days. 10[5] cells per well were plated in a 96-well plate and left to attach. After 24 h, standard cell culture medium was changed for medium containing chemotherapeutic drug cisplatin or oxaliplatin. OV90 cells were left with cisplatin or paclitaxel for 72 hours, COAV3 for 96 hours. After removal of the chemotherapeutic drug, cells were washed with PBS and left to re-grow in standard culture medium. Cell viability was assessed using the MTT upon removal of the drug, and after re-growth (ranging 18-35 days). O.D. reading was performed at 595 nm with a Microplate Reader. Background measurements were subtracted from each data point. All experiments were performed at least in duplicate for each individual cell line and drug. (**a-b**). Chemo sensitivity assays using cisplatin (**a**) or paclitaxel (**b**) in bulk (black bars), EpCAM[hi] (dark grey bars) and EpCAM[lo] (light grey bars) OV90 cells. (**c-d**) Chemo sensitivity assays using cisplatin (**c**) or paclitaxel (**d**) in bulk (black bars) and EpCAM[lo] (grey bars) CAOV3 cells.

Upregulated in OV90, CAOV3, HCT116, SW480

ZEB1

Upregulated in ovarian cancer cell lines: OV90 en CAOV3

ZEB1	VIM	PTGS2	IL6	NCAM1	NLRP1	TFPI2	FAM20A	RBM24	COL7A1
EMP1	AMIGO2	STC1	BDNF	F2R	EVI2B	DIO2			

Upregulated in colon cancer cell lines: HCT116 en SW480

ZEB1	SPARC	SUSD2	LIMS2	TGFB2	SYDE1	CNTNAP3	RGS5	HMCN1	CTNAP3B

Downregulated in OV90, CAOV3, HCT116, SW480

CDH1	ESRP1	EPCAM	PRSS22	LAMA3	LAMC2	BSPRY	AP1M2	MARVELD3	EPHA1
ST14	LAD1	CCDC64B	TMC4	KDF1	TMEM125	PKP3	C1orf210		

Downregulated in ovarian cancer cell lines: OV90 en CAOV3

CDH1	ESRP1	EPCAM	OVOL2	PRSS22	PRSS8	MSM01	LAMA3	PLEKHH1	LAMC2
COL17A1	LLGL2	LRP2	BIK	ELMO3	FA2H	TJP3	HPN	DTX4	MVK
SCNN1A	WWC1	TFCP2L1	ITGB6	FBXO2	IRF6	PPL	BSPRY	XG	RAB17
MT1G	SH2D3A	PRRG2	AP1M2	CRB3	TNS4	ITGB4	INADL	HOOK1	WNT10A
CTSV	TMPRSS4	MARVELD3	GRB7	FBN3	DCDC2	EPHA1	ST14	IGSF10	MAPK13
KRTCAP3	F11R	LAD1	CD3G	CCDC64B	TRIM17	CAPN13	CDS1	MST1R	ELOVL7
SPINT1	TMC4	SPINT2	FAM83B	NPNT	CDC42BPG	KRT19	P2RY6	DHCR7	GOLT1A
KDF1	PLEKHD1	MYO1D	ERICH5	ZNF114	TMEM125	B3GNT3	HIST1H2BC	C1orf116	RIPK4
PKP3	MFSD6L	MARC1	INSIG1	C6orf132	S100A14	LAMB3	ZNF165	DENND1C	ARHGAP8
C1orf210	EPPK1	C2orf15							

Downregulated in colon cancer cell lines: HCT116 en SW480

CDH1	ESRP1	EPCAM	MAL2	PRSS22	LAMA3	LAMC2	CDH3	AIM1	GALNT3
BSPRY	AP1M2	KLK10	MAP7	MARVELD3	EPHA1	ST14	ACOXL	LAD1	CCDC64B
SYK	TMC4	KDF1	ALOXE3	TMEM125	CLDN7	MACC1	PKP3	C1orf210	

Figure 2 – Supplement 1. Gene list of commonly differentially expressed genes in EpCAM[lo] versus EpCAM^{hi} cells in colon cancer cell lines HCT116 and SW480, and ovarian cancer cell lines OV90 and CAOV3. A total of 152 and 353 differentially regulated genes were identified between the CD44^{hi}EpCAM^{hi} and CD44^{hi}EpCAM^{lo} cells in HCT116 and SW480, respectively; and 509 and 778 differentially regulated genes were identified between the EpCAM^{hi} and EpCAM[lo]/bulk cells in OV90 and CAOV3, respectively (*P. adjusted* < 0.01, when applying a Log_2 fold change of < -1.5 and > 1.5).

Chapter 6

Figure 2 – Supplement 2. (**a**) Principal component analysis of HCT116, SW480, OV90 and CAOV3 cells based on the variable expressed genes across EpCAM^lo and EpCAM^hi populations. (**b**) Heatmap showing PID pathways of differentially expressed genes between EpCAM^lo and EpCAM^hi populations in HCT116, SW480, OV90 and CAOV3 cell lines using Gene Set Variation.
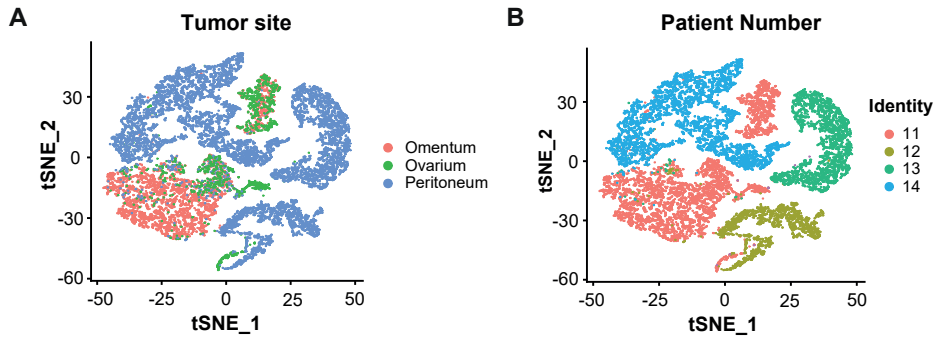
Figure 3 – supplement 1. (**a**) tSNE of gene expression of ovarian cancer cells based on different tumor sites. (**b**) tSNE of gene expression of individual tumor cells marked per individual ovarian cancer patient.
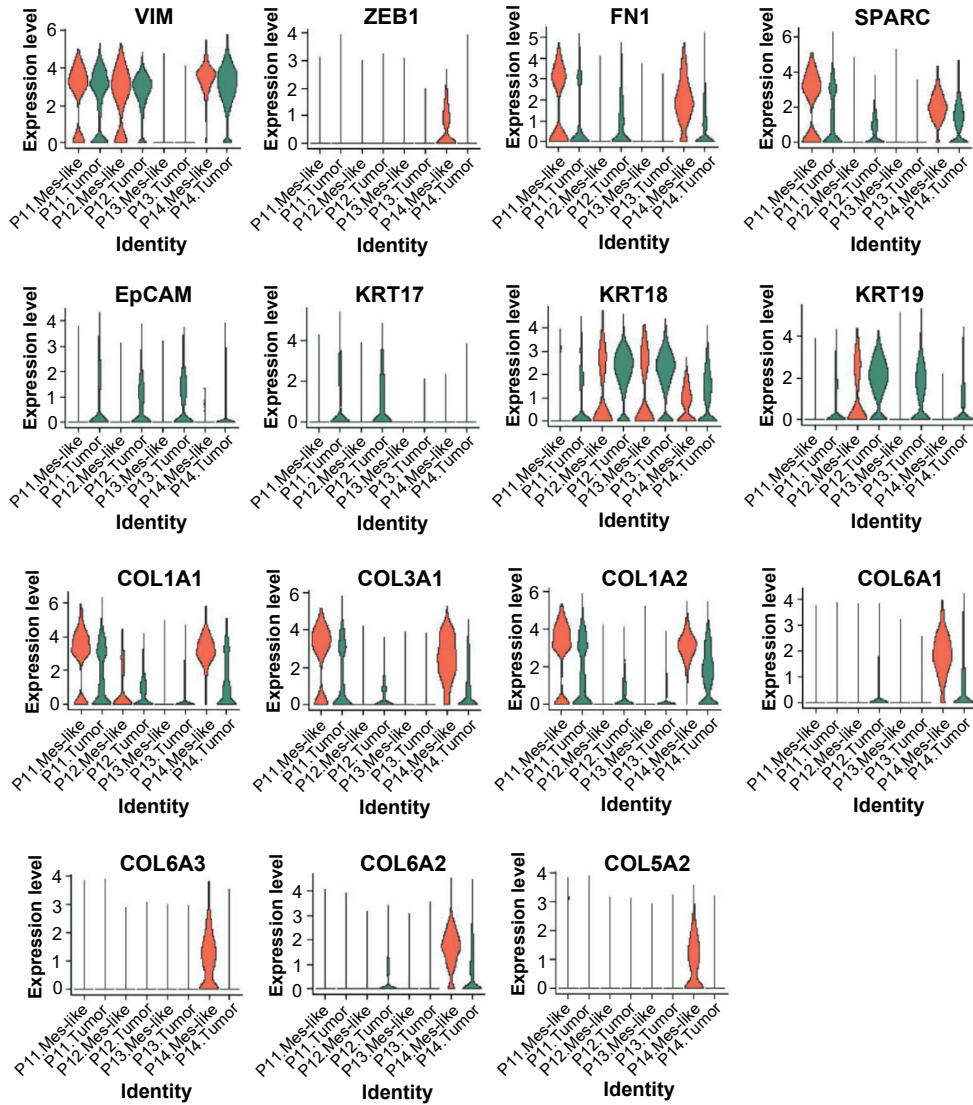
Chapter 6

Figure 3 – supplement 2. Violin plots of tumor and mesenchymal-like tumor cells (obtained from figure 4D) showing expression patterns across different genes.

CHAPTER VII

7

A dual role for Wnt signaling in high-grade serous ovarian cancer

Teeuwssen M.J., Chen T., Verhagen M.*, Joosten R., Sacchetti A., van Royen M., Fodde R.

Abstract

Epithelial ovarian cancer (EOC) is the leading cause of death amongst gynecologic malignancies. EOC is an extremely heterogeneous disease being subdivided into low-grade serous, mucinous, clear cell, endometrioid, high-grade serous and undifferentiated carcinomas. The Wnt/β-catenin signaling pathway is known to regulate stemness in a broad spectrum of stem cell niches including the ovary. Additionally, alterations in members of the Wnt cascade have been reported in endometrioid ovarian cancers. Next to that, constitutive Wnt signaling activation has been observed in other histotypes, including high grade serous ovarian cancers, even in the absence of mutations in Wnt-related genes. Importantly, the increased activation of Wnt signaling has shown to correlate with, tumor grade, resistance to chemotherapy, and poor prognosis in patients with ovarian carcinomas.

Unique for ovarian cancer is the 'transcoelomic' dissemination of tumor cells and the formation of ascites fluid in the abdominal and pelvic cavity. Malignant ascites provides a favorable tumor microenvironment (TME) enriched in secreted inflammatory cytokines, growth factors, and extracellular macromolecules such as collagen, fibronectin, and laminin interfering with the peritoneal barrier and thereby creating a favourable premetastatic environment beneficial for peritoneal metastasis of ovarian cancer. The role of Wnt signaling in this process has been unknown.

Here, we present experimental evidence for the dual role of Wnt signaling in regulating metastasis formation in high grade serous ovarian cancer. We show that the Wnt signaling cascade establishes and regulates quasi-mesenchymal cellular phenotypes through activation of the EMT transcription factor *ZEB1*. Moreover, our results suggest that Wnt participates in the establishment of pre-metastatic niches in the abdominal cavity through exosome-mediated ligand secretion from primary ovarian cancer cells.

Keywords: ovarian cancer, Wnt signaling, EMT, pre-metastatic niche, exosomes

Abstract

Introduction

Epithelial ovarian cancer (EOC) is the leading cause of death amongst gynecologic malignancies [1] as it generally manifests at advanced disease stages, i.e. when metastases have already spread to pelvic organs (stage II), the abdomen (stage III), or beyond the peritoneal cavity (stage IV) [2].

EOC is an extremely heterogeneous disease. Based on the molecular alterations underlying the deregulation of signal transduction pathways involved in DNA repair, cell proliferation, apoptosis, cell adhesion and motility, two major types of ovarian cancers have been discerned [3]. Type I tumors are slow growing, mostly restricted to the ovary and thought to arise from well-differentiated precursor lesions called "borderline" tumors. They are further subdivided into low-grade serous, mucinous, clear cell, and endometrioid subtypes. Type I lesions frequently carry mutations in *KRAS*, *BRAF*, *PTEN* and *CTNNB1* (β-catenin) and often show a relatively stable karyotype. Type II ovarian cancers instead include high-grade serous (HGS) and undifferentiated carcinomas characterized by frequent mutations in *TP53* and by genomic instability [3].

The Wnt/β-catenin signaling pathway is known to regulate stemness in a broad spectrum of stem cell niches including the ovary. Accordingly, it is also thought to play an important role in ovarian cancer [4]. In normal physiological circumstances, the Wnt signaling pathway is activated by the binding of secreted Wnt ligands to cell-surface receptors leading to the stabilization and subsequently accumulation of β-catenin in the cytoplasm. Eventually, β-catenin translocates into the nucleus where it interacts with members of the T-cell specific transcription factor/lymphoid enhancer binding factor (TCF/LEF) family of transcription factors thus modulating the expression of a broad spectrum of target genes regulating, among others, stemness, proliferation, and differentiation [5]. In the absence of Wnt ligands, a multi-protein destruction complex encompassing protein phosphatase 2A (PP2a), glycogen synthase kinase 3 (GSK3β), casein kinase 1α (CK1α), and the scaffold proteins adenomatous polyposis coli (APC) and AXIN1/2, targets intracellular β-catenin for its ubiquitination and subsequent degradation by the proteasome [5].

To date, mutations in β-catenin or, less frequently, in other members of the Wnt cascade including *APC*, *AXIN1*, and *AXIN2*, have been consistently reported in endometrioid ovarian cancers (16-54% of the cases) though not in other subtypes [6,7]. However, constitutive Wnt signaling activation as indicated by alterations in β-catenin subcellular localization (i.e., nuclear and/or cytoplasmic vs. membrane-bound) is observed in a broader spectrum of histotypes including high grade serous ovarian cancers, even in the absence of mutations in Wnt-related genes [8-10]. Of note, increased Wnt activity was shown to correlate with tumor grade [11], resistance to chemotherapy [12], and poor prognosis [13] in patients with ovarian carcinomas. Based on these observations, whereas Wnt signaling activation is likely to play an early (initiating or promoting) role in the endometrioid ovarian cancer subset, its involvement in other more commonly occurring high-grade histotypes seems to affect later disease stages.

Among the broad spectrum of its downstream effectors, activation of the Wnt/β-catenin pathway has been shown to elicit epithelial-to-mesenchymal transition (EMT) in different types of malignancies [14-18], including ovarian cancer [4,6,19-22]. EMT is a developmental program exploited by malignant cells to reversibly shift from an epithelial state with apical-basal polarity and cell–cell adhesions, to a more motile mesenchymal

Chapter 7

phenotype with spindle like morphology and front-back-end polarity [23]. In addition to the motile and invasive characteristics of the mesenchymal state, EMT is functionally linked to the acquirement of stem-like features, resistance to therapy, and immune suppression [24-26]. The reversible nature of EMT is crucial as mesenchymal-to-epithelial transitions (MET) allow metastasizing cancer (stem-like) cells to regain proliferative and epithelial characteristics to colonize distant organ site [14,23].

Next to the EMT/MET programs which allow cancer cells to disseminate and metastasize, the establishment of pre-metastatic niches is also thought to be critical for circulating tumor cells to efficiently engraft at distant organ site [27-29]. Factors secreted by primary carcinomas lead to the establishment of pre-metastatic niches encompassing a specialized and favorable micro-environment that enables colonization and promotes survival and outgrowth of metastasizing cancer cells [28]. The involvement of premetastatic niches in ovarian cancer has been suggested in several studies [30,31]. Among other pathways, Wnt signaling has been proposed to play a role in pre-metastatic niche formation [28]. Recent studies have demonstrated that Wnt ligands can be transported across tissues by exosomes [32-35], i.e. the small extracellular vesicles thought to play a key role in the formation of pre-metastatic niches, as they act as important mediators in cell-cell communication carrying molecules such as micro RNAs, mRNAs, and both membrane-bound and secreted proteins [36]. Numerous studies have demonstrated the presence of exosomes in ovarian cancer cell line cultures and in patient-derived serum and ascites [37]. Last, ovarian cancer exosomes have been shown to participate in the establishment of pre-metastatic niches [31,38].

Here, we present experimental evidence for the dual role of Wnt signaling in regulating metastasis formation in high grade serous ovarian cancer. We show that the Wnt signaling cascade establishes and regulates quasi-mesenchymal cellular phenotypes through activation of the EMT transcription factor *ZEB1*. Moreover, our results suggest that Wnt participates in the establishment of pre-metastatic niches in the abdominal cavity though exosome-mediated ligand secretion from primary ovarian cancer cells.

Results

Effects of paracrine Wnt stimulation on Ovarian Cancer Cells

As mentioned above, mutations in Wnt-related genes are in general extremely rare in most ovarian cancer histotypes with the notable exception of endometrioid tumors [6]. However, even in the absence of specific mutations, Wnt signaling has been reported to be frequently activated in the more common serous histotype, as indicated by nuclear and cytoplasmic β-catenin subcellular localization [8-11]. As shown in **Figure 1A**, β-catenin IHC analysis of primary human high grade ovarian cancer tissue is indicative of Wnt signaling activation at the invasive front, as marked by the nuclear β-catenin. In agreement with our previous observations in colon cancer [15], increased ZEB1, a transcription factor associated with EMT, expression is seen at this site.

To better understand the underlying mechanisms and the functional consequences of Wnt signaling activation in ovarian cancer, we first analyzed a panel of ovarian cancer cell lines of different histologic origins by TOP-Flash reporter assays [39,40]. Overall, the results reveal constitutive activation of Wnt signaling in 6 out of 37 ovarian cancer cell lines (**Figure 1B**). Notably, constitutive Wnt activation was found in cell lines from each of

the subtypes represented in the panel. Moreover, supplementation of the culture medium with Wnt3a conditioned medium (Wnt3a-CM) resulted in a more than two-fold induction of Wnt activity in 32 out of 37 ovarian cancer cell lines (ranging 2.0-170 fold), compared to control HEK293-cells (**Figure 1C**).

A

anti-β-catenin   anti-ZEB1

B

C
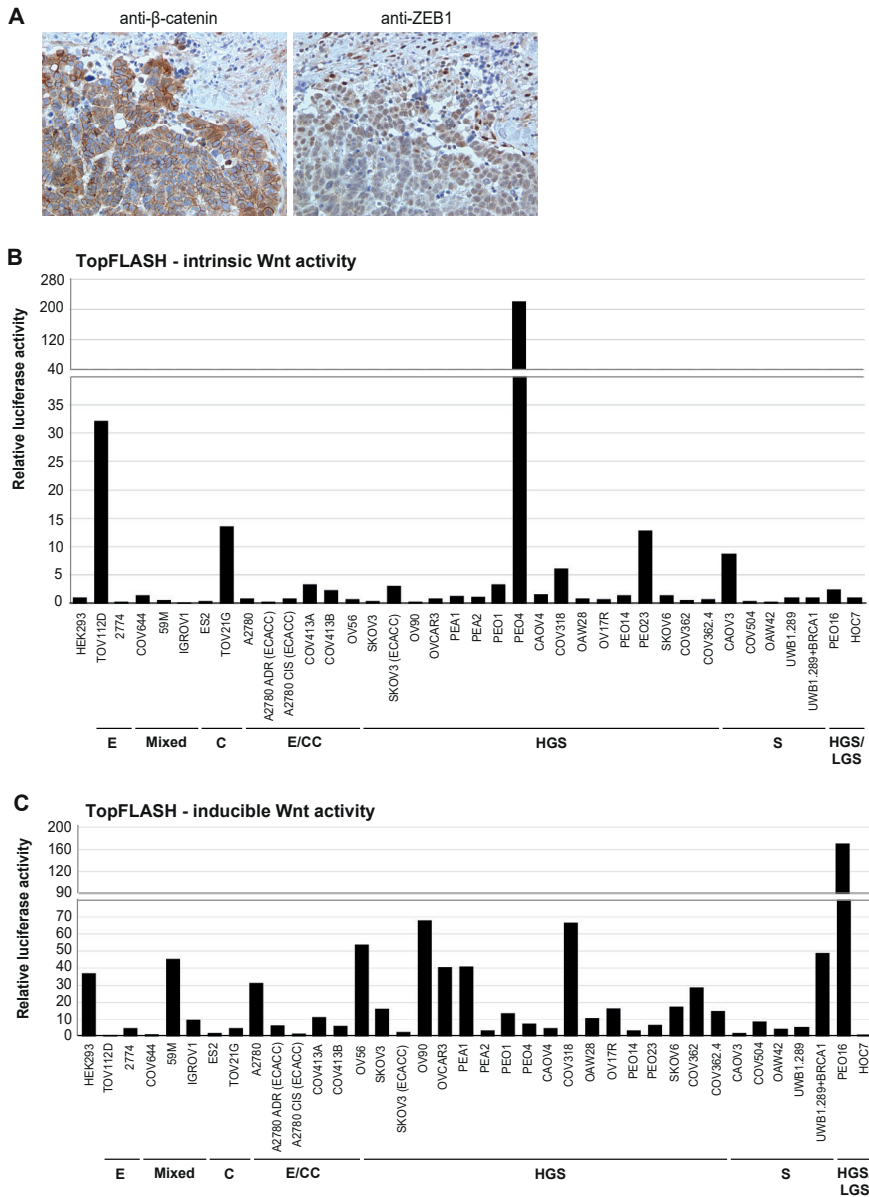
**Figure 1.** (**a**) IHC analysis with antibodies directed against β-catenin and ZEB1 in consecutive sections of an ovarian cancer patient. Scale bar100 μm. (**b**) Graph displaying the constitutive activation of Wnt signaling in a panel of 37 ovarian cancer cell lines of different histologic origins. Ovarian cancer cells were plated on 48-well dishes. When 70% confluence was reached, cells were transfected by Fugene

HD (Promega) with 125 ng of the TOP-Flash or FOP-Flash reporter constructs together with 25 ng of the Renilla luciferase vector for normalization purposes. Luciferase activity was measured using the Dual-Luciferase Reporter Assay System (Promega) 24 hrs. post-transfection. Luminescence was measured using a GloMax Luminometer. (**c**) Graph showing the induction of Wnt signaling in ovarian cancer cell lines using TOP-Flash reporter assays. Ovarian cancer cells were plated on 48-well dishes and cultured in a Wnt3a conditioned medium. The induction was measured by comparing the fold induction with ovarian cancer cells treated with control L-cell conditioned medium. HEK293 was used as a control.

To evaluate the specific effects exerted by Wnt signaling on ovarian cancer cells, we employed the OV90, SKOV3 and COV504 cells lines in colony forming assays and evaluated their clonogenicity and growth characteristics in the presence of Wnt3a-CM. An 8, 10, and 1.25-fold increase in the number of colonies was observed OV90, SKOV3 and COV504 cells cultured in Wnt3a-CM, respectively (**Figure 2A**).

The same analysis performed on the immortalized mouse ovarian cell lines STOSE [41] and ID8 [42] and demonstrated a 7.5 and 10-fold increase in number of colonies upon Wnt stimulation (**Figure 2A**). Moreover, when cultured in suspension in Wnt3a-CM, STOSE cells form larger spheres at significantly increased multiplicity when compared with the control medium (**Figure 2B**). IHC analysis of the spheres confirmed by the nuclear translocation of β-catenin in the Wnt3a-CM culture conditions (**Figure 2C**). Self-renewal was assessed by serial passaging in suspension and by plating each passage in agarose to quantify sphere formation and multiplicity. Enhanced self-renewal was observed in both STOSE and ID8 cell when grown in Wnt3a-CM (**Figure 2D**). Notably, upon exposure to the Wnt3a-CM for 24 hours, the *Lgr5* and *Axin2* genes were specifically upregulated (**Figure 2E**). This is of relevance as the *Lgr5* gene was also shown to earmark normal embryonic and neonate populations as stem/progenitor cells contributing to the development of the ovarian surface epithelial lineage, as well as epithelia of the mesovarian ligament and oviduct/fibria [43]. Hence, Wnt signaling activation and stemness are likely to be functionally related in normal and malignant ovarian cells. Accordingly, the, Wnt-inhibitors niclosamide and LGK-974 abrogated *Lgr5* and *Axin2* upregulation in both STOSE and ID8 (**Figure 2F**).

Our recent analysis of EpCAM^{lo} cells in colon cancer has revealed a key role for enhanced Wnt signaling activation upstream of *ZEB1*/EMT in the establishment and maintenance of these invasive and quasi-mesenchymal malignant cells [15]. As shown in the **Appendix** to Chapter V of this thesis, ovarian cancer cell lines show similar EpCAM$^{lo/hi}$ subpopulations with distinct quasi-mesenchymal and epithelial features. In order to assess the role played by Wnt in the establishment of the EpCAM^{lo} subpopulation in ovarian cancer cell lines, we first cultured OV90, SKOV3, and COV504 in the presence of Wnt3a-conditioned medium (Wnt3a-CM; **Figure 3A**) or supplemented with the GSK3β inhibitor Chiron (OV90 only; **Figure 3B**). As shown in **Figure 3C**, FACS analysis of Chiron- and Wnt3a-CM stimulated cells showed a 2-fold increase of the EpCAM^{lo} subpopulation in OV90, though not in of SKOV3 and COV504 (data not shown). In addition, RTqPCR analysis of ovarian cancer cells cultured in Wnt3a-CM showed moderate down-regulation of *ECAD* and a pronounced increase of *VIM* and *ZEB1* expression in OV90 and COV504 though not in SKOV3 (**Figure 3D**).
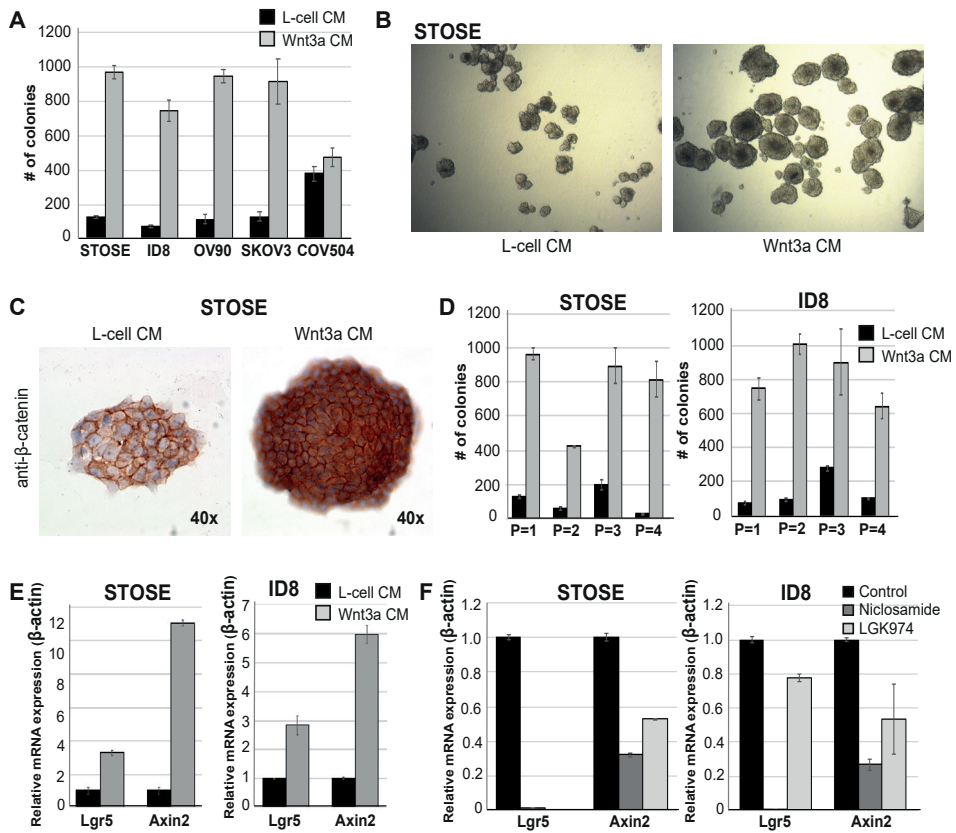
Figure 2. (**a**) Colony forming assay evaluating the proliferation and self-renewal of murine ovarian cancer cell lines STOSE and ID8 and human ovarian cancer cell lines OV90, SKOV3 and COV504 in absence (black bar) or presence (grey bar) of Wnt stimuli. (**b**) Phase contrast microscopy images of sorted STOSE cells cultured in suspension (in ultra-low attachment culture dishes) in presence and absence of Wnt3A conditioned medium. (**c**) IHC analysis with antibodies directed against β-catenin sections derived from STOSE spheroids derived from suspension cultures in presence or absence of Wnt3a conditioned medium. (**d**) Serial passaging and colony forming assay of STOSE and ID8 cells evaluating the proliferation and self-renewal of murine ovarian cancer cell lines STOSE and ID8 in presence or absence of Wnt stimuli. Cells were serially passaged in suspension and plated each passage in agarose to better evaluate sphere formation and multiplicity. Black bar: L-cell conditioned medium; grey bar: Wnt3a conditioned medium. Each bar represents the mean ± SD. (**e**) RT-qPCR expression analysis of stem cell marker *Lgr5* and Wnt target gene *Axin2* of STOSE and ID8 comparing cells cultured in L-cell conditioned medium (black bar) or Wnt3a conditioned medium (grey bars) treated cultures. *Actb* was employed for normalization. Each bar represents the mean ± SD. (**f**) RT-qPCR expression analysis of stem cell marker *Lgr5* and Wnt target gene *Axin2* of STOSE and ID8 treated with Wnt-inhibitors niclosamide (dark grey bars) or LGK-974 (light grey bars). *Actb* was employed for normalization. Each bar represents the mean ± SD.

Chapter 7
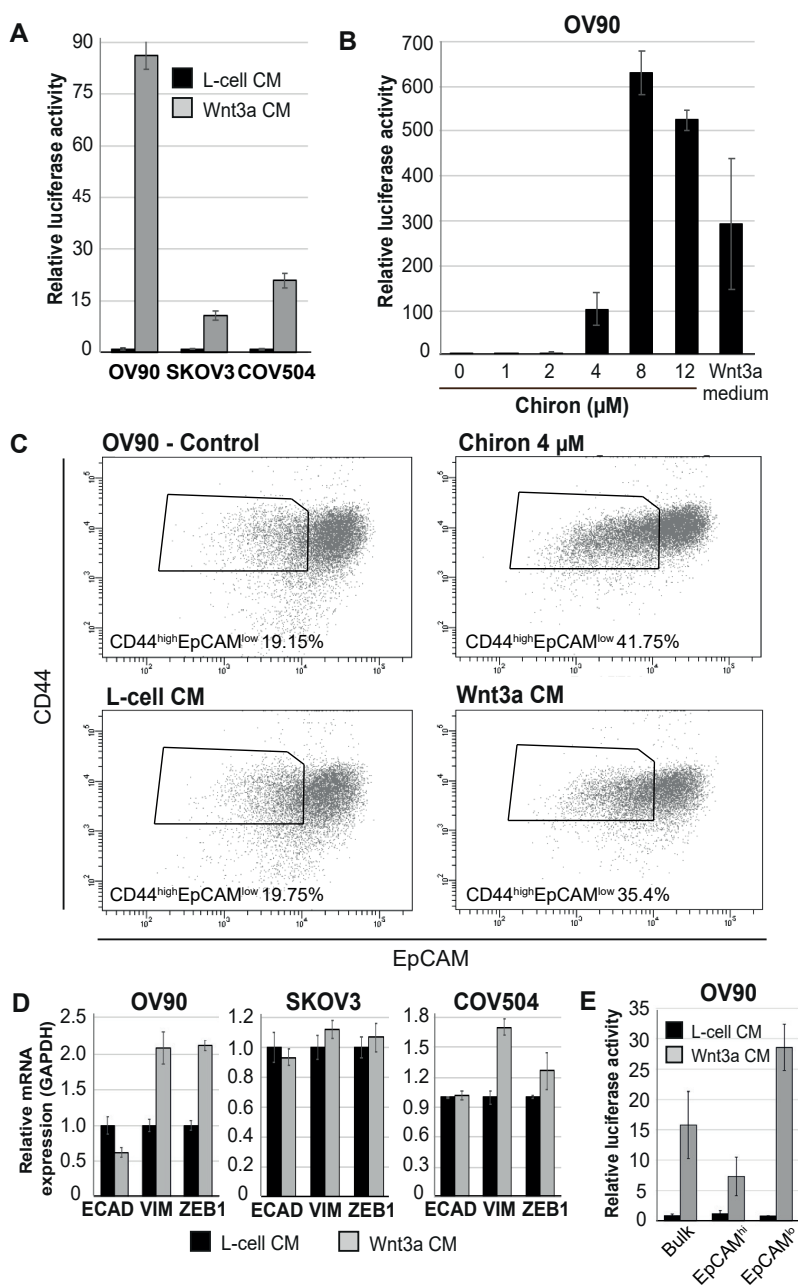
Figure 3. (**a**) TOP-Flash luciferase reporter analysis of Wnt signaling activity in ovarian cancer cell lines OV90, SKOV3 and COV504 upon treatment with Wnt3a conditioned medium. Each bar represents the mean ± SD. (**b**) TOP-Flash luciferase reporter analysis of Wnt signaling activity in OV90 upon treatment with different concentrations of Chiron for 48 hours. Each bar represents the mean ± SD. (**c**) Flow cytometric analysis of OV90 cells using antibodies directed against CD44 and EpCAM. Cells were cultured for 48 hours in L-cell conditioned medium, Wnt3a conditioned medium, standard medium and 4 µM Chiron before the analysis. Graphs show percentage of cells within the EpCAM^{hi} and EpCAM^{lo}

gates relative to the control. Each bar represents the mean ± SD. (**d**) RT-qPCR expression analysis of EMT markers (ECAD and VIM) and transcription factor ZEB1 in L-cell CM (black bar) and Wnt3a CM (grey bars) treated cultures. GAPDH was employed for normalization. Each bar represents the mean ± SD. (**e**) Top-Flash reporter assay to measure Wnt signaling activity in sorted bulk, EpCAM^{hi} and EpCAM^{lo} OV90 cells cultured in either L-cell or Wnt3a conditioned medium.

Enhanced Wnt induction was observed in sorted EpCAM^{lo} cells relative to EpCAM^{hi} and bulk OV90 cells, suggestive of the differential presence of Wnt-related receptors between subpopulations of HGS ovarian cancer cells (**Figure 3E**). However, RTqPCR expression analysis of Frizzled, R-spondins, and the LGR genes did not reveal significant differences between EpCAM^{hi} and EpCAM^{lo} OV90 cells (data not shown).

Overall, these results show that ovarian cancer cells of different histotypes are capable of responding to external Wnt cues by activating the canonical pathway. In a subset of HGS cell lines, Wnt stimulation results in increased self-renewal and EMT. In view of the apparent lack of somatic mutations in known members of the Wnt pathway among type II (HGS) ovarian cancers [4] and of the observed consequences of its activation in mouse and human ovarian cells, it is likely that Wnt signaling plays a role as a paracrine factor possibly in later stages of HGS ovarian cancer progression and dissemination.

Ovarian cancer ascites fluid stimulates Wnt signaling in paracrine fashion and underlies spheroid formation and self-renewal in ovarian cancer cell lines

More than one third of ovarian cancer patients present with malignant ascites at diagnosis, and almost all have ascites at recurrence. Malignant ascites provides a favorable tumor microenvironment and consists of a heterogenous composition of cells and a complex mixture of soluble factors which provide a pro-inflammatory and tumor-promoting microenvironment [44]. To investigate whether ascites represent the source of paracrine Wnt activation in ovarian cancer, we collected and centrifuged ascites from 22 patients, and employed the supernatant in TCF/Wnt reporter TopFLASH experiments with L cells. Overall, the results showed a more than two-fold induction of Wnt activity in 15 out of 22 ovarian cancer patients (ranging 2.5-45.1-fold), compared to control L-cell CM (**Figure 4A**). Exogenous ligands, either secreted in the ascitic fluids and/or incorporated in extracellular vesicles such as exosomes are the most likely sources of the observed Wnt stimulation.

Numerous studies have shown the presence of exosomes in ovarian cancer cell cultures, patient-derived serum, and malignant ascites [37,45-47]. Exosomes can be isolated from the supernatant of cultured cells or biological fluids by differential centrifugation [48]. They often carry molecules such as microRNAs, mRNAs, and both membrane-bound and secreted proteins [36]. As previous published by Gross et al. (2006), exosomes containing Wnt3a ligands can be derived from Wnt3a-CM by ultracentrifugation at 100,000*g*; likewise control exosomes can be derived from control L-cells [33]. We generated positive and negative exosome controls from the L-cell and Wnt3a conditioned media and evaluated their relative purity. Transmission electron microscopy (TEM) showed the presence of cup-shaped structures of 40-100 nm in 100,000*g* pellets derived from L-cell and Wnt3a CM (**Figure 4 - Supplement 1A**). Western blot analysis confirmed the presence of exosomal markers Alix, Tsg101, HSC90 and CD9 in both L-cell and Wnt3a CM derived post-100,000*g* pellets, whereas contaminating protein markers, here employed to exclude contaminations with vesicles derived from other compartments, such as calnexin, an

endoplasmic reticulum marker, and tubulin, a cytoskeletal marker, were absent (**Figure 4 - Supplement 1B**). Last, qNano analysis was performed to measure particle size and confirmed the existence of particles ranging from 40 to 100 nm in diameter in the extracted post-100,000*g* pellet (**Figure 4- Supplement 1C**). These quality control experiments confirm the purification of exosomes from L-cell and Wnt3a conditioned medium by ultra-centrifugation.
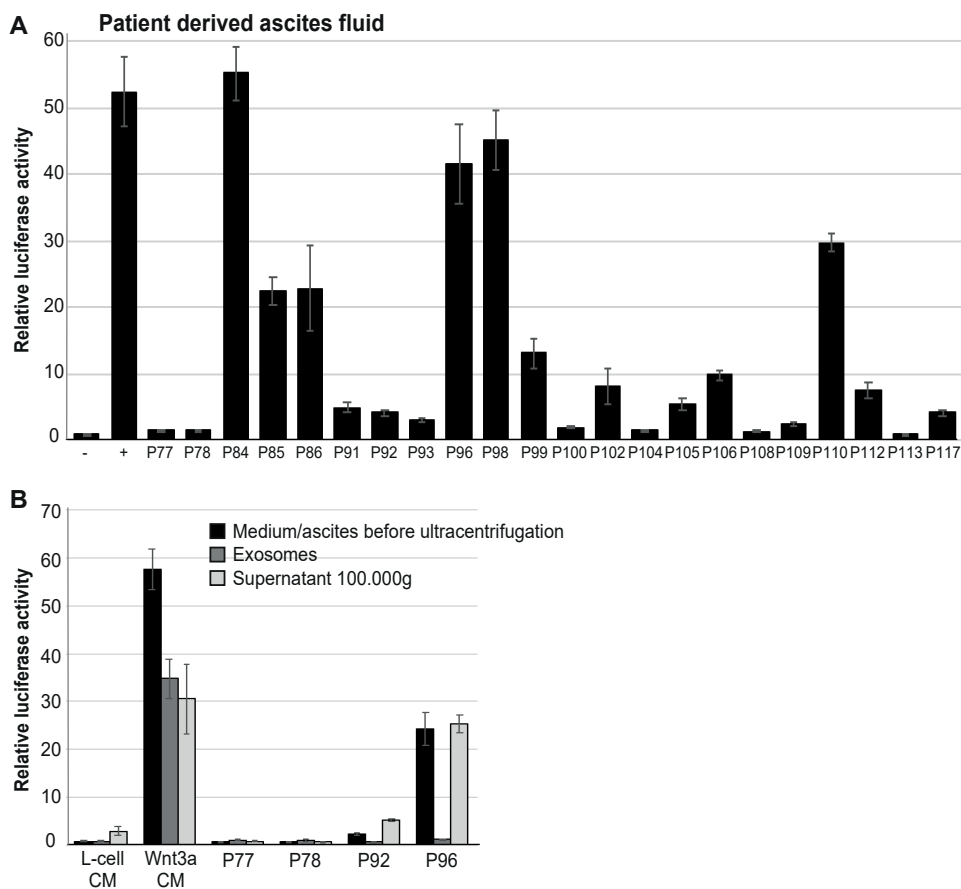
Figure 4. (**a**) TOP-Flash luciferase reporter analysis measuring induction of Wnt signaling in HEK293 after treatment with patient derived ascites. Negative control: L-cell conditioned medium; positive control: Wnt3a conditioned medium. Each bar represents the mean ± SD. (**b**) TOP-Flash luciferase reporter analysis measuring induction of Wnt signaling in HEK293 after treatment with patient derived ascites exosomes and the supernatant after the 100,000*g* centrifugation step (see materials and methods). Two Wnt positive and two Wnt negative patients as measured in Figure 4A were used. Negative control: L-cell conditioned medium; positive control: Wnt3a conditioned medium. Each bar represents the mean ± SD.

Next, the signal-inducing activity of the Wnt3a exosome pellet was tested. To this aim, HEK293 cells were transiently transfected with a luciferase-based TCF/Wnt reporter plasmid and treated with exosomes derived from L-cell and Wnt3a L-cell CM for 24 hours. In comparison to basal reporter level, addition of Wnt3a derived exosomes led to a 43-

fold induction of Wnt activity, whereas no induction was observed by the addition of exosomes from control L-cells (**Figure 4 - Supplement 1D**).

To assess the ability of exosomes derived from ovarian cancer ascites to induce Wnt signaling, we purified the fractions encompassing extracellular vesicles from two Wnt-negative and two Wnt-positive patients (as previously established by reporter assays in **Figure 4A**) and again performed a TopFLASH assay using the bulk ascites fluids (i.e. prior to ultracentrifugation), the 100,000g exosome fraction, and the supernatant after the 100,000g ultracentrifugation step. As shown in **Figure 4B**, the results show Wnt-activation by the 100,000g centrifugated supernatant, whereas no activation was observed using the isolated exosomes.

Overall, the results show that the Wnt-inducing fraction of ascites from ovarian cancer patients does not reside in the exosomes and is more likely to be due to either to diffusible ligands or to extracellular vesicles of sizes other than those characteristic of exosomes.

Wnt signaling promotes mesothelial attachments of ovarian cancer cells.

Ovarian cancers spread by shedding tumor cells (singles or clusters) from the primary lesion directly into the peritoneal fluid through which they reach distal sites within the abdominal cavity. Notably, previous studies have suggested that the formation of pre-metastatic niche is of great relevance in ovarian cancer [30,31,38,49]. Also, a role for Wnt signaling in establishing pre-metastatic niches has been demonstrated in several cancer types [29,50]. To investigate the role of Wnt signaling in pre-metastatic niche formation in ovarian cancer, we first employed the mesothelial cell lines MET5A[ref] and LP9[ref] to perform qPCR analysis of the Wnt target *AXIN2*. Wnt3a CM cultures of MET5A and LP9 revealed a 6.5- and 3-fold increase, respectively, when compared to control cells (L-cell CM) (**Figure 5A-B**). Next, in order to measure *in vitro* the effects of Wnt signaling on the attachment of tumor cells to the perithoneal surface, we co-cultured the mesothelial cells together with spheres from the OV90 and SKOV3 ovarian cell lines [51]. To this aim, spheroids of the OV90 and SKOV3 ovarian cancer cell lines were generated under nonadherent conditions, and plated on top of MET5A and LP9 mesothelial cells grown to full confluence and pretreated with L-cell or Wnt3a CM for 48 hours. To measure the ability to attach to the mesothelial layer, non-adherent spheres were washed away with PBS six hours after plating and the number of attached spheres counted. A 1.7 and 1.5-fold increase in the attachment of both OV90 and SKOV3 spheroids respectively, was observed with MET5A cells pretreated with Wnt3a CM in comparison with mesothelial cells preincubated with control L-cell medium (**Figure 5C**). In addition, the adherence of OV90 spheres on LP9 cells preincubated with Wnt3a CM was increased 1.5 times (**Figure 5D**). Comparable results were obtained with MET5A and LP9 pretreated with exosomes purified from Wnt3a CM: a 1.7 and 1.6-fold increase was observed with OV90 and SKOV3 plated on MET5A cells, whereas a 2.1 fold increase was obtained with OV90 co-cultured with LP9 cells (**Figure 5C-D**).

To further elucidate the downstream effects of Wnt-activation in mesothelial cells, a real-time qPCR analysis was performed on MET5A and LP9 cells treated with L-cell or Wnt3a conditioned media, or with exosomes derived from control and Wnt3a CM. After 48 hours of incubation, the mesenchymal marker vimentin and the EMT-related transcription factors *ZEB1* and *TWIST* were upregulated in both cell lines treated with Wnt3a CM, when compared with control (*VIM*: MET5A= 2.3x, LP9 = 5.6x; *ZEB1*: MET5A= 7.4x, LP9 = 119x; *TWIST*: MET5A= 4.0x, LP9 = 4.0x) (**Figure 5 A-B**).

Chapter 7
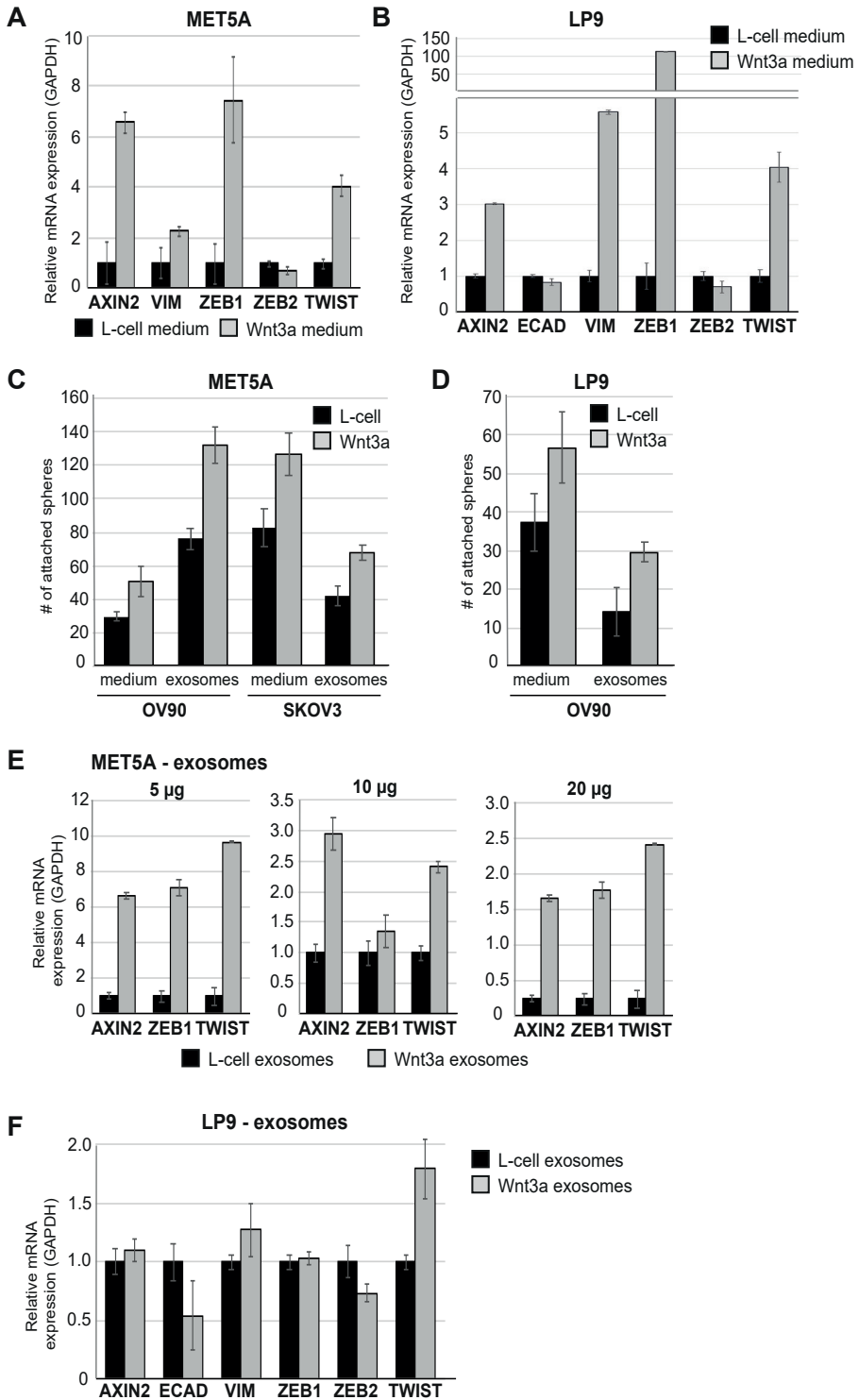
Figure 5. (Opposite) (**a-b**). RT-qPCR expression analysis of Wnt target gene *AXIN2*, mesenchymal marker *VIM* and EMT related transcription factors *ZEB1*, *ZEB2* and *TWIST* in mesothelial cells MET5A (**a**) and LP9 (**b**) upon treatment with either L-cell conditioned (black bar) or Wnt3a conditioned medium (grey bar). *GAPDH* was employed for normalization. Each bar represents the mean ± SD. (c) Spheroid-mesothelial co-culture experiment to measure the effect of Wnt-signaling on metastatic attachment of tumor cells unto mesothelial cells *in vitro*. For this, spheroids of the OV90 and SKOV3 ovarian cancer cell lines were generated under nonadherent conditions, and plated on top of MET5A mesothelial cells that were grown to full confluency and pretreated with L-cell (black bar) or Wnt3a (grey bar) conditioned medium or exosomes for 48 hours. To measure the ability to adhere, non-adherent spheres were washed away with PBS six hours after plating. The number of attached spheres was counted. Each bar represents the mean ± SD. (d) Spheroid-mesothelial co-culture experiment measuring the ability of OV90 spheres to attach to LP9 cells after pre-treatment of the LP9 cells for 48 hours with either L-cell (black bar) of Wnt3a (grey bar) CM or exosomes. (e) RT-qPCR expression analysis of *AXIN2*, *ZEB1*, and *TWIST* in mesothelial cells MET5A after treatment with 5, 10 or 20 μg L-cell (black bar) or Wnt3a (grey bar) CM derived exosomes. *GAPDH* was employed for normalization. Each bar represents the mean ± SD. (**f**) RT-qPCR expression analysis of *AXIN2*, *ZEB1*, and *TWIST* in mesothelial cells LP9 after treatment with 5 μg L-cell (black bar) or Wnt3a (grey bar) CM derived exosomes. *GAPDH* was employed for normalization. Each bar represents the mean ± SD.

No differences were measured in E-cadherin (LP9) and *ZEB2* expression (**Figure 5 A-B**). The same effect was measured upon culturing MET5A cells with WNT3a CM-derived exosomes (5 μg) in comparison with control L-cell exosomes (6.7-fold *AXIN2* = 6.7x; *ZEB1* = 7.1x; *TWIST* = 9.6x) (**Figure 5E**). No differences were measured with the LP9 cells (**Figure 5F**). Of note, increasing amounts of Wnt3a exosomes led to weaker Axin2/ZEB1/TWIST upregulation in MET5A cells (**Figure 5E**).

Overall, *in vitro* activation of Wnt signaling in mesothelial cells induces EMT and leads to an enhanced interaction with ovarian cancer spheroids. In order to validate these results in an *in vivo* model, control and Wnt3a exosomes were first labeled with the red-fluorescent lipophilic membrane dye PKH26 and injected I.P. in recipient mice to verify their uptake into the mesothelium. 24 hours after injection mice were sacrificed, and

tissue sections were made of the isolated abdominal wall. Confocal microscopy analysis confirmed the uptake of both L-cell and Wnt3a PKH26-labeled exosomes, whereas no signal was detected with the PBS control (**Figure 6A**).

Next, to study the effects of Wnt on pre-metastatic niche formation, i.e. the attachment of ovarian cancer cells, control (PBS and L-cell) and Wnt3a exosomes were injected i.p. twice a week for 3 weeks, followed by the i.p. transplantation of OV90 ovarian cancer cells. Five weeks after the injection of the cancer cells, mice were sacrificed and the ascites fluid and the peritoneal tissue collected. No differences in number of spheroids present in the ascites was observed between the three conditions (data not shown). To quantify the number of micrometastases on the mesothelial surface of the abdominal wall, isolated peritoneal tissues were fixed and stained with a human specific mitochondria antibody. Stained tissues were imaged by Opera and analyzed for the number of "objects" (see Materials and Methods) attached to the peritoneal wall (**Figure 6B-C**). The results show a significant increase of cell clusters attached to the mesothelial layer in mice treated with Wnt3a CM derived exosomes compared to both L-cell exosome and PBS injected controls. No differences were seen between PBS and L-cell exosome injected mice (**Figure 6B**). Notably, confocal images of the peritoneal wall suggest the attachment of spheroid shaped objects that invade into the muscular layer underlying the mesothelial cells (**Figure 6D**).

Chapter 7

Overall, these results, although yet preliminary, suggest an important role for Wnt signaling in the formation of a pre-metastatic niche favoring the attachment of ovarian tumor cells toto the mesothelial lining and invade through the abdominal wall.
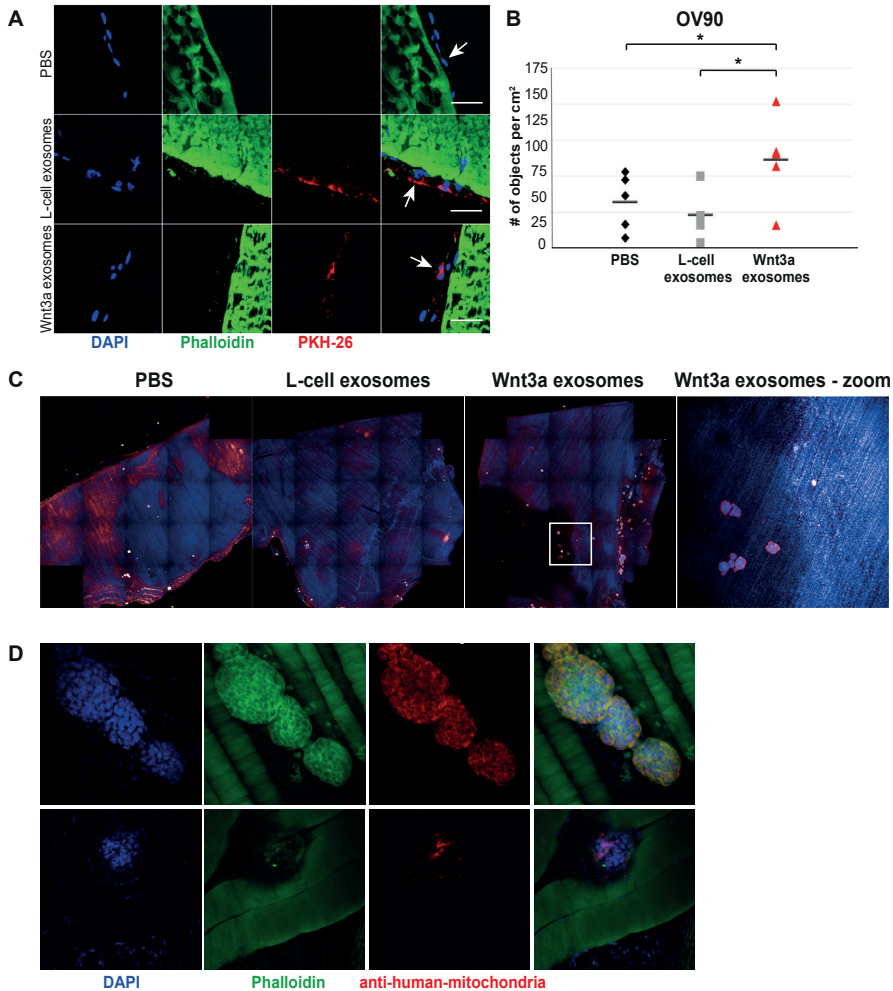
Figure 6. (**a**) Confocal microscopy showing the uptake of both L-cell (middle panel) and Wnt3a (lower panel) PKH26 labeled exosomes by the mesothelial cell *in vivo* (white arrow). Both L-cell and Wnt3a CM derived exosomes were stained with the red-fluorescent lipophilic membrane dye PKH26 and intraperitoneally injected in mice. A mouse injected with PBS was taken as a negative control (upper panel). 24 hours after injection mice were sacrificed, and fresh frozen sections were made of the isolated abdominal wall. Red: PKH26, green: phalloidin. Nuclei were visualized by DAPI staining of DNA (blue). Scale bar: 50 μm. (**b-c**) Graph (**b**) and Opera image (**c**) quantifying the number of attached objects (spheres containing cells that were double stained for DAPI and Alexa Fluor 560) to the peritoneal wall. For this experiment mice were intraperitoneally injected PBS, L-cell or Wnt3a CM derived exosomes twice a week for three weeks. Upon three weeks of exosome injection, OV90 ovarian cancer cells were peritoneally injected. Five weeks after injection of the cancer cells, when ascites developed, mice were sacrificed and the peritoneal tissue was collected. To quantify the number of metastases spread unto the mesothelium of the abdominal wall, isolated peritoneal tissues were fixed and stained with a human

specific mitochondria antibody. (**d**) Confocal images of the peritoneal wall showing the attachment of spheroid shaped objects that attached to the peritoneal wall. Red: anti-human-mitochondria, green: phalloidin. Nuclei were visualized by DAPI staining of DNA (blue). Scale bar: 50 µm.

Discussion

In ovarian cancer, constitutive Wnt signaling activation as the result of the loss of function of a tumor suppressor such as *APC* or of an oncogenic gain of function mutation seems to be limited to the endometrioid histotype (16-54% of the cases) where mutations in β-catenin have been consistently reported. As for the broader spectrum of ovarian cancers and in particular for the high-grade serous (HGS) cases, known to be associated with poor overall survival, Wnt signaling activation is more likely to result from paracrine stimuli from the microenvironment, as intracellular (nuclear or cytoplasmic) β-catenin accumulation has been observed in a sizeable percentage of the cases [6,7]. As such, it is plausible to think that the role of Wnt signaling activation in HGS ovarian cancers is mainly a promoting, rather than initiating, one.

From the perspective of the invasion-metastasis cascade, ovarian cancer represents a unique example of a tumor where the primary lesion is in direct contact with the most frequent site of metastasis, i.e. the abdominal cavity. Unique for ovarian cancer is the 'transcoelomic' dissemination of tumor cells and the formation of ascites fluid in the abdominal and pelvic cavity. Under normal physiological conditions, capillary vessels lining the peritoneal cavity constantly secrete free fluid in order to lubricate the serosal surfaces supporting the free movement of intra-abdominal structures and the passage of solutes between peritoneum and organs. Most of this peritoneal fluid is reabsorbed into lymphatic vessels and eventually drained into the blood circulation. However, in cases of metastasized intra-abdominal cancer, the production of peritoneal fluid is increased due to enhanced leakiness of the microvasculature within tumors and obstruction of the lymphatic vessels [52,53]. As a result, fluid accumulation in the peritoneal cavity exceeds its resorption, resulting in the build-up of malignant ascites which provide a favorable tumor microenvironment (TME) enriched in secreted inflammatory cytokines [54], growth factors [55], and extracellular macromolecules such as collagen, fibronectin, and laminin [56]. Here, we show that over 75% of malignant ascites obtained from late-stage ovarian cancer patients can trigger Wnt signaling activation. Our data show that ovarian cancer cells of different histotypes are capable to respond to external Wnt cues by activating the canonical pathway. In the tested cell lines, Wnt stimulation results in increased self-renewal and activation of the EMT program in spheroids grown under low-attachment conditions. As further discussed here below, we propose that these multicellular aggregates enriched in cancer stem/progenitor cells, detach from the primary tumor and eventually implant on the mesothelial lining of the peritoneum where metastatic colonization occurs.

The major event in ovarian cancer metastasis formation is the adhesion of disseminated cells to the mesothelium, i.e. the inner surface of the intraperitoneal cavity. In this context, the establishment of premetastatic niches is likely to be important for the disseminated ovarian cancer cells to engraft at the distant site [30,31,38,49]. However, studying the pre-metastatic niche in ovarian cancer has been challenging since more than one third of ovarian cancer patients present with ascites at diagnosis, and almost all have ascites at recurrence [44]. Here, we have employed experimental models to study the development

Chapter 7

of the pre-metastatic niche and the subsequent metastasis formation in ovarian cancer. We observed that the pre-treatment of mesothelial cells with Wnt ligands lead to the enhanced attachment of ovarian cancer cells both *in vitro* and *in vivo*. Wnt signaling activation in mesothelial cells leads to the induction of the EMT program, likely interfering with the peritoneal barrier and thereby creating a favourable premetastatic environment beneficial for peritoneal metastasis of ovarian cancer. This is in line with literature reports supportive of the role of Wnt signaling in mesothelial attachment [57] and pre-metastatic niche formation [29].

More recently, several studies have suggested the participation of exosomes derived from primary ovarian cancers in premetastatic niche formation. Microarry gene expression analysis of malignant extracellular vesicles (EVs) showed a significanlty upregulation of the MMP1 (Matrix Metalloproteinase 1) in both cell line as well as ovarian cancer patient derived EVs. MMP-1 was shown to be a key molecule for destructive phenotypes capable of altering the peritoneal barrier by promoting apoptotic cell death of the mesothelial cells [38]. Additionally, ovarian cancer exosomes often retain the cell surface glycoprotein CD44, a well-known Wnt target gene [58], that can be transferred onto the cell membrane of mesothelial cells of the peritoneum thereby triggering mesothelial clearance and inducing MMP9 secretion thereby facilitating ovarian cancer invasion and metastasis formation [31]. In this study, we observed that over 75% of ovarian cancer malignant ascites can induce Wnt signaling. However, this does not seem to be mediated by exosomes, but rather by either secreted Wnt agonists or by extracellular vescicles of different sizes than the canonical exosomes. Several literature studies have shown epigenetic modifications leading to overexpression of Wnt ligands [59,60], receptors [61], other Wnt agonists including *FRAT1* [11] and *PYGO2* [62], or even Wnt antagonists like secreted frizzled receptor proteins (sFRP) and Dickkopf (DKK1) [13,63-65]. In addition, several other factors found in malignant ascites and known to promote Wnt signaling including leptin [66,67], urokinase-type plasminogen activator receptor (uPAR) [68], and macrophage migrating inhibitory factor (MIF) [69], have been correlated with shorter progression-free survival in ovarian cancer [54,70]. A thorough characterization of the composition of ascites will further elucidate the underlying mechanisms leading to the establishment of a pre-metastatic niches and/or promoting metastatic dissemination and colonization. The latter will lay the basis for the development of new therapeutic interventions.

Overall, our results are indicative of a specific role of Wnt signaling in ovarian cancer stemness and progression to malignancy. Not only does the activation of this signaling pathway play a role in deregulating cells within the primary tumor, but it also contributes to the establishment of pre-metastatic niches thus facilitating ovarian cancer cells homing and colonization of the abdominal cavity.

Material and Methods

Cell culture

CAOV3, SKOV3, COV504, HEK293T, Wnt3a producing L cells (gift from R. Nusse, Stanford University), and control (i.e. non-Wnt3a producing) cell lines were cultured in DMEM medium (11965092, Thermo Fisher Scientific) supplemented with 10% heat inactivated fetal bovine serum (FBS; Thermo Fisher Scientific), 2 mM L-glutamin (200 mM; 25030081; Thermo Fisher Scientific), and 1% Penicillin/Streptomycin (Pen/Strep; penicillin: 100 U/ml, streptomycin:

100 μg/ml; 15140122 Thermo Fisher Scientific). OV90 was cultured in a 1:1 mixture of MCDB 105 medium (M6395; Sigma Aldrich containing 1.5 g/L sodium bicarbonate) and Medium 199 (31150022; Thermo Fisher Scientific containing 2.2 g/L sodium bicarbonate) supplemented with 15% heat inactivated fetal bovine serum (FBS; Thermo Fisher Scientific) and 1% Penicillin/Streptomycin (Pen/Strep). Murine STOSE and ID8 were cultured in Alpha MEM (12561056; Thermo Fisher Scientific) containing 5% FBS, 1% Pen/Strep, and 1% insulin-transferrin-sodium-selenite solution (ITSS, Roche). STOSE was a generous gift from Professor B. Vanderhyden (Ottawa Hospital Research Institute) [41].

All cell lines were maintained in a humidified atmosphere at 37°C and 5% CO_2. The identity of each cell line was confirmed by DNA fingerprinting with microsatellite markers (Amelogenin, CSF1PO, D13S317, D16S539, D5S818, D7S820, THO1, TPOX, vWA, D8S1179, FGA, Penta E, Penta D, D18S51, D3S1358, D21S11) and compared with the analogous data provided by ATCC, EACC, and https://web.expasy.org/cellosaurus/ (data not shown).

Chiron (CHIR99021, 4423, Tocris, dissolved at 20 mM in DMSO), CHIR99021 was added at 4 μM to the culture medium every 48 hours for one week.

5 μM niclosamide and 10 nM LGK794 were used to inhibit Wnt signaling in STOSE and ID8 cultures. Cells were treated 48 hours before employing further analysis.

Preparation of L-cell and Wnt 3a conditioned medium

To prepare L-cell and Wnt3a conditioned media, one T75 culture flask at 80-90% confluency was passaged to five T75 flasks and allowed to grow for 4 days. Culture medium (25 ml) was removed and centrifuged at 3,000g for 10 min. The supernatant constituted a first batch of conditioned medium. 25 mL fresh medium were added to the dish and the cells cultured for an additional 3 days. The medium was again centrifuged at 3000g for 10 min, pooled with the 1st batch, filtered through a 0.22 μm membrane, and stored at 4 °C. TopFLASH reporter assay was employed to assess the Wnt-inducing capacity of the conditioned medium.

TOP-Flash reporter assay

For the β-catenin/TCF reporter assay (TOP-Flash reporter assay), cells were plated on 48-well dishes and cultured in medium with or without 4 μM CHIR99021. After 48 hrs., when 70% confluence was reached, cells were transfected by Fugene HD (Promega) with 125 ng of the TOP-Flash or FOP-Flash reporter constructs together with 25 ng of the Renilla luciferase vector for normalization purposes. Luciferase activity was measured using the Dual-Luciferase Reporter Assay System (Promega) 24 hrs. post-transfection. Luminescence was measured using a GloMax Luminometer.

Flow cytometry and sorting

For flow cytometry and sorting purposes, cells were detached from the culture dishes using trypsin-EDTA (15400054, Thermo Fisher Scientific) and resuspended in staining buffer (PBS supplemented with 4% FCS). Antibody staining was performed on ice for 30' with CD44-APC (clone IM7, 559250, BD Pharmingon) and EpCAM-FITC (ESA-214, GTX30708, GeneTex). Single cell suspensions were then washed and resuspended in 4% FCS in PBS supplemented with 4% FCS. Flow cytometry analysis and cell sorting were carried out with a FACSAria II Cell Sorter (BD Biosciences). Forward-scatter height (FSC-H) versus Forward-scatter width (FSC-W), and side-scatter high versus side-scatter

Chapter 7

width were employed to eliminate cell aggregates and ensure single cell sorting. The DAPI nuclear dye (D9542, Sigma-Aldrich) was used at 1 µg/mL to exclude dead cells. FITC was analyzed using 488 nm laser and 502LP and 530/30BP filters and APC a 633 nm laser and a 660/20BP filter.

RNA isolation and qRT-PCR

RNA was isolated from cells using TRIzol™ Reagent (15596018, ThermoFisher Scientific) according to the manufacturer's instructions. RNA concentration was measured by NanoDrop. Subsequently, reverse transcription into cDNA was conducted using the High-Capacity cDNA Reverse Transcription Kit (4368814, Life Technologies) according to the manufacturer's instructions. RT-qPCR was performed with Fast SYBR Green Master Mix (4385617; ThermoFisher Scientific). PCR amplification and detection were implemented with the 7400 Fast Real-Time PCR System. Expression levels were normalized for the endogenous *GAPDH* or *ACTB* reference gene.

Immunofluorescence (IF) analysis

Mouse peritoneal tissues were fixed for 24 hours in 4% PFA at 4°C and washed twice with PBS. Tissues were permeabilized for 20 minutes at room temperature with 0.2% of Triton X-100 and then incubated in blocking buffer (5% milk powder in PBS-Tween) for 1 hour at room temperature. Cells were then exposed overnight at 4 °C to primary antibodies against human mitochondria (mouse, 1:250). After washing twice with PBS-Tween, coverslips were incubated for 6 hrs. at room temperature in blocking buffer containing secondary antibody monkey anti-Mouse Alexa Fluor® 568 conjugate (1:250, Thermo Fisher) and phallodin-GFP (1:200, Thermo Fisher). Cells were counterstained with DAPI to visualize the nuclei. Tissues were imaged using the Opera Phenix HCS system. DAPI was used to measure the tissue containing area per well, Alexa Fluor 560 was used to detect cells. Objects were defined as clusters that expressed both DAPI and Alexa Fluor 560. All images were processed with ImageJ (U.S. National Institutes of Health, Bethesda, MD, USA).

Immunohistochemistry (IHC) analysis

Paraffin blocks containing human ovarian cancer tissue were obtained from the department of Pathology at the Erasmus Medical Center in Rotterdam. Four µm sections were mounted on slides. Immunohistochemistry was performed using the EnVision Plus-HRP system (Dako) and antibodies directed against β-catenin (1:200, 610154, BD Biosciences) and ZEB1 (1:200, HPA027524, Sigma-Aldrich). Briefly, paraffin embedded sections were dewaxed with Xylene and hydrated in 100% and 70% ethanol. Antigen retrieval was performed using pressure cooker pretreatment in a citrate buffer (pH 6.0) for ZEB1 and in a Tris-EDTA buffer (pH 9.0) for the anti-human-mitochondria and anti-β-catenin antibodies. Subsequently, slides were incubated at room temperature in 3% hydrogen peroxidase for 15' to block endogenous peroxidase activity. Tissue sections were washed and blocked with 5% BSA in PBS-Tween for 1 hour to then incubated with the primary antibodies overnight at 4 °C. Slides were washed twice with PBS-Tween and incubated with Rabbit EnVision+ System-HRP (K4001, Dako) or Mouse EnVision+ System-HRP (K4007, Dako) for 30'. Tissues were counterstained with Mayer's Hematoxylin. Dehydration was performed by incubation in 70% and 100% ethanol followed by Xylene before sleds were mounted using Pertex (00811, Histolab).

Spheroid adhesion assays

Spheroids were generated by culturing GFP labeled (ATG-1929, #108712, Addgene) ovarian cancer cells in low attachment plates (3473, Corning). Spheroids were cultured in advanced DMEM medium/F12 (12634028, Thermo Fisher Scientific) containing 1x GlutaMAX (350500061, Thermo Fisher Scientific), 10 mM HEPES (15630056, Thermo Fisher Scientific) and Pen/Strep and supplemented with Noggin (conditioned medium), Wnt3a (conditioned medium), Rpo1 (conditioned medium), 1x B27 supplement (#17504044, Invitrogen), N-Acetylcysteine (1.25 mM, A9165-5G, Sigma-Aldrich), TGFβ receptor inhibitor A83-01 (500 nM, 2939, Bio-techne), Y27632 dihydrochloride (10 μM, Y-27632, Abole bioscience), and hEGF (50 ng/mL, AF-100-15, Proprotech). To quantify the adhesion of ovarian cancer spheroids to mesothelial monolayers, Met5A or LP9 human mesothelial cells were grown to confluence. Upon confluency, spheroids were plated and allowed to adhere for 6 hours at 37 °C. Non-adherent spheroids were gently rinsed away with PBS. The number of spheroids/well was counted under a fluorescent microscope.

Ascitic fluids

Ovarian cancer patient-derived ascites were collected from patients at the Erasmus Medical Center in Rotterdam. Tissue collection was approved by the medical ethical committee Erasmus MC. Peritoneal fluids were obtained and centrifuged at 1000 rpm for 15 minutes and supernatants were stored at -80 °C until assayed.

Exosome purification

Exosomes were purified by differential centrifugation. Supernatants from cell cultures or malignant ascites were subjected to sequential centrifugation steps from 300g and 10,000g before pelleting exosomes at 100,000g in a SW41T1 swinging bucket rotor for 1 hour (Beckman). The supernatant was collected and exosomes were resuspended in PBS.

Electron microscopy

Purified exosomes were left to settle on carbon-coated grids. After staining with 3% uranyl acetate, grids were air-dried and visualized using a transmission electron microscope (Zeiss EM900). For immunogold labelling, pelleted exosomes were plated on grids, blocked and stained in anti-Wg antibody (4D4, 1:5), then incubated in secondary anti-mouse antibody and labelled with protein A–gold particles (10 nm). Each staining step was followed by five PBS washes and finally ten washes in H_2O before contrast staining with 3% uranyl acetate.

Western blot analysis

To measure protein concentration of isolated exosomes, 5 μL sample was mixed with 5 μL of Laemmli lysis buffer [0.125 M Tris–HCl (pH 6.8), 10% glycerol, 2.3% sodium dodecyl sulphate (SDS)]. Protein concentration was determined using the Bio-Rad DC Protein Assay (Bio-Rad, Hercules, USA). For analysis, 10 μg of protein was suspended in reducing sample buffer [1 M Tris–HCl (pH 6.8), 30% glycerol, 6% SDS, 3% 2-mercaptoethanol, 0.005% bromophenol blue] or non-reducing sample buffer (without 2-mercaptoethanol) and boiled for 5 minutes at 95℃. Proteins were separated by SDS-PAGE (SDS-polyacrylamide gel electrophoresis) and transferred to polyvinylidene fluoride membranes, blocked in 5%

non-fat milk in PBS with 0.5% Tween-20, and immunostained with exosomal markers Alix, Tsg101, HSC90 and CD9.

qNano analysis

Tunable resistive pulse sensing (RPS) by qNano (Izon, Cambridge, MA, USA) was used to measure the size distribution and concentration of particles in the purified exosome fraction. To prevent protein binding to the pore, an Izon reagent kit was used, and 0.03% Tween/PBS was added to each of the collected fractions. An aliquot of exosomes from each fraction were placed in the Nanopore (NP150, A37355, Izon), calibration particles included in the reagent kit (1:1, 200 EV, Izon) were used to calibrate the machine. All samples were measured at 43.3 mm stretch with a voltage of 0.74 V at two pressure levels of 4 and 8 mbar. Particles were detected in short pulses of the current. The size and concentration of particles were determined using software provided by Izon.

Animal experiments

All protocols involving animals were approved by the Dutch Animal Experimental Committee and were conform to the Code of Practice for Animal Experiments in Cancer Research established by the Netherlands Inspectorate for Health Protections, Commodities and Veterinary Public health (The Hague, the Netherlands, 1999). Animals were bred and maintained in the Erasmus MC animal facility (EDC) under conventional specific pathogen-free (SPF) conditions.

For all experiments 6 to 8-week-old NOD.Cg-*Prkdc^{scid} Il2rg^{tm1Wjl}*/SzJ (NSG) mice were used. To test uptake of exosomes by mesothelial cells *in vivo,* mice were injected with 100 μg exosomes pre-labeled with PKH26 (PHH26GL, Sigma Aldrich). 24 hours after injection mice were sacrificed and tissues were collected for immunofluorescent analysis. For the pre-metastatic niche experiment mice were injected with 500 μL PBS containing 50 μg of purified exosomes or PBS twice a week for a total of three weeks. Thereafter, mice were injected intraperitoneally with 1 x 10^6 OV90 cells. Five weeks after the injection, mice were sacrificed and tissue was collected. Tissues were fixed and used for further analyses.

Statistical analysis

For each experiment, data are shown as mean ± SEM. IBM SPSS Statistics software was used for data analysis. The Mann-Whitney U test was used to analyze the difference between two groups of quantitative variables; α-value was set at 5%.

Conflicts of Interest: The authors declare no conflict of interest.

References

1.   Siegel, R.L.; Miller, K.D.; Jemal, A. Cancer statistics, 2018. *CA Cancer J Clin* **2018**, *68*, 7-30, doi:10.3322/caac.21442.

2.   Bast, R.C., Jr.; Hennessy, B.; Mills, G.B. The biology of ovarian cancer: new opportunities for translation. *Nat Rev Cancer* **2009**, *9*, 415-428, doi:10.1038/nrc2644.

3.   Kurman, R.J.; Shih Ie, M. Pathogenesis of ovarian cancer: lessons from morphology and molecular biology and their clinical implications. *Int J Gynecol Pathol* **2008**, *27*, 151-160, doi:10.1097/PGP.0b013e318161e4f5.

4.   Teeuwssen, M.; Fodde, R. Wnt Signaling in Ovarian Cancer Stemness, EMT, and Therapy Resistance. *J Clin Med* **2019**, *8*, doi:10.3390/jcm8101658.

5.   Reya, T.; Clevers, H. Wnt signalling in stem cells and cancer. *Nature* **2005**, *434*, 843-850, doi:10.1038/nature03319.

6.   Arend, R.C.; Londono-Joshi, A.I.; Straughn, J.M., Jr.; Buchsbaum, D.J. The Wnt/beta-catenin pathway in ovarian cancer: a review. *Gynecol Oncol* **2013**, *131*, 772-779, doi:10.1016/j.ygyno.2013.09.034.

7.   Wu, R.; Zhai, Y.; Fearon, E.R.; Cho, K.R. Diverse mechanisms of beta-catenin deregulation in ovarian endometrioid adenocarcinomas. *Cancer Res* **2001**, *61*, 8247-8255.

8.   Kildal, W.; Risberg, B.; Abeler, V.M.; Kristensen, G.B.; Sudbo, J.; Nesland, J.M.; Danielsen, H.E. beta-catenin expression, DNA ploidy and clinicopathological features in ovarian cancer: a study in 253 patients. *Eur J Cancer* **2005**, *41*, 1127-1134, doi:10.1016/j.ejca.2005.01.022.

9.   Lee, C.M.; Shvartsman, H.; Deavers, M.T.; Wang, S.C.; Xia, W.; Schmandt, R.; Bodurka, D.C.; Atkinson, E.N.; Malpica, A.; Gershenson, D.M.; et al. beta-catenin nuclear localization is associated with grade in ovarian serous carcinoma. *Gynecol Oncol* **2003**, *88*, 363-368.

10.   Rask, K.; Nilsson, A.; Brannstrom, M.; Carlsson, P.; Hellberg, P.; Janson, P.O.; Hedin, L.; Sundfeldt, K. Wnt-signalling pathway in ovarian epithelial tumours: increased expression of beta-catenin and GSK3beta. *Br J Cancer* **2003**, *89*, 1298-1304, doi:10.1038/sj.bjc.6601265.

11.   Wang, Y.; Hewitt, S.M.; Liu, S.; Zhou, X.; Zhu, H.; Zhou, C.; Zhang, G.; Quan, L.; Bai, J.; Xu, N. Tissue microarray analysis of human FRAT1 expression and its correlation with the subcellular localisation of beta-catenin in ovarian tumours. *Br J Cancer* **2006**, *94*, 686-691, doi:10.1038/sj.bjc.6602988.

12.   Chau, W.K.; Ip, C.K.; Mak, A.S.; Lai, H.C.; Wong, A.S. c-Kit mediates chemoresistance and tumor-initiating capacity of ovarian cancer cells through activation of Wnt/beta-catenin-ATP-binding cassette G2 signaling. *Oncogene* **2013**, *32*, 2767-2781, doi:10.1038/onc.2012.290.

13.   Jacob, F.; Ukegjini, K.; Nixdorf, S.; Ford, C.E.; Olivier, J.; Caduff, R.; Scurry, J.P.; Guertler, R.; Hornung, D.; Mueller, R.; et al. Loss of secreted frizzled-related protein 4 correlates with an aggressive phenotype and predicts poor outcome in ovarian cancer patients. *PLoS One* **2012**, *7*, e31885, doi:10.1371/journal.pone.0031885.

14.   Brabletz, T.; Jung, A.; Spaderna, S.; Hlubek, F.; Kirchner, T. Opinion: migrating cancer stem cells - an integrated concept of malignant tumour progression. *Nat Rev Cancer* **2005**, *5*, 744-749.

15.   Sacchetti, A.; Teeuwssen, M.; Verhagen, M.; Joosten, R.; Xu, T.; Stabile, R.; van der Steen, B.; Watson, M.M.; Gusinac, A.; Kim, W.K.; et al. Phenotypic plasticity underlies local invasion and distant metastasis in colon cancer. *Elife* **2021**, *10*, doi:10.7554/eLife.61461.

16.   Wu, Z.Q.; Li, X.Y.; Hu, C.Y.; Ford, M.; Kleer, C.G.; Weiss, S.J. Canonical Wnt signaling regulates Slug activity and links epithelial-mesenchymal transition with epigenetic Breast Cancer 1, Early Onset (BRCA1) repression. *Proc Natl Acad Sci U S A* **2012**, *109*, 16654-16659.

Chapter 7

17. Yook, J.I.; Li, X.Y.; Ota, I.; Fearon, E.R.; Weiss, S.J. Wnt-dependent regulation of the E-cadherin repressor snail. *J Biol Chem* **2005**, *280*, 11740-11748.

18. Teeuwssen, M.; Fodde, R. Cell Heterogeneity and Phenotypic Plasticity in Metastasis Formation: The Case of Colon Cancer. *Cancers (Basel)* **2019**, *11*, doi:10.3390/cancers11091368.

19. Bernaudo, S.; Salem, M.; Qi, X.; Zhou, W.; Zhang, C.; Yang, W.; Rosman, D.; Deng, Z.; Ye, G.; Yang, B.B.; et al. Cyclin G2 inhibits epithelial-to-mesenchymal transition by disrupting Wnt/beta-catenin signaling. *Oncogene* **2016**, *35*, 4816-4827, doi:10.1038/onc.2016.15.

20. Deng, Z.; Wang, L.; Hou, H.; Zhou, J.; Li, X. Epigenetic regulation of IQGAP2 promotes ovarian cancer progression via activating Wnt/beta-catenin signaling. *Int J Oncol* **2016**, *48*, 153-160, doi:10.3892/ijo.2015.3228.

21. Hojo, N.; Huisken, A.L.; Wang, H.; Chirshev, E.; Kim, N.S.; Nguyen, S.M.; Campos, H.; Glackin, C.A.; Ioffe, Y.J.; Unternaehrer, J.J. Snail knockdown reverses stemness and inhibits tumour growth in ovarian cancer. *Sci Rep* **2018**, *8*, 8704, doi:10.1038/s41598-018-27021-z.

22. Sun, J.; Yang, X.; Zhang, R.; Liu, S.; Gan, X.; Xi, X.; Zhang, Z.; Feng, Y.; Sun, Y. GOLPH3 induces epithelial-mesenchymal transition via Wnt/beta-catenin signaling pathway in epithelial ovarian cancer. *Cancer Med* **2017**, *6*, 834-844, doi:10.1002/cam4.1040.

23. Nieto, M.A.; Huang, R.Y.; Jackson, R.A.; Thiery, J.P. Emt: 2016. *Cell* **2016**, *166*, 21-45.

24. Dongre, A.; Rashidian, M.; Reinhardt, F.; Bagnato, A.; Keckesova, Z.; Ploegh, H.L.; Weinberg, R.A. Epithelial-to-Mesenchymal Transition Contributes to Immunosuppression in Breast Carcinomas. *Cancer Res* **2017**, *77*, 3982-3989.

25. Mani, S.A.; Guo, W.; Liao, M.J.; Eaton, E.N.; Ayyanan, A.; Zhou, A.Y.; Brooks, M.; Reinhard, F.; Zhang, C.C.; Shipitsin, M.; et al. The epithelial-mesenchymal transition generates cells with properties of stem cells. *Cell* **2008**, *133*, 704-715.

26. Smith, B.N.; Bhowmick, N.A. Role of EMT in Metastasis and Therapy Resistance. *J Clin Med* **2016**, *5*, doi:10.3390/jcm5020017.

27. Liu, Y.; Cao, X. Characteristics and Significance of the Pre-metastatic Niche. *Cancer Cell* **2016**, *30*, 668-681.

28. Peinado, H.; Aleckovic, M.; Lavotshkin, S.; Matei, I.; Costa-Silva, B.; Moreno-Bueno, G.; Hergueta-Redondo, M.; Williams, C.; Garcia-Santos, G.; Ghajar, C.; et al. Melanoma exosomes educate bone marrow progenitor cells toward a pro-metastatic phenotype through MET. *Nat Med* **2012**, *18*, 883-891, doi:10.1038/nm.2753.

29. Malanchi, I.; Santamaria-Martinez, A.; Susanto, E.; Peng, H.; Lehr, H.A.; Delaloye, J.F.; Huelsken, J. Interactions between cancer stem cells and their niche govern metastatic colonization. *Nature* **2011**, *481*, 85-89, doi:10.1038/nature10694.

30. Lee, W.; Ko, S.Y.; Mohamed, M.S.; Kenny, H.A.; Lengyel, E.; Naora, H. Neutrophils facilitate ovarian cancer premetastatic niche formation in the omentum. *J Exp Med* **2019**, *216*, 176-194, doi:10.1084/jem.20181170.

31. Nakamura, K.; Sawada, K.; Kinose, Y.; Yoshimura, A.; Toda, A.; Nakatsuka, E.; Hashimoto, K.; Mabuchi, S.; Morishige, K.I.; Kurachi, H.; et al. Exosomes Promote Ovarian Cancer Cell Invasion through Transfer of CD44 to Peritoneal Mesothelial Cells. *Mol Cancer Res* **2017**, *15*, 78-92, doi:10.1158/1541-7786.MCR-16-0191.

32. Dovrat, S.; Caspi, M.; Zilberberg, A.; Lahav, L.; Firsow, A.; Gur, H.; Rosin-Arbesfeld, R. 14-3-3 and beta-catenin are secreted on extracellular vesicles to activate the oncogenic Wnt pathway. *Mol Oncol* **2014**, *8*, 894-911, doi:10.1016/j.molonc.2014.03.011.

33. Gross, J.C.; Chaudhary, V.; Bartscherer, K.; Boutros, M. Active Wnt proteins are secreted on exosomes. *Nat Cell Biol* **2012**, *14*, 1036-1045, doi:10.1038/ncb2574.

34. Hu, Y.B.; Yan, C.; Mu, L.; Mi, Y.L.; Zhao, H.; Hu, H.; Li, X.L.; Tao, D.D.; Wu, Y.Q.; Gong, J.P.; et al. Exosomal Wnt-induced dedifferentiation of colorectal cancer cells contributes to chemotherapy resistance. *Oncogene* **2019**, *38*, 1951-1965, doi:10.1038/s41388-018-0557-9.

35. Luga, V.; Zhang, L.; Viloria-Petit, A.M.; Ogunjimi, A.A.; Inanlou, M.R.; Chiu, E.; Buchanan, M.; Hosein, A.N.; Basik, M.; Wrana, J.L. Exosomes mediate stromal mobilization of autocrine Wnt-PCP signaling in breast cancer cell migration. *Cell* **2012**, *151*, 1542-1556, doi:10.1016/j.cell.2012.11.024.

36. Azmi, A.S.; Bao, B.; Sarkar, F.H. Exosomes in cancer development, metastasis, and drug resistance: a comprehensive review. *Cancer Metastasis Rev* **2013**, *32*, 623-642, doi:10.1007/s10555-013-9441-9.

37. Keller, S.; Konig, A.K.; Marme, F.; Runz, S.; Wolterink, S.; Koensgen, D.; Mustea, A.; Sehouli, J.; Altevogt, P. Systemic presence and tumor-growth promoting effect of ovarian carcinoma released exosomes. *Cancer Lett* **2009**, *278*, 73-81, doi:10.1016/j.canlet.2008.12.028.

38. Yokoi, A.; Yoshioka, Y.; Yamamoto, Y.; Ishikawa, M.; Ikeda, S.I.; Kato, T.; Kiyono, T.; Takeshita, F.; Kajiyama, H.; Kikkawa, F.; et al. Malignant extracellular vesicles carrying MMP1 mRNA facilitate peritoneal dissemination in ovarian cancer. *Nat Commun* **2017**, *8*, 14470, doi:10.1038/ncomms14470.

39. Domcke, S.; Sinha, R.; Levine, D.A.; Sander, C.; Schultz, N. Evaluating cell lines as tumour models by comparison of genomic profiles. *Nat Commun* **2013**, *4*, 2126, doi:10.1038/ncomms3126.

40. Beaufort, C.M.; Helmijr, J.C.; Piskorz, A.M.; Hoogstraat, M.; Ruigrok-Ritstier, K.; Besselink, N.; Murtaza, M.; van, I.W.F.; Heine, A.A.; Smid, M.; et al. Ovarian cancer cell line panel (OCCP): clinical importance of in vitro morphological subtypes. *PLoS One* **2014**, *9*, e103988, doi:10.1371/journal.pone.0103988.

41. McCloskey, C.W.; Goldberg, R.L.; Carter, L.E.; Gamwell, L.F.; Al-Hujaily, E.M.; Collins, O.; Macdonald, E.A.; Garson, K.; Daneshmand, M.; Carmona, E.; et al. A new spontaneously transformed syngeneic model of high-grade serous ovarian cancer with a tumor-initiating cell population. *Front Oncol* **2014**, *4*, 53, doi:10.3389/fonc.2014.00053.

42. Roby, K.F.; Taylor, C.C.; Sweetwood, J.P.; Cheng, Y.; Pace, J.L.; Tawfik, O.; Persons, D.L.; Smith, P.G.; Terranova, P.F. Development of a syngeneic mouse model for events related to ovarian cancer. *Carcinogenesis* **2000**, *21*, 585-591, doi:10.1093/carcin/21.4.585.

43. Ng, A.; Tan, S.; Singh, G.; Rizk, P.; Swathi, Y.; Tan, T.Z.; Huang, R.Y.; Leushacke, M.; Barker, N. Lgr5 marks stem/progenitor cells in ovary and tubal epithelia. *Nat Cell Biol* **2014**, *16*, 745-757, doi:10.1038/ncb3000.

44. Ahmed, N.; Stenvers, K.L. Getting to know ovarian cancer ascites: opportunities for targeted therapy-based translational research. *Front Oncol* **2013**, *3*, 256, doi:10.3389/fonc.2013.00256.

45. Liang, B.; Peng, P.; Chen, S.; Li, L.; Zhang, M.; Cao, D.; Yang, J.; Li, H.; Gui, T.; Li, X.; et al. Characterization and proteomic analysis of ovarian cancer-derived exosomes. *J Proteomics* **2013**, *80*, 171-182, doi:10.1016/j.jprot.2012.12.029.

46. Runz, S.; Keller, S.; Rupp, C.; Stoeck, A.; Issa, Y.; Koensgen, D.; Mustea, A.; Sehouli, J.; Kristiansen, G.; Altevogt, P. Malignant ascites-derived exosomes of ovarian carcinoma patients contain CD24 and EpCAM. *Gynecol Oncol* **2007**, *107*, 563-571, doi:10.1016/j.ygyno.2007.08.064.

47. Taylor, D.D.; Gercel-Taylor, C. MicroRNA signatures of tumor-derived exosomes as diagnostic biomarkers of ovarian cancer. *Gynecol Oncol* **2008**, *110*, 13-21, doi:10.1016/j.ygyno.2008.04.033.

48. Thery, C.; Amigorena, S.; Raposo, G.; Clayton, A. Isolation and characterization of exosomes from cell culture supernatants and biological fluids. *Curr Protoc Cell Biol* **2006**, *Chapter 3*, Unit 3 22, doi:10.1002/0471143030.cb0322s30.

Chapter 7

49. Etzerodt, A.; Moulin, M.; Doktor, T.K.; Delfini, M.; Mossadegh-Keller, N.; Bajenoff, M.; Sieweke, M.H.; Moestrup, S.K.; Auphan-Anezin, N.; Lawrence, T. Tissue-resident macrophages in omentum promote metastatic spread of ovarian cancer. *J Exp Med* **2020**, *217*, doi:10.1084/jem.20191869.

50. Oskarsson, T.; Acharyya, S.; Zhang, X.H.; Vanharanta, S.; Tavazoie, S.F.; Morris, P.G.; Downey, R.J.; Manova-Todorova, K.; Brogi, E.; Massague, J. Breast cancer cells produce tenascin C as a metastatic niche component to colonize the lungs. *Nat Med* **2011**, *17*, 867-874, doi:10.1038/nm.2379.

51. Bilandzic, M.; Stenvers, K.L. Assessment of ovarian cancer spheroid attachment and invasion of mesothelial cells in real time. *J Vis Exp* **2014**, doi:10.3791/51655.

52. Adam, R.A.; Adam, Y.G. Malignant ascites: past, present, and future. *J Am Coll Surg* **2004**, *198*, 999-1011, doi:10.1016/j.jamcollsurg.2004.01.035.

53. Feldman, G.B.; Knapp, R.C.; Order, S.E.; Hellman, S. The role of lymphatic obstruction in the formation of ascites in a murine ovarian carcinoma. *Cancer Res* **1972**, *32*, 1663-1666.

54. Matte, I.; Lane, D.; Laplante, C.; Rancourt, C.; Piche, A. Profiling of cytokines in human epithelial ovarian cancer ascites. *Am J Cancer Res* **2012**, *2*, 566-580.

55. Mills, G.B.; May, C.; Hill, M.; Campbell, S.; Shaw, P.; Marks, A. Ascitic fluid from human ovarian cancer patients contains growth factors necessary for intraperitoneal growth of human ovarian adenocarcinoma cells. *J Clin Invest* **1990**, *86*, 851-855, doi:10.1172/JCI114784.

56. Burleson, K.M.; Casey, R.C.; Skubitz, K.M.; Pambuccian, S.E.; Oegema, T.R., Jr.; Skubitz, A.P. Ovarian carcinoma ascites spheroids adhere to extracellular matrix components and mesothelial cell monolayers. *Gynecol Oncol* **2004**, *93*, 170-181, doi:10.1016/j.ygyno.2003.12.034.

57. Burkhalter, R.J.; Symowicz, J.; Hudson, L.G.; Gottardi, C.J.; Stack, M.S. Integrin regulation of beta-catenin signaling in ovarian carcinoma. *J Biol Chem* **2011**, *286*, 23467-23475, doi:10.1074/jbc.M110.199539.

58. Wielenga, V.J.; Smits, R.; Korinek, V.; Smit, L.; Kielman, M.; Fodde, R.; Clevers, H.; Pals, S.T. Expression of CD44 in Apc and Tcf mutant mice implies regulation by the WNT pathway. *Am J Pathol* **1999**, *154*, 515-523, doi:10.1016/S0002-9440(10)65297-2.

59. Ricken, A.; Lochhead, P.; Kontogiannea, M.; Farookhi, R. Wnt signaling in the ovary: identification and compartmentalized expression of wnt-2, wnt-2b, and frizzled-4 mRNAs. *Endocrinology* **2002**, *143*, 2741-2749, doi:10.1210/endo.143.7.8908.

60. Tothill, R.W.; Tinker, A.V.; George, J.; Brown, R.; Fox, S.B.; Lade, S.; Johnson, D.S.; Trivett, M.K.; Etemadmoghadam, D.; Locandro, B.; et al. Novel molecular subtypes of serous and endometrioid ovarian cancer linked to clinical outcome. *Clin Cancer Res* **2008**, *14*, 5198-5208, doi:10.1158/1078-0432.CCR-08-0196.

61. Badiglian Filho, L.; Oshima, C.T.; De Oliveira Lima, F.; De Oliveira Costa, H.; De Sousa Damiao, R.; Gomes, T.S.; Goncalves, W.J. Canonical and noncanonical Wnt pathway: a comparison among normal ovary, benign ovarian tumor and ovarian cancer. *Oncol Rep* **2009**, *21*, 313-320.

62. Popadiuk, C.M.; Xiong, J.; Wells, M.G.; Andrews, P.G.; Dankwa, K.; Hirasawa, K.; Lake, B.B.; Kao, K.R. Antisense suppression of pygopus2 results in growth arrest of epithelial ovarian cancer. *Clin Cancer Res* **2006**, *12*, 2216-2223, doi:10.1158/1078-0432.CCR-05-2433.

63. Duan, H.; Yan, Z.; Chen, W.; Wu, Y.; Han, J.; Guo, H.; Qiao, J. TET1 inhibits EMT of ovarian cancer cells through activating Wnt/beta-catenin signaling inhibitors DKK1 and SFRP2. *Gynecol Oncol* **2017**, *147*, 408-417, doi:10.1016/j.ygyno.2017.08.010.

64. Gray, J.W.; Suzuki, S.; Kuo, W.L.; Polikoff, D.; Deavers, M.; Smith-McCune, K.; Berchuck, A.; Pinkel, D.; Albertson, D.; Mills, G.B. Specific keynote: genome copy number abnormalities in ovarian cancer. *Gynecol Oncol* **2003**, *88*, S16-21; discussion S22-14.

65. Takada, T.; Yagi, Y.; Maekita, T.; Imura, M.; Nakagawa, S.; Tsao, S.W.; Miyamoto, K.; Yoshino, O.; Yasugi, T.; Taketani, Y.; et al. Methylation-associated silencing of the Wnt antagonist SFRP1 gene in human ovarian cancers. *Cancer Sci* **2004**, *95*, 741-744, doi:10.1111/j.1349-7006.2004.tb03255.x.

66. Endo, H.; Hosono, K.; Uchiyama, T.; Sakai, E.; Sugiyama, M.; Takahashi, H.; Nakajima, N.; Wada, K.; Takeda, K.; Nakagama, H.; et al. Leptin acts as a growth factor for colorectal tumours at stages subsequent to tumour initiation in murine colon carcinogenesis. *Gut* **2011**, *60*, 1363-1371, doi:10.1136/gut.2010.235754.

67. Yan, D.; Avtanski, D.; Saxena, N.K.; Sharma, D. Leptin-induced epithelial-mesenchymal transition in breast cancer cells requires beta-catenin activation via Akt/GSK3- and MTA1/Wnt1 protein-dependent pathways. *J Biol Chem* **2012**, *287*, 8598-8612, doi:10.1074/jbc.M111.322800.

68. Asuthkar, S.; Gondi, C.S.; Nalla, A.K.; Velpula, K.K.; Gorantla, B.; Rao, J.S. Urokinase-type plasminogen activator receptor (uPAR)-mediated regulation of WNT/beta-catenin signaling is enhanced in irradiated medulloblastoma cells. *J Biol Chem* **2012**, *287*, 20576-20589, doi:10.1074/jbc.M112.348888.

69. Zhang, X.; Chen, L.; Wang, Y.; Ding, Y.; Peng, Z.; Duan, L.; Ju, G.; Ren, Y.; Wang, X. Macrophage migration inhibitory factor promotes proliferation and neuronal differentiation of neural stem/precursor cells through Wnt/beta-catenin signal pathway. *Int J Biol Sci* **2013**, *9*, 1108-1120, doi:10.7150/ijbs.7232.

70. Thibault, B.; Castells, M.; Delord, J.P.; Couderc, B. Ovarian cancer microenvironment: implications for cancer dissemination and chemoresistance acquisition. *Cancer Metastasis Rev* **2014**, *33*, 17-39, doi:10.1007/s10555-013-9456-2.

Chapter 7

Supplementary figures
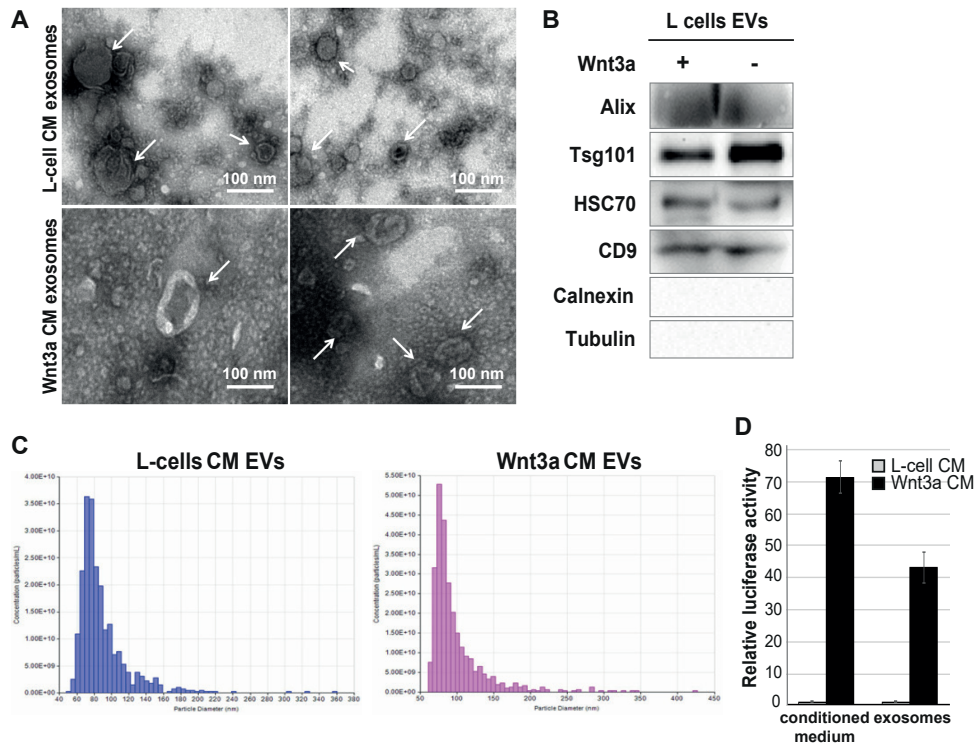
Figure 4 – Supplement 1. (**a**). Transmission electron microscopy (TEM) showing the presence of cup-shaped structures of 40-100 nm in both L-cell and Wnt3a CM cell derived post 100,000g pellets. (**b**). Western blot analysis showing the presence of exosomal markers Alix, Tsg101, HSC90 and CD9 in both L-cell and Wnt3a CM derived post-100,000g pellets. Contaminating protein such as calnexin and tubulin were absent. (**c**). qNano analysis measuring particle size and confirmed the existence of particles ranging from 40 to 100 nm in diameter in the extracted post-100,000g L-cell CM and Wnt3a CM pellets. (**d**). TOP-Flash luciferase reporter analysis measuring induction of Wnt signaling in HEK293 after treatment with patient derived ascites exosomes and the supernatant after the 100,000g centrifugation step. Two Wnt positive and two Wnt negative patients as measured in Figure 4A were used. Negative control: L-cell CM; positive control: Wnt3a CM. Each bar represents the mean ± SD.

CHAPTER VIII

General discussion

Teeuwssen M.J.

The success of cytotoxic and targeted therapies in cancer treatment has been hindered by a variety of mechanisms that contribute to therapy resistance. Historically, most efforts on the elucidation of therapy resistance have been made on resistance-conferring genetic mutations, such as alterations that avoid target inhibition through impaired binding of the cytotoxic drug, activation of downstream targets in the same signaling pathway, or engagement of alternative survival pathways components [1]. The development of therapy resistance by targeting these mechanisms resulted from either the selection of rare drug-tolerant cells with pre-existing genetic alterations upon drug treatment, or the acquisition of *de novo* mutations during treatment [2,3]. However, notwithstanding the potential and innovative therapeutic strategies currently in development that specifically target genetic mechanisms, emerging evidence indicate the significance of non-mutational and plasticity-related escape mechanisms that promote therapy resistance [4,5]. Here, plasticity of the tumor cell contributes to a phenotypic state that enable the adaptation and consequentially the survival of carcinoma cells that are no longer dependent on the drug targeted pathway [6,7]. In the last few years, cell plasticity has emerged as a novel anti-cancer treatment strategy in various cancer types. In the final chapter of this thesis, novel therapeutic strategies to target cancer cell plasticity will be discussed including their associated challenges.

1. Phenotypic plasticity and EMT

Phenotypic plasticity can be described as the ability of a cell to significantly alter its identity to adapt to changes in its direct environment [6]. In cancer treatment, such plasticity allows tumor cells to reversible transition to a cell state, independently of the drug targeted pathway. Epithelial-to-mesenchymal transition (EMT) is one of the best described examples of molecular and cellular processes underlying phenotypic plasticity [8] and is normally defined as a process through which cancer cells lose part of their epithelial characteristics by downregulating E-cadherin and apical-basal polarity and cell-cell junctions proteins, and acquire mesenchymal features by upregulating vimentin and other fibroblast-specific genes, together with increased migrative and invasive properties. As such, EMT has been suggested to play a critical role in malignant progression, local invasion and dissemination, and in distant metastasis [8]. In addition to the metastatic process, EMT has been functionally associated with 1. the acquisition of stem cell behavior, 2. escape from apoptosis and senescence, 3. extracellular matrix and tumor-microenvironment remodeling, and 4. resistance to anti-cancer treatments [6].

Yet, as comprehensively discussed in *Chapter 2* of this thesis, EMT should not be envisaged as a binary system but rather as a dynamic process where carcinoma cells can acquire intermediate and highly metastable EMT phenotypes characterized by the co-expression of both epithelial and mesenchymal genes (partial or hybrid EMT), and the capacity to revert back to a more epithelial state through mesenchymal-to-epithelial transitions (MET) [8,9].

The EMT-induction of a slow-cycling stem-like state, downregulation of apoptotic signaling pathways, and upregulation of drug efflux, all contribute to the development of resistance of tumor cells to cytotoxic drugs [10-15] (*Chapters 4 and 6*). In addition, EMT-associated transcription factors have been demonstrated to underlie resistance against molecular targeted therapies [16-18]. For example, the EMT-transcription factor

Snail induces the expression of the AXL receptor tyrosine kinase on the surface of non-small-cell lung carcinoma cells. AXL-signaling, activated by the GAS6 ligand (growth arrest-specific protein 6), empowers Snail-expressing tumor cells to overrule the cytotoxic effects of the EGFR blockage with small-molecule inhibitors or antagonistic monoclonal antibodies [17,18]. Lastly, EMT also stimulates several processes that enable cancer cells to escape the deadly effects of cytotoxic T-cells [19,20]. In this case, ZEB1 expression leads to upregulation of the expression of programmed cell death ligand 1 (PD-L1), which binds to the programmed cell death protein 1 (PD-1) inhibitory immune-checkpoint receptor expressed by cytotoxic T-cells and thereby reducing their function [19]. Moreover, Snail expression in melanoma cells contributes to enhanced secretion of thrombospondin (TSP-1), which promotes the development of regulatory T-cells within the tumor microenvironment thus eventually suppressing the anti-tumor activity of cytotoxic T-cells [20].

Hence, although the link between cellular plasticity and therapy resistance is well-established, the molecular mechanisms accounting for the induction and maintenance of the cellular plasticity upon drug treatment are yet poorly understood. Nevertheless, interfering with cancer cell plasticity might represent an alternative way to prevent therapy resistance and could therefore improve anti-cancer treatment responses. In the following section I will review and summarize distinct potential treatment strategies targeting cellular plasticity, together with the associated challenges.

2. Future perspectives: can we treat cancer cell plasticity?

Targeting cell plasticity may represent a novel approach to prevent the appearance of drug-resistant cells and to improve response to targeted treatments. At least three different approaches could be pursued to target cancer cell plasticity: *i*. the inhibition of the development of plasticity by antagonizing the underlying molecular mechanisms, *ii*. the selective targeting of cancer cells in their new therapy resistant state, and *iii*. by reversing the conversion process through the induction of differentiation and/or trans-differentiation. Below, each of these strategies will be discussed, including the associated challenges of each approach.

2.1. Preventing cancer cell plasticity

Cancer cell plasticity can be prevented by interfering with the processes that are critical for the activation and subsequent maintenance of the programs regulating it. In order to target cellular plasticity, the underlying upstream epigenetic mechanisms such as chromatin remodeling and transcriptional adaptation, can be specifically inhibited. In addition, targeting of downstream signaling pathways underlying plasticity, together with specific components of the tumor microenvironment known to play key roles in endowing cancer cells with stem-like features, may also represent promising therapeutic targets.

2.1.1. The epigenetic regulation of cellular plasticity

Rather than genetic aberrations that would result in permanent changes, the transient and reversible modifications of cell identity elicited by anti-cancer treatments highlight the critical role played by epigenetic re-programming of tumor cells. Chromatin remodeling

complexes, such as Nucleosome Remodeling and Deacetylase (NuRD), SWI/SNF, and Polycomb, play central roles in this regulation by affecting the accessibility of regulatory DNA elements and positioning of nucleosomes [21]. In addition, post-translational histone modifications which regulate chromatin folding, and the direct recruitment of regulatory proteins that control gene expression, are also involved [22]. Yet, although they facilitate entirely different biochemical reactions, remodelers and histone-modifying enzymes function in a closely related manner to regulate chromatin state [23]. Cancer studies have revealed frequent alterations in remodelers and histone-modifying enzymes across a broad spectrum of cancer types contributing to oncogenesis and cancer progression [24-26]. In *Chapter 3* we show that loss of the Deleted in Oral Cancer 1 (DOC1; also known as CDK2AP1: cyclin-dependent kinase 2-associated protein 1) tumor suppressor in oral squamous cell carcinoma (OSCC) cells leads to the failure of remodeler complex NuRD to bind and repress EMT-related transcriptional regulators thereby promoting the acquisition of quasi-mesenchymal states. Accordingly, rescue of DOC1 expression in OSCC cells results in the reversal of EMT, i.e. MET (**Figure 1**). Mechanistically, we show that DOC1 is an integral subunit of the MBD2/3/CHD3/4/5-NuRD family and that it is essential for the gene-selective binding of the NuRD complex to the promoters of the EMT master regulators *TWIST1, TWIST2*, and *ZEB2*. Upon DOC1-dependent NuRD recruitment, SWI/SNF is displaced resulting in the transition from active to repressive chromatin. Moreover, next to the eviction of SWI/SNF by NuRD, recruitment of the Polycomb Repressive Complex 2 (PRC2) and KDM1A is promoted, followed by H3K27 methylation and H3K4 demethylation (**Figure 1**). Interestingly, depletion of SWI/SNF mimics the effects of DOC1 re-expression (**Figure 1**). In the absence of SWI/SNF, the NuRD complex lacking DOC1 still binds to the *TWIST1/2* and *ZEB2* promoters, suggesting that these promoters are permanently targeted by a remodeler. Binding of either SWI/SNF or NuRD determines opposite epigenetic states, thereby committing OSCC cells to either EMT or MET.

Thus, our report suggests a dynamic equilibrium between antagonistic chromatin modulating enzymes, and that disturbances in this balance can promote a cascade of chromatin reprogramming events that drives cancer progression. Such an intertwined system of epigenetic regulation offers therapeutic options aimed at restoring this equilibrium between opposing activities. Indeed, several reports have recently showed that the use of epigenetic therapies in combination with conventional chemotherapy re-sensitizes resistant cancer stem cells (CSCs) to anti-cancer treatment [27,28]. For example, DNA methyltransferase (DNMT) inhibitor SGI-110 drives ovarian CSCs towards a differentiated phenotype and sensitize them to platinum treatment [29]. In addition, supplementary studies have demonstrated the re-sensitization of tumors cells to chemotherapeutic agents by epigenetic drugs through EMT inhibition in several cancers including head and neck, thyroid, pancreatic, and breast cancer [30-33]. For instance, in head and neck cancer, the inhibition of histone deacetylases (HDAC) revealed a synergistic effect with chemotherapeutic drugs, suppressed the stemness and EMT character, stopped the cell cycle, and induced apoptosis [34].

Chapter 8
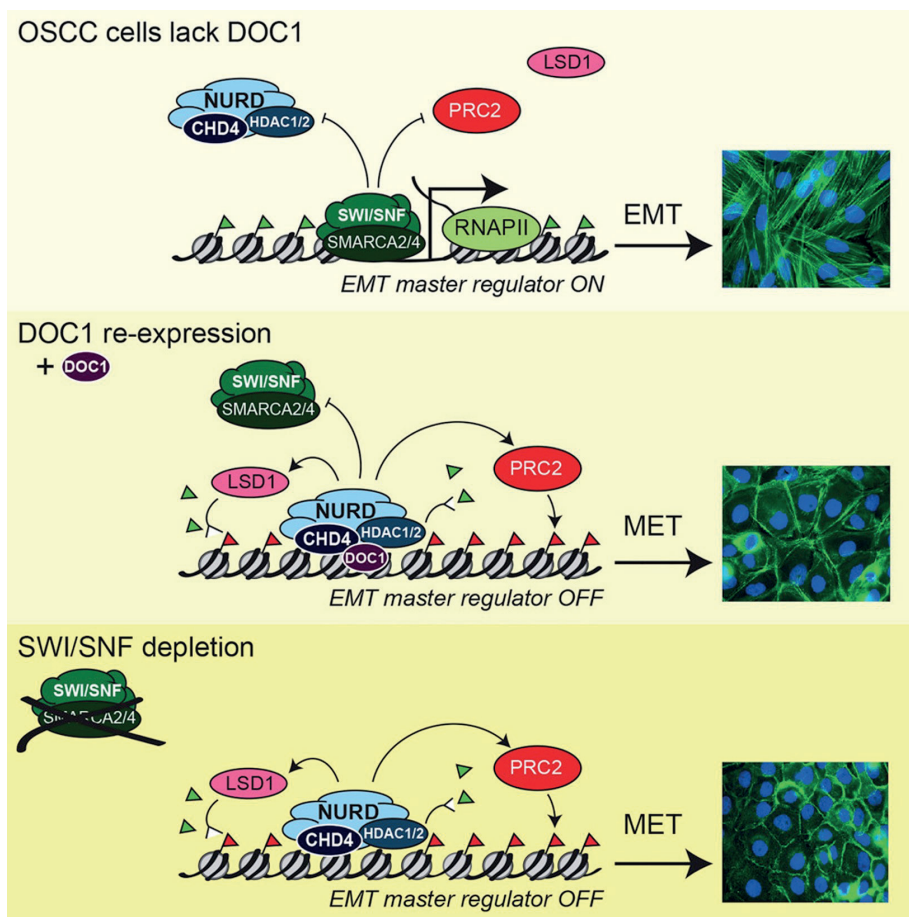
Figure 1. Loss of the NuRD subunit DOC1 (Deleted in Oral Cancer 1) is associated with human oral squamous cell carcinomas (OSCC). Restoration of DOC1 expression in OSCC cells leads to a reversal of epithelial-to-mesenchymal transition (EMT). This is caused by the DOC1-dependent targeting of NuRD to repress key transcriptional regulators of EMT. NuRD recruitment drives extensive epigenetic reprogramming, including eviction of the SWI/SNF remodeler, formation of inaccessible chromatin, H3K27 deacetylation, and binding of PCR2 and KDM1A, followed by H3K27 methylation and H3K4 demethylation. Strikingly, depletion of SWI/SNF mimics the effect of DOC1 re-expression [35].

Though, the effects of epigenetic drugs on cellular plasticity differ in various types of cancers. Whereas the repression of EMT by certain epigenetic inhibitors has been demonstrated in some models, others have shown opposite effects, namely the activate the expression of EMT transcription factors [36-39]. Valproic acid (VPA) is a member of the short-chain fatty acid family and a HDAC inhibitor. In renal cell carcinoma cells, VPA was shown to inhibit EMT by decreasing SMAD4 expression [40]. Furthermore, it reduces proliferation and invasion of bladder cancer cells, and increases sensitivity to paclitaxel in thyroid carcinoma cells [30,41]. In contrast, VPA and trichostatin A (TSA), another HDAC inhibitor, induced mesenchymal characteristics in colon cancer cells by a decrease in E-cadherin and an increase in vimentin expression at both mRNA and protein levels. Here,

colon cancer cells changed from a cobble stone-appearance to a spindle like-morphology with increased migration and invasion ability following treatment with TSA or VPA [39].

Furthermore, most HDAC inhibitors target multiple HDAC isoforms leading to side effects and variable outcomes [42]. Thus, epigenetic drugs like DNMT and HDAC inhibitors require careful attention before their administration as new anti-cancer drugs. Future research may result in more specific epigenetic drugs that minimize the off-target side effects and the variable results of the targeted treatment. To illustrate an example of this, Mocetinostat is a HDAC inhibitor that, in contrast to other HDAC inhibitors, specifically interferes with ZEB1 expression leading to the reversion of therapy resistance by sensitizing cancer cells to chemotherapy [31].

Alternatively, rather than targeting the chromatin landscape, non-coding RNAs such as microRNAs (miRNA) and long coding RNAs (lncRNA) known to play key roles in the regulation of the expression of EMT-TFs and of epigenetic-regulating enzymes, could potentially represent an alternative target to treat cancer plasticity and prevent therapy resistance. For example, in non-small cell lung carcinoma (NSCLC) cells, the miR-200 family has been demonstrated to enhance the sensitivity to nintedanib by influencing EMT [43]. In contrast, miR-223 has been shown to induce EMT in gemcitabine-resistant pancreatic cancer cells by down-regulating the ubiquitin protein ligase Fbw7. Inhibition of miR-223 reversed the EMT state and enhanced the sensitivity of the carcinoma cells to gemcitabine [44]. Lastly, decreased miR-186 expression features cisplatin-resistant ovarian cancer cells leading to the induction of EMT by increased Twist1 expression. Overexpression of miR-186 in these ovarian cancer cells provokes a decreased expression of Twist, reversed EMT, and sensitized the cells to cisplatin [45]. These results point to non-coding RNAs as attractive candidates for overcoming drug resistance. Although several new insights have been recently gathered on the role of miRNA families and lncRNAs in tumorigenesis and cancer progression, there is still a long way ahead to fully comprehend the stability and specificity of these molecules in cancer treatment [46].

2.1.2. The role of the microenvironment in cellular plasticity

It is well-established that the tumor microenvironment plays important roles in cellular plasticity and treatment resistance. The reciprocal interactions between a tumor cell and its tumor microenvironment allows the former to regulate the response to the changing environment and remodel the latter to facilitate its survival and proliferation. Numerous reports have shown that EMT programs in carcinoma cells are provoked by a range of signals originating from different components of the stroma [8]. Among them, cancer associated fibroblasts (CAFs), tumor associated macrophages (TAMs), infiltrating T-lymphocytes, and myeloid-derived suppressor cells (MDSCs), play vital roles through the paracrine regulation of EMT induction by cytokines and growth factors, including tumor necrosis factor alpha (TNFα), interleukin-6 (IL-6), transforming growth factor β (TGF-β), and hepatocyte growth factor (HGF). As such, targeting specific components of the stroma (e.g. CAFs, TAMs, T-lymphocytes and MDSCs), their secreted cytokines, and/or the ECM, may be of great potential clinical value in preventing cell plasticity.

CAFS are the most abundant non-cancer cell types in the stroma surrounding most solid tumors. CAFs show remarkable degree of heterogeneity with different subsets within individual tumors. This heterogeneity is due to different developmental origin of CAFs as well as the influence of the local micro-environment within a tumor on these cells [47].

Chapter 8

For example, TGF-β can induce a process called endothelial to mesenchymal transition (EndMT) that drives proliferating endothelial cells to undergo a phenotypic conversion into fibroblast-like cells displaying mesenchymal markers such as fibroblast-specific protein-1, α-SMA, N-cadherin and type I/III collagen, together with the corresponding loss of endothelial markers like CD31, platelet endothelial cell adhesion molecule-1 (PECAM1), Tie-2, and vascular endothelial (VE) cadherin [48,49]. Neutralizing antibodies or chemical inhibitors targeting molecules required for EndMT could be instrumental in the inhibition of this process, thereby preventing the formation of CAFs and reversing therapy resistance. Indeed, reduced resistance to cisplatin and gefitinib was shown in a multicellular lung carcinoma spheroid model upon EndMT inhibition in endothelial cells [50]. Although the role of EndMT needs to be further explored and fully understood, it represents yet a novel potential therapeutic target in anti-cancer strategy.

Alternatively, DNA vaccines targeting fibroblast activation protein (FAP), a fibroblast marker that is highly expressed in CAFs compared to normal fibroblasts, have been shown to enhance CD8+ T-cell-mediated killing of CAFs in pre-clinical studies. Combining the vaccination with chemotherapy resulted in a 70% increase in the uptake of the chemotherapeutic drugs in tumor xenografts [51]. In addition, several other targets, such as tenascin C and connective tissue growth factor (CTGF), both highly expressed in CAFs, represent additional promising therapeutic targets against CAFs [52,53]. Also, the genetic or pharmacological inhibition of the crosstalk between tumor cells expressing platelet-derived growth factor (PDGF)-CC and CAFs expressing the equivalent receptors in human basal-like mammary carcinomas have also been demonstrated to confer sensitivity to endocrine therapy with tamoxifen of the aromatase inhibitor letrozole in previously resistant tumors [54].

Growing evidence has shown that tumor-associated macrophages or TAMs are actively involved in resistance to anti-cancer drugs, and that depletion or inhibition of these cells can attenuate therapy resistance *in vitro* and *in vivo*. For example, inhibition of macrophages by exploiting a CSF-1 (colony stimulating factor 1) neutralizing antibody reverses chemotherapy resistance in a human breast cancer xenograft [55]. In addition, other anti-CSF-1 antibodies and small molecules inhibitors [56-58], agents that directly kill macrophages such as trabectedin and zoledronic acid [59,60], and various other clinical trials focused on macrophages are currently advancing [61,62]. Hence, targeting TAMs could potentially inhibit malignant progression and therapy resistance in cancer, and therefore have synergistic effects with anti-cancer therapy.

Different from targeting stromal cells themselves, numerous studies have shown that inhibition of the pro-tumorigenic factors present in the stromal compartment also interferes with the induction of cellular plasticity and its related therapy resistance. Recently, Ebbing et al. (2019) showed the involvement CAF-derived IL6 in the development of therapy resistance in esophageal adenocarcinoma (EAC) [63]. Here, EAC cells treated with either recombinant or CAF-derived IL-6 acquire a mesenchymal phenotype together with increased migratory capacity and enhanced resistance to treatment. Accordingly, IL6 inhibition reverted the EMT state and sensitized patient derived EAC organoids and cancer cells lines to therapy [63]. Similarly, decreasing the bioavailability of inflammation-stimulated IL6 with a specific blocking antibody increased cancer cell sensitivity to erlotinib treatment in NSCLC cells [64]. Likewise, stromal HGF induced a mesenchymal phenotype with enhanced expression of the EMT-related transcription factor Snail in

small cell lung cancer (SCLC) by activating Met-signaling. This EMT-switch improved tumorigenesis, enhanced cancer cell invasion, and induced the development of resistance to the chemotherapeutic drug etoposide. Vice versa, the blockage of this process with Met inhibitors sensitized cells to chemotherapy both *in vitro* and *in vivo* [65]. Comparably, blocking HGF-mediated signaling in melanoma by either a HGF neutralizing antibody or the Met inhibitor crizotinib, repressed stroma-mediated resistance to BRAF inhibitor PLX4720 [66]. At present, several Met inhibitors but also other inhibitors specifically targeting cytokines and growth factors are being tested in clinical trials [67].

Last, hypoxia is important in the context of the tumor microenvironment that promotes tumor cells to undergo EMT and acquire therapy resistance. In fast-growing solid cancer, the central area of the tumor mass becomes progressively hypoxic and acid. These environmental changes enhance the expression and stabilization of the hypoxia-inducible factor 1-alpha (HIF1α). HIF1α is critical for the transcriptional initiation of genes involved in the re-establishment of local oxygen perfusion [68]. Moreover, HIF1α is able to regulate the expression of EMT-related genes [69] and the related resistance to therapy. For instance, HIF1α induces EMT and promotes chemotherapy resistance under hypoxic circumstances in hepatocellular carcinoma (HCC) [70]. Knock-down of HIF1α, however, reversed the EMT state and eliminated the drug resistance of HCC under hypoxia, supporting the role of hypoxia in EMT-initiated therapy resistance [71,72].

Notwithstanding the above positive results, caution must be taken when considering treating the tumor microenvironment, in view of the stroma's tumor suppressive roles [73,74]. In pancreatic ductal adenocarcinoma (PDAC), the presence of CAFs is related to an improvement in immune surveillance. These CAFs produce a tumor-suppressing rather than a tumor-supporting ECM [73,74]. An additional complicating factor is represented by potential off-target effects. Many cytokines are involved in several different homeostatic signaling pathways. As such, targeting the cytokine itself can affect signaling pathways not originally intended to be targeted. Furthermore, changes in the tumor microenvironment can contribute to development of resistance by preventing the elimination of the tumor by the immune system. For example, alterations in the balance of cytokines, e.g. TGF-β, VEGF, IL6 and others, can inhibit the maturation of dendritic cells (DCs), thus leading to the reduced antigen presenting function of DCs, which on its turn may result in immune tolerance [75]. Thus, significant challenges still lie ahead before the implementation of stromal targeting in clinical anti-cancer practice.

2.1.3. The signalings pathways involved in cellular plasticity
The identification and characterization of the molecular signaling pathways that regulate cellular plasticity in cancer cells has been the subject of intense investigation. In *Chapter 4 and 7* we highlight the relevance of Wnt signaling in the establishment and maintenance of a therapeutic resistant cell population through *ZEB1* upregulation and the induction of phenotypic plasticity in both colon and ovarian cancer. Targeting cellular plasticity by interfering with these signaling pathways presents an approach to prevent the appearance of therapy resistance and accomplish better therapy responses. For instance, overexpression of Wnt3 activates the Wnt signaling pathway and promotes EMT in trastuzumab resistant HER2-overexpressing breast cancer cells [76]. Likewise, expression of the secreted frizzle-related protein 5 (*SFRP5*) gene, encoding for an extracellular antagonist of the Wnt pathway that prevents ligand-receptor interaction by directly binding to Wnt

ligands, is frequently downregulated in ovarian cancer by epigenetic silencing through promoter hypermethylation leading to downstream activation of EMT-TF *TWIST* and *AKT2* signaling [77]. Accordingly, restoration of *SFRP5* expression inhibits Wnt signaling and EMT thereby sensitizing ovarian cancer cells to chemotherapy [77]. Similary, restoration of Wnt antagonist *SFRP1* expression in lung adenocarcinoma cells inhibits the activation of Wnt-signaling and reverses its related taxane chemoresistance. Futhermore, the Wnt inhibitor FH535 enhances the sensitivity of taxane-resistant lung adenocarcinoma cells to taxanes [78]. Overall, numerous Wnt signaling inhibitors, including biological agents and small molecule reagents, have been developed which could overcome EMT-induced therapy resistance [79].

TGF-β signaling is amongst the best-characterized pathways known to drive EMT activation. Among many other studies from the scientific literature, rapamycin, together with 17-AAG and LY294002, have been shown to inhibit EMT through interference with TGF-β signaling [80]. In addition, TGF-β mediated immune-suppression, EMT and tumor dormancy could be reversed by galunisertib, a small molecule inhibitor of TGF-β receptor I [81]. Related to therapy resistance, treatment of animals bearing alkylating resistant tumors with TGF-β neutralizing antibodies increased the sensitivity to cyclophosphamide and cisplatin [82]. Similarly, the increase of paclitaxel-induced autocrine TGF-β secretion leading to the enrichment of drug-resistant CSCs could be blocked by the TGF-β type I receptor kinase inhibitor LY2157299, or by neutralizing TGF-β type II receptor antibodies in triple-negative breast cancer (TNBC) cell lines and mouse xenografts [83]. Currently, several specific TGF-β inhibitors are undergoing both preclinical and clinical testing. However, due to the complicated and multidimensional effects of TGF-β signaling during different stages of tumor development and progression, attentive patient selection and monitoring, and optimization of drug-administration protocols need to be implemented for the effective and safe use of these inhibitors in the clinic [84-86].

Apart from Wnt and Tgf-β, other signaling pathways are known to contribute to EMT-related drug resistance. For example, the acquisition of gemcitabine resistance in pancreatic cancer cells is driven by EMT activation downstream of the Akt/GSK3β/Snail-pathway [87]. Zidovudine, an antiviral agent, inhibits this pathway and restores the gemcitabine sensitivity in the tumor cells. Co-treatment of zidovudine with gemcitabine in mice grafted with gemcitabine-resistant pancreatic cancer cells significantly suppressed tumorigenesis and inhibited the onset EMT (quasi-mesenchymal) cellular phenotypes [87]. In addition, studies have shown that Erk [88] and mTOR inhibitors [89-92] are able to re-establish drug sensitivity by interfering with EMT. Also, metformin has demonstrated to trigger an EMT reversion through the inhibition of the Erk, mTOR, and JAK/STAT3 pathways [93,94].

Overall, a substantial proportion of the experimental therapeutic approaches presently being assessed aims at the inhibition of EMT-inducing upstream pathways and/or their downstream effectors [95]. Notwithstanding these potential and innovative therapeutic strategies specifically target key signaling pathways, plasticity of cancer cells still represents an escape mechanism leading to therapy resistance. For example, MEK inhibition, a therapeutic approach to target the Ras-MAP kinase pathway in tumors, leads to increased Wnt signaling activity and stem cell plasticity, thus exposing a potential side effect of RAS pathway inhibition [96]. Moreover, because of their essential role in tissue homeostasis and regeneration upon damage, its inhibition is likely to result in

adverse events. Therefore, the identification and elucidation of the complex network of intrinsic and extrinsic mechanisms driving cancer progression and therapy resistance still represents the major future research challenge in the translation of the fundamental understanding of metastasis and therapy.

2.2. Targeting the new cell identity

Another approach to prevent and/or interfere with cancer cell plasticity is by targeting the therapy resistant phenotype. This can be achieved by either targeting the malignant cells in their cancer stem cell (CSC) state, by therapeutic blocking of the function of classic EMT-associated markers, or by disturbing plasticity-associated metabolic profiles.

2.2.1. The cancer stem cells (CSC) concept

As previously stated, the activation of the EMT program is functionally linked to the conversion of epithelial tumor cells into the CSC state. According to the CSC concept, a subpopulation of cells exists within tumors that are endowed with self-renewal and the capacity to differentiate, thereby continuously fueling the growth of the tumor mass [97,98]. CSCs are in general refractory to current conventional therapy. Therapeutic strategies specifically targeting and eliminating CSC may therefore represent an attractive approach to achieve tumor regression.

The transcriptomic and proteomic profiles of CSCs are clearly distinct from the more differentiated tumor cells thus offering novel opportunities to target them by exploiting these differences. For example, antibodies directed against CSC-specific cell surface markers such as LGR5, CD133 or CD44, could be utilized [99-103]. Indeed, selective ablation of LGR5+ cancer stem cells with antibody-drug conjugates in gastro-intestinal tumors caused induced cytotoxicity of these CSCs, hindered tumor growth, and impeded the development of metastatic lesions [100-103]. However, within weeks after discontinuation of the targeted therapy, LGR5- cancer cells were able to de-differentiate and acquire LGR5 expression together with their stem-like features, thereby reinstating growth of the primary tumor and metastatic lesions [102,103]. Furthermore, since CSC-specific markers are often shared by normal stem cells, their pharmacologic targeting is likely to result in significant side effects on healthy tissues [101,104]. Thus, although targeting CSC represents on paper the most straightforward and rationale approach, it is likely to pose main challenges due to cellular plasticity and side effects.

Alternatively, with the objective to selectively eradicate CSCs, much effort has been committed to identify molecular targets specific for cancer cells undergoing EMT [95,105,106]. A chemical compound screen taking advantage of immortalized human mammary epithelial cells with or without prior experimental EMT activation, led to the identification of the potassium ionophore salinomycin as an cytotoxic agent specific for cells that have undergone EMT [95]. Interestingly, salinomycin induced the differentiation of mesenchymal-like tumors *in vivo*, as evaluated by increased E-cadherin and reduced vimentin expression. In addition, a comparable screen for kinase antagonists revealed that a protein kinase C α (PKCα) inhibitor specifically targets CSCs, with little effects on non-CSCs. The transition from non-stem cells to CSC involves a change from epidermal growth factor receptor (EGFR) to platelet-derived growth factor receptor (PDGFR) pathway signaling, and results in the PKCα-dependent activation of FRA-1. PKCα and FRA-

Chapter 8

1 expression are both associated with aggressive triple-negative breast cancers and the reduction of FRA1 results in MET [107].

As also discussed in more details here above on the use of epigenetic drugs, targeting key signaling pathways involved in regulation of cancer stem cells affecting EMT- and CSC-inducible components from the micro-environment, might represent an alternative and promising strategy to affect CSC maintenance. Last, ABC transporters, i.e. ATP-dependent drug efflux pumps expressed by therapy-resistant CSCs, can also be specifically targeted by using ATP-competitive molecules [108,109]

In view of the challenges posed by targeting CSCs due to cellular plasticity of bulk tumor cells and to the expected cytotoxic effects on healthy stem cells, one would ideally prefer to ablate both bulk tumor cells by employing combinational therapies. Hence, recognizing molecular characteristics involved in the identity shift between cell states can be used to affect cellular mechanisms essential to CSCs. In addition, as discussed in more detail here below, the general concept according to which poorly differentiated cancer with high CSC contents can be treated by inducing terminal differentiation lay the basis for novel treatment modalities. However, before these re/trans-differentiation-based strategies will be discussed, two approaches aimed at the "simple" targeting of the newly obtained cellular identity will be highlighted.

2.2.2. Selective targeting cells that have undergone EMT

When considering targeting CSCs with specific therapeutics directed at molecules that distinguish them from more committed tumor cells, robust regiments aimed at the mesenchymal cell state have been tested [110,111]. Degradation of vimentin, an EMT-related filament, is accomplished by withaferin A treatment. Withaferin A has been revealed to inhibit breast cancer cell invasion metastasis formation both *in vitro* and *in vivo* [110]. Likewise, similar results were obtained by treating prostate cancer cells with monoclonal antibodies directed against the ectodomain of the EMT marker N-cadherin [111]. Notwithstanding the promising preliminary data, the therapeutic efficacy of these reagents remains to be further investigated. Mesenchymal markers are commonly expressed by non-cancerous mesenchymal cells suxh as fibroblast, potentially resulting in toxicity. Yet, alternative strategies are currently explored which target cells undergoing an EMT program.

2.2.3. Metabolic targeting

Recently, it has been reported that the deregulation of common metabolic processes, including glucose and metabolism, and amino acid utilization affect the consumption of cellular energy sources, regulate the expression of EMT-related genes, and lead to therapy resistance (**Figure 2**) [112]. Therefore, interfering with the metabolic regulation through gene-specific or pharmacological inhibition targeting specific metabolic pathways may suppress cellular plasticity leading to the inhibition of tumor progression and improvement of anti-cancer efficacy.

The Warburg effect, i.e. the modified cellular metabolism that favors anaerobic glycolysis rather than oxidative phosphorylation, enables tumor cells to compensate for the higher demand of energy determined by enhanced cell proliferation [113]. Lately, besides their function in proliferation, the role of glycolytic enzymes in regulating the EMT process has also emerged (**Figure 2**). For example, phosphoglucose isomerase (PGI),

an glycolytic enzyme that converts glucose-6-phosphate and fructose-6-phosphate in the cytoplasm, has been shown to be secreted by tumor cells where it functions as a cytokine, often referred to as autocrine motility factor (AMF). Ectopic expression of PGI/AMF in normal epithelial breast cells induces EMT [114]. Also, its overexpression in breast cancer cells leads to EMT by the stabilization of ZEB1 and ZEB2 through NFkB signaling [115]. Accordingly, suppression of PGI/AMF triggered a MET in aggressive mesenchymal-type human breast cancer MDA-MB-231 cells [114], in endometrial cancer cells [116], and in lung fibrosarcoma [117]. In addition, downregulation of the glycolytic enzyme fructose-1,6-biphosphatase (FBP1) has been shown to promote EMT and is a poor prognosis predictor in gastic cancer [118]. In contrast, FBP1 expression inhibits the induction of SNAI1-mediated EMT in luminal breast cancer cells [119]. Moreover, the overexpression of lactate dehydrogenase (LDH), the enzyme that converts pyruvate to lactate, promotes malignant progression via EMT activation and confers stemness in muscle-invasice bladder cancer [120]. Lastly, inhibition of glyceraldehyde-3-phosphate dehydrogenase (GAPDH) blocks EMT by repressing SNAI1 in colon cancer [121].

Functional connection between mitochondrial dysfunction and EMT has also been shown (**Figure 2**). A comprehensive analysis across 20 different cancer types revealed a correlation between the downregulation of mitochondrial genes and the expression of an EMT gene signature and a worst clinical outcome [122]. Tumors containing mutations in genes encoding for tricarboxylic acid cycle (TCA) enzymes FH, IDH, and SDH, were also demonstrated to feature EMT-related signature [123-125]. Here, a common pathway affected by these metabolites is the epigentic suppression of the miR200 family, through inhibition of histone and DNA demethylases [126]. Furthermore, induced mitochondrial dysfunction by depletion of mitochondrial DNA in breast cancer cells activates EMT through enhanced expression of EMT-TFs and metalloproteases, and E-cadherin suppression in Calcineurin A (CaN)-dependent fashion [127].

Similarly, numerous reports support the correlation between EMT and alterations in lipid metabolism (**Figure 2**). Proteomic and lipidomic studies have identified major differences between epithelial and mesenchymal cancer cells and in particular in the activity of specific metabolic enzymes and metabolites including fatty acids and phospholipids. In epithelial cells increased levels of mono-unsaturated fatty acids together with increased expression of enzymes involved in *de novo* fatty acid synthesis, is often observed whereas mesenchymal cancer cells dispay reduced lipogenesis with higher polyunsaturated fatty acid levels and enhanced expression of genes regulating triacylglycerol synthesis and lipid droplet formation [128]. In addition, other lipid modifying networks have also been demonstrated to regulate EMT. For example, the acyl-CoA synthetase/stearoyl-CoA desaturase (ACSL/SCD) complex causes EMT and promotes migration and invasion of colon cancer cells. This mesenchymal state is reversed by the reactivation of AMPK signaling. Of note, the expression of this network correlates with poor clinical outcome in stage-II colon cancer patients. Treatment with chemical inhibitors of ACSL/SCD selectively decreases cancer cell viability without affecting normal cells [129]. Moreover, integrity of the plasma membrane has also been shown to play an important role by remodeling of the lipidome during EMT [130]. An important characteristic of the plasma membrane is the compositional and functional subdivision of signaling domains, including the organisation of dynamic lipid and protein complexes called lipid rafts [131]. Upon EMT induction, lipid drafts become destabilized, an essential step for the maintenance of

the stem cell phenotype and of EMT-induced changes in plasma membrane coordinated pathways [132]. Treating tumor cells with ω-3 polyunsaturated fatty acid docosahexaenoic acid (DHA) reversed mesenchymal features to more epithelial characteristics, especially with respect to mobility and stem cell properties, though retaining expression of some mesenchymal markers. Hence, the stabilized rafts suppress the activity of EMT-associated signaling pathways and impaired the ability of tumor cells to colonize the lung [132].
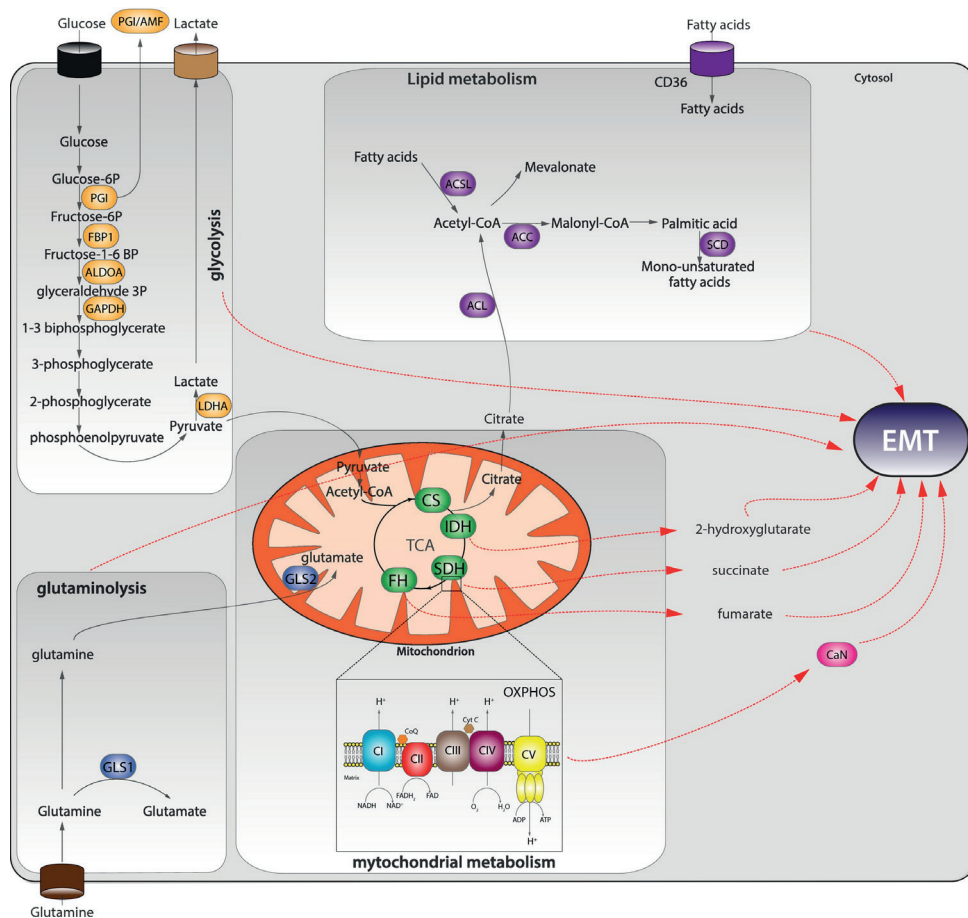
Figure 2. Metabolic genes control EMT. Aberrant expression of metabolic enzymes of glycolysis (orange), lipid metabolism (purple), glutaminolysis (blue), and mitochondrial metabolism (green) leads to EMT. Red dashes indicate the link between specific metabolic pathway/metabolites and EMT. ACSL: acetyl-CoA synthetase; CI-CV: respiratory chain complexes I-V; CoQ: coenzyme Q; CS: citrate synthase; CytC: cytochrome C; LDHA: lactic dehydrogenase A. Adapted from [126].

The functional link between EMT and metabolic reprogramming offer attractive prospects for the targeting of phenotypic plasticity in cancer. EMT could be reversed by targeting specific metabolic enzymes or by affecting metabolism-dependent epigenetic reprogramming, eventually hindering cancer metastasis and EMT-induced therapy resistance. For instance, AGI-5198, a selective isocitrate dehydrogenase 1 (IDH1) inhibitor

that specifically inhibits R132H/C mutants (mIDH1) and not wild-type IDH1, was identified through a high-throughput screen, and was shown to induce demethylation of histone H3K9me3 reverting glioma cells to a more differentiated state [133]. In addition, in *SDH* mutant paraganglioma cells, the migratory phenotype was reversed by the DNA methylation inhibitor, decitabine [134]. In recent years, the small molecule 3-BrPA (3-bromopyruvate) has been shown to function as a metabolic inhibitor not only by targeting the glycolysis process, but also by inhibiting mitochondrial OXPHOS in cancer cells [135]. Indeed, 3-BrPA inhibited glycolysis and sensitized pancreatic cancer cells to geldanamycin [136]. Also, it enhanced the antiproliferative effects of both cisplatin and oxaliplatin in p53-deficient HCT116 cells [137]. Recently, it was demonstrated that a simvastatin targets cholesterol metabolism by disrupting lipid rafts leading to a conversion of EMT and to the sensitization of drug-resistant cancer cells to paclitaxal. Furthermore, simvastatin was able to repolarize TAMs via the cholesterol-associated LXR/ABCA1 regulation. The repolarization diminished TGF-β affecting tumor microenvironment remodeling and suppressed EMT [138].

Yet, the precise regulation of the metabolic pathway necessary for EMT and drug-resistance is still unknown for several cancer types. Also, whether one or more networks are involved in these regulatory mechanisms is poorly understood. Moreover, despite the substantial understanding gathered on the metabolic control of EMT, little is known about the metabolic control of MET. As MET occurs at the metastatic site, where it is important for the metastatic colonization, it is likely that these cancer cells rely on different metabolic reprogramming strategies. Therefore, elucidation of the metabolic networks is needed to help in identifying potential therapeutic targets affecting EMT-associated therapy resistance.

2.3. Reversing cell plasticity

Rather than preventing cellular plasticity or targeting the newly acquired stem-like identity, some lines of experimentation have attempted to reverse the process, i.e. induce plastic cells to commit to a terminally differentiated and post mitotic lineage in order to regain sensitivity to chemotherapeutic drugs. By doing so, tumor cells normally driven into a CSC state by EMT will be compelled to differentiate into non-CSCs by MET and consequently regain epithelial characteristics, thereby losing both their innate malignancy and resistance to cytotoxic drugs.

2.3.1. Inducing differentiation

As described above, the spectrum of novel (and under development) therapeutic strategies to minimize EMT-induced treatment chemo-resistance in cancer is very broad and encompass widely diverse experimental approaches. The MET-driven induction of epithelial differentiation is expected to place cells in a state where they become more vulnerable to conventional cytotoxic therapies that mainly target proliferating cells [139]. With the aim to identify compounds inducing MET in mesenchymal breast cancer cells, Pattabiraman et al., (2016) performed a drug screen to identify compounds that could induce transcription of *CDH1* gene encoding for E-cadherin. This screen revealed that two adenylate cyclase activators, cholera toxin and forskolin, increase intracellular levels of cycling AMP thereby enhancing protein kinase A (PKA) signaling in tumor cells [139]. Treatment of mesenchymal derivatives of immortalized human mammary epithelial cells with either two agents resulted in the induction of MET and the associated reduction

in invasiveness and stem cell function. Remarkably, these epithelialization effects were accompanied by the sensitization of the breast cancer cells to different anti-cancer drugs including paclitaxel, doxorubicin, EGFR inhibitors, and proteasome inhibitors [139]. This result is in line with previous described discovery that the HDAC inhibitor mocetinostat interferes with ZEB1 expression and function in cancer cells thereby restoring the sensitivity to chemotherapeutics [31].

Further studies will be required to assess the general applicability and clinical efficacy of these agents. Of note, given the necessity for migrating cancer cells to reacquire epithelial characteristics as the very last step in the metastatic cascade, the therapeutic stimulation of MET might result in the undesirable effect of stimulating metastatic colony formation. In addition, inadequate or insufficient reversion of the mesenchymal characteristics of migrating cancer cells into more epithelial-like features may paradoxically lead to increased plasticity. A possible adverse outcome of an incomplete induction of differentiation would be, for example, the increase in cancer cells with partial EMT and highly metastable and metastatic features [9]. Last, toxicity due to side effects caused by off-targeting of healthy mesenchymal cells such as fibroblasts, should be assessed. Accordingly, treatment strategy and timing of MET induction will have to be determined with care. Nonetheless, the induction of differentiation still represents a very attractive opportunity for the future of anticancer therapies.

Recently, an alternative strategy to inhibit cellular plasticity, metastasis, and therapy resistance was presented: by forcing cancer cells with enhanced plasticity to differentiate into terminal and post-mitotic lineages, one could think of preventing EMT/MET and the associated phenotypic plasticity and therapy resistance [140]. This strategy was first demonstrated in breast cancer mouse models where metastatic cells were induced to differentiate into adipocytes at the interface of EMT-driven plasticity [140] (**Figure 3**). The combination of rosiglitazone (an inhibitor of peroxidase proliferator-activated receptors) and BMP2 (part of the transforming growth factor-beta (TGF-β) superfamily) was demonstrated to trigger mesenchymal, but not epithelial, murine mammary cancer cells to undergo adipogenesis, as shown by increased expression of the adipogenesis regulator C/ebpα and by the formation of intracellular lipid droplets. Mechanistically, it was demonstrated that expression of the EMT-TFs Zeb1, Zeb2, and Klf4 underlie the potential of cancer cells to activate adipogenesis. Remarkably, the cancer-derived adipocytes were pre-dominantly localized at the invasive front of the tumors, the location where migrating cancer (stem) cells reside. Additionally, the cancer-derived adipocytes were identified to be in a post-mitotic cell-cycle arrested state. As mentioned before, partial EMT has been associated with enhanced plasticity [9]. It can therefore be hypothesized that cancer cell plasticity defined by partial EMT, may also underlie cancer cell transformation into terminally differentiated and post-mitotic lineages such as adipocytes.

Since cancer cell plasticity is considered a general characteristic of malignant solid tumors, it would be interesting to explore whether the same mechanisms would apply for other tumor types. However, considering that the connective tissue compartment of the fully differentiated breast is mainly composed of fat tissue, conversion of mammary cancer cells into adipocytes might be the preferred mechanisms in breast cancer, yet not be the case for other tumor types. Hence, further studies delineating the molecular mechanisms of cancer cell (trans)differentiation in other malignancies may open new avenues for future therapies. Furthermore, additional studies are necessary to test the stability and

durability of the cancer-derived terminally-differentiated cells. Recent work has indicated that terminally differentiated Paneth cells and late-stage entero-endocrine cells, still have the capacity to switch back to an intestinal stem cell state [141-143]. In our laboratory we have demonstrated that the activation of the stem cell factor (SCF)/c-Kit signaling axis upon inflammation induced cell cycle re-entry, dedifferentiation, and acquisition of stem cell properties in post-mitotic Paneth cells by enhancing Wnt through PI3K/Akt activation and GSK3β inhibition [142]. Hence, further preclinical assessment will be required to test the inducibility of dedifferentiation of the trans-differentiated cancer derived post-mitotic cells.
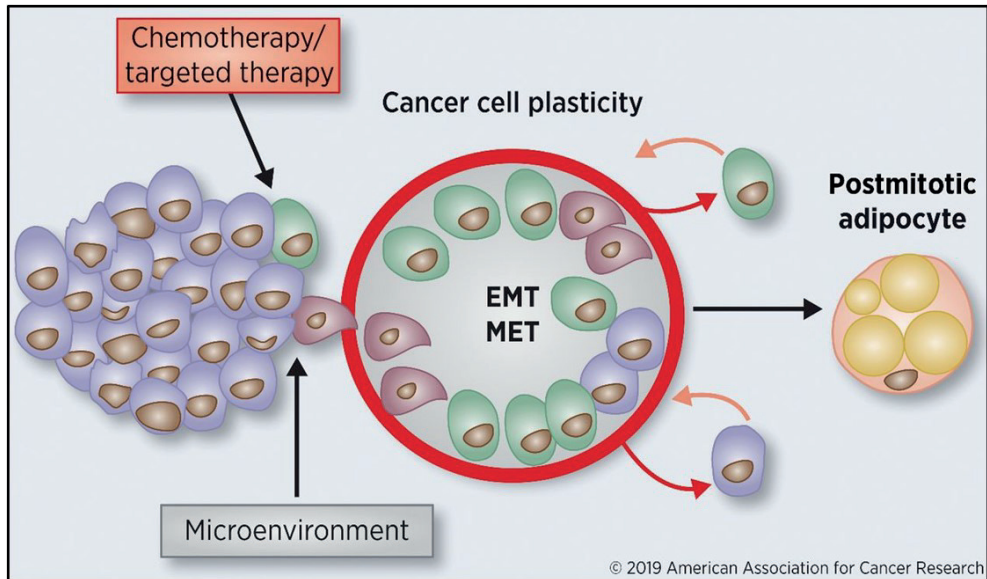
Figure 3. Targeting cancer cell plasticity by forcing (trans)differentiation into adipocytes. Tumor cells adapt to changing signals from the microenvironment and to drug treatments by increasing cellular plasticity and survival. EMT and MET facilitate a dynamic cell response and enhance cancer cell plasticity. Reverting cells back into an epithelial state can potentially maintain plasticity response. Forcing cells with increased plasticity into post-mitotic adipocytes interferes with EMT/MET transitions and prevent cellular plasticity, metastasis, and therapy resistance. Adapted from [140].

3. Concluding remarks

An steadily increasing body of evidence is emerging connecting cellular plasticity and the development of therapy resistance in cancer cells, not only in experimental models but also in clinical settings. Indeed, residual tumor cells after diverse anti-cancer therapy modalities (chemotherapy, immunotherapy, and molecularly targeted therapy) frequently present with signs of active EMT. Accordingly, the effectiveness of these therapeutic strategies in resulting in long-lasting clinical responses might be increased by targeting tumor cells that have activated EMT as a mean to undergo plasticity and circumvent cytotoxic events. However, the mechanisms responsible for the induction and/or maintenance for the EMT in cancer cells remain largely unknown. Cellular plasticity

Chapter 8

is executed by highly complex and intricated mechanisms, presenting a serious challenge to the effective and selective targeting of these processes. Overcoming these challenges will lay the ground for new treatment strategies aimed at preventing the development of therapy resistance and eventually leading to the eradication of the malignant disease.

This thesis presents the identification of quasi-mesenchymal tumor cells displaying phenotypic plasticity. By using conventional cancer cell lines, organoid models, and pre-clinical mouse models, we discovered and characterized a subpopulation of cancer cells marked with enhanced competence to undergo phenotypic changes in colon and ovarian cancer (*Chapter 4*, *6 and 7*). These cells demonstrated an increased capacity to metastasize and to survive conventional cytotoxic therapies commonly employed in the clinical management of cancer patients. We show that this process is likely to occur through activation of Wnt signaling upstream of EMT induction through *ZEB1*. In another study (*Chapter 3*), we demonstrate an epigenetic mechanism involving the antagonistic control of chromatin remodeling by NURD and SWI/SNF in human oral squamous cell carcinomas (OSCCs). This "tug-of-war" between two main chromatin remodeling complexes explains how the EMT/MET phenotypic switch is regulated in oral and possibly other types of cancer. The importance of epigenetics and the elucidation of the mechanisms underlying transient changes in the cellular identity of individual circulating and metastasizing tumor cells will lay the basis for the development of novel treatment modalities. These will complement the current cancer treatment options that are mainly directed against somatic gene mutations arisen at the primary site and unlikely to be rate-limiting in the clinical management of a more advanced malignant disease.

References

1. Redmond, K.M.; Wilson, T.R.; Johnston, P.G.; Longley, D.B. Resistance mechanisms to cancer chemotherapy. *Front Biosci* **2008**, *13*, 5138-5154, doi:10.2741/3070.

2. Roesch, A. Tumor heterogeneity and plasticity as elusive drivers for resistance to MAPK pathway inhibition in melanoma. *Oncogene* **2015**, *34*, 2951-2957, doi:10.1038/onc.2014.249.

3. Hata, A.N.; Niederst, M.J.; Archibald, H.L.; Gomez-Caraballo, M.; Siddiqui, F.M.; Mulvey, H.E.; Maruvka, Y.E.; Ji, F.; Bhang, H.E.; Krishnamurthy Radhakrishna, V.; et al. Tumor cells can follow distinct evolutionary paths to become resistant to epidermal growth factor receptor inhibition. *Nat Med* **2016**, *22*, 262-269, doi:10.1038/nm.4040.

4. Salgia, R.; Kulkarni, P. The Genetic/Non-genetic Duality of Drug 'Resistance' in Cancer. *Trends Cancer* **2018**, *4*, 110-118, doi:10.1016/j.trecan.2018.01.001.

5. Sharma, S.V.; Lee, D.Y.; Li, B.; Quinlan, M.P.; Takahashi, F.; Maheswaran, S.; McDermott, U.; Azizian, N.; Zou, L.; Fischbach, M.A.; et al. A chromatin-mediated reversible drug-tolerant state in cancer cell subpopulations. *Cell* **2010**, *141*, 69-80, doi:10.1016/j.cell.2010.02.027.

6. Varga, J.; Greten, F.R. Cell plasticity in epithelial homeostasis and tumorigenesis. *Nat Cell Biol* **2017**, *19*, 1133-1141, doi:10.1038/ncb3611.

7. Holohan, C.; Van Schaeybroeck, S.; Longley, D.B.; Johnston, P.G. Cancer drug resistance: an evolving paradigm. *Nat Rev Cancer* **2013**, *13*, 714-726, doi:10.1038/nrc3599.

8. Nieto, M.A.; Huang, R.Y.; Jackson, R.A.; Thiery, J.P. Emt: 2016. *Cell* **2016**, *166*, 21-45.

9. Pastushenko, I.; Brisebarre, A.; Sifrim, A.; Fioramonti, M.; Revenco, T.; Boumahdi, S.; Van Keymeulen, A.; Brown, D.; Moers, V.; Lemaire, S.; et al. Identification of the tumour transition states occurring during EMT. *Nature* **2018**, *556*, 463-468.

10. Saxena, M.; Stephens, M.A.; Pathak, H.; Rangarajan, A. Transcription factors that mediate epithelial-mesenchymal transition lead to multidrug resistance by upregulating ABC transporters. *Cell Death Dis* **2011**, *2*, e179, doi:10.1038/cddis.2011.61.

11. Wu, W.S.; Heinrichs, S.; Xu, D.; Garrison, S.P.; Zambetti, G.P.; Adams, J.M.; Look, A.T. Slug antagonizes p53-mediated apoptosis of hematopoietic progenitors by repressing puma. *Cell* **2005**, *123*, 641-653, doi:10.1016/j.cell.2005.09.029.

12. Wu, D.W.; Lee, M.C.; Hsu, N.Y.; Wu, T.C.; Wu, J.Y.; Wang, Y.C.; Cheng, Y.W.; Chen, C.Y.; Lee, H. FHIT loss confers cisplatin resistance in lung cancer via the AKT/NF-kappaB/Slug-mediated PUMA reduction. *Oncogene* **2017**, *36*, 5439, doi:10.1038/onc.2017.249.

13. Vega, S.; Morales, A.V.; Ocana, O.H.; Valdes, F.; Fabregat, I.; Nieto, M.A. Snail blocks the cell cycle and confers resistance to cell death. *Genes Dev* **2004**, *18*, 1131-1143, doi:10.1101/gad.294104.

14. Escriva, M.; Peiro, S.; Herranz, N.; Villagrasa, P.; Dave, N.; Montserrat-Sentis, B.; Murray, S.A.; Franci, C.; Gridley, T.; Virtanen, I.; et al. Repression of PTEN phosphatase by Snail1 transcriptional factor during gamma radiation-induced apoptosis. *Mol Cell Biol* **2008**, *28*, 1528-1540, doi:10.1128/MCB.02061-07.

15. Lu, M.; Marsters, S.; Ye, X.; Luis, E.; Gonzalez, L.; Ashkenazi, A. E-cadherin couples death receptors to the cytoskeleton to regulate apoptosis. *Mol Cell* **2014**, *54*, 987-998, doi:10.1016/j.molcel.2014.04.029.

16. Byers, L.A.; Diao, L.; Wang, J.; Saintigny, P.; Girard, L.; Peyton, M.; Shen, L.; Fan, Y.; Giri, U.; Tumula, P.K.; et al. An epithelial-mesenchymal transition gene signature predicts resistance to EGFR and PI3K inhibitors and identifies Axl as a therapeutic target for overcoming EGFR inhibitor resistance. *Clin Cancer Res* **2013**, *19*, 279-290, doi:10.1158/1078-0432.CCR-12-1558.

Chapter 8

17. Sequist, L.V.; Waltman, B.A.; Dias-Santagata, D.; Digumarthy, S.; Turke, A.B.; Fidias, P.; Bergethon, K.; Shaw, A.T.; Gettinger, S.; Cosper, A.K.; et al. Genotypic and histological evolution of lung cancers acquiring resistance to EGFR inhibitors. *Sci Transl Med* **2011**, *3*, 75ra26, doi:10.1126/scitranslmed.3002003.

18. Zhang, Z.; Lee, J.C.; Lin, L.; Olivas, V.; Au, V.; LaFramboise, T.; Abdel-Rahman, M.; Wang, X.; Levine, A.D.; Rho, J.K.; et al. Activation of the AXL kinase causes resistance to EGFR-targeted therapy in lung cancer. *Nat Genet* **2012**, *44*, 852-860, doi:10.1038/ng.2330.

19. Chen, L.; Gibbons, D.L.; Goswami, S.; Cortez, M.A.; Ahn, Y.H.; Byers, L.A.; Zhang, X.; Yi, X.; Dwyer, D.; Lin, W.; et al. Metastasis is regulated via microRNA-200/ZEB1 axis control of tumour cell PD-L1 expression and intratumoral immunosuppression. *Nat Commun* **2014**, *5*, 5241, doi:10.1038/ncomms6241.

20. Kudo-Saito, C.; Shirako, H.; Takeuchi, T.; Kawakami, Y. Cancer metastasis is accelerated through immunosuppression during Snail-induced EMT of cancer cells. *Cancer Cell* **2009**, *15*, 195-206, doi:10.1016/j.ccr.2009.01.023.

21. Tam, W.L.; Weinberg, R.A. The epigenetics of epithelial-mesenchymal plasticity in cancer. *Nat Med* **2013**, *19*, 1438-1449, doi:10.1038/nm.3336.

22. Zentner, G.E.; Henikoff, S. Regulation of nucleosome dynamics by histone modifications. *Nat Struct Mol Biol* **2013**, *20*, 259-266, doi:10.1038/nsmb.2470.

23. Swygert, S.G.; Peterson, C.L. Chromatin dynamics: interplay between remodeling enzymes and histone modifications. *Biochim Biophys Acta* **2014**, *1839*, 728-736, doi:10.1016/j.bbagrm.2014.02.013.

24. Laugesen, A.; Helin, K. Chromatin repressive complexes in stem cells, development, and cancer. *Cell Stem Cell* **2014**, *14*, 735-751, doi:10.1016/j.stem.2014.05.006.

25. Masliah-Planchon, J.; Bieche, I.; Guinebretiere, J.M.; Bourdeaut, F.; Delattre, O. SWI/SNF chromatin remodeling and human malignancies. *Annu Rev Pathol* **2015**, *10*, 145-171, doi:10.1146/annurev-pathol-012414-040445.

26. Morgan, M.A.; Shilatifard, A. Chromatin signatures of cancer. *Genes Dev* **2015**, *29*, 238-249, doi:10.1101/gad.255182.114.

27. Easwaran, H.; Tsai, H.C.; Baylin, S.B. Cancer epigenetics: tumor heterogeneity, plasticity of stem-like states, and drug resistance. *Mol Cell* **2014**, *54*, 716-727, doi:10.1016/j.molcel.2014.05.015.

28. Juo, Y.Y.; Gong, X.J.; Mishra, A.; Cui, X.; Baylin, S.B.; Azad, N.S.; Ahuja, N. Epigenetic therapy for solid tumors: from bench science to clinical trials. *Epigenomics* **2015**, *7*, 215-235, doi:10.2217/epi.14.73.

29. Wang, Y.; Cardenas, H.; Fang, F.; Condello, S.; Taverna, P.; Segar, M.; Liu, Y.; Nephew, K.P.; Matei, D. Epigenetic targeting of ovarian cancer stem cells. *Cancer Res* **2014**, *74*, 4922-4936, doi:10.1158/0008-5472.CAN-14-1022.

30. Catalano, M.G.; Poli, R.; Pugliese, M.; Fortunati, N.; Boccuzzi, G. Valproic acid enhances tubulin acetylation and apoptotic activity of paclitaxel on anaplastic thyroid cancer cell lines. *Endocr Relat Cancer* **2007**, *14*, 839-845, doi:10.1677/ERC-07-0096.

31. Meidhof, S.; Brabletz, S.; Lehmann, W.; Preca, B.T.; Mock, K.; Ruh, M.; Schuler, J.; Berthold, M.; Weber, A.; Burk, U.; et al. ZEB1-associated drug resistance in cancer cells is reversed by the class I HDAC inhibitor mocetinostat. *EMBO Mol Med* **2015**, *7*, 831-847, doi:10.15252/emmm.201404396.

32. Eades, G.; Yao, Y.; Yang, M.; Zhang, Y.; Chumsri, S.; Zhou, Q. miR-200a regulates SIRT1 expression and epithelial to mesenchymal transition (EMT)-like transformation in mammary epithelial cells. *J Biol Chem* **2011**, *286*, 25992-26002, doi:10.1074/jbc.M111.229401.

33. Cicchini, C.; de Nonno, V.; Battistelli, C.; Cozzolino, A.M.; De Santis Puzzonia, M.; Ciafre, S.A.; Brocker, C.; Gonzalez, F.J.; Amicone, L.; Tripodi, M. Epigenetic control of EMT/MET dynamics: HNF4alpha impacts DNMT3s through miRs-29. *Biochim Biophys Acta* **2015**, *1849*, 919-929, doi:10.1016/j.bbagrm.2015.05.005.

34. Chikamatsu, K.; Ishii, H.; Murata, T.; Sakakura, K.; Shino, M.; Toyoda, M.; Takahashi, K.; Masuyama, K. Alteration of cancer stem cell-like phenotype by histone deacetylase inhibitors in squamous cell carcinoma of the head and neck. *Cancer Sci* **2013**, *104*, 1468-1475, doi:10.1111/cas.12271.

35. Mohd-Sarip, A.; Teeuwssen, M.; Bot, A.G.; De Herdt, M.J.; Willems, S.M.; Baatenburg de Jong, R.J.; Looijenga, L.H.J.; Zatreanu, D.; Bezstarosti, K.; van Riet, J.; et al. DOC1-Dependent Recruitment of NURD Reveals Antagonism with SWI/SNF during Epithelial-Mesenchymal Transition in Oral Cancer Cells. *Cell Rep* **2017**, *20*, 61-75, doi:10.1016/j.celrep.2017.06.020.

36. Lee, J.; Yakubov, B.; Ivan, C.; Jones, D.R.; Caperell-Grant, A.; Fishel, M.; Cardenas, H.; Matei, D. Tissue Transglutaminase Activates Cancer-Associated Fibroblasts and Contributes to Gemcitabine Resistance in Pancreatic Cancer. *Neoplasia* **2016**, *18*, 689-698, doi:10.1016/j.neo.2016.09.003.

37. Tang, H.M.; Kuay, K.T.; Koh, P.F.; Asad, M.; Tan, T.Z.; Chung, V.Y.; Lee, S.C.; Thiery, J.P.; Huang, R.J. An epithelial marker promoter induction screen identifies histone deacetylase inhibitors to restore epithelial differentiation and abolishes anchorage independence growth in cancers. *Cell Death Discov* **2016**, *2*, 16041, doi:10.1038/cddiscovery.2016.41.

38. Kong, D.; Ahmad, A.; Bao, B.; Li, Y.; Banerjee, S.; Sarkar, F.H. Histone deacetylase inhibitors induce epithelial-to-mesenchymal transition in prostate cancer cells. *PLoS One* **2012**, *7*, e45045, doi:10.1371/journal.pone.0045045.

39. Ji, M.; Lee, E.J.; Kim, K.B.; Kim, Y.; Sung, R.; Lee, S.J.; Kim, D.S.; Park, S.M. HDAC inhibitors induce epithelial-mesenchymal transition in colon carcinoma cells. *Oncol Rep* **2015**, *33*, 2299-2308, doi:10.3892/or.2015.3879.

40. Mao, S.; Lu, G.; Lan, X.; Yuan, C.; Jiang, W.; Chen, Y.; Jin, X.; Xia, Q. Valproic acid inhibits epithelialmesenchymal transition in renal cell carcinoma by decreasing SMAD4 expression. *Mol Med Rep* **2017**, *16*, 6190-6199, doi:10.3892/mmr.2017.7394.

41. Chen, C.L.; Sung, J.; Cohen, M.; Chowdhury, W.H.; Sachs, M.D.; Li, Y.; Lakshmanan, Y.; Yung, B.Y.; Lupold, S.E.; Rodriguez, R. Valproic acid inhibits invasiveness in bladder cancer but not in prostate cancer cells. *J Pharmacol Exp Ther* **2006**, *319*, 533-542, doi:10.1124/jpet.106.106658.

42. Falkenberg, K.J.; Johnstone, R.W. Histone deacetylases and their inhibitors in cancer, neurological diseases and immune disorders. *Nat Rev Drug Discov* **2014**, *13*, 673-691, doi:10.1038/nrd4360.

43. Nishijima, N.; Seike, M.; Soeno, C.; Chiba, M.; Miyanaga, A.; Noro, R.; Sugano, T.; Matsumoto, M.; Kubota, K.; Gemma, A. miR-200/ZEB axis regulates sensitivity to nintedanib in non-small cell lung cancer cells. *Int J Oncol* **2016**, *48*, 937-944, doi:10.3892/ijo.2016.3331.

44. Ma, J.; Fang, B.; Zeng, F.; Ma, C.; Pang, H.; Cheng, L.; Shi, Y.; Wang, H.; Yin, B.; Xia, J.; et al. Down-regulation of miR-223 reverses epithelial-mesenchymal transition in gemcitabine-resistant pancreatic cancer cells. *Oncotarget* **2015**, *6*, 1740-1749, doi:10.18632/oncotarget.2714.

45. Zhu, X.; Shen, H.; Yin, X.; Long, L.; Xie, C.; Liu, Y.; Hui, L.; Lin, X.; Fang, Y.; Cao, Y.; et al. miR-186 regulation of Twist1 and ovarian cancer sensitivity to cisplatin. *Oncogene* **2016**, *35*, 323-332, doi:10.1038/onc.2015.84.

46. Berman, M.; Mattheolabakis, G.; Suresh, M.; Amiji, M. Reversing epigenetic mechanisms of drug resistance in solid tumors using targeted microRNA delivery. *Expert Opin Drug Deliv* **2016**, *13*, 987-998, doi:10.1080/17425247.2016.1178236.

Chapter 8

47. Xing, F.; Saidou, J.; Watabe, K. Cancer associated fibroblasts (CAFs) in tumor microenvironment. *Front Biosci (Landmark Ed)* **2010**, *15*, 166-179, doi:10.2741/3613.

48. Zeisberg, E.M.; Tarnavski, O.; Zeisberg, M.; Dorfman, A.L.; McMullen, J.R.; Gustafsson, E.; Chandraker, A.; Yuan, X.; Pu, W.T.; Roberts, A.B.; et al. Endothelial-to-mesenchymal transition contributes to cardiac fibrosis. *Nat Med* **2007**, *13*, 952-961, doi:10.1038/nm1613.

49. Potenta, S.; Zeisberg, E.; Kalluri, R. The role of endothelial-to-mesenchymal transition in cancer progression. *Br J Cancer* **2008**, *99*, 1375-1379, doi:10.1038/sj.bjc.6604662.

50. Kim, S.H.; Song, Y.; Seo, H.R. GSK-3beta regulates the endothelial-to-mesenchymal transition via reciprocal crosstalk between NSCLC cells and HUVECs in multicellular tumor spheroid models. *J Exp Clin Cancer Res* **2019**, *38*, 46, doi:10.1186/s13046-019-1050-1.

51. Loeffler, M.; Kruger, J.A.; Niethammer, A.G.; Reisfeld, R.A. Targeting tumor-associated fibroblasts improves cancer chemotherapy by increasing intratumoral drug uptake. *J Clin Invest* **2006**, *116*, 1955-1962, doi:10.1172/JCI26532.

52. Reardon, D.A.; Rich, J.N.; Friedman, H.S.; Bigner, D.D. Recent advances in the treatment of malignant astrocytoma. *J Clin Oncol* **2006**, *24*, 1253-1265, doi:10.1200/JCO.2005.04.5302.

53. Aikawa, T.; Gunn, J.; Spong, S.M.; Klaus, S.J.; Korc, M. Connective tissue growth factor-specific antibody attenuates tumor growth, metastasis, and angiogenesis in an orthotopic mouse model of pancreatic cancer. *Mol Cancer Ther* **2006**, *5*, 1108-1116, doi:10.1158/1535-7163.MCT-05-0516.

54. Roswall, P.; Bocci, M.; Bartoschek, M.; Li, H.; Kristiansen, G.; Jansson, S.; Lehn, S.; Sjolund, J.; Reid, S.; Larsson, C.; et al. Microenvironmental control of breast cancer subtype elicited through paracrine platelet-derived growth factor-CC signaling. *Nat Med* **2018**, *24*, 463-473, doi:10.1038/nm.4494.

55. Paulus, P.; Stanley, E.R.; Schafer, R.; Abraham, D.; Aharinejad, S. Colony-stimulating factor-1 antibody reverses chemoresistance in human MCF-7 breast cancer xenografts. *Cancer Res* **2006**, *66*, 4349-4356, doi:10.1158/0008-5472.CAN-05-3523.

56. Coussens, L.M.; Zitvogel, L.; Palucka, A.K. Neutralizing tumor-promoting chronic inflammation: a magic bullet? *Science* **2013**, *339*, 286-291, doi:10.1126/science.1232227.

57. Quail, D.F.; Joyce, J.A. Microenvironmental regulation of tumor progression and metastasis. *Nat Med* **2013**, *19*, 1423-1437, doi:10.1038/nm.3394.

58. Mitchem, J.B.; Brennan, D.J.; Knolhoff, B.L.; Belt, B.A.; Zhu, Y.; Sanford, D.E.; Belaygorod, L.; Carpenter, D.; Collins, L.; Piwnica-Worms, D.; et al. Targeting tumor-infiltrating macrophages decreases tumor-initiating cells, relieves immunosuppression, and improves chemotherapeutic responses. *Cancer Res* **2013**, *73*, 1128-1141, doi:10.1158/0008-5472.CAN-12-2731.

59. Germano, G.; Frapolli, R.; Belgiovine, C.; Anselmo, A.; Pesce, S.; Liguori, M.; Erba, E.; Uboldi, S.; Zucchetti, M.; Pasqualini, F.; et al. Role of macrophage targeting in the antitumor activity of trabectedin. *Cancer Cell* **2013**, *23*, 249-262, doi:10.1016/j.ccr.2013.01.008.

60. Hiroshima, Y.; Maawy, A.; Hassanein, M.K.; Menen, R.; Momiyama, M.; Murakami, T.; Miwa, S.; Yamamoto, M.; Uehara, F.; Yano, S.; et al. The tumor-educated-macrophage increase of malignancy of human pancreatic cancer is prevented by zoledronic acid. *PLoS One* **2014**, *9*, e103382, doi:10.1371/journal.pone.0103382.

61. Mantovani, A.; Marchesi, F.; Malesci, A.; Laghi, L.; Allavena, P. Tumour-associated macrophages as treatment targets in oncology. *Nat Rev Clin Oncol* **2017**, *14*, 399-416, doi:10.1038/nrclinonc.2016.217.

62.   Komohara, Y.; Fujiwara, Y.; Ohnishi, K.; Takeya, M. Tumor-associated macrophages: Potential therapeutic targets for anti-cancer therapy. *Adv Drug Deliv Rev* **2016**, *99*, 180-185, doi:10.1016/j. addr.2015.11.009.

63.   Ebbing, E.A.; van der Zalm, A.P.; Steins, A.; Creemers, A.; Hermsen, S.; Rentenaar, R.; Klein, M.; Waasdorp, C.; Hooijer, G.K.J.; Meijer, S.L.; et al. Stromal-derived interleukin 6 drives epithelial-to-mesenchymal transition and therapy resistance in esophageal adenocarcinoma. *Proc Natl Acad Sci U S A* **2019**, *116*, 2237-2242, doi:10.1073/pnas.1820459116.

64.   Yao, Z.; Fenoglio, S.; Gao, D.C.; Camiolo, M.; Stiles, B.; Lindsted, T.; Schlederer, M.; Johns, C.; Altorki, N.; Mittal, V.; et al. TGF-beta IL-6 axis mediates selective and adaptive mechanisms of resistance to molecular targeted therapy in lung cancer. *Proc Natl Acad Sci U S A* **2010**, *107*, 15535-15540, doi:10.1073/pnas.1009472107.

65.   Canadas, I.; Rojo, F.; Taus, A.; Arpi, O.; Arumi-Uria, M.; Pijuan, L.; Menendez, S.; Zazo, S.; Domine, M.; Salido, M.; et al. Targeting epithelial-to-mesenchymal transition with Met inhibitors reverts chemoresistance in small cell lung cancer. *Clin Cancer Res* **2014**, *20*, 938-950, doi:10.1158/1078-0432.CCR-13-1330.

66.   Straussman, R.; Morikawa, T.; Shee, K.; Barzily-Rokni, M.; Qian, Z.R.; Du, J.; Davis, A.; Mongare, M.M.; Gould, J.; Frederick, D.T.; et al. Tumour micro-environment elicits innate resistance to RAF inhibitors through HGF secretion. *Nature* **2012**, *487*, 500-504, doi:10.1038/nature11183.

67.   Hughes, V.S.; Siemann, D.W. Have Clinical Trials Properly Assessed c-Met Inhibitors? *Trends Cancer* **2018**, *4*, 94-97, doi:10.1016/j.trecan.2017.11.009.

68.   Taddei, M.L.; Giannoni, E.; Comito, G.; Chiarugi, P. Microenvironment and tumor cell plasticity: an easy way out. *Cancer Lett* **2013**, *341*, 80-96, doi:10.1016/j.canlet.2013.01.042.

69.   Jiang, J.; Tang, Y.L.; Liang, X.H. EMT: a new vision of hypoxia promoting cancer progression. *Cancer Biol Ther* **2011**, *11*, 714-723, doi:10.4161/cbt.11.8.15274.

70.   Jiao, M.; Nan, K.J. Activation of PI3 kinase/Akt/HIF-1alpha pathway contributes to hypoxia-induced epithelial-mesenchymal transition and chemoresistance in hepatocellular carcinoma. *Int J Oncol* **2012**, *40*, 461-468, doi:10.3892/ijo.2011.1197.

71.   Qin, Y.; Liu, H.J.; Li, M.; Zhai, D.H.; Tang, Y.H.; Yang, L.; Qiao, K.L.; Yang, J.H.; Zhong, W.L.; Zhang, Q.; et al. Salidroside improves the hypoxic tumor microenvironment and reverses the drug resistance of platinum drugs via HIF-1alpha signaling pathway. *EBioMedicine* **2018**, *38*, 25-36, doi:10.1016/j.ebiom.2018.10.069.

72.   Zhou, Q.Y.; Tu, C.Y.; Shao, C.X.; Wang, W.K.; Zhu, J.D.; Cai, Y.; Mao, J.Y.; Chen, W. GC7 blocks epithelial-mesenchymal transition and reverses hypoxia-induced chemotherapy resistance in hepatocellular carcinoma cells. *Am J Transl Res* **2017**, *9*, 2608-2617.

73.   Ozdemir, B.C.; Pentcheva-Hoang, T.; Carstens, J.L.; Zheng, X.; Wu, C.C.; Simpson, T.R.; Laklai, H.; Sugimoto, H.; Kahlert, C.; Novitskiy, S.V.; et al. Depletion of carcinoma-associated fibroblasts and fibrosis induces immunosuppression and accelerates pancreas cancer with reduced survival. *Cancer Cell* **2014**, *25*, 719-734, doi:10.1016/j.ccr.2014.04.005.

74.   Rhim, A.D.; Oberstein, P.E.; Thomas, D.H.; Mirek, E.T.; Palermo, C.F.; Sastra, S.A.; Dekleva, E.N.; Saunders, T.; Becerra, C.P.; Tattersall, I.W.; et al. Stromal elements act to restrain, rather than support, pancreatic ductal adenocarcinoma. *Cancer Cell* **2014**, *25*, 735-747, doi:10.1016/j. ccr.2014.04.021.

75.   Zou, W. Immunosuppressive networks in the tumour environment and their therapeutic relevance. *Nat Rev Cancer* **2005**, *5*, 263-274, doi:10.1038/nrc1586.

Chapter 8

76. Wu, Y.; Ginther, C.; Kim, J.; Mosher, N.; Chung, S.; Slamon, D.; Vadgama, J.V. Expression of Wnt3 activates Wnt/beta-catenin pathway and promotes EMT-like phenotype in trastuzumab-resistant HER2-overexpressing breast cancer cells. *Mol Cancer Res* **2012**, *10*, 1597-1606, doi:10.1158/1541-7786.MCR-12-0155-T.

77. Su, H.Y.; Lai, H.C.; Lin, Y.W.; Liu, C.Y.; Chen, C.K.; Chou, Y.C.; Lin, S.P.; Lin, W.C.; Lee, H.Y.; Yu, M.H. Epigenetic silencing of SFRP5 is related to malignant phenotype and chemoresistance of ovarian cancer through Wnt signaling pathway. *Int J Cancer* **2010**, *127*, 555-567, doi:10.1002/ijc.25083.

78. Ren, J.; Wang, R.; Song, H.; Huang, G.; Chen, L. Secreted frizzled related protein 1 modulates taxane resistance of human lung adenocarcinoma. *Mol Med* **2014**, *20*, 164-178, doi:10.2119/molmed.2013.00149.

79. Zhang, X.; Hao, J. Development of anticancer agents targeting the Wnt/beta-catenin signaling. *Am J Cancer Res* **2015**, *5*, 2344-2360.

80. Reka, A.K.; Kuick, R.; Kurapati, H.; Standiford, T.J.; Omenn, G.S.; Keshamouni, V.G. Identifying inhibitors of epithelial-mesenchymal transition by connectivity map-based systems approach. *J Thorac Oncol* **2011**, *6*, 1784-1792, doi:10.1097/JTO.0b013e31822adfb0.

81. Yingling, J.M.; McMillen, W.T.; Yan, L.; Huang, H.; Sawyer, J.S.; Graff, J.; Clawson, D.K.; Britt, K.S.; Anderson, B.D.; Beight, D.W.; et al. Preclinical assessment of galunisertib (LY2157299 monohydrate), a first-in-class transforming growth factor-beta receptor type I inhibitor. *Oncotarget* **2018**, *9*, 6659-6677, doi:10.18632/oncotarget.23795.

82. Teicher, B.A.; Holden, S.A.; Ara, G.; Chen, G. Transforming growth factor-beta in in vivo resistance. *Cancer Chemother Pharmacol* **1996**, *37*, 601-609, doi:10.1007/s002800050435.

83. Bhola, N.E.; Balko, J.M.; Dugger, T.C.; Kuba, M.G.; Sanchez, V.; Sanders, M.; Stanford, J.; Cook, R.S.; Arteaga, C.L. TGF-beta inhibition enhances chemotherapy action against triple-negative breast cancer. *J Clin Invest* **2013**, *123*, 1348-1358, doi:10.1172/JCI65416.

84. Tsai, J.H.; Donaher, J.L.; Murphy, D.A.; Chau, S.; Yang, J. Spatiotemporal regulation of epithelial-mesenchymal transition is essential for squamous cell carcinoma metastasis. *Cancer Cell* **2012**, *22*, 725-736, doi:10.1016/j.ccr.2012.09.022.

85. Akhurst, R.J.; Hata, A. Targeting the TGFbeta signalling pathway in disease. *Nat Rev Drug Discov* **2012**, *11*, 790-811, doi:10.1038/nrd3810.

86. Neuzillet, C.; Tijeras-Raballand, A.; Cohen, R.; Cros, J.; Faivre, S.; Raymond, E.; de Gramont, A. Targeting the TGFbeta pathway for cancer therapy. *Pharmacol Ther* **2015**, *147*, 22-31, doi:10.1016/j.pharmthera.2014.11.001.

87. Namba, T.; Kodama, R.; Moritomo, S.; Hoshino, T.; Mizushima, T. Zidovudine, an anti-viral drug, resensitizes gemcitabine-resistant pancreatic cancer cells to gemcitabine by inhibition of the Akt-GSK3beta-Snail pathway. *Cell Death Dis* **2015**, *6*, e1795, doi:10.1038/cddis.2015.172.

88. Buonato, J.M.; Lazzara, M.J. ERK1/2 blockade prevents epithelial-mesenchymal transition in lung cancer cells and promotes their sensitivity to EGFR inhibition. *Cancer Res* **2014**, *74*, 309-319, doi:10.1158/0008-5472.CAN-12-4721.

89. Lamouille, S.; Connolly, E.; Smyth, J.W.; Akhurst, R.J.; Derynck, R. TGF-beta-induced activation of mTOR complex 2 drives epithelial-mesenchymal transition and cell invasion. *J Cell Sci* **2012**, *125*, 1259-1273, doi:10.1242/jcs.095299.

90. Lamouille, S.; Derynck, R. Cell size and invasion in TGF-beta-induced epithelial to mesenchymal transition is regulated by activation of the mTOR pathway. *J Cell Biol* **2007**, *178*, 437-451, doi:10.1083/jcb.200611146.

91. Maru, S.; Ishigaki, Y.; Shinohara, N.; Takata, T.; Tomosugi, N.; Nonomura, K. Inhibition of mTORC2 but not mTORC1 up-regulates E-cadherin expression and inhibits cell motility by blocking HIF-2alpha expression in human renal cell carcinoma. *J Urol* **2013**, *189*, 1921-1929, doi:10.1016/j.juro.2012.11.010.

92. Kim, E.Y.; Kim, A.; Kim, S.K.; Kim, H.J.; Chang, J.; Ahn, C.M.; Chang, Y.S. Inhibition of mTORC1 induces loss of E-cadherin through AKT/GSK-3beta signaling-mediated upregulation of E-cadherin repressor complexes in non-small cell lung cancer cells. *Respir Res* **2014**, *15*, 26, doi:10.1186/1465-9921-15-26.

93. Li, L.; Han, R.; Xiao, H.; Lin, C.; Wang, Y.; Liu, H.; Li, K.; Chen, H.; Sun, F.; Yang, Z.; et al. Metformin sensitizes EGFR-TKI-resistant human lung cancer cells in vitro and in vivo through inhibition of IL-6 signaling and EMT reversal. *Clin Cancer Res* **2014**, *20*, 2714-2726, doi:10.1158/1078-0432.CCR-13-2613.

94. Cufi, S.; Vazquez-Martin, A.; Oliveras-Ferraros, C.; Martin-Castillo, B.; Joven, J.; Menendez, J.A. Metformin against TGFbeta-induced epithelial-to-mesenchymal transition (EMT): from cancer stem cells to aging-associated fibrosis. *Cell Cycle* **2010**, *9*, 4461-4468, doi:10.4161/cc.9.22.14048.

95. Gupta, P.B.; Onder, T.T.; Jiang, G.; Tao, K.; Kuperwasser, C.; Weinberg, R.A.; Lander, E.S. Identification of selective inhibitors of cancer stem cells by high-throughput screening. *Cell* **2009**, *138*, 645-659, doi:10.1016/j.cell.2009.06.034.

96. Zhan, T.; Ambrosi, G.; Wandmacher, A.M.; Rauscher, B.; Betge, J.; Rindtorff, N.; Haussler, R.S.; Hinsenkamp, I.; Bamberg, L.; Hessling, B.; et al. MEK inhibitors activate Wnt signalling and induce stem cell plasticity in colorectal cancer. *Nat Commun* **2019**, *10*, 2197, doi:10.1038/s41467-019-09898-0.

97. Foster, R.; Buckanovich, R.J.; Rueda, B.R. Ovarian cancer stem cells: working towards the root of stemness. *Cancer Lett* **2013**, *338*, 147-157, doi:10.1016/j.canlet.2012.10.023.

98. Reya, T.; Morrison, S.J.; Clarke, M.F.; Weissman, I.L. Stem cells, cancer, and cancer stem cells. *Nature* **2001**, *414*, 105-111.

99. Deonarain, M.P.; Kousparou, C.A.; Epenetos, A.A. Antibodies targeting cancer stem cells: a new paradigm in immunotherapy? *MAbs* **2009**, *1*, 12-25, doi:10.4161/mabs.1.1.7347.

100. Gong, X.; Azhdarinia, A.; Ghosh, S.C.; Xiong, W.; An, Z.; Liu, Q.; Carmon, K.S. LGR5-Targeted Antibody-Drug Conjugate Eradicates Gastrointestinal Tumors and Prevents Recurrence. *Mol Cancer Ther* **2016**, *15*, 1580-1590, doi:10.1158/1535-7163.MCT-16-0114.

101. Junttila, M.R.; Mao, W.; Wang, X.; Wang, B.E.; Pham, T.; Flygare, J.; Yu, S.F.; Yee, S.; Goldenberg, D.; Fields, C.; et al. Targeting LGR5+ cells with an antibody-drug conjugate for the treatment of colon cancer. *Sci Transl Med* **2015**, *7*, 314ra186, doi:10.1126/scitranslmed.aac7433.

102. de Sousa e Melo, F.; Kurtova, A.V.; Harnoss, J.M.; Kljavin, N.; Hoeck, J.D.; Hung, J.; Anderson, J.E.; Storm, E.E.; Modrusan, Z.; Koeppen, H.; et al. A distinct role for Lgr5(+) stem cells in primary and metastatic colon cancer. *Nature* **2017**, *543*, 676-680, doi:10.1038/nature21713.

103. Shimokawa, M.; Ohta, Y.; Nishikori, S.; Matano, M.; Takano, A.; Fujii, M.; Date, S.; Sugimoto, S.; Kanai, T.; Sato, T. Visualization and targeting of LGR5(+) human colon cancer stem cells. *Nature* **2017**, *545*, 187-192, doi:10.1038/nature22081.

104. Tian, H.; Biehs, B.; Warming, S.; Leong, K.G.; Rangell, L.; Klein, O.D.; de Sauvage, F.J. A reserve stem cell population in small intestine renders Lgr5-positive cells dispensable. *Nature* **2011**, *478*, 255-259, doi:10.1038/nature10408.

Chapter 8

105. Feng, Y.X.; Sokol, E.S.; Del Vecchio, C.A.; Sanduja, S.; Claessen, J.H.; Proia, T.A.; Jin, D.X.; Reinhardt, F.; Ploegh, H.L.; Wang, Q.; et al. Epithelial-to-mesenchymal transition activates PERK-eIF2alpha and sensitizes cells to endoplasmic reticulum stress. *Cancer Discov* **2014**, *4*, 702-715, doi:10.1158/2159-8290.CD-13-0945.

106. Vijay, G.V.; Zhao, N.; Den Hollander, P.; Toneff, M.J.; Joseph, R.; Pietila, M.; Taube, J.H.; Sarkar, T.R.; Ramirez-Pena, E.; Werden, S.J.; et al. GSK3beta regulates epithelial-mesenchymal transition and cancer stem cell properties in triple-negative breast cancer. *Breast Cancer Res* **2019**, *21*, 37, doi:10.1186/s13058-019-1125-0.

107. Tam, W.L.; Lu, H.; Buikhuisen, J.; Soh, B.S.; Lim, E.; Reinhardt, F.; Wu, Z.J.; Krall, J.A.; Bierie, B.; Guo, W.; et al. Protein kinase C alpha is a central signaling node and therapeutic target for breast cancer stem cells. *Cancer Cell* **2013**, *24*, 347-364, doi:10.1016/j.ccr.2013.08.005.

108. Kuhnle, M.; Egger, M.; Muller, C.; Mahringer, A.; Bernhardt, G.; Fricker, G.; Konig, B.; Buschauer, A. Potent and selective inhibitors of breast cancer resistance protein (ABCG2) derived from the p-glycoprotein (ABCB1) modulator tariquidar. *J Med Chem* **2009**, *52*, 1190-1197, doi:10.1021/jm8013822.

109. Robey, R.W.; Shukla, S.; Steadman, K.; Obrzut, T.; Finley, E.M.; Ambudkar, S.V.; Bates, S.E. Inhibition of ABCG2-mediated transport by protein kinase inhibitors with a bisindolylmaleimide or indolocarbazole structure. *Mol Cancer Ther* **2007**, *6*, 1877-1885, doi:10.1158/1535-7163.MCT-06-0811.

110. Thaiparambil, J.T.; Bender, L.; Ganesh, T.; Kline, E.; Patel, P.; Liu, Y.; Tighiouart, M.; Vertino, P.M.; Harvey, R.D.; Garcia, A.; et al. Withaferin A inhibits breast cancer invasion and metastasis at sub-cytotoxic doses by inducing vimentin disassembly and serine 56 phosphorylation. *Int J Cancer* **2011**, *129*, 2744-2755, doi:10.1002/ijc.25938.

111. Tanaka, H.; Kono, E.; Tran, C.P.; Miyazaki, H.; Yamashiro, J.; Shimomura, T.; Fazli, L.; Wada, R.; Huang, J.; Vessella, R.L.; et al. Monoclonal antibody targeting of N-cadherin inhibits prostate cancer growth, metastasis and castration resistance. *Nat Med* **2010**, *16*, 1414-1420, doi:10.1038/nm.2236.

112. Kang, H.; Kim, H.; Lee, S.; Youn, H.; Youn, B. Role of Metabolic Reprogramming in Epithelial(-)Mesenchymal Transition (EMT). *Int J Mol Sci* **2019**, *20*, doi:10.3390/ijms20082042.

113. Pavlova, N.N.; Thompson, C.B. The Emerging Hallmarks of Cancer Metabolism. *Cell Metab* **2016**, *23*, 27-47, doi:10.1016/j.cmet.2015.12.006.

114. Funasaka, T.; Hogan, V.; Raz, A. Phosphoglucose isomerase/autocrine motility factor mediates epithelial and mesenchymal phenotype conversions in breast cancer. *Cancer Res* **2009**, *69*, 5349-5356, doi:10.1158/0008-5472.CAN-09-0488.

115. Ahmad, A.; Aboukameel, A.; Kong, D.; Wang, Z.; Sethi, S.; Chen, W.; Sarkar, F.H.; Raz, A. Phosphoglucose isomerase/autocrine motility factor mediates epithelial-mesenchymal transition regulated by miR-200 in breast cancer cells. *Cancer Res* **2011**, *71*, 3400-3409, doi:10.1158/0008-5472.CAN-10-0965.

116. Li, Y.; Che, Q.; Bian, Y.; Zhou, Q.; Jiang, F.; Tong, H.; Ke, J.; Wang, K.; Wan, X.P. Autocrine motility factor promotes epithelial-mesenchymal transition in endometrial cancer via MAPK signaling pathway. *Int J Oncol* **2015**, *47*, 1017-1024, doi:10.3892/ijo.2015.3091.

117. Funasaka, T.; Hu, H.; Yanagawa, T.; Hogan, V.; Raz, A. Down-regulation of phosphoglucose isomerase/autocrine motility factor results in mesenchymal-to-epithelial transition of human lung fibrosarcoma cells. *Cancer Res* **2007**, *67*, 4236-4243, doi:10.1158/0008-5472.CAN-06-3935.

118. Li, J.; Wang, Y.; Li, Q.G.; Xue, J.J.; Wang, Z.; Yuan, X.; Tong, J.D.; Xu, L.C. Downregulation of FBP1 Promotes Tumor Metastasis and Indicates Poor Prognosis in Gastric Cancer via Regulating Epithelial-Mesenchymal Transition. *PLoS One* **2016**, *11*, e0167857, doi:10.1371/journal.pone.0167857.

119. Dong, C.; Yuan, T.; Wu, Y.; Wang, Y.; Fan, T.W.; Miriyala, S.; Lin, Y.; Yao, J.; Shi, J.; Kang, T.; et al. Loss of FBP1 by Snail-mediated repression provides metabolic advantages in basal-like breast cancer. *Cancer Cell* **2013**, *23*, 316-331, doi:10.1016/j.ccr.2013.01.022.

120. Jiang, F.; Ma, S.; Xue, Y.; Hou, J.; Zhang, Y. LDH-A promotes malignant progression via activation of epithelial-to-mesenchymal transition and conferring stemness in muscle-invasive bladder cancer. *Biochem Biophys Res Commun* **2016**, *469*, 985-992, doi:10.1016/j.bbrc.2015.12.078.

121. Liu, K.; Tang, Z.; Huang, A.; Chen, P.; Liu, P.; Yang, J.; Lu, W.; Liao, J.; Sun, Y.; Wen, S.; et al. Glyceraldehyde-3-phosphate dehydrogenase promotes cancer growth and metastasis through upregulation of SNAIL expression. *Int J Oncol* **2017**, *50*, 252-262, doi:10.3892/ijo.2016.3774.

122. Gaude, E.; Frezza, C. Tissue-specific and convergent metabolic transformation of cancer correlates with metastatic potential and patient survival. *Nat Commun* **2016**, *7*, 13041, doi:10.1038/ncomms13041.

123. Sciacovelli, M.; Goncalves, E.; Johnson, T.I.; Zecchini, V.R.; da Costa, A.S.; Gaude, E.; Drubbel, A.V.; Theobald, S.J.; Abbo, S.R.; Tran, M.G.; et al. Fumarate is an epigenetic modifier that elicits epithelial-to-mesenchymal transition. *Nature* **2016**, *537*, 544-547, doi:10.1038/nature19353.

124. Grassian, A.R.; Lin, F.; Barrett, R.; Liu, Y.; Jiang, W.; Korpal, M.; Astley, H.; Gitterman, D.; Henley, T.; Howes, R.; et al. Isocitrate dehydrogenase (IDH) mutations promote a reversible ZEB1/microRNA (miR)-200-dependent epithelial-mesenchymal transition (EMT). *J Biol Chem* **2012**, *287*, 42180-42194, doi:10.1074/jbc.M112.417832.

125. Loriot, C.; Burnichon, N.; Gadessaud, N.; Vescovo, L.; Amar, L.; Libe, R.; Bertherat, J.; Plouin, P.F.; Jeunemaitre, X.; Gimenez-Roqueplo, A.P.; et al. Epithelial to mesenchymal transition is activated in metastatic pheochromocytomas and paragangliomas caused by SDHB gene mutations. *J Clin Endocrinol Metab* **2012**, *97*, E954-962, doi:10.1210/jc.2011-3437.

126. Sciacovelli, M.; Frezza, C. Metabolic reprogramming and epithelial-to-mesenchymal transition in cancer. *FEBS J* **2017**, *284*, 3132-3144, doi:10.1111/febs.14090.

127. Guha, M.; Srinivasan, S.; Ruthel, G.; Kashina, A.K.; Carstens, R.P.; Mendoza, A.; Khanna, C.; Van Winkle, T.; Avadhani, N.G. Mitochondrial retrograde signaling induces epithelial-mesenchymal transition and generates breast cancer stem cells. *Oncogene* **2014**, *33*, 5238-5250, doi:10.1038/onc.2013.467.

128. Giudetti, A.M.; De Domenico, S.; Ragusa, A.; Lunetti, P.; Gaballo, A.; Franck, J.; Simeone, P.; Nicolardi, G.; De Nuccio, F.; Santino, A.; et al. A specific lipid metabolic profile is associated with the epithelial mesenchymal transition program. *Biochim Biophys Acta Mol Cell Biol Lipids* **2019**, *1864*, 344-357, doi:10.1016/j.bbalip.2018.12.011.

129. Sanchez-Martinez, R.; Cruz-Gil, S.; Gomez de Cedron, M.; Alvarez-Fernandez, M.; Vargas, T.; Molina, S.; Garcia, B.; Herranz, J.; Moreno-Rubio, J.; Reglero, G.; et al. A link between lipid metabolism and epithelial-mesenchymal transition provides a target for colon cancer therapy. *Oncotarget* **2015**, *6*, 38719-38736, doi:10.18632/oncotarget.5340.

130. Nieva, C.; Marro, M.; Santana-Codina, N.; Rao, S.; Petrov, D.; Sierra, A. The lipid phenotype of breast cancer cells characterized by Raman microspectroscopy: towards a stratification of malignancy. *PLoS One* **2012**, *7*, e46456, doi:10.1371/journal.pone.0046456.

Chapter 8

131. Sengupta, P.; Baird, B.; Holowka, D. Lipid rafts, fluid/fluid phase separation, and their relevance to plasma membrane structure and function. *Semin Cell Dev Biol* **2007**, *18*, 583-590, doi:10.1016/j.semcdb.2007.07.010.

132. Tisza, M.J.; Zhao, W.; Fuentes, J.S.; Prijic, S.; Chen, X.; Levental, I.; Chang, J.T. Motility and stem cell properties induced by the epithelial-mesenchymal transition require destabilization of lipid rafts. *Oncotarget* **2016**, *7*, 51553-51568, doi:10.18632/oncotarget.9928.

133. Rohle, D.; Popovici-Muller, J.; Palaskas, N.; Turcan, S.; Grommes, C.; Campos, C.; Tsoi, J.; Clark, O.; Oldrini, B.; Komisopoulou, E.; et al. An inhibitor of mutant IDH1 delays growth and promotes differentiation of glioma cells. *Science* **2013**, *340*, 626-630, doi:10.1126/science.1236062.

134. Letouze, E.; Martinelli, C.; Loriot, C.; Burnichon, N.; Abermil, N.; Ottolenghi, C.; Janin, M.; Menara, M.; Nguyen, A.T.; Benit, P.; et al. SDH mutations establish a hypermethylator phenotype in paraganglioma. *Cancer Cell* **2013**, *23*, 739-752, doi:10.1016/j.ccr.2013.04.018.

135. Fan, T.; Sun, G.; Sun, X.; Zhao, L.; Zhong, R.; Peng, Y. Tumor Energy Metabolism and Potential of 3-Bromopyruvate as an Inhibitor of Aerobic Glycolysis: Implications in Tumor Treatment. *Cancers (Basel)* **2019**, *11*, doi:10.3390/cancers11030317.

136. Cao, X.; Bloomston, M.; Zhang, T.; Frankel, W.L.; Jia, G.; Wang, B.; Hall, N.C.; Koch, R.M.; Cheng, H.; Knopp, M.V.; et al. Synergistic antipancreatic tumor effect by simultaneously targeting hypoxic cancer cells with HSP90 inhibitor and glycolysis inhibitor. *Clin Cancer Res* **2008**, *14*, 1831-1839, doi:10.1158/1078-0432.CCR-07-1607.

137. Ihrlund, L.S.; Hernlund, E.; Khan, O.; Shoshan, M.C. 3-Bromopyruvate as inhibitor of tumour cell energy metabolism and chemopotentiator of platinum drugs. *Mol Oncol* **2008**, *2*, 94-101, doi:10.1016/j.molonc.2008.01.003.

138. Jin, H.; He, Y.; Zhao, P.; Hu, Y.; Tao, J.; Chen, J.; Huang, Y. Targeting lipid metabolism to overcome EMT-associated drug resistance via integrin beta3/FAK pathway and tumor-associated macrophage repolarization using legumain-activatable delivery. *Theranostics* **2019**, *9*, 265-278, doi:10.7150/thno.27246.

139. Pattabiraman, D.R.; Bierie, B.; Kober, K.I.; Thiru, P.; Krall, J.A.; Zill, C.; Reinhardt, F.; Tam, W.L.; Weinberg, R.A. Activation of PKA leads to mesenchymal-to-epithelial transition and loss of tumor-initiating ability. *Science* **2016**, *351*, aad3680, doi:10.1126/science.aad3680.

140. Ishay-Ronen, D.; Diepenbruck, M.; Kalathur, R.K.R.; Sugiyama, N.; Tiede, S.; Ivanek, R.; Bantug, G.; Morini, M.F.; Wang, J.; Hess, C.; et al. Gain Fat-Lose Metastasis: Converting Invasive Breast Cancer Cells into Adipocytes Inhibits Cancer Metastasis. *Cancer Cell* **2019**, *35*, 17-32 e16, doi:10.1016/j.ccell.2018.12.002.

141. Yan, K.S.; Gevaert, O.; Zheng, G.X.Y.; Anchang, B.; Probert, C.S.; Larkin, K.A.; Davies, P.S.; Cheng, Z.F.; Kaddis, J.S.; Han, A.; et al. Intestinal Enteroendocrine Lineage Cells Possess Homeostatic and Injury-Inducible Stem Cell Activity. *Cell Stem Cell* **2017**, *21*, 78-90 e76, doi:10.1016/j.stem.2017.06.014.

142. Schmitt, M.; Schewe, M.; Sacchetti, A.; Feijtel, D.; van de Geer, W.S.; Teeuwssen, M.; Sleddens, H.F.; Joosten, R.; van Royen, M.E.; van de Werken, H.J.G.; et al. Paneth Cells Respond to Inflammation and Contribute to Tissue Regeneration by Acquiring Stem-like Features through SCF/c-Kit Signaling. *Cell Rep* **2018**, *24*, 2312-2328 e2317, doi:10.1016/j.celrep.2018.07.085.

143. Yu, S.; Tong, K.; Zhao, Y.; Balasubramanian, I.; Yap, G.S.; Ferraris, R.P.; Bonder, E.M.; Verzi, M.P.; Gao, N. Paneth Cell Multipotency Induced by Notch Activation following Injury. *Cell Stem Cell* **2018**, *23*, 46-59 e45, doi:10.1016/j.stem.2018.05.002.

CHAPTER IX

Summary

Malignant cells, and in particular those responsible for local invasion, dissemination and distant metastasis, are often endowed with plasticity, i.e. the capacity to undergo transient and reversible morphological and functional changes. In particular, epithelial to mesenchymal transition (EMT), namely the loss of epithelial identity and the acquisition of a migratory and more mesenchymal phenotype, is regarded as the crucial event in invasion and dissemination. In addition to promoting cellular migration and invasion, the transient phenotypic changes associated with the formation of the mesenchymal state during EMT have been associated with the acquisition of stem-like properties, resistance to therapy, immune suppression, extracellular matrix and tumor microenvironment remodeling, and escape from apoptosis and senescence. The epigenetic, and as such reversible nature of EMT is crucial as the reverse mesenchymal to epithelial (MET) process allows migrating cancer (stem-like) cells to regain proliferative and epithelial characteristics to colonize distant organ sites. However, rather than leading to a complete epithelial or mesenchymal state, the EMT/MET programs generate migrating cancer cells displaying intermediate phenotypes featuring both epithelial and mesenchymal characteristics. These hybrid E/M cancer cells have been the focus of much attention in the most recent scientific literature as they are likely to be metastable and as such very efficient in causing metastasis. In this thesis, I report on my studies towards the elucidation of the molecular and cellular mechanisms underlying phenotypic plasticity in oral cell squamous cell carcinoma, colon tumors and ovarian cancer.

Chapter I provides a short and general introduction on the development of cancer and a brief outline of the metastatic cascade. The latter is more extensively reviewed in **Chapter II** with focus on the current debate on the role of cancer heterogeneity and phenotypic plasticity in metastasis formation. The importance of EMT, and in particular hybrid epithelial/mesenchymal (E/M), in collective and/or single cell migration during local dissemination at the primary and more systemic spreading is here highlighted.

In **Chapter III** we report on the epigenetic mechanisms underlying MET in tongue cancer. We show that loss of Deleted in Oral Cancer 1 (DOC1; also known as CDK2AP1: cyclin-dependent kinase 2-associated protein 1) in oral squamous cell carcinoma (OSCC) cells leads to the failure of the remodeler complex NuRD to bind and repress EMT-related transcriptional regulators thereby promoting an EMT state. Mechanistically, upon DOC1-dependent NuRD recruitment to the promoters of specific EMT master regulator genes, SWI/SNF is displaced resulting in the transition from an active to a repressive chromatin state.Accordingly, re-expression of DOC1 expression in OSCC (i.e. DOC1-deficient) cells results in the reversal of EMT, i.e. MET. We suggest that SWI/SNF and NURD function antagonistically to control chromatin state and transcription of EMT master regulators.

In **Chapter IV**, we report on the identification and characterization of a subpopulation of colon cancer cells endowed with phenotypic plasticity and responsible for local invasion and distant metastasis. These CD44^{hi}/EpCAM^{lo} (EpCAM^{lo}) cells are highly motile, invasive, chemoresistant, and metastatic both *in vitro* and *in vivo*. Bulk and single-cell RNAseq analysis indicate that they comprise a broad spectrum of degrees of EMT activation, together with stem/progenitor-like features, enhanced Wnt/β-catenin signaling, and a high correlation with the CMS4 subtype, accounting for ~25% of colon cancer cases with poor prognosis. Enhanced Wnt and the downstream upregulation of EMT transcription factors such as ZEB1 represent key events in eliciting phenotypic plasticity to cancer cells along the invasive front of primary colon carcinomas. Additional analysis reveals

Chapter 9

that different combinations of distinct sets of epithelial and mesenchymal genes define transcriptional trajectories through which state transitions arise. Here, hybrid E/M stages are predicted to represent the origin of these differentiation routes through biologically-distinct cellular states and as such to underlie the phenotypic plasticity of colon cancer cells.

In **Chapter VI** we show that a similar dichotomy between epithelial and quasi-mesenchymal subpopulations of cancer cells exist in ovarian cancer. Accordingly, patients with ovarian cancers characterized by increased *ZEB1* expression are usually associated with worse progression-free and overall survival. By taking advantage of an EMT signature derived from RNAseq data we show the presence of quasi-mesenchymal cells in ovarian cancer tumors.

Chapter V reviews the current knowledge of the role of Wnt signaling in ovarian cancer. Importantly, Wnt activity has been shown to correlate with grade, EMT, chemotherapy resistance, and poor prognosis in ovarian cancer. In addition, malignant ascites provides in the paracrine activation of Wnt signaling and pre-metastatic niche formation. This review provides the basis for **Chapter VII**, where we present experimental evidence for the dual role of Wnt signaling in regulating metastasis formation in high grade serous ovarian cancer. We show that the Wnt signaling cascade establishes and regulates quasi-mesenchymal cellular phenotypes through activation of the EMT transcription factor *ZEB1*. Moreover, our results suggest that Wnt participates in the establishment of pre-metastatic niches in the abdominal cavity through exosome-mediated ligand secretion from primary ovarian cancer cells.

Overall, this thesis presents a series of original studies and literature reviews on the characterization of cellular and molecular mechanisms underlying phenotypic plasticity along the invasion-metastasis cascade in oral squamous cell carcinoma, colon cancer, and ovarian tumors. These results are of relevance for the development of future and therapeutic approaches. EMT and especially hybrid E/M tumor cells feature a high degree of phenotypic plasticity coupling the capacity to undergo phenotypic switching with therapy resistance and other stem cell features (**Chapter VIII**).

A

Appendices

Appendix I – Nederlandse samenvatting

Kankercellen, en vooral de cellen die verantwoordelijk van voor lokale invasie en het uitzaaien van kanker, zijn vaak plastisch. Zij beschikken over de eigenschap om tijdelijk van morfologie en functie te veranderen. Vooral het proces genaamd epitheliale tot mesenchymale transitie (EMT), waarin cellen hun epitheliale identiteit verliezen en een invasief mesenchymaal fenotype krijgen, wordt gezien als een cruciale gebeurtenis in het metastaseren. Naast het invasieve karakter dat geassocieerd is met het mesenchymale fenotype tijdens EMT, is het ondergaan van EMT door kankercellen ook geassocieerd met het verkrijgen van stamceleigenschappen, het ontwikkelen van resistentie tegen kankerbehandelingen, het ontstaan van immuunsuppressie, het remodelleren van de extracellulaire matrix en het tumormilieu, en het ontsnappen aan geprogrammeerde celdood.

Het epigenetische, en dus reversibele karakter, van EMT is essentieel omdat het omgekeerde mesenchymale tot epitheliale transitie ervoor zorgt dat invasieve (kankerstam)cellen hun proliferatieve en epitheliale eigenschappen weer terug krijgen om zo de metastase te vormen. Echter, in plaats dat kankercellen zich in een compleet epitheliale of mesenchymale toestand bevinden, genereert het EMT/MET programma ook invasieve kankercellen die zowel epitheliale als mesenchymale eigenschappen hebben. Recente literatuur heeft laten zien dat deze hybride EMT/MET kankercellen nog effectiever zijn het metastaseren dan volledig mesenchymale cellen. In dit proefschrift beschrijf ik de onderzoeken dit ik gedaan heb naar de onderliggende moleculaire en cellulaire mechanismen die aan fenotypische plasticiteit ten grondslag leggen in plaveiselcelcarcinomen van de mond, in colontumoren en ovariumkanker.

Een korte en algemene introductie naar het ontstaan van kanker en de route van het uitzaaien wordt gegeven een **hoofdstuk I**. Dit laatste zal meer uitgebreid worden belicht in **hoofdstuk II** waarbij de focus wordt gelegd op kankerheterogeniteit en de fenotypische plasticiteit tijdens het uitzaaien. Het belang van EMT, en vooral ook de hybride epitheliale/mesenchymale status wordt hier bediscussieerd. Daarnaast wordt de migratie van kankercellen in collectief of als één enkele cel besproken.

Hoofdstuk III is een stuk waarin de epigenetische mechanismen betrokken bij EMT/MET in tongkanker worden besproken. Wij laten zien dat het verlies van DOC1 (Deleted in Oral Cancer 1; ook wel bekend als CDK2AP1: cyclin-dependent kinase 2-associated protein 1) in orale plaveiselcelcarcinomen leidt tot falen van het onderdrukken EMT-betrokken transcriptie regulatoren door DNA remodeller NuRD. Dit falen leidt tot een EMT-actief programma in kankercellen. Mechanisch zorgt DOC1 voor de rekrutering van NuRD op de promoteren van specifieke EMT regulatie genen, hierop wordt SWI/SNF van het DNA ontbonden wat resulteert in de transitie van actief naar inactief chromatine. Re-expressie van DOC-1 in tongkanker (welke vaak DOC1 deficiënt zijn) resulteert in MET. Wij suggereren dat SWI/SNF en NuRD antagonistisch aan elkaar werken in het controleren van actief/inactief chromatine en daardoor de transcriptie van EMT regulatoren.

Vervolgens wordt in **hoofdstuk IV** de identificatie en het karakteriseren van een subpopulatie van colonkanker cellen die gekenmerkt wordt met fenotypische plasticiteit

en verantwoordelijk zijn voor lokale invasie en het vormen van metastasen besproken. Deze CD44^{hi}/EpCAM^{lo} (EpCAM^{lo}) cellen zijn invasief, chemoresistent en zorgen voor uitzaaiingen zowel *in vitro* als wel *in vivo*. Bulk en single-cell RNAseq analyse voorspelt de aanwezigheid van een breed spectrum aan levels van EMT activatie. Deze analyses bevestigen de aanwezigheid van stamceleigenschappen in deze cellen. Tevens wordt een toename van Wnt/β-catenin signalering gedetecteerd in deze EpCAM^{lo} cellen en wordt een correlatie met het CMS4 subtype van colonkanker die verantwoordelijk is voor de 25% van de kankergevallen met een slechte prognose gezien. Wnt en de daarop volgende activatie van EMT transcriptiefactoren zoals ZEB1 is essentieel voor het teweegbrengen van fenotypische plasticiteit van kankercellen aan het invasieve front in primaire colontumoren. Aanvullende analyse laat zien dat verschillende combinaties van epitheliale en mesenchymale genen verantwoordelijk zijn voor verschillende routes die leiden tot EMT/MET transities. De hybrid E/M fase lijkt hierin de origine te zijn van deze verschillende differentiatie paden en zullen daardoor ten grondslag liggen aan fenotypische plasticitiet in colonkanker.

In **hoofdstuk VI** laten we een gelijke tweedeling tussen epitheliale en quasi-mesenchymale subpopulaties zien in ovariumkanker. Hierbij wordt een slechtere progressie-vrije en overlevingskans gezien in ovariumkankerpatiënten die een toegenomen genexpressie hebben van ZEB1. Door middel van een EMT-lijst die verkregen is door middel van RNAseq data laten we de aanwezigheid van quasi-mesenchymale cellen zien in ovariumkanker.

Hoofdstuk V bespreekt de huidige kennis van de rol van Wnt signalering in ovariumkanker. Belangrijk is de correlatie van Wnt activatie met tumorgraad, EMT, chemotherapieresistentie en een slechtere prognose in ovariumkanker. Daarnaast zorgt maligne ascites voor een paracriene activatie van Wnt signalering en de vorming van een pre-metastatische niche. Deze review legt de basis voor **hoofdstuk VII** waar experimenteel bewijs gepresenteerd wordt waarin Wnt signalering een tweedelige rol heeft in het vormen van uitzaaiingen in hoog gradige sereuze ovariumkankers. Wnt signalering veroorzaakt een quasi-mesenchymaal fenotype door de activatie van EMT transcriptiefactor ZEB1. Daarnaast suggereren de resultaten dat Wnt betrokken is bij de vorming van de pre-metastatische niche in de buikholte voor secretie van exosomen door primaire ovariumkankercellen.

Al met al presenteert dit proefschrift een serie van originele onderzoeken en reviews van de literatuur over het karakteriseren van de cellulaire en moleculaire mechanismes betrokken bij fenotypische plasticiteit gedurende de invasie-uitzaaiingscascade in orale plaveiselcelcarcinomen, colonkanker en ovariumtumoren. Deze resultaten zijn van belang voor het ontwikkelen van toekomstige therapeutische mogelijkheden. EMT maar vooral ook hybride EMT kankercellen bezitten stamceleigenschappen en staan daarom bekend om hun therapieresistentie. Opheldering van de mechanismes die verantwoordelijk zijn voor de epigenetische veranderingen die kankercellen ondergaan tijdens het metastaseren zullen daarom belangrijk zijn voor het ontwikkelen van nieuwe therapeutische mogelijkheden (**hoofdstuk VIII**).

Appendix II – Acknowledgements

Fellow *arts-assistenten Interne Geneeskunde* and *beschouwende pool,* it has been a crazy period with the COVID-units and extra shifts we had to cover. But I think we make a great team, that takes care of each other. Thank you also for the warm welkom in Brabant and for all the experiences we pick up along the way.

Of course, this PhD journey would not have been possible without the financial support of KWF Kankerbestrijding and the Erasmus MRACE grant, to whom I am sincerely grateful.

Fortunately, I have the privilege of having a lovely family and friends who had a fundamental role in getting me through the PhD process successfully:

First of all, my dearest friends Danny and Lisette Fiere. *Samen Sterk*, the best team ever. Since the day we met, you are like a brother and sister to me. No words can explain how proud I was when we finished Tour for Life in 2017. And again in 2018. All the hard work on the bike, the beautiful trips to the Alps and Zeeland, the million Easter eggs we wrapped and the many Skip-Bo matches in your waterproof tent are just a selection of the precious moments with you that I will never forget.

Lisette, you are the sweetest, most caring and strongest person I have ever met. Thank you for being my friend. You are such an inspiration for me. I miss you very much and I will never forget you. I love you so much.

Danny, last year was incredible hard and very emotional. But despite all this, thank you for being there for me. You made it possible to help me grow, and most importantly to believe in myself. Although team *Samen Sterk* will never be the same, we will continue to be a team that will make our dearest Lisette proud.

A recurring theme during my time as a PhD-student was the Tour for Life. Starting as a cyclist in the Erasmus MC team in 2016 was the start of a period that has changed me as a person. Thanks to all the riders, *ploegleiders*, volunteers and supporters that I met during the Tour for Life editions of 2016, 2017, 2018 and 2021. The positivity and support during the actual ride, but also the friendships that were made are very important to me. Especially I want to thank Johannes and Renée, Patrick, Ilse, Jochem, Laurent, Sylvia, Sheila Gemin, Jannie and Leo, Ada and Arie, Desirée, and Joke and Henk van Raamsdonk.

Also, thanks to Annemarie de Witte. *Sparren* about our PhD life during our bike or run sessions were very helpful.

Special thanks to Désirée Mark for helping me out. Your sessions really made a difference and make me how I am today.

Thank you to Michael, LuAnn, Carly and Brett Farrell, my American family. Although writing this thesis in was quite hard. It would have been so much harder if I did not get the opportunity to become more fluent in English as I am now.

Also, many thanks to all my high school friends Roxanne, Angelique, Marlène and Linda. It started all with a *stroopwavel* in our second year, but it broke the ice and was starting of a beautiful friendship.

Of course I cannot forget my team mates from Triathlon Vereniging Rijnmond and all the people I met along the way that supported or listened to me.

Next my family in law Yvonne, Ben and Alie, Mitchell and Sifra, Cheline and Ron, and off course little Noé. Thank you for your support!

Frank, my brother, and Emilyn thank you putting things in perspective for me. Thanks you for your paptalks when I needed them the most!

Many thanks to my parents Frank and Ans Teeuwssen for all the love, support and opportunities you gave and still give me. This journey was challenging at times and I would not have finished it with so much proud without your support.

And at last, Samantha Kraaijveld. Although we met after finishing my time in the lab, you supported me during the last struggles finishing this thesis. And yes, I know you don't like these personal 'thank yous' and special words directed to you. So, I just want to say that I love you and that I am looking forward to our next project (renovating our new house) and future adventures!

Appendix III – List of publications

A. Sacchetti*, M. Teeuwssen*, M. Verhagen*, R. Joosten, A. Gusinac, M.M. Watson, R. Stabile, W. K. Kim, I. Ubink, H. J.G. van Werken, A. Fumagalli, M. Paauwe, J. van Rheenen, O. Sansom, O. Kranenburg, R. Fodde, *Phenotypic plasticity and partial EMT underlie local invasion and distant metastasis in colon cancer,* **eLife***,* 2021 May 26;10e61461

M. Teeuwssen and R. Fodde, *Wnt signaling in ovarian cancer stemness, EMT, and therapy resistance,* **Journal of Clinical Medicine***,* 2019 Oct 11;8(10)

M. Teeuwssen and R. Fodde, *Cell heterogeneity and phenotypic plasticity in metastasis formation: the case of colon cancer,* **Cancers (Basel)***,* 2019 Sept 14;11(9)

M. Schmitt, M. Schewe, A. Sacchetti, D. Feijtel, W.S. van de Geer, M. Teeuwssen, H.F. Sleddens, R. Joosten, M.E. van Royen, H.J.G. van de Werken, J. van Es, H. Clevers, R. Fodde, *Paneth cells respond to inflammation and acquiring stem-like features through SCF/c-Kit Signaling,* **Cell Reports**, 2018 Aug 28;24(9)

A. Mohd-Sarip, M. Teeuwssen, A.G. Bot, M.J. de Herdt, S.M. Willems, R.J. Baatenburg-de Jong, J. van Riet, E. Oole, W.F.J. van IJcken, H.J.G. van de Werken, J.A. Demmers, R. Fodde, C.P. Verrijzer, *DOC-1-dependent recruitment of NURD reveals antagonism with SWI/SNF during epithelial mesenchymal transition in oral cancer cells*, **Cell Reports**, 2017 Jul 5;20(1)

M. van der Zee, A. Sacchetti, M. Cansoy, R. Joosten, M. Teeuwssen, C. Heijmans-Antonissen, P.C. Ewing, Graham, C.W. Burger, L.J. Blok, R. Fodde, *IL6/JAK1/STAT3 signaling blockade in endometrial cancer affects the ALDHhigh/CD126+ stem-like component and reduces tumor burden,* **Cancer Research**, 2015 Sept 1;75(17)

C. van de Werken, G. W. van der Heijden, C. Eleveld, M. Teeuwssen, M. Albert, W. M. Baarends, J. S. E. Laven, A. H.F.M. Peters, E. B. Baart, *The build-up of paternal heterochromatin in human embryos is directed by the H3K9/HP1 pathway and primed by sperm-derived histone modifications*, **Nature Communications**, 2014 Dec 18;5
*equal contributions

Appendix IV – Curriculum Vitae

Miriam Teeuwssen was born in Delft on August 17th 1988. In 2007 she attended Medical School at the Erasmus University Medical Centre in Rotterdam, where she graduated in 2014. During the same period, she also enrolled to the research master Molecular Medicine, where she performed her master internship under the supervision of prof. R. Fodde at the department of Pathology at the Erasmus Medical Centre. After defending her master thesis studying the cellular and molecular mechanisms underlying liver metastasis in colon cancer, she continued this work as a PhD student in the same laboratory. In addition to studying the mechanisms underlying metastasis in colon cancer, she expanded her research to ovarian cancer and oral squamous cell carcinoma. From September 2020 onwards, Miriam started working as a resident not in training in Internal Medicine at the Elizabeth-TweeSteden Ziekenhuis in Tilburg. In January 2022 she was accepted to start her residency in training in Internal Medicine under de supervision of dr. M.E.E. van Kasteren (Elisabeth-Tweesteden Ziekenhuis) and dr. A.M. van Zandbergen (Erasmus Medical Center).

Appendix V – PhD portfolio

Name PhD student: M. J. Teeuwssen
Department: Pathology
Research school: Molecular Medicine
PhD period: 2014-2020
Promotor: Prof. R. Fodde
Co-promotor   Prof. C. P. Verrijzer

	Year	Workload (ECTS)
Courses		
Article 9 – Laboratory Animal Science	2013	3.0
The course: Research management for PhD-students	2014	1.0
Erasmus MC – Basic Course on 'R'	2016	2.0
Conferences		
100 year Daniël den Hoed symposium	2014	1.0
EMBO: Cancer Stem Cells 20 years later – achievements, controversies, emerging concepts and technologies (poster presentation)	2014	2.5
KWF Tumor Cell Biology Annual Meeting	2016	1.0
5th Daniël den Hoeddag (oral presentation)	2017	1.5
Liver Metastasis Research Network (oral presentation)	2017	2.0
6th International Zoo meeting (oral and poster presentation)	2019	2.5
Seminars		
JNI Oncology lectures	2014-2019	5.0
JNI meetings (oral presentations)	2014-2019	5.0
Pathology Laboratory Meeting (oral presentations)	2016-2018	3.0
Teaching		
VO pathology - digital microscopy	2014-2019	5.0
Journal club Nanobiology	2015-2016	3.0
Supervision HLO-student	2017	5.0
Supervision master student	2018	5.0